UNIVERSITA' DEGLI STUDI DI PARMA

Dottorato di ricerca in Ingegneria Industriale

Ciclo XXIV

Modeling and Analysis of Hydraulic Load Sensing Strategies in Off Highway Equipment

Modellazione e Analisi di Sistemi Idraulici Load Sensing in Macchine Movimento Terra

Coordinatore:

Chiar.mo Prof. Ing. Marco Spiga

Tutor:

Chiar.mo Prof. Ing. Paolo Casoli

Dottorando:
Dott. Ing. Alvin Anthony

To

Mythili, Michelle and Arielle

PREFACE

This thesis titled "Modeling and Analysis of Hydraulic Load Sensing Strategies in Off Highway Equipment" consists of two parts. The first part is called "Modeling and Analysis of an Excavator System' and the title of the second part is "Modeling and Analysis of Tractor Rear Hitch Controls." The topics discussed in this thesis include modeling of an excavator sytem and the modeling of an agricultural tractor's rear hitch controls. The objectives of this thesis have been to develop a fast simulation model to replicate the functioning of an excavators system and the analysis of a tractor rear hitch controls. Both topics are of substantial importance in today's industrial research scenario. With a large demand being placed on more intelligent development of construction and agricultural equipment to meet the changing needs of the worlds economy, this thesis offers its contribution in the meeting of these requirements. These two parts of this thesis are based on the following papers published at various conferences and journals.

- Casoli P., Vacca A., Anthony A., Berta G.L. (2010) *Numerical and Experimental Analysis of the Hydraulic Circuit for the Rear Hitch Control in Agricultural Tractors*. 7th International Fluid Power Conference, (pp. 51-63, vol. 1) Aachen, 22-24/03 2010, ISBN 978-3-940565-90-7

- Alvin Anthony, Paolo Casoli, Andrea Vacca. (2010) .*Analysis of a tractor rear hitch control system.* Proc. Of 6th FPNI-PhD Symposium West Lafayette, 15-19 June 2010, pp. 589-602. FPNI Fluid Power Net Publications, 2010

- Casoli P., Vacca A., Anthony A., Berta G.L. (2011) *Modellazione e verifica sperimentale del circuito oleodinamico di controllo del sollevatore posteriore di trattori agricoli*. Proc of UNACOMA, 13 April 2011, Bologna, Italy.

- Paolo Casoli, Alvin Anthony, *Modeling of an Excavator – Pump Nonlinear Model and Structural Linkage/Mechanical Model*, Proc. Of 12th Scandinavian International Conference on Fluid Power, May 18-20, 2011, Tampere, Finland

- Paolo Casoli, Alvin Anthony, Manuel Rigossi (2011), *Modeling of an Excavator System - Semi Empirical Hydraulic Pump Model*, SAE Commercial Vehicle Congress 2011, September 2011, Rosemont, IL, USA

- Paolo Casoli, Alvin Anthony, Manuel Rigossi (2011), *Modeling of an Excavator System - Semi Empirical Hydraulic Pump Model*, SAE Commercial Vehicle Journal, October 2011, Rosemont, IL, USA

- Paolo Casoli, Alvin Anthony, *Gray Box Modeling of an Excavator's Variable Displacement Hydraulic Axial Piston Pump for Fast Simulation of Excavation Cycles,* Journal of Control Engineering Practice – Elsevier Publciations *(under review)*

- Paolo Casoli, Andrea Vacca, A. Anthony, Gian Luigi Berta, *Modellazione della valvola di controlloo di un sollevatore agricolo,* O&P - Oleodinamica Pneumatica - Gennaio 2012

- Alvin Anthony, Alessandro Ottala, Paolo Casoli, Cesare Dolcin, Antonio Lettini, *Modeling and Verification of an Excavator System – Axial Piston Pump, Kinematics and Prime Mover Models,* Proc. Of 7^{h} FPNI-PhD Symposium Modena. FPNI Fluid Power Net Publications, 2012

PART 1

This part describes the results of a study focused on the mathematical modeling of an excavator hydraulic system. From the viewpoint of designing and tuning an efficient control system, an excavator is a very complex nonlinear plant. To design and tune such a complex control system an extremely good nonlinear model of the plant is necessary. The problem of modeling an excavator is considered in this document; a nonlinear mathematical model of an excavator has been developed using the AMESim® modeling environment to replicate actual operating conditions. The excavator model is described by detailed models of the main pump, mobile valve block, actuators and a completely developed kinematic model. The objective of this research is to develop a complete simulation model of an excavator with the capability of reproducing the actual characteristics of the system. This part presents the developed model of a complete excavator system with detailed verification of individual components and preliminary results of a complete excavator system.

PART 2

This part of the thesis describes the work carried out towards mathematical modeling and analysis of a tractor rear hitch control valve (HCV). The HCV operates in two modes namely lifting and lowering. The lifting circuit incorporates a pressure compensated flow control valve, while the lowering circuit is gravity assisted. The HCV is a load-sensing system; load-sensing systems and pressure compensated valves are classified as feedback systems. Systems with feedback offer scope for tuning and towards this objective the pressure compensator has been linearised and its characteristics analyzed. The objective of this study is to develop a complete mathematical model of the HCV. This would help to better understand its functionality and to quantify the energy losses across its components.

UNIVERSITY OF PARMA

Modeling and Analysis of an Excavator System

PART - I

This part describes the results of a study focused on the mathematical modeling of an excavator hydraulic system. From the viewpoint of designing and tuning an efficient control system, an excavator is a very complex nonlinear plant. To design and tune such a complex control system an extremely good nonlinear model of the plant is necessary. The problem of modeling an excavator is considered in this document; a nonlinear mathematical model of an excavator has been developed using the AMESim® modeling environment to replicate actual operating conditions. The excavator model is described by detailed models of the main pump, mobile valve block, actuators and a completely developed kinematic model. The objective of this research is to develop a complete simulation model of an excavator with the capability of reproducing the actual characteristics of the system. This part presents the developed model of a complete excavator system with detailed verification of individual components and preliminary results of a complete excavator system.

Index

CHAPTER 1

Introduction

An excavator is a typical hydraulic heavy-duty human-operated machine used in general versatile construction operations, such as digging, ground leveling, carrying loads, dumping loads and straight traction. These operations require coordinated movement of boom, arm and bucket in order to control the bucket tip position to follow a desired trajectory. An excavator is comprised of three planar implements connected through revolute joints known as the boom, arm, and bucket, and one vertical revolute joint known as the swing joint [1].

Kinematics is the science of motion which treats motion without regard to the forces that cause it. Within the science of kinematics one studies the position, velocity, acceleration, and all higher order derivatives of the position variables (with respect to time or any other variables) [3]. The excavator linkage, however, is a complex link mechanism whose motion is controlled by hydraulic cylinders and actuators. To program the bucket motion and joint-link motion, a mathematical model of the link mechanism is required to refer to all geometrical and/or time-based properties of the motion. Kinematic model describes the spatial position of joints and links, and position and orientation of the bucket. The derivatives of kinematics deal with the mechanics of motion without considering the forces

that cause it [4]. Their common structure consists of a traveling body, a swing body and a front manipulator. The boom, arm and bucket, as shown in Figure 1.1, are three main links comprising the front manipulator of an excavator. Boom, arm and bucket motions are the most frequent motions of an excavator when it works in a parked condition.
In this document, the mechanical dynamics refers to the multi-body dynamics of the front manipulator and the hydraulic system dynamics. Hydraulic actuators such as hydraulic cylinders drive the boom, arm and bucket of an excavator. Hydraulic cylinders are used for boom, arm and bucket motion respectively. Since the hydraulic system has its own dynamics due to compressibility of hydraulic oil and has highly nonlinear characteristics, it is necessary to consider its effect on the overall dynamic behavior of the excavator. An exact knowledge of the coupled dynamics is crucial for designing the hydraulic system, determining the required mechanical strengths of the major parts, improving efficiency and handling for excavator operators.

A dynamic model is essential for dynamics-related studies of an excavator, such as controllability. Since the hydraulic system, which controls the actuators of an excavator, has its own dynamics due to compressibility of hydraulic oil, it is required that the dynamics of the hydraulic system be incorporated into that of the mechanical system to study the coupled dynamic behavior of the excavator. Base compliance, non-linearity and coupled dynamics result in positioning inaccuracies which in turn give rise to control problems.

In order to design, improve performance, simulate the behavior, and finally control a system or "plant", it is necessary to obtain its dynamics. In Figure 1.1 a schematic drawing of a typical excavator under consideration is shown. It consists of a chain track and the hydraulic propel drive which is used to maneuver the machine but usually not during a work cycle. On top of that is a carriage where the operator sits. It can rotate around a vertical axis with respect to the chain track. It also holds the Diesel engine, the hydraulic pumps and control system. Furthermore, there is a boom, an arm and at the end a bucket which is attached via a planar kinematic loop to the arm. Boom, arm and bucket can be rotated by the appropriate cylinders.

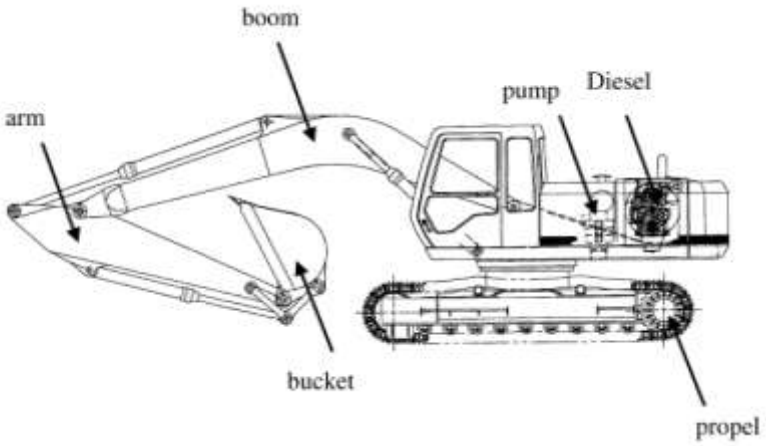

Figure 1.1: Schematic drawing of an excavator

The advantages of such a model are:

- Optimally tune the area curves of control valves for improved excavator motion by iterating the coupled dynamic simulations, without performing cost-intensive experiments with precision-machined spools which have varied area characteristics.
- Increase durability of the various mechanical parts of an excavator by using information on the dynamic forces obtained from simulations of the real working conditions of the excavator.
- Simulate the transient dynamic behavior of an excavator on the computer, and get insight into how much effect each mechanical or hydraulic design parameter has on the ride comfort.
- The coupled dynamic model is indispensable for designing a model-based control system for an automated excavator.

In all these processes, a simulation environment for an excavator, in which not only the Mechanical dynamics but also the hydraulic actuator dynamics can be considered, plays an essential role. It can greatly help to reduce the development costs and shorten the time to market. Without loss of generality, some assumptions were made to simplify the mechanical system model of the excavator.

- Inertial effects of moving parts, e.g., cylinders and pistons, of the hydraulic actuators are neglected. Masses and mass moments of inertia of the hydraulic actuators are much smaller than those of the boom, arm and bucket. Therefore, they can be reasonably neglected. Otherwise, they can be assumed to be constant and included in the masses and mass moments of inertia of the boom, arm and bucket, if needed.
- Hydraulic cylinders can transmit axial forces only. There exist no radial force components.
- Passive revolute joints have no friction. The major sources of friction are the stiction and viscous friction between the inner wall and the piston in the hydraulic cylinder assembly. These frictional forces can be treated in the hydraulic system model.

To provide a deeper understanding into the dynamics of an excavator as it carries out different functions. Let us look at figures 1.2 which represent the excavator in different operating conditions.

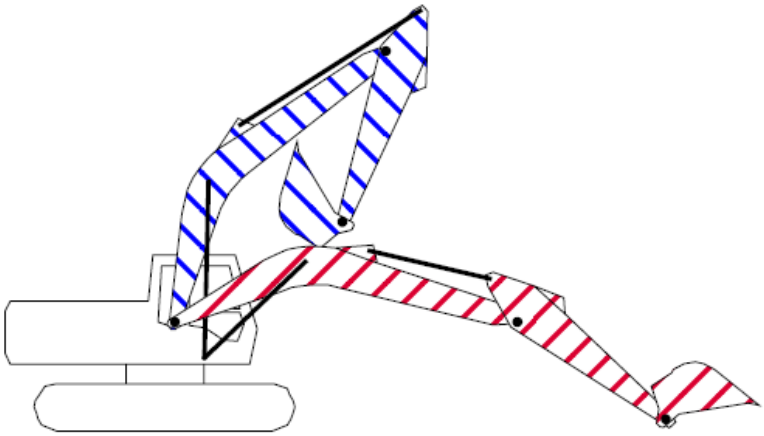

Figure 1.2: Different working conditions of an Excavator's Implements

Figure 1.2 shows that the required pressures in the cylinders depend on the position. For the "stretched" situation the pressure in the boom cylinder is 60 % higher than in the retracted position. Not only the position but also the movements have to be taken into account. The figure demonstrate's that a simulation model must take into account the couplings between the four degrees of freedom this excavator has. A simpler model that uses a constant load for each cylinder and the swivel drive leads to erroneous results [5].

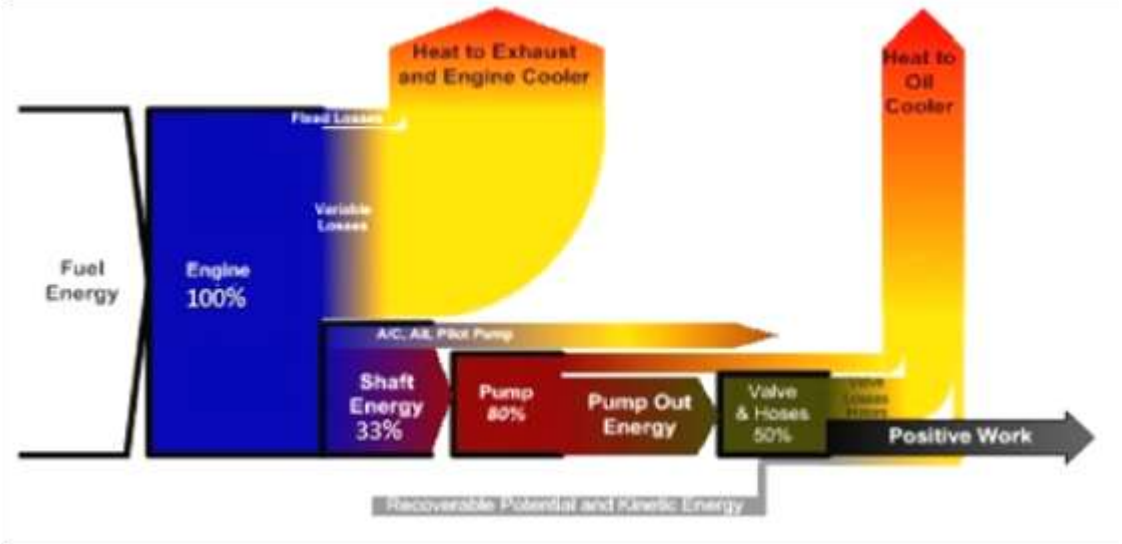

Figure 1.3: Skankey diagram of energy consumption in an excavator

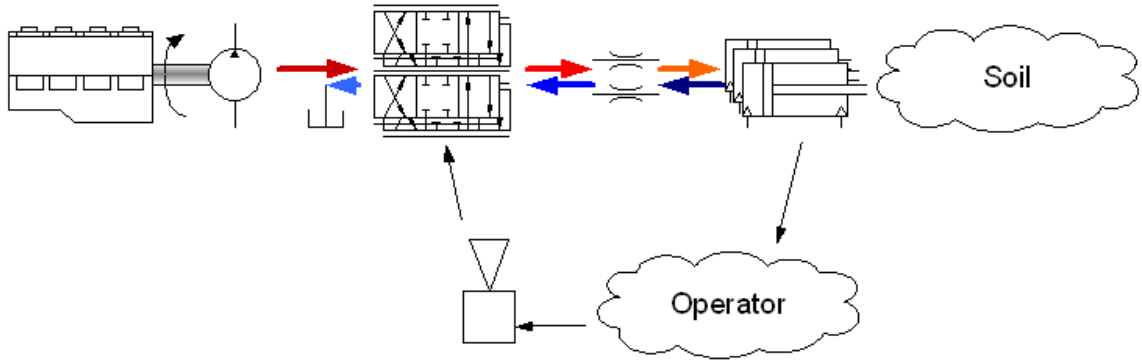

Figure 1.4: Schematic diagram of the integration of hydraulic components in an excavator

Excavators have typically one Diesel engine, two hydraulic motors and three cylinders. There exist different hydraulic circuits to provide the consumers with the required hydraulic energy. A typical design is a Load Sensing circuit that is energy efficient and user friendly. The idea is to have a flow rate control system for the pump such that it delivers exactly the needed flow rate. As a sensor the pressure drop across an orifice is used. The reference value is the resistance of the orifice. A schematic drawing is shown in figure 1.4; a good introduction to that topic is given in [6].

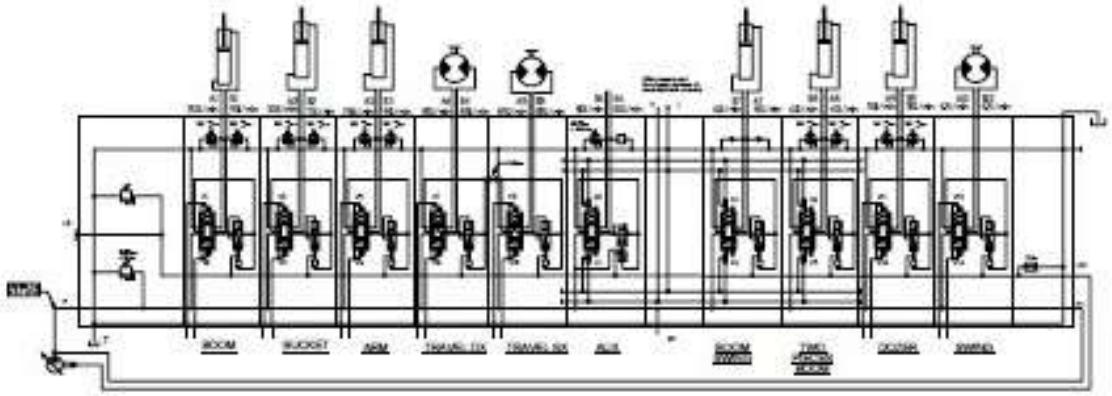

Figure 1.5: Hydraulic circuit of the Sanpierana 850 ZT

The pump control valve maintains a pressure at the pump port that is typically 15 bar higher than the pressure in the LS line (Load Sensing line). If the directional valve is closed the pump has therefore a stand-by pressure of 15 bar. If it is open the pump delivers a flow rate that leads to a pressure drop of 15 bar across that directional valve. Note: The directional valve is *not* used to throttle the pump flow but as a flow control (pressure drop that is fed back) and as a reference (resistance). The circuit is energy efficient because the pump delivers only the needed flow rate; the throttling losses are small compared to other circuits. If more than one cylinder is used the circuit becomes more complicated, see figure 1.5. e.g. if the boom requires a pressure of 100 bar and the bucket a pressure of 300 bar the pump pressure must be above 300 bar which would cause an unwanted movement of the boom cylinder. Therefore compensators are used that throttle the oil flow and thus achieve a pressure drop of 15 bar across the particular directional valve. These compensators can be installed upstream or downstream of the directional valves. An additional valve reduces the nominal pressure differential if the maximum pump flow rate or the maximum pressure is reached [7].

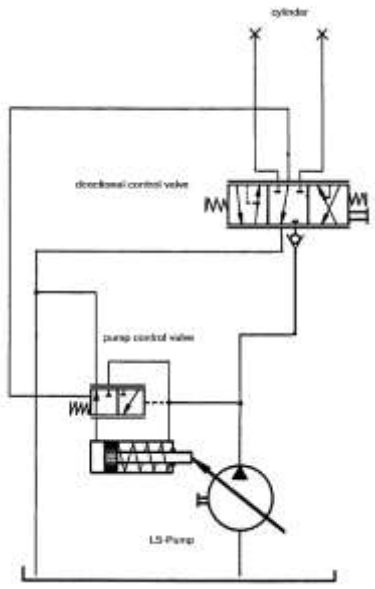

Figure 1.6: Schematic diagram of a simple LS system

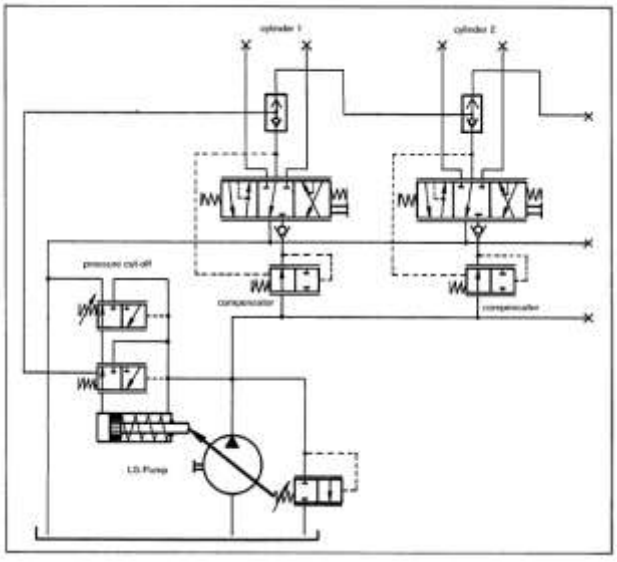

Figure 1.7: Schematic diagram of a LS System

1.1 Hydraulic System Model

The hydraulic system of an excavator consists of various components such as pumps, control valves, auxiliary valves, motors and cylinders. Hydraulic pumps convert the mechanical energy supplied by the diesel engine to the fluid-power energy stored in hydraulic oil. The main role of control valves is to control the actuator velocities by properly metering the flows of hydraulic oil into and out of the actuators. The area

characteristics of the control valves are very important since their profiles directly determine the actuator responses. Auxiliary valves are used to protect the hydraulic circuits and ensure safety during the excavating motion. Hydraulic motors and cylinders are used as the actuators. They generate torques and forces necessary for swing, boom, arm and bucket motion. These forces and torques are determined by the pressures of the chambers in each actuator, and these pressures, in turn, are determined by the velocity and displacement of the actuator which are calculated from the mechanical dynamics of the excavator. Therefore, it is in these actuators where the dynamic coupling between the mechanical and hydraulic system model of the excavator takes place.

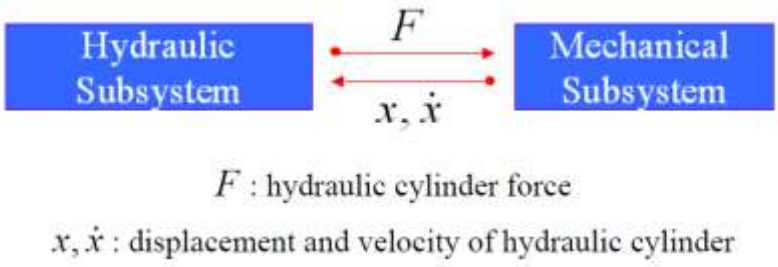

Figure 1.8: Dynamic coupling between the mechanical and hydraulic system of an excavator

The differential equations of a hydraulic system are generally stiff in the numerical point of view. Moreover, the governing equations of a hydraulic system are mostly strongly nonlinear. Hence, solving the models of a hydraulic system is numerically challenging. Hence, two important requirements for software pertaining to the hydraulic system of an excavator are to have stiff ODE solvers suited for the hydraulic system, and to have appropriate interfaces to as many multi-body dynamics programs as possible.

The pump-controlled system consists of a variable delivery pump supplying fluid to an actuation device. The fluid flow is controlled by the stroke of the pump to vary output speed and the pressure generated matches the load. It is usually difficult to closely couple the pump to the actuator and this causes large contained volumes and slow response [2]. The valve-controlled system consists of a valve controlling the flow from a hydraulic power supply to an actuation device. The hydraulic power supply is usually a constant pressure type (as opposed to constant flow) and there are two basic configurations. One consists of a constant delivery pump with a relief valve to regulate pressure whereas the

other is much more efficient because it uses a variable delivery pump with a stroke control to regulate pressure.

1.2 Modelling

The concept of bond graphs was originated by Paynter [5]. The idea was further developed by Karnopp and Rosenberg in their textbooks [6]–[8], such that it could be used in practice. By means of the formulation by Breedveld [9] of a framework based on thermodynamics, bond graph model description evolved to a systems theory. More information about bond graphs can be found in [6] and [12]. The Bond graph method can be used to obtain more intricate information such as the power required to drive each joint Actuator or the power interaction at the interface with the environment. Such information can also be used to study the stability of the manipulator system during contact interaction with the environment. Modifications and additions to the system can be easily incorporated by connecting suitable bond graphic sub-systems to its existing bond graph. In this thesis the bond graph methodology has been implemented in the software AMESim®.

1.3 Objectives

The objective of this thesis is to develop a fast simulation model of an excavator which can recreate the simulation of excavator dig cycles without compromising on computation time. Towards achieving this objective this thesis will present:

- The semi empirical model that has been adopted to replicate the pumps dynamic behaviour.
- The mathematical model developed to recreate the valve dynamics of the mobile load sensing flow sharing valve block.
- Model of the kinematics developed to recreate the dynamic loads on the hydraulic system.

- Empirical Soil interaction model integrated into the kinematics model to recreate the effects of soil interaction.
- Experimental verification of all hydraulic models developed for simulating the excavator simulation.

1.4 Outline of Thesis

This thesis is organized in the following sequence to describe the development of the excavator model:

Chapter 1 describes the basic functioning of an excavator.

Chapter 2 describes the theory and the model development approach for the semi empirical pump model. Development of mathematical models of FC, PC and the complete LS valriable displacement LS Pump.

Chapter 3 presents the theory behind flow sharing and the mathematical model development process for the complete LS flow sharing valve DPX100.

Chapter 4 presents the development of the excavator upper carriage system kinematics along with a soil interaction model.

Chapter 5 presents an overall model of the developed excavator and its capabilities.

Chapter 6 presents the details of the experimental test facilities in the laboratory and the tests carried on the field.

Chapter 7 details the comparisons between the predicted and experimental results for the model of the pump, valve and the complete excavator.

Chapter 8 Presents conclusion and recommendation for future work.

1.5 References

1 Peter B., Martin O., *Multi –Domain Simulation: Mechanics and Hydraulics of an Excavator*, Proceedings of the 3rd International Modelica Conference, Linkong, November 3-4, 2003

2 Cheol-Gyu P., Kwang-Ho L., *A Simulation Environment for Excavator Dynamics*, Daewoo Heavy Industries Limited

3 Juma Y. A., *Mathematical Modeling for Pump Controlled System of Hydraulic Drive Unit of Single Bucket Excavator Digging Mechanisms*, JJMIE, Volume 2, Number 3, September 2008, ISSN 1995-6665

4 Joe P., *Energy Efficient Fluid Power: Valve Efficiency through Machine System Know – How*, Design News Editorial

5 Manfred Hiller. (1996). *Modeling, simulation and control design for large and heavy manipulators*, Journal of Robotics and Autonomous Systems 19 (1996) 167-177

6 Mutku Mvengei and john Kihiu (2009), *Bond Graph Modeling of Mechanical Dynamics of an Excavator for Hydraulic System Analysis and Design*, International Journal of Aerospace and Mechanical Engineering 3:4 2009

7 Grzesikiewicz W. (1998). *Dynamics of a ground digging tool*. XI scientific Conference Problems of Work Machines, konferencja Naukova Problem Maszyn Roboczych) Polska: Zakopane, 1998

8 Gennaro Monacelli, Haibo Guo, Michele Russo, Salvatore Strano, Fausto Di Genova, Stefano Scala (2011), *Model of the excavator arm of CNH wheeled excavator for HIL application*

9 Blakburn J. F., Reethof G. & Shearer J. L. (1966) *Fluid Power Control*. USA: MIT Press, 1966. ISBN 0262520044.

10 Amalendu Mukherjee, Ranjit Karmakar, A.K. Samatry (2006) *Bond Graph in Modeling Simulation and Fault Identification*, I.K International Publishing

House

11 Paolo Casoli, Alvin Anthony, Manuel Rigossi (2011), *Modeling of an Excavator System - Semi Empirical Hydraulic Pump Model*, SAE Commercial Vehicle Congress 2011, September 2011, Rosemont, IL, USA

12 LMS Imagine Reference Manual 2009

Chapter 2

LOAD SENSING VARIABLE DISPLACEMENT AXIAL PISTON PUMP

2.1 Introduction - Load Sensing Variable Displacement Axial Piston Pump

The pump model described and developed in this chapter is that of a load sensing variable displacement axial piston pump. This is a standard line production pump developed by Casappa SpA and belongs to the MVP series. This chapter will outline the modeling methodologies adopted to model the behavior of the pump along with its associated valving. The complexity of modeling pump behavior is that it requires excessive simulation time to recreate the pumps dynamic behavior. The methods adopted to recreate the pump behavior have been described in this chapter. This chapter will also offer an introduction to load sensing and standard pump model equations to provide future researchers a reference source for the equations used to model a pump and how these equations have been recreated by the author in this document.

The study of optimal displacement control of variable displacement pumps has been a topic of interest for fluid power researchers' world over and continues to provide scope for development with electro hydraulics and recent advances in robust control strategies. To set the pace of study, this chapter describes the current stage of model development and will detail the actual pump being produced, i.e. with classical hydraulic feedback. As depicted in Figure 2.1, the pump model comprises of three sub-models a flow compensator, pressure compensator and the flow characteristics.

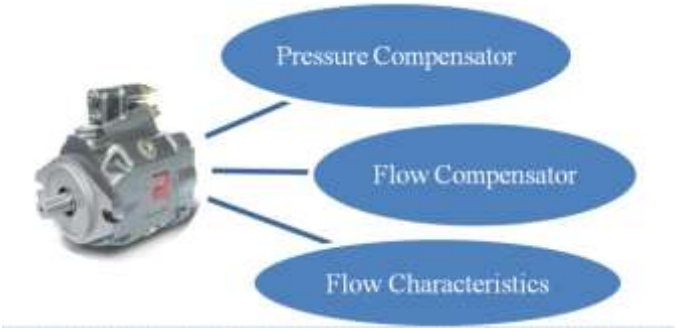

Figure 2.1. Model breakup of the MVP series, Load Sensing Variable Displacement Pump

The pump model has been conceived as a grey box model, i.e. A model based on both insight into the system and experimental data as can be seen in Figure 2.1. The flow and pressure compensators have been modeled as white box models and that of the flow characteristics as a black box model. The grey box model of the pump correlates the control piston pressure and the system pressure to provide the equilibrium of forces that defines the swash plate angle. This model approach has been adopted to provide the manufacturer with the flexibility of selecting pumps with discrete maximum displacements to vary the complete system's gain.

To better understand the system at hand let us start by defining load sensing and how the idea was conceived [1]. Very simply stated, it is a hydraulic system that senses and provides only the pressure and flow required by the hydraulic system. The components required to accomplish the characteristics of the load sensing system are: A variable

volume piston pump, which has a compensator that will allow the pump to standby at low pressure when the system is not being actuated. It will sense the flow requirements of the system when it is being actuated and provide a variable flow rate as the flow demands of the hydraulic system are varied. The pump must also sense and respond to the varying pressure requirements of the hydraulic system. Most hydraulic systems do not operate at constant pressure. The hydraulic pressure will vary as the load on the hydraulic system changes. A control valve, with special sensor passages and checks, is also required to get the full benefit of the load sensing system. When the hydraulic system is not being operated, and is in the standby mode, the control valve must cut off the pressure signal from the actuating cylinder (or motor) to the pump. This causes the pump to automatically go into low pressure standby when the system is not being operated. When the control valve is actuated, the control valve will pick up the pressure requirement from the actuating cylinder (or motor) and send that pressure signal back to the pump where the pump starts to respond to the system pressure. The flow requirement of the system is dictated by the movement of the spool. The system flow requirement is sent back to the pump, through the signal line, from the control valve. This combination of a load sensing pump and load sensing control valve allows the total system to provide only the flow and pressure required by the load sensing system. This description in a nutshell was the original idea behind the development of the load sensing technology.

Figure 2.2: Variable Displacement Pump MVP 60

To gain a deeper understanding let us reference Figure 2.3 to understand how the load sensing technology works [13]. A load sensing pump is one in which a pressure (or pressure differential) is fed back to a controller within a pump to adjust the swash-plate angle and subsequently, the pump's flow. The LS pump system consists of a variable displacement pump (A), the actuating yoke and control piston (B) of the swash-plate, and the critically lapped adjusting valve (C). When the physical load (D) experiences an incremental increase, then a corresponding incremental increase in pressure *PL* is sensed in the feedback sensing line (E); the pressure change acts on the spool of the compensator piston (G). A force unbalance on the spool translates the spool to the right porting fluid in the swash-plate piston (B) to the tank. A decrease in the fluid pressure at this point increases the swash-plate angle, which in turn increases the flow rate from the pump. This increase in flow encounters the controlling orifice (higher resistance) (F) and as a result, the pressure increases. This pressure is sensed in the pump feedback line (H), which acts on the right hand side of the compensator piston (G). The pressure rises until a force balance across the compensator is re-established. At this point, the pressure drop across the controlling orifice (F) is re-established and the flow restored to its original value. Flow control is thus established. This type of pump is called a “load sensing” pump. A system that consists of a load sensing pump, a simple proportional valve and its load(s) is commonly called as load sensing (LS) system.

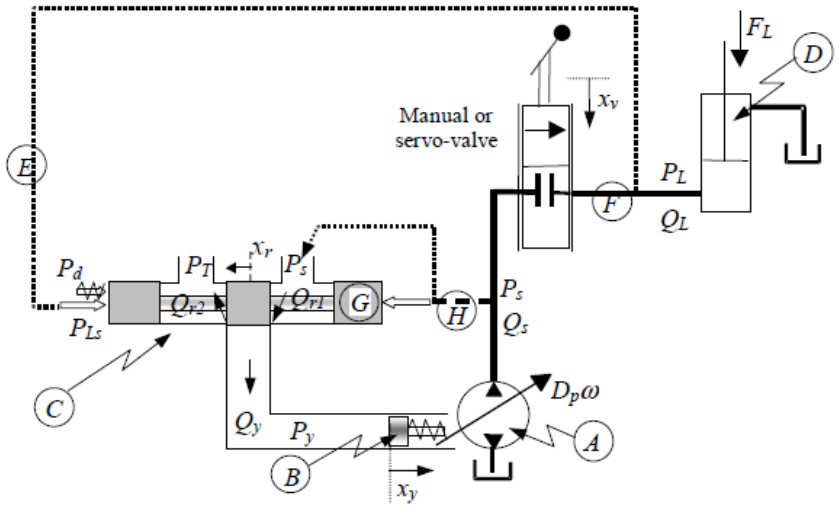

Figure 2.3 : Schematic of a Load Sensing System

In LS systems, the system response is affected by dynamic changes in the load conditions. This can be illustrated in Figure 2.4. With reference to this figure, consider the following scenario.

a) Steady state loading conditions are shown.
b) A sudden increase in *PL* occurs.
c) Flow through the valve decreases momentarily.
d) *Ps* increases but at a smaller rate than *PL* because of the capacitance in the lines between the pump and valve. But the pressure difference across the load sensing compensator forces the spool to respond such that the pump starts to increase its stroke; therefore, the pump flow *Qs* increases as illustrated.
e) *QL* starts to increase because of the small increase in *Ps*. As a result of the increase in pump flow, *Ps* increases rapidly. *QL* increases because the pressure drop across the valve increases, the pump flow starts to decrease due to the reestablishment of the pressure balance across the pump compensator.
f) This continues until the pressure drop across the control valve is re-established.

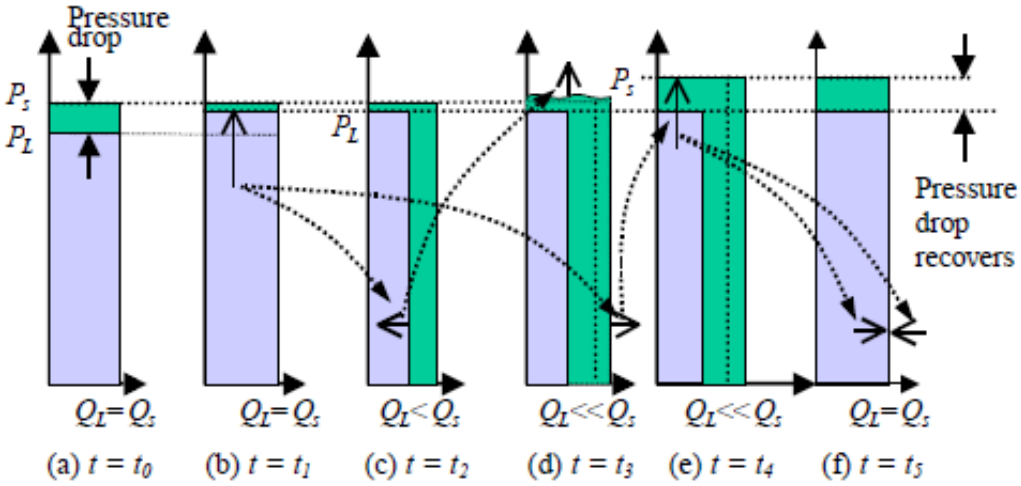

Figure 2.4 Time Sequenced Pressure and Flow of a LS System during Transition

The LS pump system consists of three main hydraulic components as shown in Figure 2.5; pressure control pump, LS regulator (three-position three-way valve with critical center spool), and a control piston (the control piston makes contact with the yoke upon which the swash plate is fixed).

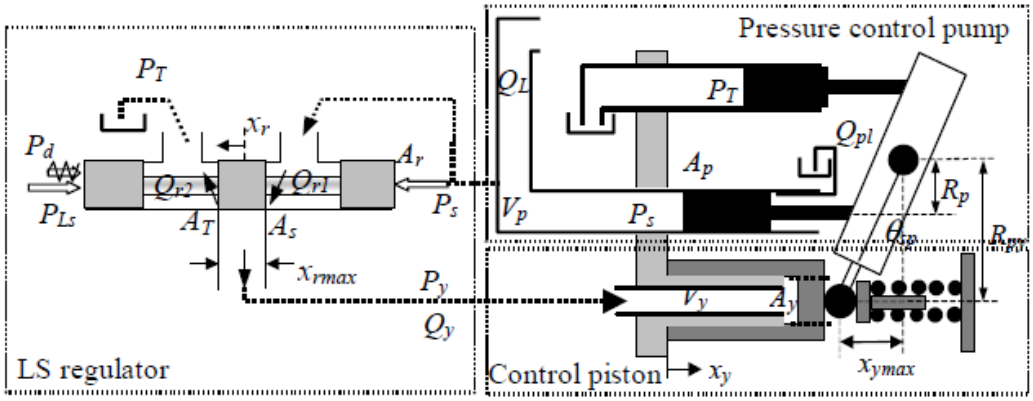

Figure 2.5 Schematic of the Load Sensing Pump System

The dynamic mathematical model consists of two equations of mechanical movement and one flow continuity equation.

- *Force Equilibrium Equation for the LS Regulator Spool*

The equation of motion for the spool of the LS regulator (Figure 2.5) can be described as

$$\ddot{x}_r = \frac{1}{m_r}(-B_r\dot{x}_r - k_r x_r + A_r((P_s - P_{LS}) - P_d \qquad (2.1)$$

Where x_r is the spool displacement. m_r, B_r, and k_r are spool mass, damping coefficient, and preset spring coefficient respectively. A_r is the cross sectional area of the spool. P_s, P_{LS} and Pd are the pump pressure, the load pressure at the end of LS line, and the pressure differential setting respectively. It is noted that Pd is not a true "physical" pressure but an equivalent pressure term caused by the pre-compression force of the spring (P = F/A). Pd controls the pressure drop across an adjustable orifice and is a designed value of pressure differential, Ps - P_L. It is also noted that Equation (2.1) does not include the steady state flow force and the transient flow force exerted on the spool of the LS regulator. This is

because the flow rate (i.e. the leakage for the critically lapped LS spool) through orifices around the spool sleeve is small resulting in a flow force that is very small compared to the force produced by (*Ps – PLs - Pd*). A dynamic simulation in which the steady state flow force and the transient flow force were considered has been conducted to verify that the flow forces are negligible for the LS regulator in this study.

- *Dynamic Equation of the Yoke Control Cylinder and Swash Plate*

Referring to the control piston (Figure 2.5), the relationship between the swash plate angle, θ*sp*, and the yoke displacement, *xy*, is

$$\tan\theta_{sp} = \frac{x_{ymax} - x_y}{R_{py}} \qquad (2.2)$$

The pre-compression spring normally pushes the yoke piston back and maintains the displacement, *xy*, of the yoke at the original position (*xy* = 0 in Figure 2.4). That is, the pre-compression spring value is such that the pump is at full displacement before the pump operates. When the yoke chamber pressure, *Py*, increases, the yoke piston does not move until the yoke chamber pressure overcomes the pre-compression pressure *Pys*. When *Py* increases beyond *Pys*, the yoke piston begins to move forward and the swash plate angle begins to decrease correspondingly. When *xy* increases to the maximum, the pump swash plate angle decreases to zero. In this case, the pump is "destroked" and pump flow is zero. In order to describe the dynamic behavior of the swash plate and the control yoke, the displacement of the control piston, *y x,* or the swash plate angle, θ*sp,* can be assigned as the state variable. The swash plate angle, θ*sp*, is usually used as the variable in modeling because:

1. The non-linearity of the pump is mainly caused by the pressure control pump, rather than the control piston
2. Measuring θ*sp* is easier than measuring *xy*. The dynamic model of the swash plate angle depends on the structure of the variable displacement axial piston pump. Depending on the eccentricity of the swash plate axis, the external active torque on

the swash plate assembly is dictated by both the yoke control pressure and the pumping piston pressure.

Numerous models for axial displacement pump have been developed. [3] has developed a mathematical model of a variable displacement axial piston pump and investigated the effect of internal pump dynamics on control piston pressure ripple. However, this model was too complex to consider in the LS system-level models. Another model, which reflects the "back pressure" on the pump due to the pump pressure acting on the pistons, was developed by [4] and is reproduced here as equation 2.3 The non-linear dynamic equation was developed to be

$$J_{sp}\ddot{\theta}_{sp} = -B_{sp}\dot{\theta}_{sp} - K_{sp}\theta_{sp} + T_{sp} + K_{pr2}P_s - K_{pr3}P_s\theta_{sp} - R_{py}A_yP_y \qquad (2.3)$$

Where:

J_{sp}	Average total moment of inertia of swash plate, yoke and piston assembly Nms^2
B_{sp}	Simplified constant (damp coefficient) of the control piston and swash plate assembly, Nms
K_{sp}	Angular effective spring coefficient, Nm-rad^{-1}
T_{sp}	Angular effective spring pretension Nm
K_{pr2}	Pressure torque constant NmPa^{-1}
K_{pr3}	Pressure torque constant NmPa^{-1}rad^{-1}
R_{py}	Distance between centerline of control piston guide and swash plate pivot
A_y	Effective control piston area m^2

- *Flow Continuity Equation of Chamber Volume of the Pump Swash Plate Control Cylinder*

Consider the chamber between the LS regulator and the control piston in Figure 2.5. For the adjusting valve with a critically lapped spool the flow continuity equations can be described as

$$\dot{P}_y = \frac{\beta}{V_y}(Q_{r1} - A_y\dot{x}_y - Q_{r2}) \qquad (2.4)$$

Where β is the bulk modulus of the hydraulic oil, V_y is the volume of the yoke chamber which is given in equation, Q_{r1} is the flow through the "charging orifice on the right side and Q_{r2} is the flow through the discharging orifice on the left side.

$$V_y = V_{y0} + A_y x_y \qquad (2.5)$$

The control piston position is defined such that an increase in x_y will cause an increase in the volume V_y, of the yoke chamber. The flow through the charge and discharge orifices Q_{r1} and Q_{r2} are described by the orifice equation.

- *Flow Supply of the LS Pump*

The figure shows schematically the flow through the LS Pump. Consider the control volume defined as illustrated by the dashed line. Three flows are illustrated, the flow $D_p\omega$ from the tank, the flow $Q_{r1}$to the regulator and $Q_s$the flow to the load.

From the flow continuity consideration of the pump outlet volume,

$$Q_s = D_p\omega - Q_{r1} \qquad (2.6)$$

D_p is the dispalcement of the pump and is linearly related to the tangent of the swash plate angle, that is

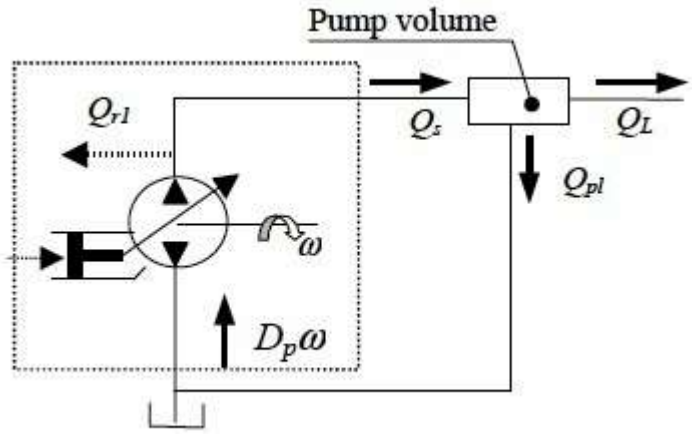

Figure 2.6: Flow Diagram LS Pump

$$D_p = f(\theta_{sp}) = \frac{NA_pR_p tan\theta_{sp}}{\pi} \quad (2.7)$$

Where:

D_p	Volumetric displacement of the pump, m^3
N	Number of pump pistons
A_p	Cross sectional area of pistons, m^2
R_p	Moment arm of pump piston, m
θ_{sp}	Swash plate angle of the pump, rad

- *Pump Volume*

Consider Figure 2.5. The pump pressure is dictated by the pump flow Q_s, the leakage flow Q_{pl}, and the load flow, Q_L. The pump pressure in the outlet volume is thus given as

$$\dot{P}_s = \frac{\beta}{V_p}((Q_s - Q_L) - Q_{pl}) \quad (2.8)$$

where V_p is the pump outlet volume which includes the volume of pipeline. The load flow, Q_L, will be discussed in the next section. It should be noted that if the pump volume

is small and the leakage is negligible, then the pump pressure is dictated by the loading condition and thus the causality of all the relationships do change. In most applications, the pipeline volume between the pump and valves is larger than the effective volume of pump pistons.

2.2 Modeling MethOdology

With the above considerations in mind and to find a method which could be used to best recreate the dynamics, one could build a so-called white-box model based on first principles but in many cases such models will be overly complex and possibly even impossible to obtain in reasonable time due to the complex nature of many systems and processes.

To overcome the problem of having to develop a white box model whilst still being fairly accurate a much more common approach is therefore to start from measurements of the behavior of the system and the external influences (inputs to the system) and try to determine a mathematical relation between them without going into the details of what is actually happening inside the system. This approach of system identification that was utilized in this study was that of:

- **Grey box modeling:** although the peculiarities of what is going on inside the system are not entirely known, a certain model based on both insight into the system and experimental data is constructed. This model does however need a number of unknown free parameters which can be estimated. Grey box modeling is also known as semi-physical modeling.

In the context of non-linear model identification greybox modeling is described as assuming a model structure a priori and then estimating the model parameters. This model

structure can be specialized or more general so that it is applicable to a larger range of systems or devices. The parameter estimation is the tricky part the search for a good fit to experimental data tends to lead to an increasingly complex model.

Thus the model was approached in the above described method of gray box modeling methodologies. Where the pump valving Flow Compensator and Pressure Compensator were modeled in great detail as white box models and the actual Pump has been modeled as a Black Box Model as illustrated in Figure 2.7.

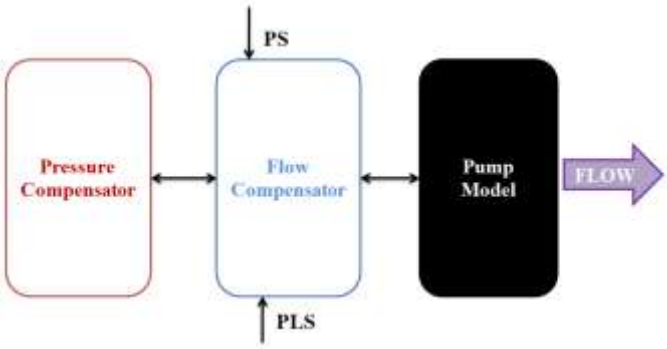

Figure. 2.7 Grey Box modeling methodology

The mathematical models of the flow compensator, pressure compensator and flow characteristics have been developed using the bond graph methodology realized through the AMESim® simulation software. This methodology uses the transfer of power between elements to describe the dynamics of the system. The basic idea being - the direction of power flow at any moment in a system is invariant. Power may be expressed as a multiplication of two factors – generalized effort and generalized flow. Bond graphs are far more powerful in modeling complex systems which involve the interaction of several energy domains [5].

2.3 Flow Compensator Model

The flow compensator (FC) has the most important function of offsetting the pump displacement for a set preload by regulating the swash plate angle. This component has been modeled and verified in great detail [6]

The logic integrated in the FC is to compare the dominant load pressure (PLS) with the pump's output pressure (PS) to modulate the flow through the FC, hence regulating the pump's displacement. The objective of the FC is to maintain a fixed differential pressure across the control orifice accomplished by modulating the pump's flow. The FC's spring comprises of two springs one being a snubber spring. This arrangement has been adopted to provide a snubbing function - thereby resiliently biasing the spool from the first operating position to the second operating position, when the fluid pressure in the LS chamber is increased from a first pressure level to a second pressure level. This feature has an attribute of controlling pressure spikes more carefully due to the precise metering characteristics of the valve, thus reducing the oscillations on the swash plate.

The functioning of the FC as depicted in Figure 3 and Figure 4 is such that the pump pressure enters the FC valve through the chamber A. The pressure entering this chamber acts on the area of spool 1 to create a force. This is realized in the model by means of a transformer element, in the form of spool 1, where the modulus of the transformer is the ratio between the spool - piston and rod area. The force created by the pump pressure on spool 1 is countered by the force created by the springs 5 and the LS pressure which is sensed in chamber D. The sum of these two forces i.e. spring 5 and the LS pressure acting on the area of piston 4 is the force value used to maintain the force balance of the spool. When the pump pressure is greater than the force on piston 4, the spool is displaced to the left creating a flow path between chamber A and chamber B, referred to as the intermediate chamber. The flow through this chamber has the function of varying the pump's swash plate angle, and in this way the pump displacement is regulated. Chamber C is connected to tank and its function is to drain the oil from the intermediate chamber. Spool 2, has been modeled as a transformer element with the modulus being the area ratio between the spool - piston and rod. Leakage models have been included as depicted in 3 (Figure 2.9) to describe internal leakage between chambers and to increase the system damping.

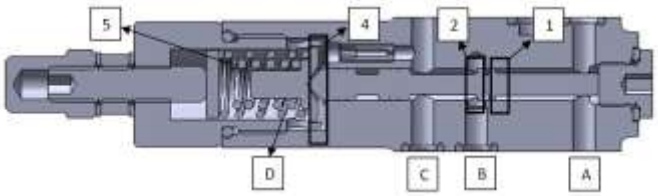

Figure. 2.8. CAD model of the Flow Compensator

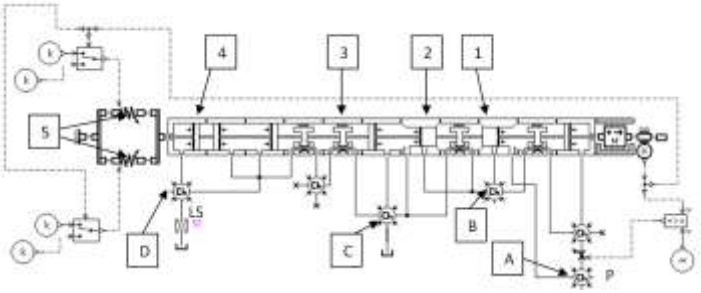

Figure. 2.9. AMESim® model of the Flow Compensator

The governing equations are described by the interaction between a fluid-dynamic model (FDM) and a mechanical-geometrical model (MGM). The FDM calculates the pressures inside the chambers and the flow rate between adjacent chambers, while the MGM calculates the forces acting on the spool and determines its dynamics and the flow areas. The FDM is based on a lumped parameter framework. The pressure inside each control volume is assumed uniform and time dependent, and is determined by the pressure-rise rate equation:

$$\frac{dp_i}{dt} = \frac{\beta}{\rho_i}\frac{1}{V_i(x)}\left(\sum \dot{m} - \rho_i \frac{dV_i(x)}{dt}\right) \qquad (2.9)$$

The model assumes a constant value of fluid temperature. The fluid density is evaluated as a function of pressure as described in [7]. The summation term represents the net mass flow rate entering or leaving the volume. This is obtained by considering the contribution of all orifices connected with the considered volume. The mass exchange occurring through the orifices is calculated using the generalized Bernoulli's equation under quasi-steady conditions, Eq. (2.10):

$$\dot{m} = C_d\, A(x) \sqrt{\frac{2\,|\Delta p|}{\rho}} \tag{2.10}$$

The user sets an appropriate saturated value for the coefficient of discharge of each connection, on the basis of experimental data or using values reported in literature, such as [7]; thereafter the instantaneous coefficient of discharge value is evaluated as a function of Reynolds number, to account for partially developed or fully turbulent conditions. Annular leakages past spool bodies have been evaluated using Eq. (2.11) as reported in [8]:

$$\dot{m} = \rho \frac{\pi \cdot R \cdot h^3}{6 \cdot \mu} \cdot \frac{|\Delta p|}{L} \tag{2.11}$$

The mechanical model calculates the instantaneous position and velocity of the spool using Newton's second law:

$$\sum_i F_i = ma \tag{2.12}$$

The forces acting on the spool, Figure 4, are: hydrostatic forces; spring force; friction forces; hydrodynamic forces. Static and dynamic friction forces are evaluated by use of the Karnopp friction model and considering the Stribeck effect; static and dynamic friction coefficients are assumed constant; the hydrodynamic forces are proportional to the orifice flow sectional area and pressure drop across the orifice, the model implements the equation:

$$F = 2 \cdot C_d \cdot A \cdot \Delta p \cdot \cos\theta \tag{2.13}$$

Where, the jet or flow angle θ is affected by chamber geometry, orifice clearance and sharpness; for spool valves with a sharp edged orifice and no clearance between spool and sleeve, θ can be assumed equal to 69° [9]. The other assumptions are that fluid inertia is neglected; springs are assumed linear.

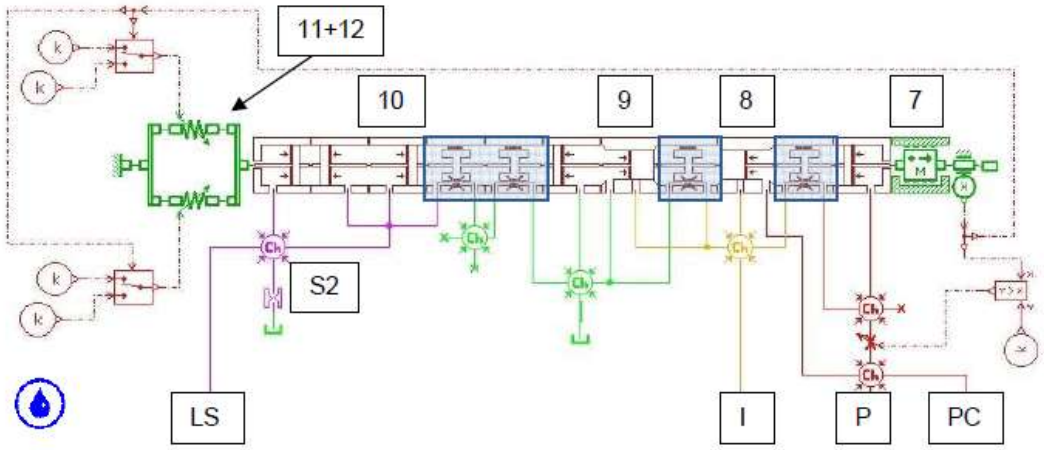

Figure 2.10: Representation of the physical parameters of the Flow Compensator in AMESim

Table 2.1: Physical Parameters of Flow Compensator

Element	Parameter	Value	Unit of Measure
7	*Spool Mass*	*11.67* 10^{-3}*	*kg*
	Spool Mass with LVDT	*23.14* 10^{-3}*	*kg*
	Spool Displacement	*-3* 10^{-3}*	*m*
	Spool Displacement with LVDT	*-4.8* 10^{-3}*	*m*
	Coefficient of Viscous Friction	*10*	*N/(m/s)*
8	*Cylinder Diameter*	*7*	*mm*
	Piston Diameter	*5*	*mm*
	Hole Diameter	*4*	*mm*
	Underlap	*-2.09*	*mm*
	Underlap with LVDT	*-3.9*	*mm*
9	*Cylinder Diameter*	*7*	*mm*
	Piston Diameter	*5*	*mm*
	Hole Diameter	*4*	*mm*
	Underlap	*2.17*	*mm*
	Underlap with LVDT	*3.98*	*mm*
10	*Cylinder Diameter*	*7*	*mm*
	Piston Diameter	*0*	*mm*
Leakage Submodels	*Cylinder Diameter*	*7*	*mm*

	Tolerence	*0.01*	*mm*
	Contact Length - Left	*2.6*	*mm*
	Contact Length - Right	*7*	*mm*
11	*Precompression (17bar)*	*$-0.75*10^{-3}$*	*m*
	Elastic Constant	*9'950*	*N/mm*
12	*Precompression (17bar)*	*$-3.55*10^{-3}$*	*m*
	Elastic Constant	*61'450*	*N/mm*
S2	*Orifice Diameter*	*0.38*	*mm*
Ch	*Volume*	*2*	*cm^3*
Ch (LS)	*Volume*	*10*	*cm^3*
Ch (I)	*Volume*	*5*	*cm^3*
Oil Prop.	*Temperature*	*40*	*° C*
	Density	*850*	*kg/m^3*
	Modulus of Compressibility	*17'000*	*bar*

2.4 Pressure Compensator Model

The function of the pressure compensator (PC) is that of a relief valve and its function is to limit the maximum pressure of the system, Figure 2.11. The relief valve provides an alternate flow path to tank while keeping the system pressure at the relief valve setting. The relief valve realized in the PC is that of the direct operated type, it operates with a spring to pre-load the valve spool. Since a small flow rate is passed through the spool, the set pressure can be maintained with nearly no effect on the pressure flow characteristics of the valve. The functioning of the PC is such that the system pressure enters the PC through chamber E (Figure 2.12) and the pressure acts on the area of spool 6 to create a force, which resists the force created by the spring 8 and spool 9, creating a relief setting pressure. When the system pressure is greater than the relief setting pressure, the spool 6 is displaced and creates a flow path to the swash plate actuating piston and to tank through an orifice S1 (Figure.2.12), which is housed in the PC valve. The governing equations describing the physical behavior of the PC are the same as those described in the section on the modeling of the flow compensator.

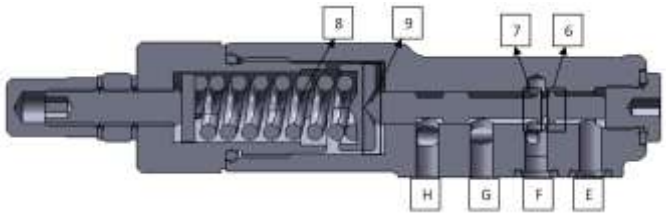

Figure. 2.11. CAD model of the Pressure Compensator

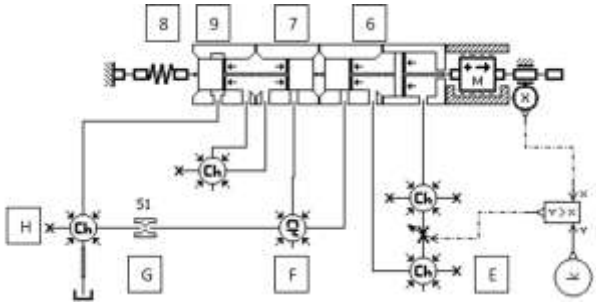

Figure 2.12. AMESim® model of the Pressure Compensator

Parameters used to model the Pressure Compensator

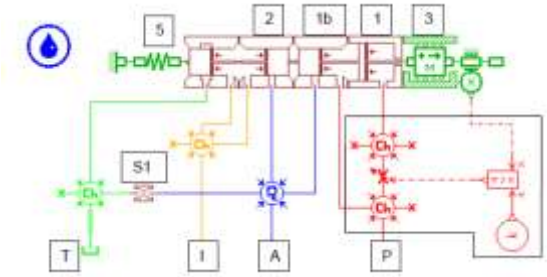

Figure 2.13: Pressure Compensator Model in AMESim

Table 2.2 of Physical Parameters for Pressure Compensator

Element	Parameter	Value	Unit
3	*Mass*	*$9.9* 10^{-3}$*	*kg*
	Spool Displacement	*$-2.67* 10^{-3}$*	*m*
1	*Cylinder Diameter*	*5*	*mm*
	Piston Diameter	*0*	*mm*

1b	*Cylinder Diameter*	*7*	*mm*
	Piston Diameter	*5*	*mm*
	Hole Diameter	*4*	*mm*
	Underlap	*-2.08*	*mm*
2	*Cylinder Diameter*	*7*	*mm*
	Piston Diameter	*4.5*	*mm*
	Hole Diameter	*4*	*mm*
	Underlap	*2.17*	*mm*
5	*Number of Active Spirals*	*8*	*adim*
	Preload - 250 bar	*609*	*N*
	Spring Diameter	*10.8*	*mm*
	Diametro spira	*3.5*	*mm*
S1	*Orifice Diameter*	*0.5*	*mm*
Ch	*Volume*	*2*	*cm^3*
Ch (A)	*Volume*	*10*	*cm^3*
Oil Prop.	*Temperature*	*40*	*° C*
	Density	*850*	*kg/m^3*
	Modulus of Compressibility	*17'000*	*bar*

The above two sections describing the white box model development of the Pressure and Flow Compensator result in the following assembly as described in Figure. The figure illustrates the flow path to the control piston actuator used to vary the pumps displacement. The lines marked in orange symbolize the drain flow from control piston actuator to tank T.

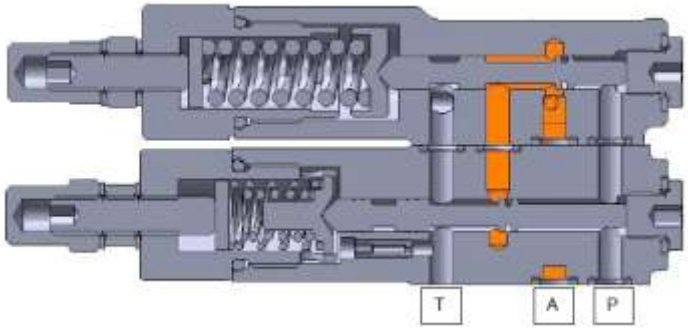

Figure 2.14: Assembly of the Pressure and Flow Compensator describing flow through the intermediate chamber

2.5 Flow Characteristics Model

To understand the complexity involved in modeling the actual pump let us first study the defining equations used to model the pump.

2.5.1 Description of the Pump Components and Operation

A variable displacement axial piston pump contains five key components within its housing. These important components are the barrel, piston/slipper assembly, swash plate, valve plate, and swash plate control device, which is usually a control piston. These components and their relative positions are illustrated in the Figure 2.15.

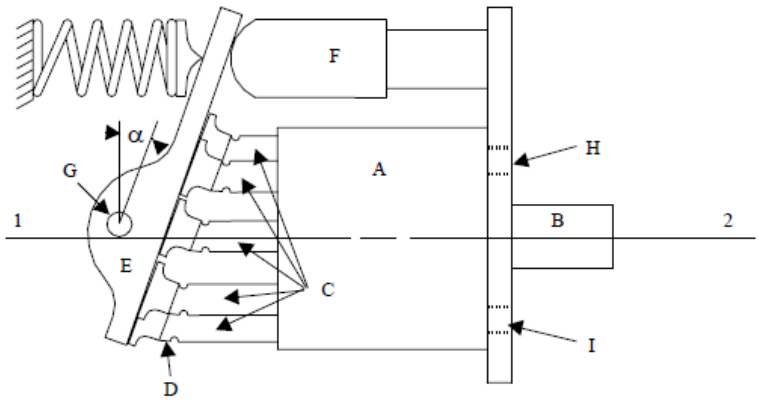

Figure 2.15 Side view of the key components of a variable displacement axial piston pump

The barrel (A) is attached rigidly to the pump input shaft (B). Torque applied to this shaft causes the barrel to rotate about the axis (1-2). The piston/slipper assemblies (C) are contained by the barrel and are arrayed radial about axis (1-2). As a result, when the shaft and barrel rotate, the pistons also rotate about the same axis.

The piston/slipper assembly consists of two joined components. The pistons are fitted to the slippers by means of a ball joint (D). This ball joint allows the slippers to slide along the surface of the swash plate (E) regardless of any angle imparted on the swash plate. The angle of the swash plate is controlled by an externally applied torque. In the case of the pump modeled for this thesis it is supplied by a control piston (F). A control pressure applied to this piston must counteract the torque produced by the pumping pistons in order to maintain a desired swash plate at steady state.

If the swash plate is rotated about the axis of its support spindle (G) to an angle (denoted hereafter as "α"), a periodic linear translation will occur in the piston/slipper assemblies as the barrel rotates. The amplitude of this linear translation is dictated by the swash plate angle as the piston/slipper assemblies slide on the swash plate surface. This linear translation creates the pumping motion. The pistons are exposed to the discharge port of the valve plate (H) as they move upward, and this upward motion causes fluid to be expelled. The fluid expelled from this port is commonly referred to as the supply flow. As a result, the pressure at the discharge port of the valve plate shall be referred to as the supply pressure or, P_s. As the pistons travel downward, they are exposed to the suction port (I) of the valve plate and draw fluid in.

Equations of Motion

The change in modeling philosophy after 1985 involved a move from a lumped parameter approach to a sub-component level time based approach. This change was reflected in the increased attention paid to the equations of motion for the internal components of the pump. Several excellent examples of this are described in the following paragraphs. Since several similar approaches exist in the literature, a general summary of the modeling approach will be presented. [10] had proposed a model based on the motion of the swash plate given the instantaneous torque applied by the pumping pistons and a constant torque applied by the control piston. They concluded that the average response could be determined from a fourth order model. [3] Described similar approaches and also concluded that reduced order models provided good approximations of the input/output

response of a pump. Although these simplified models show decreased accuracy at various operating ranges, and do not reflect the high frequency characteristics of swash plate behavior, the model limitations do not devalue the importance of the general describing equations developed in those publications.

The equations of motion for the internal components of a variable displacement axial piston pump have been developed in the aforementioned publications, as well as several others, through similar geometric developments. Variations in development of these equations are due to differing levels of detail in the sub-component level describing equations. As an example, [10] solved for the instantaneous pressure in a pumping piston during transition while [11] chose a linear estimate for the pumping piston pressure during transition. Regardless of the detail involved in the sub-component level mathematics, models of this type share a common approach in that they endeavor to predict the behavior of the swash plate.

In general, motion of the swash plate determines the behavior of variable displacement axial piston pumps. Therefore, the equation of consequence is that which describes the motion of the swash plate. This equation can be found in general terms when the forces that tend to rotate the swash plate are examined, as illustrated in Figure 2.16.

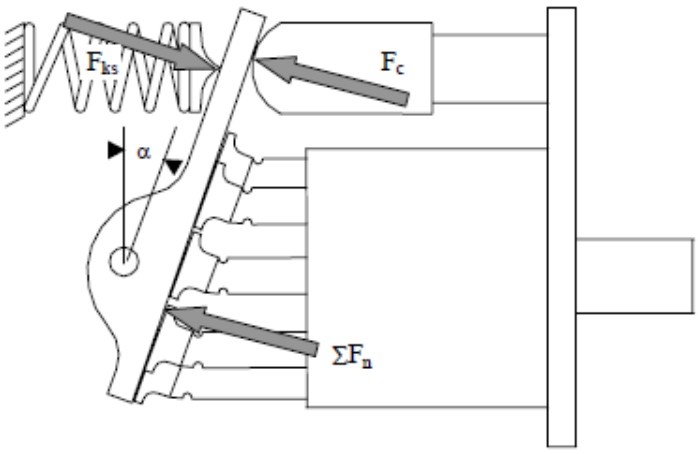

Figure 2.16: Forces that tend to rotate a swash plate

These forces create a net torque about the swash plate axis of rotation. The swash plate angular displacement, α, is the variable which describes the swash plate motion. The equation describing that motion is widely accepted and takes the form of a torque balance as follows:

$$J\ddot{\alpha} = M_c(t) - C_s(t) - M_{ks}(t) \qquad (2.14)$$

The terms of this equation represent the control piston torque (M_c), the summed torque of the pumping pistons (M_n), the effects of swash plate friction (C_s), and the torque applied by the return spring (M_{ks}). These terms have been examined in many papers and from many perspectives.

Friction

Phenomena due to friction are seldom included in overall pump modeling. This stems from the inherently nonlinear nature of friction. Friction interfaces are present between the cylinder and bore, slipper and piston, slipper and swash plate, swash plate and spindle, and the barrel and valve plate. There are losses associated with the bearings, but only those cases which depend on hydrostatic or hydrodynamic lubrication are considered in this review.

2.5.2 Black Box Model of the Pump

A model of the pump's flow characteristics must permit the examination of dominant characteristics influencing the pump's behavior. In a load sensing pump this would include the response of the pressure and flow compensators in addition to the sensitivity of swash plate motion which defines the pump's displacement. Due to intricacies encountered in the control, design and implementation of this type of pump, it is advantageous to have a comprehensive model of the pump. Such a model would include determining the motion of the pump's swash plate based on the instantaneous operating conditions. To achieve this, the model must include the effects of friction acting on internal components, accurate determination of pressure in the pumping pistons and the effects of the swash plate motion

on the control actuator. The model must reflect both the supply flow characteristics of the pump as well as the dynamic behavior associated with the internal components in the pump itself.

In practice the accurate prediction of swash plate motion is the exclusive parameter required to represent an axial piston pump, as all pump components interact with the swash plate to determine its motion. The angle of the swash plate determines the stroke of the pumping pistons, the length of which dictates the flow characteristics. The prediction of the swash plate motion is made difficult due to the exciting forces imparted on the swash plate by the pumping pistons as well as the compressibility of the fluid in the control piston. The bond graph model of the pump Figure 2.17, describes that the net torque acting on the swash plate comprises of the torque contributed by the swash plate inertia, pumping pistons torque, return spring torque, control piston torque and damping effects. The bond graph model of the pump describes the swash plate to be modeled as a Modulated Transformer, deriving its modulus value (the swash angle) from the balance of torques acting on the swash plate and in turn modulates the pump's displacement. Regrettably the white box model approach is quite elaborate and does not afford the flexibility required to examine pumps of different sizes as all the constants (piston mass, lengths and diameters, swash plate mass, damping, valve plate geometry etc.) would have to be modified to adopt a different pump as described in the preceding section. The convenience with the gray box model approach as will be evident in the following sections is that it offers the flexibility to change the complete pump's flow characteristic values by changing the gain values of the linear equation as described in Figure 2.19. The required data set can be found by carrying out tests, post processing the data and modifying the equation. From the steps described in Chapter 6 and 7, this description will be made clear.

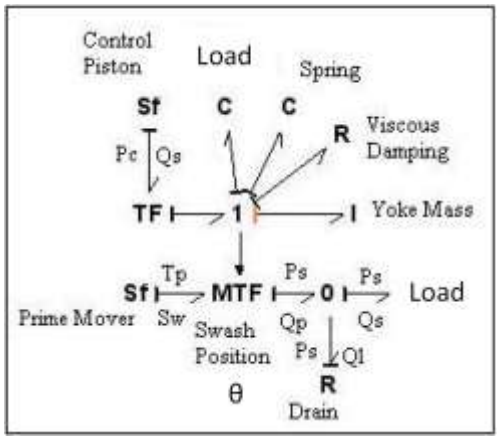

Figure.2.17**.** Bond graph representation of the Pump

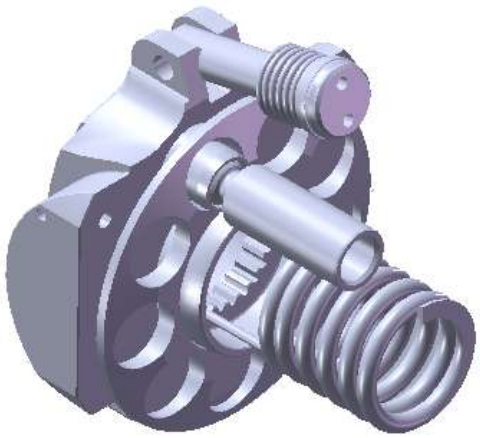

2.18 Kinematics of the Casappa MVP 60 Pump

The objective of this research has been to adopt a technique for identifying the dominant characteristics of a pump and to facilitate the study of different pump sizes in a feasible manner. This flexibility has been integrated into the model to study the flow gain offered by different pumps to the system. The black box system identification was identified as the best model methodology to integrate this flexibility. The black-box model is defined as a model which is very general and thus containing little a priori information on the problem at hand and at the same time being combined with an efficient method for parameter estimation.

This choice of modeling methodology was also attributed to the availability of an instrumented test facility and a large sample of experimental data. The black box model was realized by taking into account that the position of the swash plate could be determined by solely balancing the parameters of the control piston pressure and the system pressure. The control piston pressure is the pressure in the actuator that is used to displace the swash plate. The control piston receives its input from the flow/pressure compensator, depending on the state of the system. The system pressure is the pressure that generates the forces on the swash plate to try to keep the pump stroked. The forces acting on the swash plate affected by the system pressure comprises of the forces exerted by the pumping pistons exposed to the load and the internal friction forces.

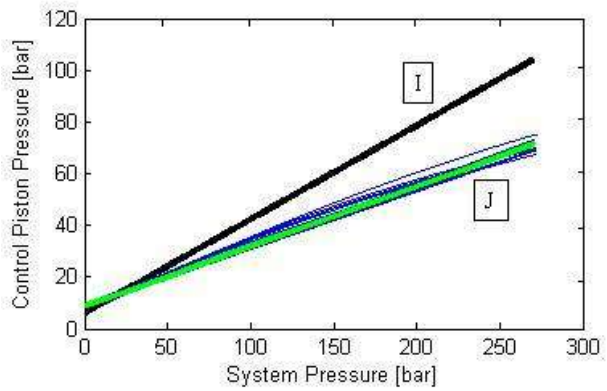

Figure.2.19. Correlation between control pressure and system pressure for swash angle position at 1000 r/min

A linear relation between the control piston pressure and the system pressure was obtained, the details of the test and detailed results can be found in Chapter 6 and 7. It was found that the functioning of the pump in different swash angle positions can be defined by two equations. The first equation (6), as depicted in Figure 2.19 curve I, describes the control piston pressure (PC) versus the system pressure (PS) that would be needed to initially displace the pump from its maximum swash angle position.

$$PC = 0.362 \cdot PS + 6.02 \qquad (2.15)$$

The second equation (2.16) is the pressure balance relation for the intermediate positions. Experiments were carried out by maintaining the swash plate at different positions and varying the load. From these tests it was observed that for the various intermediate swash

angle positions, the pressure relationships were found to overlap. Equation (2.16) was derived by interpolating the family of curves depicted in Figure 2.19 curve J.

$$P_C = 0.233 \cdot P_S + 8.50 \qquad (2.16)$$

The flow characteristics model has been realized by the use of two pistons – the control piston, 10, and the barrel forces piston, 11 (Figure 2.21), defined by the system pressure. The relation between these two equations has been realized by a constant value in the simulation model which has been used to switch between the two equations when the swash plate is displaced from its initial position. After the swash plate angle shifts from maximum swash position, the model utilizes a correction factor of 0.644 and a different constant force to modify the pressure relationship described by equation (2.15) into equation (2.16). A transformer element in the form of a lever is used to balance the forces from the two pistons. The linear displacement of the control piston actuator is measured and converted into the swash plate angle. An orifice 13, (Figure 2.21) with a fixed area has been used to realize the function of internal leakages of the pump and to simulate the pump's drain characteristics.

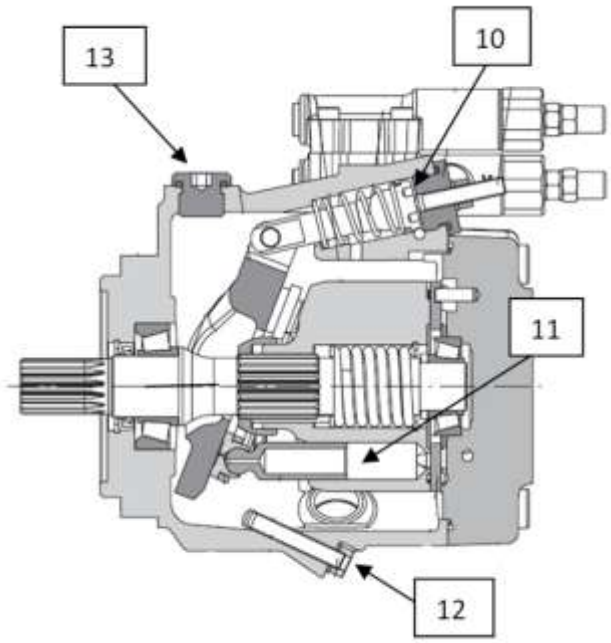

Figure 2.20. Cross section view of the swash plate and control piston

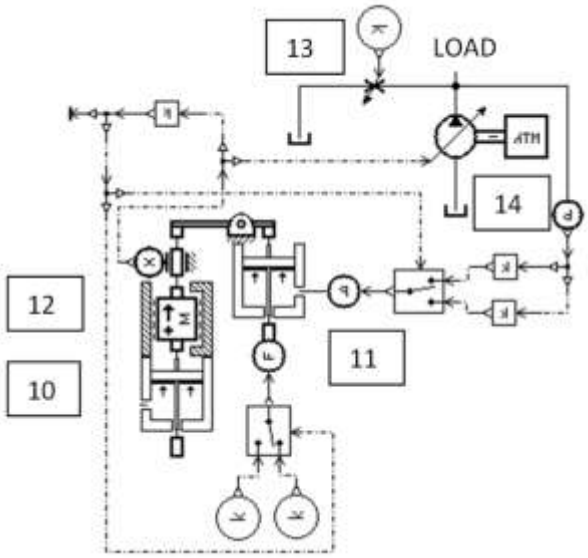

Figure 2.21. AMESim® representation of Fig.9

Although it is known that the leakage flow is a complex term and is best represented experimentally, it was found that the use of a specific flow area provided fairly reliable flow characteristics.

The pump's end stop has been simulated by the use of element 12. The model of the pump's flow characteristics has been created by use of an ideal pump element 14 (Figure 2.21). The use of the fixed orifice to replicate the drain characteristics provides for fairly reliable flow characteristics.

Future work would include maps of the mechanical and volumetric efficiency to replace the drain orifice 13 and to drive the pump's flow characteristics model.

2.6 Overview of the Pump Model

Figure 2.22 provides a complete overview of the assembled pump model. As can be seen in the illustration the complete pump consists of the pressure compensator, flow compensator and the pump model.

The pump model functions as a system in the following manner. The pump starts at maximum displacement and delivers an equivalent flow based on the rotation speed of the

prime mover. The pump output pressure or system pressure is sensed at the Pressure compensator and flow compensator.

If the load on the system causes the system pressure to rise higher than the pressure compensator's setting. The pressure compensator would open there by creating a flow path to the intermediate chamber, resulting in the pump getting de-stroked.

If the system pressure is not high enough to de-stroke the pump through the pressure compensator the pump system would function in load sensing mode. Where the flow compensator would balance its spool position based on a pressure comparison between the system pressure and the feedback pressure from the load otherwise called the Load sensed pressure. In this manner depending on the position of the flow compensator spool position the flow path to the intermediate chamber would either be connected to the system pressure or to the tank line, thereby either stroking or de-stroking the pump.

Model Capabilities

The developed models capabilities would describe the dynamics of the pump in terms of:

1. Swash plate angle – the dynamic position of the swash plate that is identified by first order equations that balances the system pressure and the actuator pressure to define the swash plate position.
2. Flow characteristics of the pump - The flow out of the pump would account for the internal leakage through the fixed orifice which would define the leakage of the pump and in this way would describe the actual flow output from the pump.
3. Pressure dynamics – The systems pressure dynamics is defined by the pressure rate rise equation.
4. Flow compensator dynamics – The flow compensator dynamics provide information of the instantaneous spool position. The LS pressure and System pressures. Spring compressibility, displacement and position. Flow through the damping orifice. Flow and pressure characteristics into and out of the intermediate chamber.
5. Pressure compensator dynamics - The pressure compensator dynamics provide information of the instantaneous spool position. system pressures. spring

compressibility, displacement and position. Flow through the damping orifice. Flow and pressure characteristics into and out of the intermediate chamber.

6. Intermediate chamber pressure – The dynamics of the intermediate chamber pressure between the pressure and flow compensator and the control piston chamber can be determined.
7. Intermediate flow characteristics - The dynamics of the intermediate flow between the pressure and flow compensator and the control piston chamber can be determined.
8. Flow and pressure compensator spring dynamics – The dynamics of the spring compressibility, spring constant and displacement can be determined.

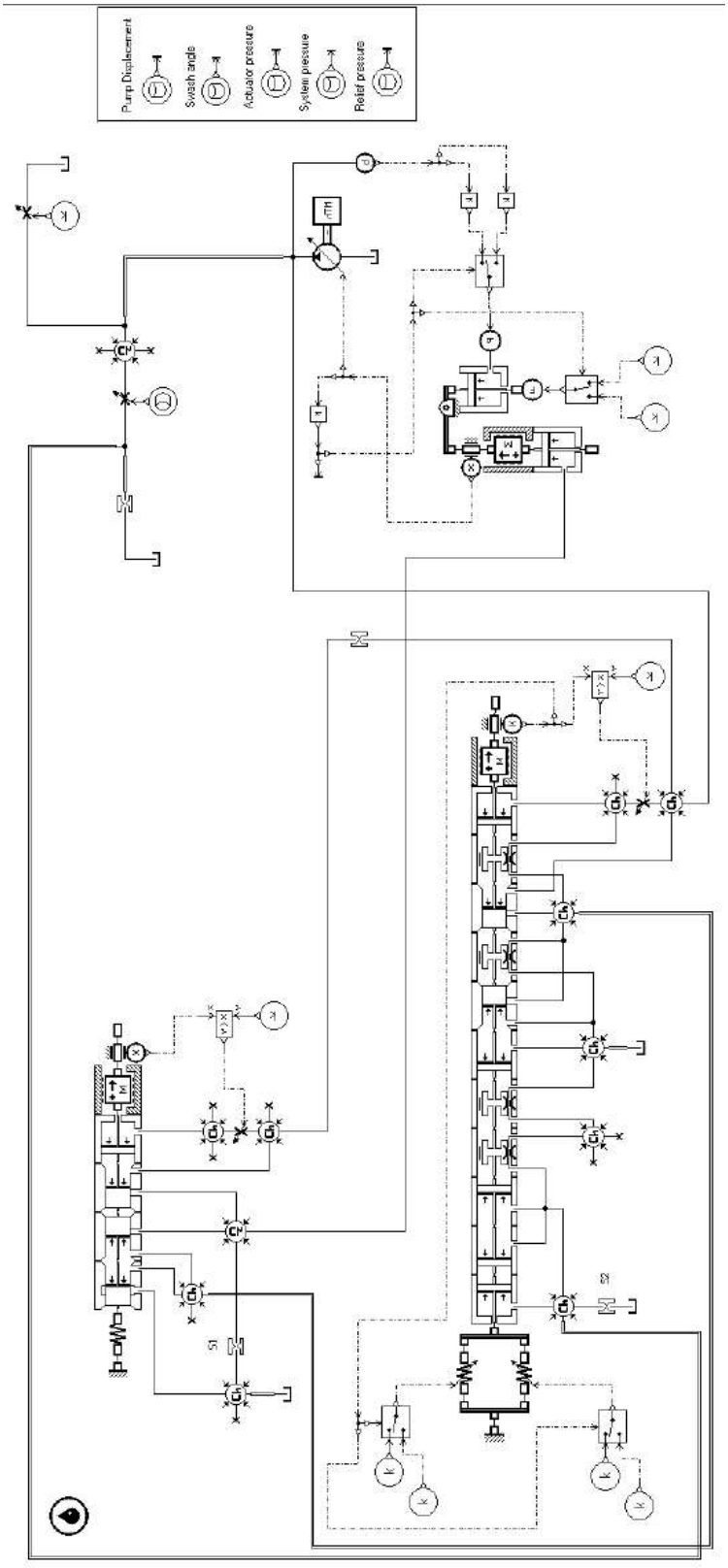

Figure 2.22: AMESim representation of the complete pump model

2.6 References

1. Alvin Anthony, Paolo Casoli, Andrea Vacca. (2010) .*Analysis of a tractor rear hitch control system.* Proc. Of 6th FPNI-PhD Symposium West Lafayette, 15-19 June 2010, pp. 589-602. FPNI Fluid Power Net Publications, 2010

2. Amalendu Mukherjee, Ranjit Karmakar, A.K. Samatry (2006) *Bond Graph in Modeling Simulation and Fault Identification*, I.K International Publishing House

3. Blakburn J. F., Reethof G. & Shearer J. L. (1966) Fluid *Power Control*. USA: MIT Press, 1966. ISBN 0262520044.

4. Casoli P., Vacca A., Anthony A., Berta G.L. (2010) .*Numerical and Experimental Analysis of the Hydraulic Circuit for the Rear Hitch Control in Agricultural Tractors*. 7th International Fluid Power Conference, (pp. 51-63, vol. 1) Aachen, 22-24/03 2010, ISBN 978-3-940565-90-7

5. Grzesikiewicz W. (1998). *Dynamics of a ground digging tool*. XI scientific Conference Problems of Work Machines, konferencja Naukova Problem Maszyn Roboczych) Polska: Zakopane, 1998

6. LMS Imagine – AMESim® Reference manual 2009

7. Manfred Hiller. (1996). *Modeling, simulation and control design for large and heavy manipulators*, Journal of Robotics and Autonomous Systems 19 (1996) 167-177

8. McCloy, D., Martin, H. M. (1973). The control of Fluid Power, Longman, London, 1973

9. Merrit, H.E. (1967) *Hydraulic Control Systems*, Wiley, New York.

10. *Paolo Casoli, Alvin Anthony, Modeling of an Excavator – Pump Nonlinear Model and Structural Linkage/Mechanical Model, Proc. Of 12th Scandinavian International Conference on Fluid Power, May 18-20, 2011, Tampere, Finland*

11. Shih-Tin Lin. (2002) *Stabilization of Baumgarte's Method Using the Runge-Kutta Approach*, ASME Journal of Mechanical Design, December 2002

12. Wu, D., Burton, R., Schoenau, G., Bitner, D.(2007) , *Analysis of a Pressure – Compensated Flow Control Valve*, ASME Journal of Dynamic Systems, Measurement and Control, March 2007

13. Wu, D., *Modeling of LS Systems*, PhD Thesis, University of Sasketchwan

Chapter 3

MOBILE LOAD SENSING FLOW SHARING VALVE

3.1 Introduction

This chapter describes the functioning and the modeling of the Walvoil – DPX 100 Load Sensing Flow Sharing Valve Block. This valve block is a mobile direction control valve used in Mobile applications, specifically for excavator controls. It includes a downstream pressure compensator to incorporate the Load sensing flow sharing capabilities of the valve. The valve bock has principally three modes of operation as a single user load sensing feedback valve as a multi user load sensing flow sharing valve and as a piston check valve to mechanically close the pressure compensator when the work port pressures are higher than the system pressure. In the third mode of operation the operator can take advantage of the meter out notches on the valve spool to precisely control gravity assisted loads. The discussion of the functioning of the valve block is described in the following sections. To start with a discussion on flow sharing is provided to better understand the logic behind flow sharing and its functioning.

3.2 Flow Sharing Theory

For a conventional LS system that uses pre-compensators, the absolute flow level for each function is controlled by the valve signal given by the operator. The pump has to be pressure controlled under these circumstances since the pump flow is already determined by the valve signals. Otherwise, if the absolute pump flow is controlled by the pump, the flow condition in the system becomes over-determined. This phenomenon is sometimes referred to as the "flow matching problem" [4].

Several different flow control system layouts have been studied by other researchers. One solution to the flow matching problem is presented in [5], where an additional bleed off valve equipped with a position sensor has been introduced in the system. In [6], several different solutions are shown, all including additional sensors and/or additional valves. The flow matching problem can also be solved without introducing extra components or sensors in the system. The key is to implicate the highest load pressure into the compensators and thus achieve a flow sharing functionality, resulting in the entire pump flow being distributed relative to the individual valve openings. Several different types of flow sharing compensators are available. One design approach is the so-called post-compensators. In such a design the compensator valve is located downstream of the directional valve. The difference compared to the conventional pre-compensator design, where the compensator valve is located upstream of the directional valve, is that all valve sections sense the highest load. This approach has been studied, for example in [7], where post-compensators were used in combination with a flow controlled pump, and in [8], which is an early work on post-compensators. It is also possible to design a system that uses pre-compensators with similar characteristics by replacing the spring in a conventional pre-compensator with two pressure control areas that sense the pressure difference between the pump and the highest load, a flow sharing functionality is achieved.

A flow sharing system overcomes the flow matching problem. This can be done by using the pump to control the total absolute flow in the system and letting the directional valves control the relative flow to the different functions. Since the flow sharing valves distribute

the total pump flow proportionally to the different active functions, the flow condition in the system is not over-determined. A more detailed analysis of this can be found in [4] and [9].

3.2.1 Flow Sharing Pressure Compensator

This section of the thesis has been included as a reference for the design and analysis of flow sharing valves. This section is a compilation of different research publications on flow sharing valves.

This type of pressure compensator has a pre-set pressure which varies according to the pressure drop of the highest load.

$$Q_{Li} = K_{qpci}X_{PCi} + K_{cpci}(P_p - P_{mi}) \tag{3.1}$$

$$Q_{Li} = K_{qvi}X_{vi} + K_{cvi}(P_{mi} - P_{Li}) \tag{3.2}$$

$$\frac{A_{PCi}}{\frac{s}{\omega_{PCi}} + 1}(P_p - P_{Li} - P_{mi} + P_{Li}) = k_{PCi}X_{PCi} \tag{3.3}$$

The following transfer functions are derived:

$$G_{xvi} = K_{qvi}\frac{K_{cpci} + \frac{K_{qpci}A_{PCi}}{k_{PCi}(\frac{s}{\omega_{PCi}} + 1)}}{K_{Cvi} + K_{CPCi} + \frac{K_{qpci}A_{PCi}}{k_{PCi}(\frac{s}{\omega_{PCi}} + 1)}} \tag{3.4}$$

$$G_{vi} = K_{cvi}\frac{K_{cpci}}{K_{Cvi} + K_{CPCi} + \frac{K_{qpci}A_{PCi}}{k_{PCi}(\frac{s}{\omega_{PCi}} + 1)}} \tag{3.5}$$

$$G_{vi} = K_{cvi}\frac{\dfrac{K_{qpci}A_{PCi}}{k_{PCi}(\dfrac{s}{\omega_{PCi}}+1)}}{K_{Cvi}+K_{CPCi}+\dfrac{K_{qpci}A_{PCi}}{k_{PCi}(\dfrac{s}{\omega_{PCi}}+1)}} \quad (3.6)$$

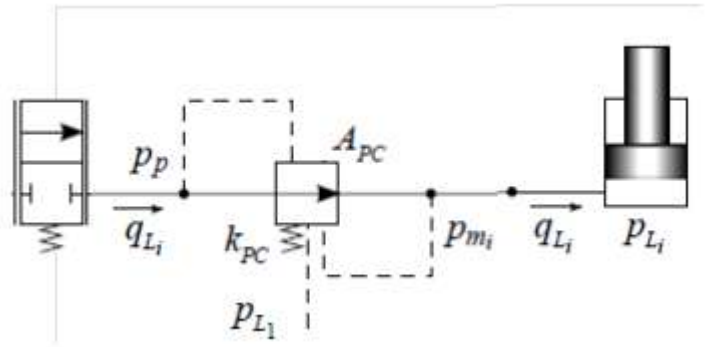

Figure 3.1: Control valve with a flow sharing pressure compensator

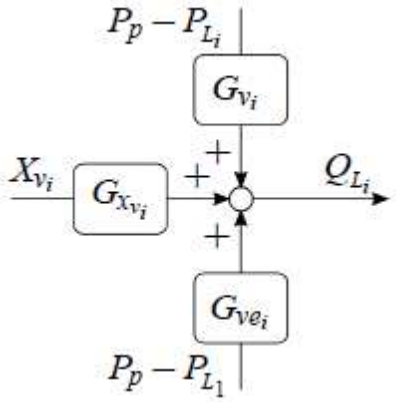

Figure 3.2: Block diagram derived from flow sharing pressure compensators transfer functions equations

Flow sharing pressure compensators are appropriate in flow controlled systems since the entire pump flow will be distributed relative to the individual valve openings. But there are dynamic differences related to this kind of compensator compared to conventional pressure compensators.

According to figure below, all lighter loads will be affected by the heaviest load via *Gvei*, which is equal to *Kcvi* if the pressure compensator is assumed to be fast and ideal. Hence, there will be dynamic load interaction between the highest load and all other functions.

This phenomenon can be studied by looking at the open loop transfer function for a flow sharing pressure compensated system. If the compensator is assumed to be fast and ideal, which means that *Gvi* ≈ 0, the open loop transfer function can be derived according to equation

$$G_{pLS}G_o = G_{PlS}\frac{H_s}{1 + G_{ve1}Z_{L1} + H_s\sum_{i=1}^{n} G_{vei}} \tag{3.7}$$

This equation shows that the dynamics, mainly of the highest load (*ZL*1), will affect the stability of the pump in LS systems, while the pump volume (*Hs*) is damped by its surrounding control valves (*Gvei*). If the pump volume is given insufficient damping, the dynamic load interaction may result in pump-load instability at small valve openings in LS systems according to figure 8. The pump controller and all loads will then oscillate.

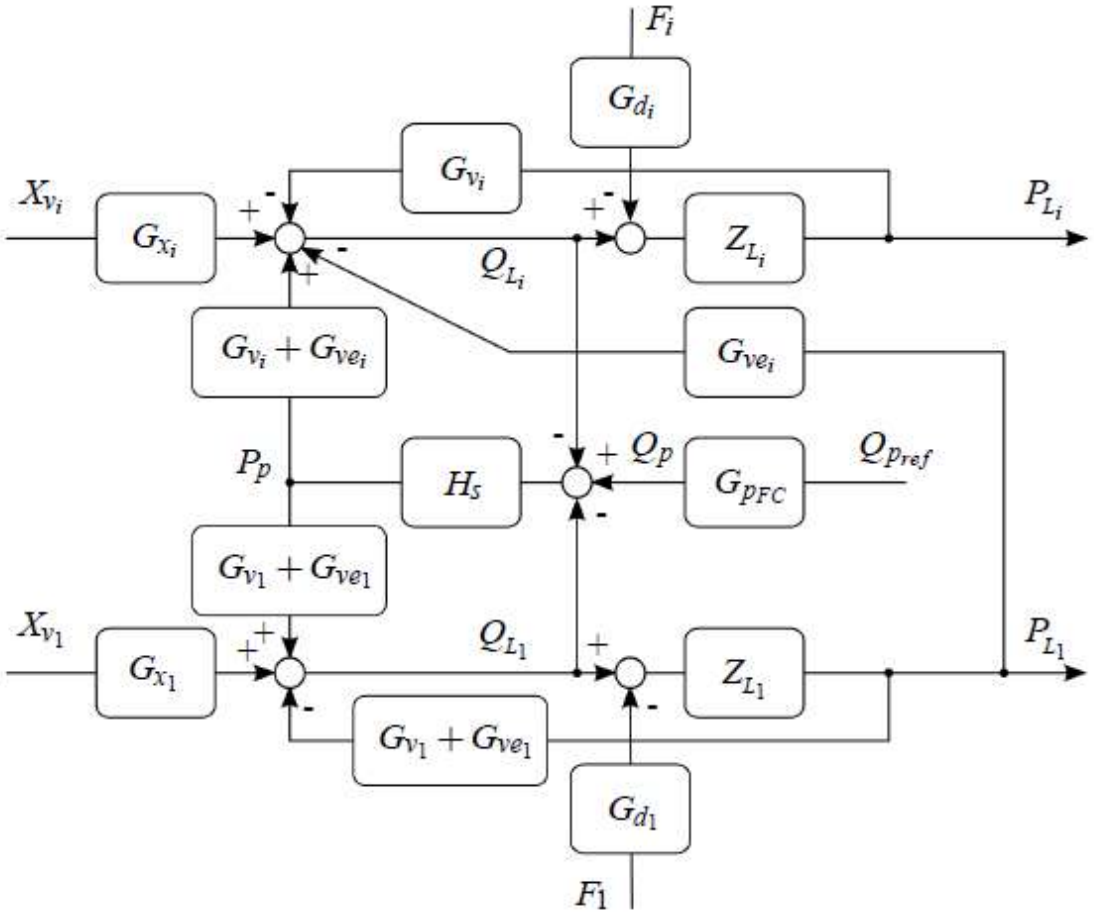

Figure 3.3: General block diagram of flow controlled systems

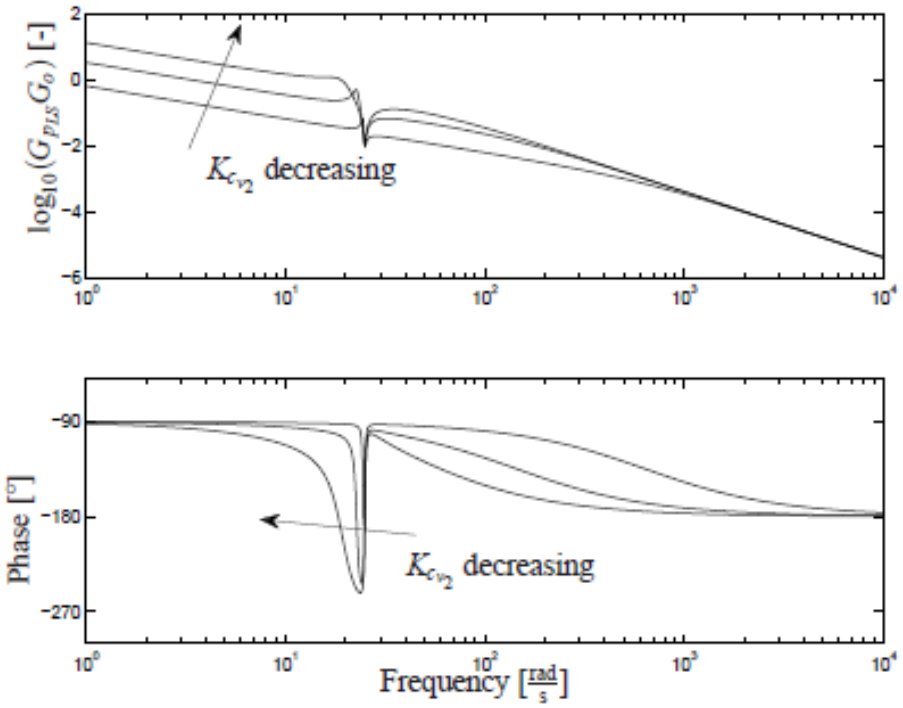

Figure 3.4. Bode plot of the open loop gain in equation (3.7), GpLSGo.

Flow sharing compensators have the feature that the meter-in orifice will add damping to the highest load in a similar way as non-compensated control valves. This can be realized by looking at figure 4, where the highest load has a feedback to the load flow, $Gv1 + Gve1 \approx Kcv1$ according to the block diagram of the flow compensator. Consequently, the highest load is less prone to oscillate. If the highest load does not oscillate, it will not cause the lighter loads to oscillate either.

In flow controlled systems, the flow sharing pressure compensator will distribute the entire pump flow relative to the individual valve openings, which gives the control system one extra degree of freedom.

$$q_L = C_q w_v x_v \sqrt{\frac{2}{\rho}\Delta p_v} \tag{3.8}$$

3.3 Functioning of the DPX 100

This section pertains to the functioning of the sectional directional control valve, particularly a load sensing flow sharing valve. In mobile machinery with this type of hydraulic circuit, under saturation conditions, i.e. when global flow rate required by the various elements exceeds the maximum pump flow rate, the pump cannot maintain a constant pressure differential, whereby a pressure drop occurs across all the elements and causes a proportional flow rate reduction of all the elements. This feature is particularly needed in machinery such as excavators, as they are required to perform several simultaneous movements as it affords proper control of the moving machine even under saturation conditions, which occurs quite often. The various functions of an excavator are each controlled by a valve element/slice, at times there could be the need to exclude at least one of such functions from proportional flow rate reduction, under saturation conditions, so that it has a fixed flow rate value, although still irrespective of the load according to the load sensing concept: the flow rate will be still proportionally reduced across all other elements except the element that has been excluded from the operation under saturation conditions.

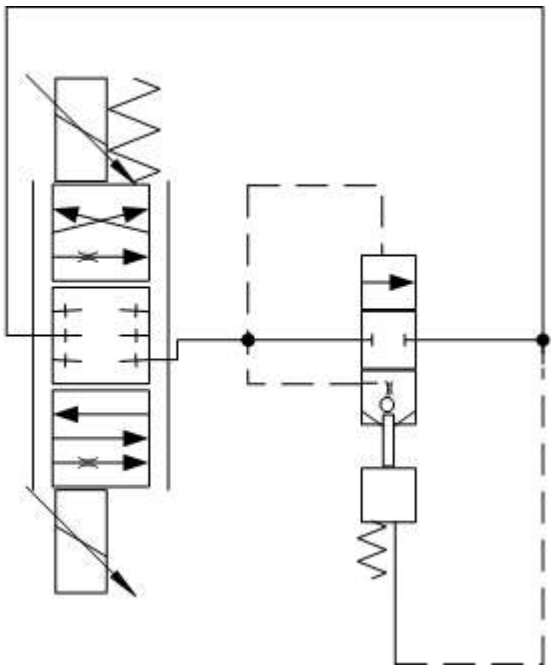

Figure 3.5: ISO Schematic of Load Sensing Flow Sharing Valve DPX 100

The DPX100 control valve adds to the standard Load Sensing valve the benefit of Flow Sharing technology. The DPX100 patented compensator maintains the margin pressure as a constant pressure drop across the spool metering area. The result is a flow to the work port dependent only on spool position. In case of flow saturation, the effective pressure drop across all spools is reduced equally. This results in proportional flow reduction at each section.

3.3.1 Single section operation

The main flow enters from the inlet line. Crosses the metering area to the compensator and enters the bridge. The spool selects flow to work port A (as shown), performing work at the actuator with return flow to work port B, crossing spool metering as it passes to tank. With only one section active, the imbalanced compensator fully shifted to the right giving priority control to either the DPX100 inlet compensator (fixed displacement pump) or to the pump compensator (variable displacement pump) which provides spool stroke proportional flow. This action drives the piston and selector sphere to the right. The piston rod prevents the selector sphere from seating, allowing flow to the load sensing line.

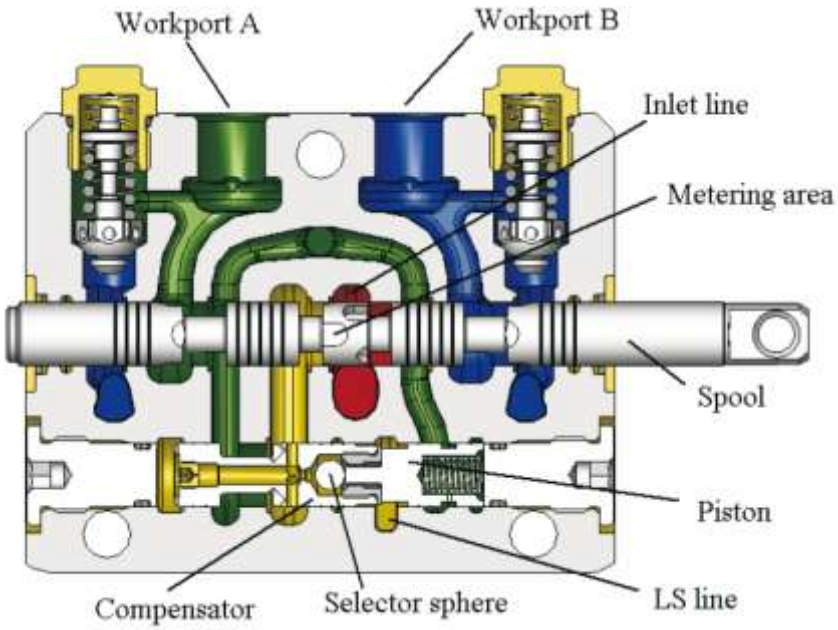

Figure 3.6: Single section operation

3.3.2 Multi Section Operation

When two functions are working at the same time, the higher pressure function is dominant. The dominant valve section performs as described in "single section operation". The function at lower pressure becomes a dependent section.

Dependent section (with lower load): refer to picture 3.7

In the dependent section, function pressure is sensed in the spring chamber of the piston. The higher load sense pressure from the dominant section is sensed at the piston rod end, pushing the piston to the right. At the same time, load sense pressure pushes the compensator left, separating the piston and compensator. The compensator metering notches are now working in order to create an artificial pressure drop that will add to the lower load. The pressure drop across the spool metering area will then remain equal to the margin. This will guarantee the flow to be only a function of the spool position.

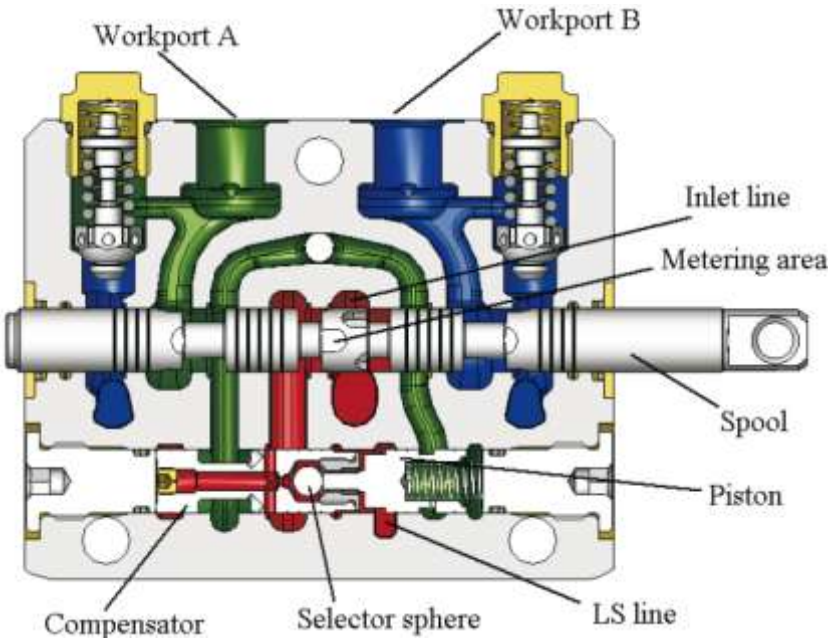

Figure 3.7: Dependent section with lower load

3.3.3 Flow sharing condition

In case of flow saturation, the flow demand is higher than the maximum pump flow therefore the margin pressure is reduced according to the formula:

$$Q \; \alpha \; A \sqrt{\frac{\Delta P}{\rho}} \qquad (3.9)$$

Since all spools have the same pressure drop across the metering area, then all flows are reduced proportionally. This allows the operator to maintain control of all function, though at reduced speed of active functions.

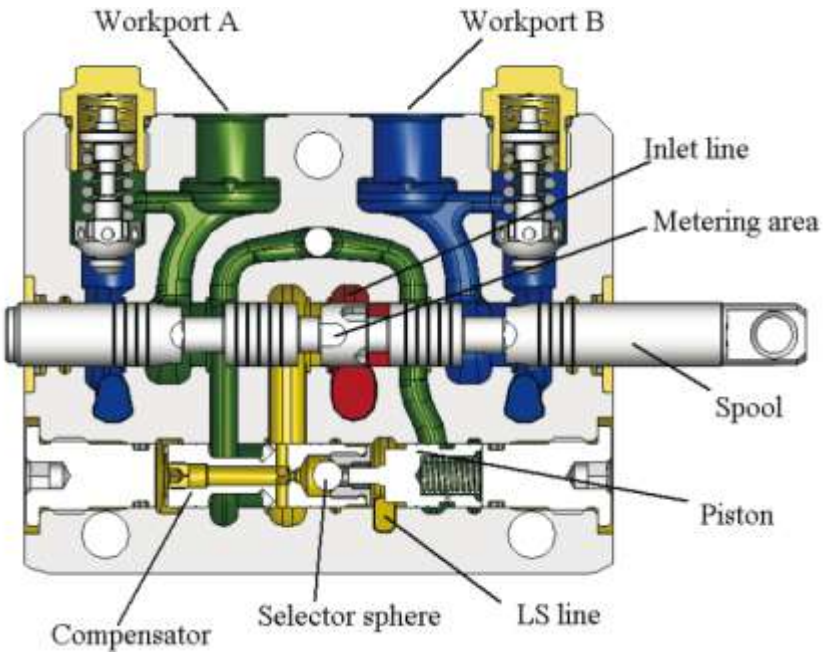

Figure 3.8: Compensator as check valve

3.3.4 Compensator as check valve: refer to picture 3.8

When actuator or function pressure is higher than inlet pressure, the group formed by the compensator, selector sphere and piston work together as a check valve. Work port pressure in the spring chamber of the piston is higher than inlet pressure, resulting in the entire group moving to the left. The movement seats the compensator against the left plug. The passage between inlet and work Port Bridge is now closed, preventing backflow from the actuator. Moreover the load sensing flow is generated by the pump and is not taken from the work port, preventing backflow from the actuator.

3.4 Modeling of the DPX 100

3.9 Multisection valve block Walvoil DPX 100

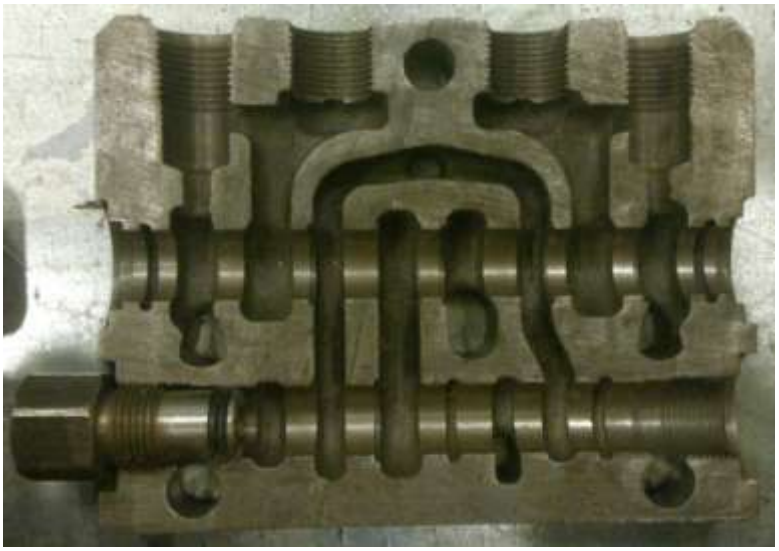

Figure 3.10: Casting cavity details of the DPX 100

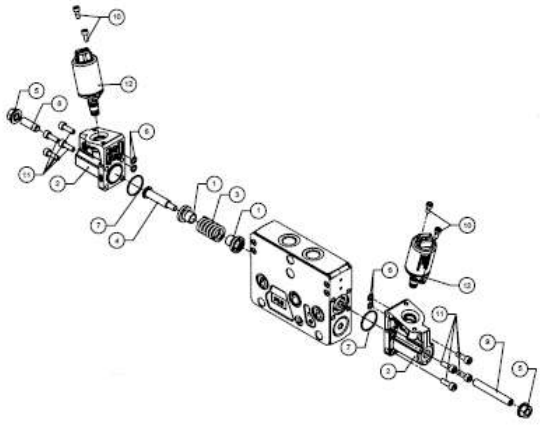

Figure 3.11: Exploded view of the DPX 100

Table 3.1 Concise data sheet of the valve block

Nominal Flow	*With compensator set at* *stand-by pressure of 14 bar* *Regulated by the load*	*120* *90*	*l/min* *l/min*
Maximum Nominal Pressure	*Port P* *Ports A/B*	*300* *300*	*bar* *bar*
Back Pressure Maximum	*Port T* *With manual command*	*30* *10*	*bar* *bar*
Internal leakage A/B → T	*Δp = 100 bar with oil temperature at 40 °C*	*max. 9*	*cm^3/min*
Fluid	*Oil or mineral based*		
Fluid Temperature	*NBR seals* *FPM seals*	*-20÷80* *-20÷100*	*°C* *°C*
Viscosity	*Working area* *Maximum*	*15÷75* *400*	*mm^2/s* *mm^2/s*

3.4.1 Modeling of the Main Spool

The most important parameter in modeling the main spool is the study of the metering areas. The main spool is fairly complex with the pressure compensators orifice integral in the spool. This orifice is a bidirectional orifice, with detailed geometry and flow characteristics.

One of the preliminary steps needed to create the model has been to study the flow areas – orifice openings. These flow paths are created by the metering grooves as the main spool is shifted to the left or the right, depending on the control requirement. The study of these flow paths would define the value of the minimum opening area for the oil inlet and exit for each position of the main spool, ie geometric area. This creates the flow path for transition of the medium between different chambers within the valve. The calculation of the opening area is based entirely on the orifice geometry and does not take into account the curvature of the flow direction, which will define the effective area.

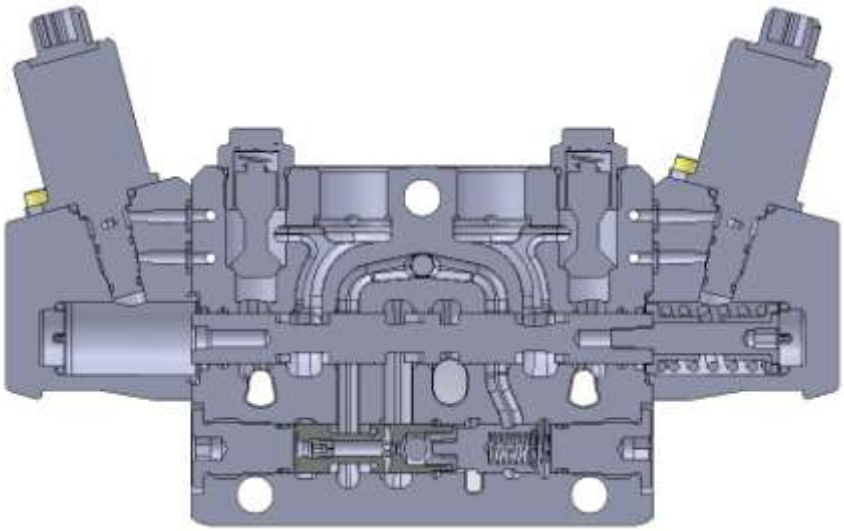

3.12 Cross Sectional view of DPX 100

The main spool (Figure 3.13) is a cylindrical symmetrical spool. The layout of the valve, center (highlighted in red in Figure 3.13) the metering grooves are semicircular and run perpendicular to the main axis. When the main spool is shifted to the left or to the right, it opens an equivalent orifice area to allow the inlet pressure to the pressure compensator. The stroke or displacemnt of the main spool is 6.6 mm in either direction. The main spool contains a bidirectional spring that is used to center the main spool when the main spool is not actuated. The other important components of the main spool are the meter out notches (indicated in green in Figure 3.13) The meter out notches are used to provide extra controllability to the main spool. These meter out notches are used to lower the load in certain conditins when the pressure compensator is closed and does not allow the system pressure to see the load. This is achieved by accurately metering out the load flow to the tank line. This is a summary of the description of the main spool geometry.

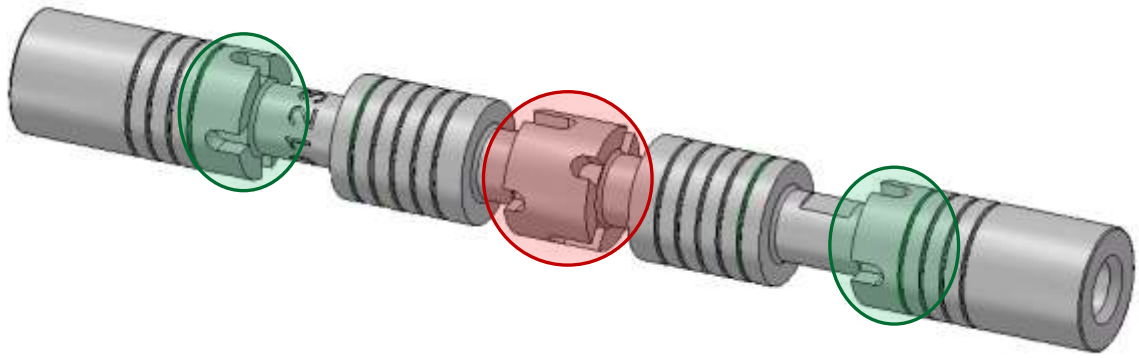

3.13 Main Spool of the DPX 100

To understand the functioning of the main orifice, consider the spool shifting inside its housing and for simplicity only two of the four grooves in the component (longer ones): it turns out that the area will be defined by two curved segments with a circular circumference radius equal to 1.25 mm (Figure 3.16). It is noted that during the initial opening, the area will surely be limited by these semi-circular segments, after the opening area 1.25 mm along the surface of the cylinder will increase linearly as the grooves

provide a stretch constant width (green area in Figure 3.14)

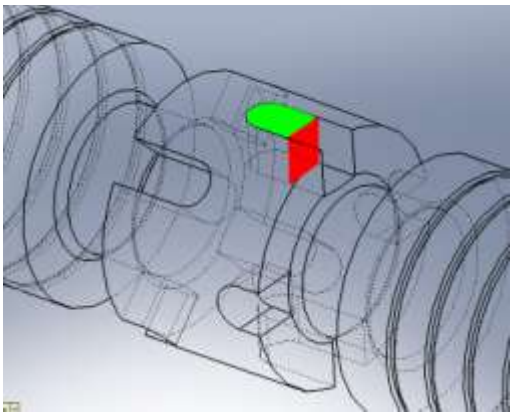

3.14 Zoom of the flow areaa in the center of the spool

However, it should also consider the transition area (in red in Figure 3.14) where the oil enters through the grooves must first pass the left chamber. The area of vertical passage, which is determined on a cross section of the spool should however, be constant with the position of the spool as the depth of the grooves is constant, and a certain point will limit the passage of more fluid. By combining the above we obtain the evolution of the minimum opening in the event that there are only two grooves (Figure 3.15).

3.15 Minimum flow area for the main spool central position

With regard to the calculation of the circular segments which are opened during the movement of the spool, the equations given below (3.10, 3.11) are used. Bearing in mind the curvature of these surfaces which uses a value of the radius (r = 1,257).

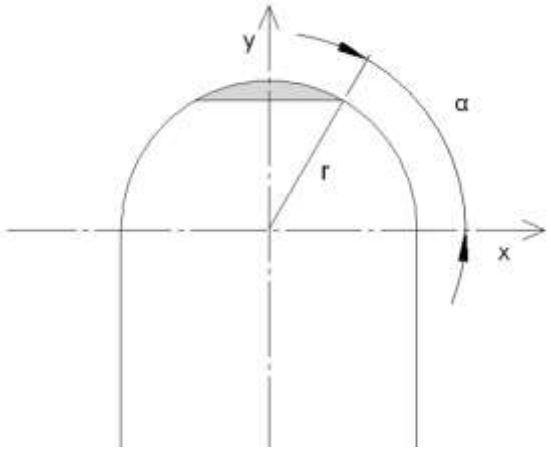

3.16 Representation of the Circular Segment of the spool central orifice

$$\alpha = \arccos\left(\frac{\sqrt{r^2 - y^2}}{r}\right) \tag{3.10}$$

$$Area = \frac{\pi \cdot r^2}{2} - 2 \cdot \left(\frac{\alpha \cdot \left(\frac{2\pi}{360}\right) \cdot r^2}{2}\right) - 2 \cdot \left(\frac{r \cdot cos\alpha \cdot (r - y)}{2}\right) \tag{3.11}$$

At this point we can return to the real case with four grooves of different lengths: what is known is that before the vertical sections of the circumference restrict the passage, then we find that the other two grooves, from the point where the transition area is double and don't feature in the movement. Based on these details we obtain the following linear graph which defines the opening of the spool's central orifice.

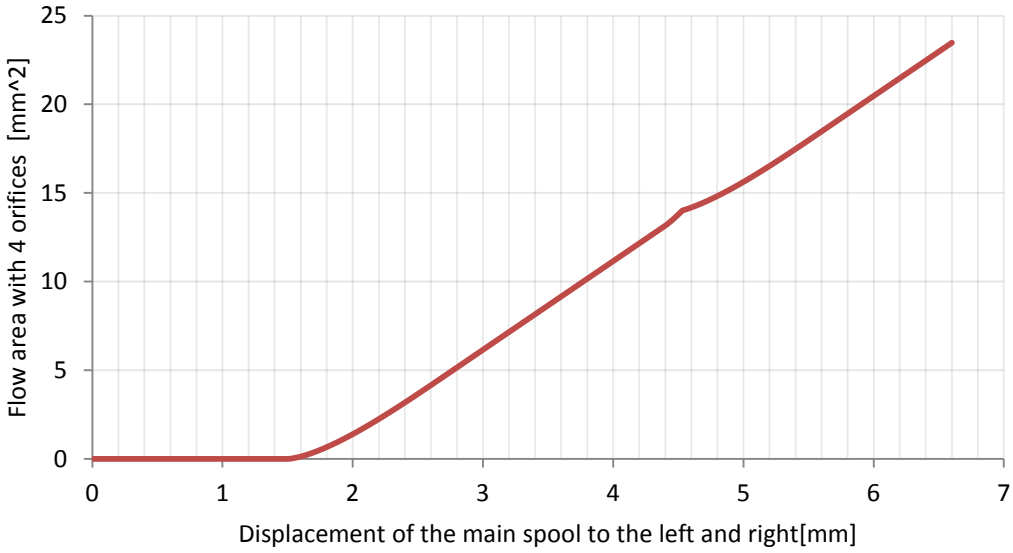

3.17 Orifice flow area for spool central position with 4 orifices open

To complete the work on the main spool with the same methodology for calculating the lateral flow areas (highlighted in green in Figure 3.17) that connect the two ports of the user to the tank (metering out). This connection occurs whenever the main spool is displaced from the central position and one of the lateral ports in connected to tank while the other is closed. In this case the grooves, which are of the same shape and radius of the circular part is always equal to 1.25 mm, and all four are equal. What is clear from the calculations is that, in spite of what happens in the central area, there comes a point where the transition area is limited more by the passage section and remains constant for a certain movement of the spool. The final feature that is obtained describs that the orifice opening is highly non- linear (Figure 3.18).

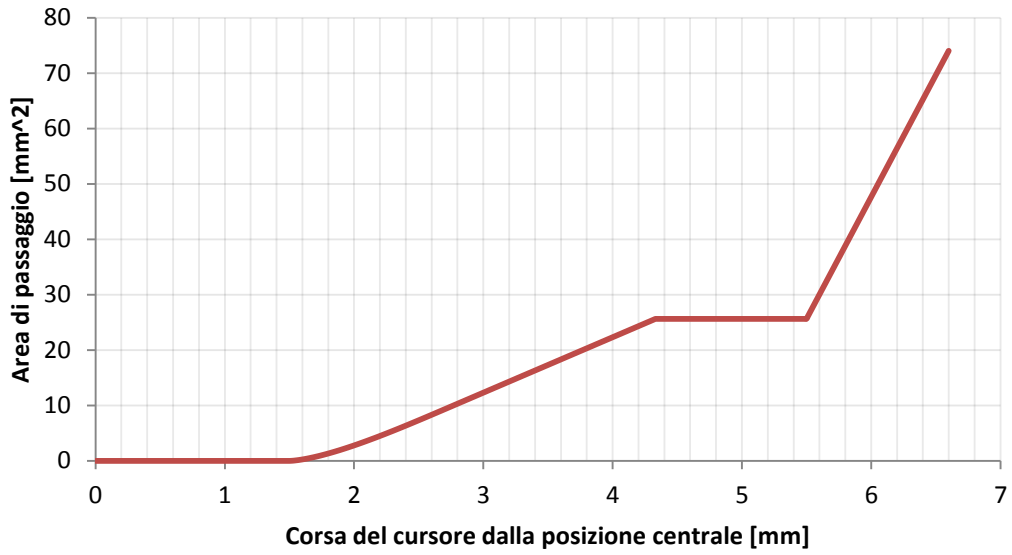

3.18 Flow area at the meter out ports

Having completely defined the geometric characteristics of the main spool, the next step was to model the system in the AMESim® environment. The input signal P, connected with an ideal pressure source (Figure 3.20) energizes the central zone 1 and the annular surface 2: the latter has been realised with a transformer whose form has the usual definition, given by ratio of area of the cylinder and area of the spool. The central element 1 has been split into two sub-models that of a "piston orifice" whose orifice parameters are read by a table that reads the ASCII data, the two sub-model allows to consider the spool displacement from the left to right.

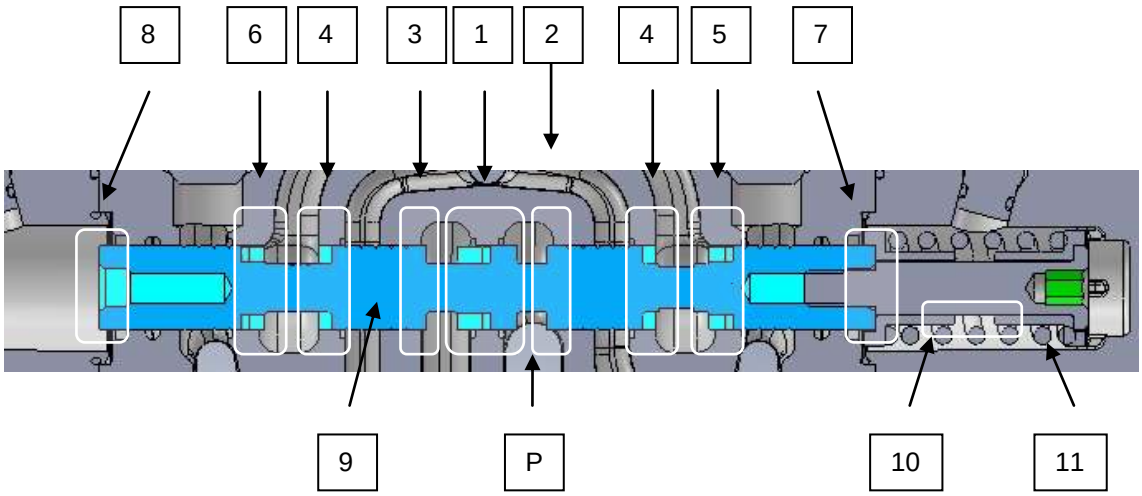

3.19 Main Spool

Piston 3 is realised by a transformer with the pressure drop generated by the metering surfaces described above. Element 3 and the elements 1 are linked with the intermediate chamber which connects to the pressure compensator. After this the medium flows past the pressure compensator and enters into the bridge, and thus flows past element 4, which has been defined as a transformer with an annular orifice cross section to recreate the geometry of the valve body; both elements connect the bridge to one of two user ports. Elements 5 and 6 reproduce the force of pressure that the user causes on the spool, both openings in terms of area (Table ASCII data) which are conncted to the tank drain line. Finally, there are elements 7 and 8 which are connected to the pilot pressures, which usually vary between 0 and 50 bar.

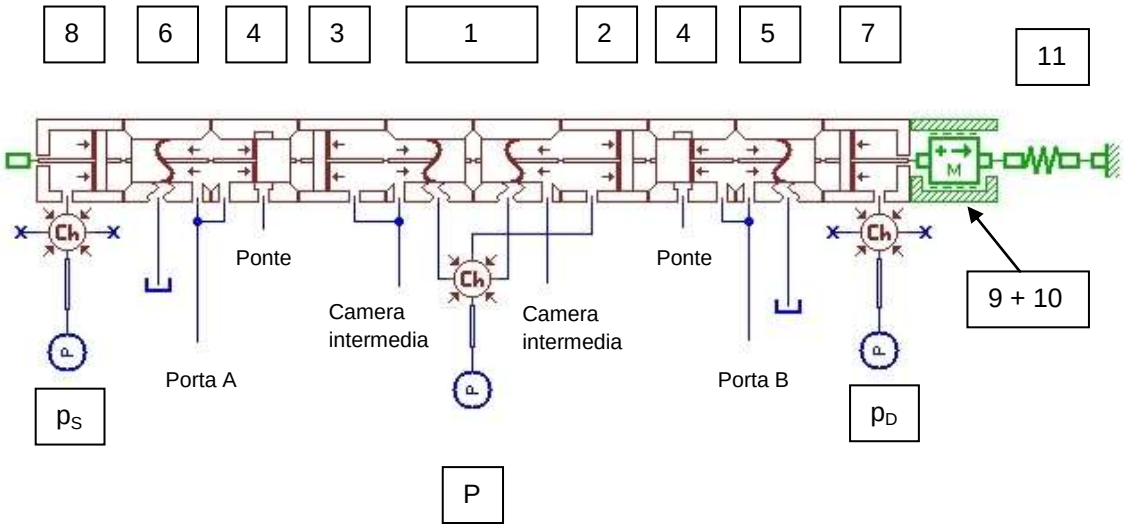

3.20 Representation of the main spool in the AMESim environment

As has already been discussed in previous models the effects of inertia and limits physical movement of the cursor have been reproduced by means of mass submodel 9 + 10, it was finally connected to the centering spring 11, whose geometric characteristics have been reproduced in the model as an ideal linear spring. Once the layout and connections between the elements have moved to introduce all the important geometric and physical

data model that makes the "white box". Among the required data volumes which play an important role of the environments in which the working oil to be introduced in the sub-models of "pressure chamber" to reproduce the dynamic response of the system, they were calculated with the aid of three-dimensional modeling software, of which a drawing of the distributor was already available. The table below includes the parameters needed to complete the model.

Table 3.2: Data parameters to model the main spool

Element	**Parameter**	**Value**	**Unit**
1	*Cylinder Diameter*	*14*	*mm*
	Piston Diameter	*8*	*mm*
	Flow Area	*file .txt con dati di Figure 2.4.12*	
2	*Cylinder Diameter*	*14*	*mm*
	Piston Diameter	*8*	*mm*
3	*Cylinder Diameter*	*14*	*mm*
	Piston Diameter	*8*	*mm*
4	*Cylinder Diameter*	*14*	*mm*
	Piston Diameter	*8*	*mm*
	Underlap at zero position	*-1.4*	*mm*
5 - 6	*Cylinder Diameter*	*14*	*mm*
	Piston Diameter	*8*	*mm*
	Flow Area	*file .txt con dati di Figure 2.4.13*	
7 - 8	*Cylinder Diameter*	*14*	*mm*
	Piston Diameter	*0*	*mm*
9 - 10	*Mass*	$121.4 * 10^{-3}$	*kg*
	Spool Displacement	*-6.6 ÷ 6.6*	*mm*
11	*Number of active spirals*	*5*	*adim*
	Pretension	*0*	*N*

	Spring Diameter	*16*	*mm*
	Wire Diameter	*2.91*	*mm*
Ch center	*Volume*	*10*	*cm^3*
Ch p_S	*Volume*	*15*	*cm^3*
Ch p_D	*Volume*	*8*	*cm^3*
Oil Prop.	*Oil Temperature*	*40*	*° C*
	Density	*850*	*kg/m^3*
	Modulus of Compressibility	*17'000*	*bar*

3.4.2 Modeling of the Pressure COMPENSATOR

The modeling of the pressure compensator has proved to be rather difficult because, in addition to the geometric complexity, there are several interdependent moving parts. Geometric calculations were carried out to determine the metering areas of the pressure compensator. This component has six circular grooves which are at an angle of 45° to the longitudinal axis. The area highlighted in Figure 3.21 of the pressure compensator is the portion of the compensator where it makes contact with the intermediate chamber to allow flow of the medium. After passing through the pressure compensator the medium flows into the bridge then feeds one of two user ports.

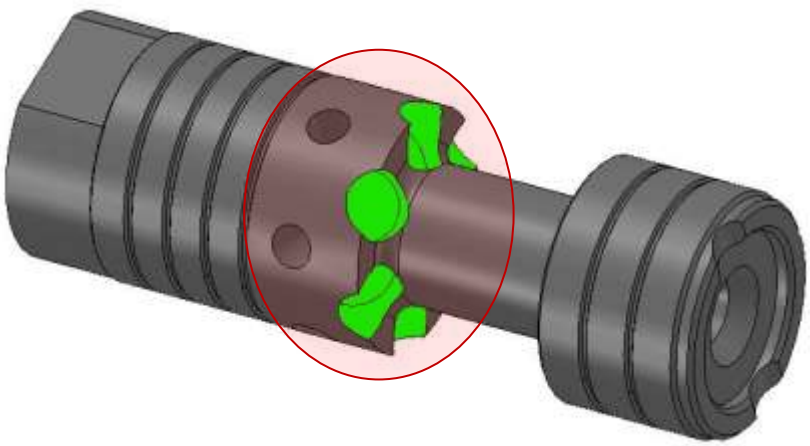

3.21 3D Model of the pressure compensator

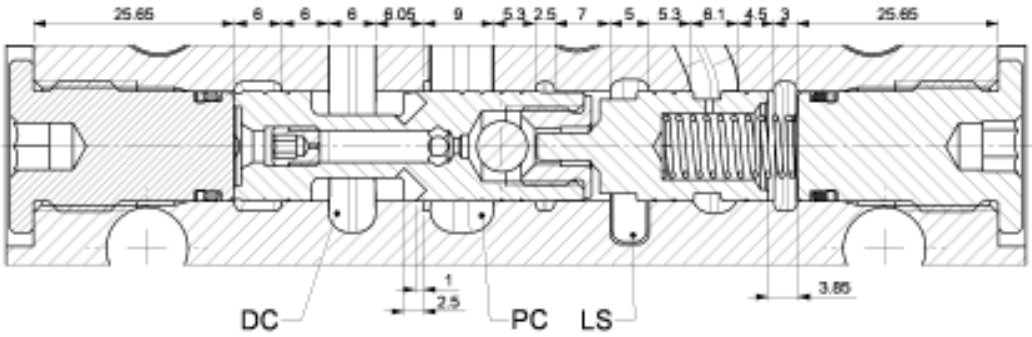

Figure 3.22: Layout of the pressure compensator

The Figure 3.22 offers a detailed view of the complexity of the complete pressure compensator setup. The fluid enters the compensator from the intermediate chamber. Initially the fluid enters through the sensing holes (totally six) and enters into a small chamber with a fine orifice of 0.5mm diameter, which creates the initial displacement of the pressure compensator. Simultaneously the fluid enters to the right of the pressure compensator which houses a selector sphere and double tapered seat that is connected with the Load Sensing chamber. In the case of the pressure compensator the transition areas have not been determined by means of analytical tools, but by calculation of the surfaces using software 3D CAD. The characteristic of discharge is obtained, as shown in Figure 3.18, we see that the transition area allows for a displacement of the compensator greater than 1 mm and 2.5 mm after which a flow path is established.

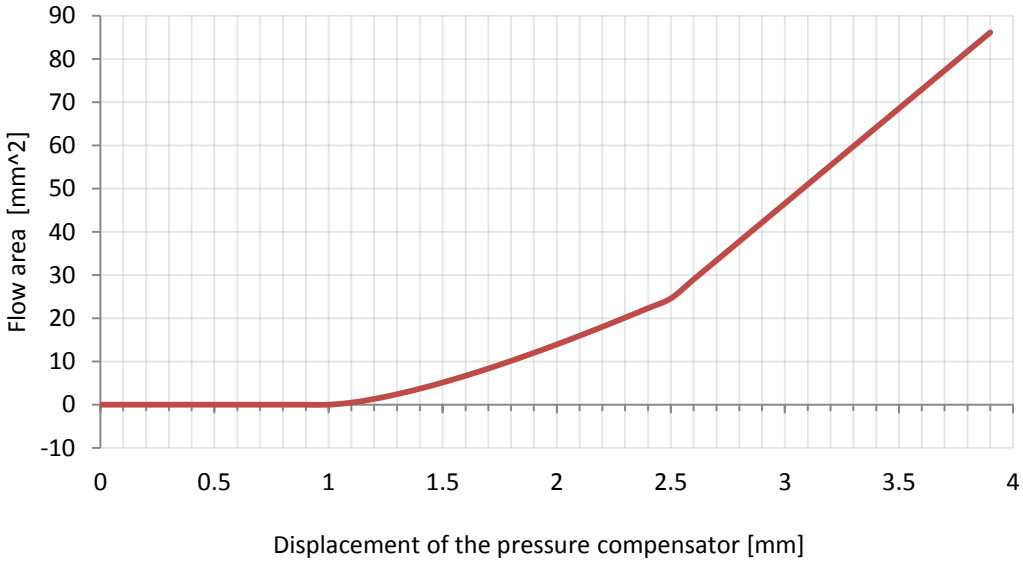

3.23 Graph of the flow area of the Pressure Compensator

The model of the pressure compensator, shown in Figure 3.25, consists essentially of three moving parts shown in Figure 3.24:

- The pressure compensator - colored blue,
- The piston – colored in orange,
- The selector sphere between the conical seats - colored in purple.

To model the pressure compensator submodels of simple transformer piston 12 and 13 to recreate the pressure forces of the fluid medium from the intermediate chamber to the bridge chamber. The module 15 reproduces the effect of metering in which the component creates a pressure drop: it can be read from an ASCII table with the characteristic outflow of Figure 3.23, and finally consider the element 18 and the force generated from the pressure existing in the chamber trying to divide the LS from the piston. The flow inside the compensator 14 and the restriction in the vicinity of the sphere 16 are reproduced with fixed orifices placed in the middle line, coming from the main valve. The asymmetric geometry of which the ball selector works to use two transformers with a spherical body linked together in the cone. Both contain movable sleeves rigidly connected to the compensator tray. Element 17 which is a double mass element is used to reproduce the

inertial effects and the limits which will not only offset but also placed the ball inside. This element 17 is a body in body element which is used to describe the relative motions of the displacement of the pressure compensator with that of the selector sphere. To describe the piston check assembly, element 18 is a transformer element modeled as a piston and recieves its control pressure from the LS chamber. Element 19 is a transformer element modeled as a piston and recieves its control pressure from the bridge chamber.

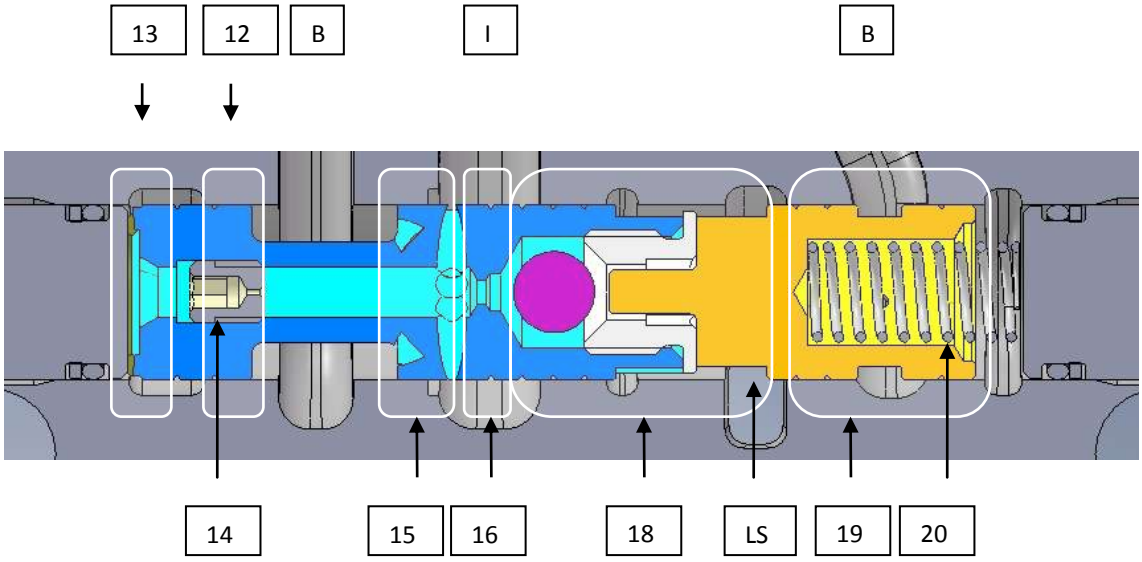

Figure 3.24: Pressure compensator sections

Element 20 is modeled as a light spring which is used to add a slight pretension to the piston. It uses a simple logic that uses the position information of the piston to decide whether to activate the elastic element: this is necessary because the spring is not rigidly connected to the piston and can only push it from left to right, but not pull it. The most complex physical condition to recreate in the modeling of the pressure compensator assembly is that of the mechanilcal / fluid contact condition. This is because at certain times the pressure compensator has a mechanical contact from the piston check assembly to displace the pressure compensator to the right and at other conditions the LS signal causes the piston check assembly and the pressure compensator to be displced to the right and to the left respectively. This peculiar operating condition has been recreated by elements 23 and 22. Where element 22 is a spring air gap damper, where the properties of the spring have been set to one of a rigid element and the air gap to define the positions in

which the fluid medium will come in contact. Element 22 is a modulated transformer element which receives its modulation signal from element 21 which sums the displacement of both the pressure compensator as well as the piston check assembly to define if the elements are in mechanical contact to transfer the force from a mechanical contact or if the elements have a gap and must transfer the pressure of the medium to determine the position of the elements. The displacement control logic is such that if the sum reaches the value of 3.25 mm, the tip of the plunger can touch the ball to move to the left by a force value from the transformer 22.

The table below defines the elements and the logic we have described of all the geometric data and physical parameters to complete the compilation of the model. As in the previous case all the volumes have been carefully calculated by the main valve in order to recreate the same effects of delay due to the compressibility of the oil.

Table 3.3: Parameter data for modeling the Pressure Compensator of DPX 100

Element	Parameter	Value	Unit
$M_{compensator}$	*Mass*	*36.2/1000*	*kg*
	Displacement(→)	*0 – 3.85*	*mm*
M_{sfera}	*Mass*	*1.15/1000*	*kg*
	Displacement	*-0.93 – 0.93*	*mm*
$M_{pistone}$	*Mass*	*18/1000*	*kg*
	Displacement(←)	*0 – 3.85*	*mm*
12	*Cylinder Diameter*	*14*	*mm*
	Piston Diameter	*8*	*mm*
13	*Cylinder Diameter*	*14*	*mm*
	Piston Diameter	*0*	*mm*
14	*Orifice Diameter*	*0.5*	*mm*
15	*Cylinder Diameter*	*14*	*mm*
	Piston Diameter	*8*	*mm*
	Flow Area	*file .txt con dati di Figure*	

		2.4.17	
16	*Orifice Diameter*	*2*	*mm*
$18_{compens.}$	*Cylinder Diameter*	*14*	*mm*
	Piston Diameter	*9*	*mm*
$18_{pistone}$	*Cylinder Diameter*	*14*	*mm*
	Piston Diameter	*0*	*mm*
19	*Cylinder Diameter*	*14*	*mm*
	Piston Diameter	*0*	*mm*
20 **(geometric value)**	*Number of active spirals*	*8*	*adim*
	Pretension	*0*	*N*
	Spring Diameter	*7.2*	*mm*
	Diameter wire	*0.8*	*mm*
20	*Precompression*	$-3.5*10^{-4}$	*mm*
	Elastic Constant	*1176*	*N/mm*
21	*Function*	*3.85-(1000*(x+y))*	
23	*Gap right side*	*0*	*mm*
	Gap left side	*3.85*	*mm*
24	*Orifice Diameter*	*1*	*mm*
Ch I	*Volume*	*9*	cm^3
Ch B	*Volume*	*17*	cm^3
Oil Prop.	*Temperature*	*40*	*° C*
	Density	*850*	kg/m^3
	Modulus of Compressibility	*17'000*	*bar*

3.5 Complete Model of the DPX 100

The figure describes the complete model of the DPX 100 – Main Spool + Pressure Compensator with chamber areas integrated in the AMESim modeling environment. The

model also includes the Counter balance valve developed by Michele Greco in his Masters thesis [11]. The model functions in the following manner. When the main spool is energised by the pilot pressure the main spool is shifted to the left or to the right. When the main spool is shifted it creates a flow path through the orifice in the center of the spool and the fluid enters from the inlet chamber to the intermediate chamber. Once in the intermediate chamber the medium enters into the sensing hole of the pressure compensator to cause the displacement of the pressure compensator. Simultaneously a part of the medium passes through the selector sphere to provide the LS feedback of the system. Once the pressure compensator is displaced it creates a flow path from the intermediate chamber to the bridge. The flow of the fluid from the intermediate chamber to the bridge chamber is through the metering notches of the pressure compensator. Once the fluid medium is in the bridge chamber the fluid can pass either to work port A or B depending on the spool position, while the other port which is draining would drain the fluid medium to tank through the meter out notches.

Model Capabilities

The developed models capabilities would describe the dynamics of the valve in terms of:

1. Main Spool – the dynamic position of the main spool and it's characteristics of inlet orifice and meter out orifice.
2. Flow characteristics of the valve - The flow through the different chambers of the valve would account for the internal leakage through the main spool and pressure compensator. This would define the actual flow output from the valve.
3. Pressure dynamics – The systems pressure dynamics is defined by the pressure rate rise equation and describes the pressure characteristics in the different chambers of the valve.
4. Pressure compensator dynamics – The pressure compensator dynamics provide information of the instantaneous spool position. The LS pressure and System pressures. Spool displacement and position. Flow through the damping orifice. Flow and pressure characteristics into and out of the intermediate chamber and the bridge.
5. Piston Check Assembly - The piston check assembly provides information of the instantaneous spool position, the bridge pressure used to displace the piston check assembly. System pressures. Spring compressibility, displacement and position.

Flow and pressure characteristics from the bridge chamber.

6. Intermediate chamber pressure – The dynamics of the intermediate chamber pressure between the main spool and pressure compensator can be determined.
7. Spool Meter out - The dynamics of the meter out flow to tank can be determined as the work port drains the pressure and flow compensator and the control piston chamber can be determined.
8. Load Sensing Signal – The dynamics of the LS signal can be determined.

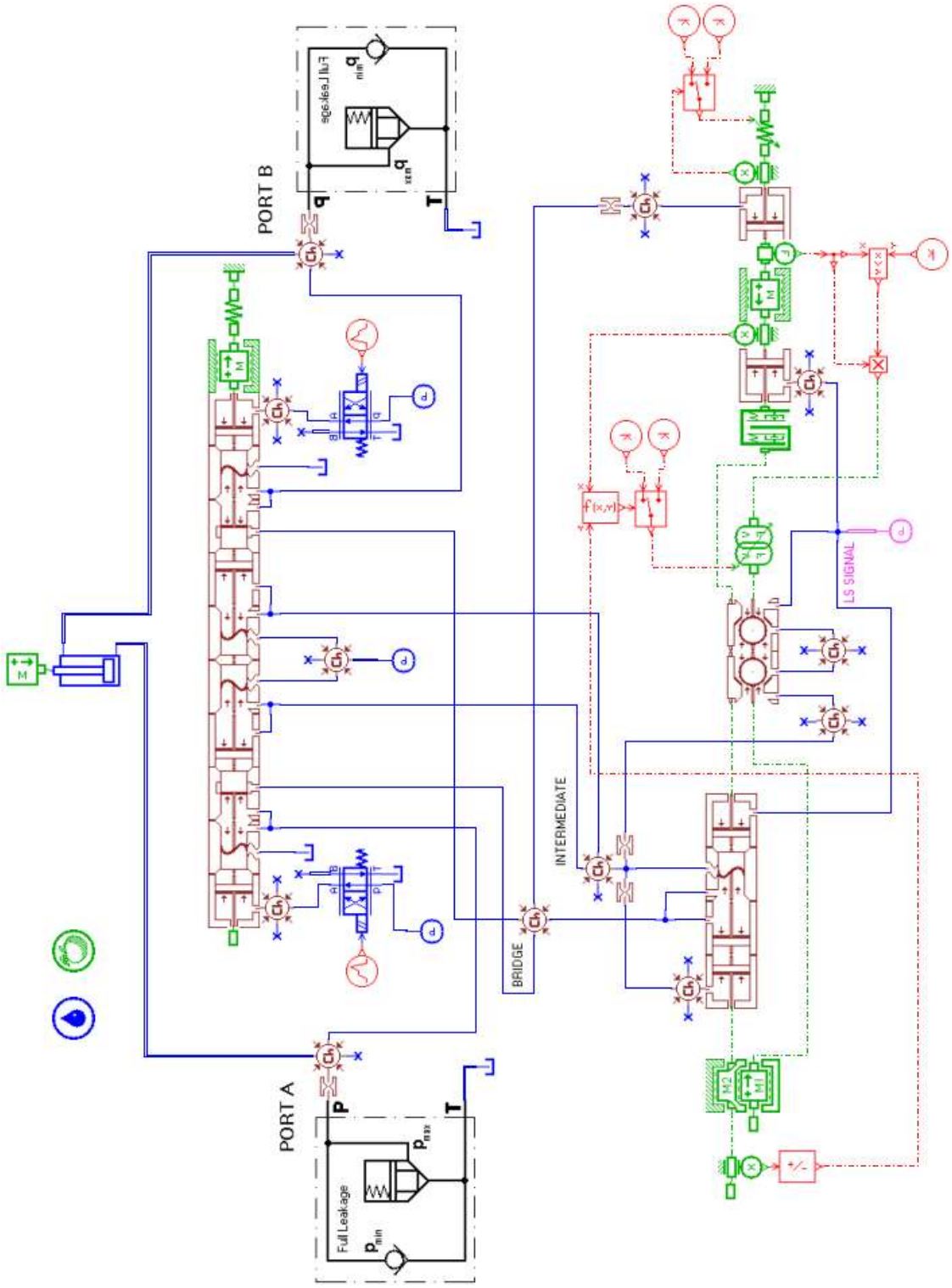

3.26 Complete model of the Walvoil DPX 100 in AMESim

3.6 References

[1] R. Finzel and S. Helduser. *New electro-hydraulic control systems for mobile machinery.* In Dr D N Johnston and Professor A R Plummer, editors, Fluid Power and Motion Control (FPMC), pages 309–321, 2008.

[2] R. Rahmfeld and M. Ivantysynova. *Displacement controlled linear actuator with Differential cylinder – a way to save primary energy in mobile machines*. In Fifth International Conference on Fluid Power Transmission and Control (ICFP), volume 1,Pages 316–322, 2001.

[3] Kim Heybroek. *Saving Energy in Construction Machinery using Displacement Control Hydraulics.* Licentiate thesis, LiTH, Linköping, 2008.

[4] Björn Eriksson and J.-O. Palmberg. *How to handle auxiliary functions in energy Efficient, single pump, flow sharing mobile systems*. In The 7th International Fluid Power Conference (IFK), 2010.

[5] K. Mettälä, M. Djurovic, G. Keuper, and P. Stachnik. *Intelligent oil flow management with EFM: The potentials of electro hydraulic flow matching in tractor hydraulics.*In J. Vilenius and K. T. Koskinen, editors, The Tenth Scandinavian International Conference on Fluid Power (SICFP), volume 3, pages 25–34, 2007.

[6] Milan Djurovic. *Energiesparende Antriebssysteme für die Arbeitshydraulik mobile Arbeitsmaschinen "Elektrohydraulisches Flow Matching".* PhD thesis, Institut für Fluidtechnik der Technischen Universität Dresden, 2007.

[7] R. Finzel, S. Helduser, and Dal-Sik Jang. *Electro-hydraulic control systems forMobile machinery with low energy consumption*. In Proceedings of the Seventh International Conference on Fluid Power Transmission and Control (ICFP), pages 214–219, 2009.

[8] Birgitta Lantto. *On Fluid Power Control with Special Reference to Load-Sensing Systems and Sliding Mode Control. PhD thesis*, LiTH, Linköping, 1994.

[9] Mikael Axin, Björn Eriksson, and J.-O. Palmberg. *Energy efficient load adapting System without load sensing - design and evaluation.* In The 11th Scandinavian International Conference on Fluid Power (SICFP), 2009.

[10] Petter Krus. *On Load Sensing Fluid Power Systems - With Special Reference toDynamic Properties and Control Aspects*. PhD thesis, LiTH, Linköping, 1988

CHAPTER 4

Kinematics

4.1 Introduction

This chapter details the modeling of the excavator's kinematics. The kinematics of the excavator modeled here pertains to the upper carriage system – namely the boom, arm and bucket implements. The model of the kinematics was integrated with the model of the hydraulics in the AMESim modeling environment. In this way realistic loads effected by the implements at different positions can be transferred to the hydraulic system. The advantage of such a model is that the effects of the loads on the system can be used to study the reaction on the pump and the valves.

4.2 Modeling of the Kinematics of an Excavator

This chapter focuses on the development of bond graph dynamic model of the mechanical dynamics of an excavator. To develop a mechanical dynamics model of the manipulator, forward recursive equations similar to those applied in iterative Newton-Euler method were used to obtain kinematic relationships between the time rates of joint variables and the generalized cartesian velocities for the centroids of the links. Representing the obtained kinematic relationships in bond graphic form, while considering the link weights and moments as the elements lead to a detailed bond graph model of the manipulator. The

bond graph method was found to reduce significantly the number of recursive computations performed on a 3 DOF manipulator for a mechanical dynamic model to result, hence indicating that bond graph method is more computationally efficient than the Newton-Euler method in developing dynamic models of 3 DOF planar manipulators. Since bond graph method is based on the interaction of power between elements, it can be used to model multi-energy domains. Mechanical manipulators and mechanisms, the bond graph model can be developed based on kinematic relationships between the time rates of joint variables and the generalized cartesian velocities (translational and angular velocities). It is not necessary to have higher order time rates of variables involved, that is translational and angular accelerations.

Kinematic modeling is helpful for understanding and improving the operating performance of the backhoe excavation machine. A dynamic model is essential for dynamics-related studies of an excavator, e.g., controllability, durability, and so on. Since the hydraulic system, which controls the actuators of an excavator, has its own dynamics due to compressibility of hydraulic oil, it is required that the dynamics of the hydraulic system be incorporated into that of the mechanical system to study the coupled dynamic behavior of the excavator.

An excavator is comprised of three planar implements connected through revolute joints known as the boom, arm, and bucket, and one vertical revolute joint known as the swing joint [2]. Kinematics is the science of motion which treats motion without regard to the forces that cause it. Within the science of kinematics one studies the position, velocity, acceleration, and all higher order derivatives of the position variables (with respect to time or any other variables) [3]. The excavator linkage, however, is a complex link mechanism whose motion is controlled by hydraulic cylinders and actuators. To program the bucket motion and joint-link motion, a mathematical model of the link mechanism is required to refer to all geometrical and/or time-based properties of the motion. Kinematic model describes the spatial position of joints and links, and position and orientation of the bucket. The derivatives of kinematics deal with the mechanics of motion without considering the forces that cause it [4].

The basic problem in the study of mechanical link mechanism is of computing the position and orientation of bucket of the backhoe attachment when the joint angles are known, which is referred to as forward kinematics. The inverse kinematics problem is, thus to calculate all possible sets of joint angles, which could be used to attain a given position and orientation of the bucket tip of the backhoe attachment. The problem of link mechanism control requires both the direct and inverse kinematic models of the backhoe attachment of the excavator [4]. The kinematic model is helpful to follow the defined trajectory as well as digging operation can be carried out successfully at required location of the terrain using proper positioning and orientation of the bucket [2], have described the kinematics of the excavator with the coordinate frame in 1993. To describe the position of the points on the mechanism of an excavator, coordinate systems are first defined. A fixed Cartesian coordinate system is assigned to the body of the excavator. The local coordinate frames are assigned to each link of the mechanism. A systematic method to define the local coordinate systems for the serially connected links (upper structure, boom, arm, and bucket) of the excavator is accomplished by applying the Denavit and Hartenberg procedure. The resulting coordinate flames for the links of the excavator are shown in figure 4.1.

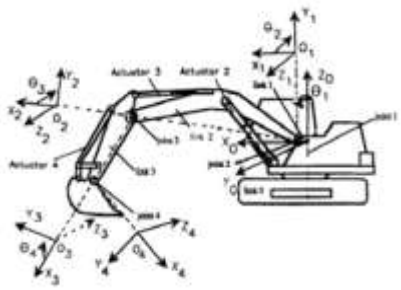

Figure 4.1: Typical excavator and its coordinate frames

In order to develop the dynamics of a manipulator, a kinematic model of the manipulator is required first. The kinematics modeling is done first by attaching frames to every link. The kinematics of the manipulator deals with the geometrical and time-based properties of motion. Hence it deals with the position, velocity and acceleration of the manipulator without regard to the forces/torques that cause them. The study of the kinematics focuses on the motion of the manipulator with respect to a fixed co-ordinate system. The complete kinematic and dynamic modeling of the manipulator has been done step by step.

The modeling of the excavator kinematics has been used to create the realistic forces on the hydraulic actuators. Considering the benefits of having the kinematic model integral with the hydraulic model, the linkage parameters were coupled to the hydraulic model using the Planar Mechanics library of AMESim®. This facilitates the understanding of dynamic loads on the hydraulic cylinder. The driving joint torques of the boom, arm and bucket are generated by the forces of the hydraulic ram actuators. The translational and rotational motions of these links are described by the dynamic model of the excavator system. The kinematic model has been incorporated as a lumped parameter model, which accounts for angular position, relative coordinates, distances between links, relative velocity, relative acceleration and the output forces. Joint forces of contact and stiffness, are also considered in the model. The equations of motion can be derived by applying the Euler–Lagrange equations to a Lagrangian energy function. The revolute pairs have been modeled as Lagrange multipliers and are calculated from the Baumgarte stabilization method applied to the constraint equations.

To develop a dynamics model of the manipulator, forward recursive equations similar to those applied in iterative Newton-Euler method were used to obtain kinematic relationships between the time rates of joint variables and the generalized Cartesian velocities for the centroid of the links. The obtained kinematic relationships were represented in bond graph form, while considering the link weights and moment as the elements led to a detailed bond graph model of the manipulator. Forward recursive equations for motion of manipulators similar to those used in Newton-Euler method are used to derive the kinematic relationships between the time rates of joint variables, and the generalized cartesian velocities (translational and angular velocities) of mass centers of the links. These kinematic relations are further used for graphical representation of the system dynamics using Bond graphs. Inertial effects of cylinders and their pistons are negligibly small compared to those of manipulator links, the hydraulic cylinders transmit axial forces only, the revolute joints have no friction, and all the links and supports are rigid, a bond graph model representing the mechanical dynamics of the excavating manipulator was developed.

One of the problems in studying the dynamics of an excavator is the soil excavation process. It is quite complicated, partly because the bucket cutting edge can move along an arbitrary path and excavations often are carried out in non homogeneous material. Thus the forces acting on the bucket are difficult to evaluate. They depend mainly on the type of soil, weight of the excavated material as well as the velocity and position of the bucket against the soil. The shape of the bucket itself is also important. The type of the soil depends on many components: its humidity, internal structure, porosity, as well as hardness. Usually these values vary in the course the whole excavation process. To further enhance the force simulation of the model, the visco-elastic properties of the material being handled have been recreated as a force during the excavation process. A model that accounts for the material being retained in the bucket, which was developed by Reece's fundamental earthmoving equation in soil mechanics was applied in this study to determine the force exerted by the excavator bucket to the soil. An impulse force which acts on the bucket during soil penetration has been included. The motion of the excavator implements would be to follow a pre-planned digging trajectory. Following industry best practices the quintic trajectory planning approach has been employed for the excavation cycles. During digging, three main tangential resistance forces arise: the resistance to soil cutting, the frictional force acting on the bucket surface in contact with the soil and the resistance to movement of the soil ahead of and in the bucket. The magnitude of the digging resistance forces depends on many factors such as the digging angle, volume of the soil, volume of material ripped into the bucket, and the specific resistance to cutting. These factors are generally variable and unavailable. Moreover, due to soil plasticity, spatial variation in soil properties, and potentially severe heterogeneity of material under excavation, it is impossible to exactly define the force needed for certain digging conditions. Taking into account the variable force conditions of the soil while including the parameters from the study of its effect on the system during the digging cycle have led to a well developed model of the kinematic system of the excavator.

Assuming that; the inertial effects of cylinders and their pistons are negligibly small compared to those of manipulator links, the hydraulic cylinders transmit axial forces only, the revolute joints have no friction, and all the links and supports are rigid, a bond graph

model representing the mechanical dynamics of the excavating manipulator was developed.

To further enhance the force simulation of the model, the visco-elastic properties of the material being handled have been recreated as a force during the excavation process. An impulse force which acts on the bucket during soil penetration has been included as described in [5]. The motion of the excavator implements would be to follow a pre-planned digging trajectory..

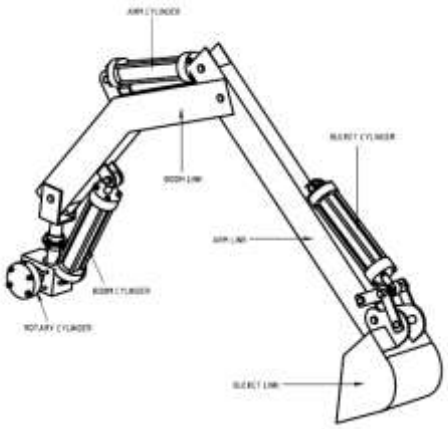

Figure 4.2. Schematic drawing of a part of assembled excavator

4.3 Modeling the Bucket Digging Force

A model that accounts for the material being retained in the bucket, which was developed by [10] using force equilibrium and fundamental earthmoving equation in soil mechanics was applied in this study to determine the force *F* exerted by the excavator bucket to the soil. From Figure the force *F* is given in (8).

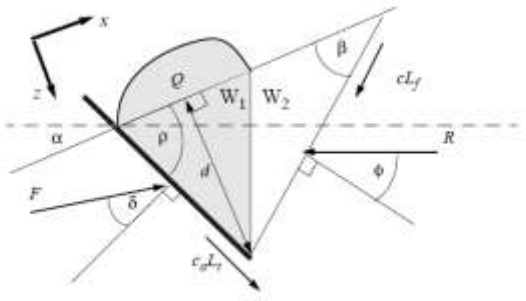

Figure 4.3. Wedge model that accounts for the material being retained in the bucket

$$F = d^2\omega\gamma g N_\omega + c\omega d N_c + V_s\gamma g N_q \qquad (4.1)$$

Vs is the swept volume, *Q* is the surcharge, W_1 is the weight of the material above the bucket, W_2 is the weight of the rest of material in the wedge, *Lt* is the length of the tool, *Lf* is the length of the failure surface, *R* is the force of the soil resisting the moving of the wedge, *F* is the force exerted by the tool on the wedge, *ca* is the adhesion between the soil and the blade, *c* is the cohesiveness of the soil media, β is the failure surface angle (slip angle), α is the surface terrain slope (cutting angle), φ is the soil-soil friction angle, ρ is the rake angle of the tool relative to the soil surface, σ is the soil-tool friction angle, *d* is the depth of the bucket tool perpendicular to the soil surface, *w* is the width of the bucket, γ is the bulk density of the soil media and *g* is the gravitational acceleration.

Nw, *Nc Nq* are N-factors which depend on: the soil's frictional strength, the bucket tool geometry and soil-to-tool strength properties, and are given by the following equations.

$$N_\omega = \frac{(\cot\beta - \tan\alpha)(\cos\alpha + \sin\alpha\cot(\beta+\varphi)}{2\{cos(\rho+\sigma) + \sin(\rho+\sigma)\cot(\beta+\varphi)\}} \qquad (4.2)$$

$$N_c = \frac{1 + (\cot\beta\cot(\beta+\varphi)}{\{cos(\rho+\sigma) + \sin(\rho+\sigma)\cot(\beta+\varphi)\}} \qquad (4.3)$$

$$N_q = \frac{\cos\alpha + \sin\alpha\cot(\beta+\varphi)}{\{cos(\rho+\sigma) + \sin(\rho+\sigma)\cot(\beta+\varphi)\}} \qquad (4.4)$$

Equations (8) to (11) show that the magnitude of the digging force depends on many factors such as the cutting angle, specific resistance to cutting, volume of the bucket,

amount of the material ripped into the bucket and the volume of the material surcharged. These factors are always varying during the bucket digging operation and indicate complicated interactions of the bucket and the soil, hence making modeling of the bucket digging force throughout the digging process a complex and bulk process.

In this study, a simplified model is presented by considering the situation of critical force, and then assuming the force to remain constant throughout the digging process. The critical value of the cutting angle is given by [17].

$$\alpha_c = \frac{1}{2}\left(\pi - \sigma - sin^{-1}(sin\sigma sin\rho)\right) \tag{4.5}$$

The soil-tool force *F* is assumed to be applied at the cutting edge of the bucket. From the Newton's third law of motion, the soil applies an opposite and equal reaction force at the bucket, which can be resolved to a normal and tangential force components as shown in Figure 4.4

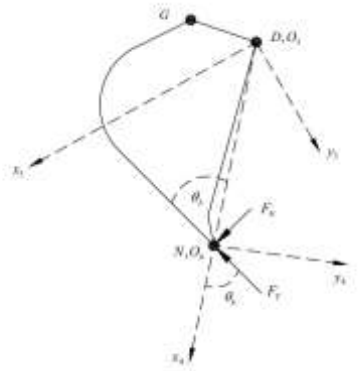

Figure 4.4. Bucket digging force at the tip

The horizontal and vertical components of the bucket reaction force are given as;

$$\begin{aligned} F_x = &-(F_T cos\theta_b - F_N sin\theta_b)cos(\theta_2 + \theta_3 + \theta_4) \\ &+ (F_T cos\theta_b + F_N sin\theta_b)sin(\theta_2 + \theta_3 + \theta_4) \end{aligned} \tag{4.6}$$

$$\begin{aligned} F_y = &-(F_T cos\theta_b - F_N sin\theta_b)sin(\theta_2 + \theta_3 + \theta_4) \\ &- (F_T sin\theta_b + F_N cos\theta_b)cos(\theta_2 + \theta_3 + \theta_4) \end{aligned} \tag{4.7}$$

These forces are included at the translational velocity of the origin of the 4*th* link coordinate frame but referenced to the base coordinate frame.

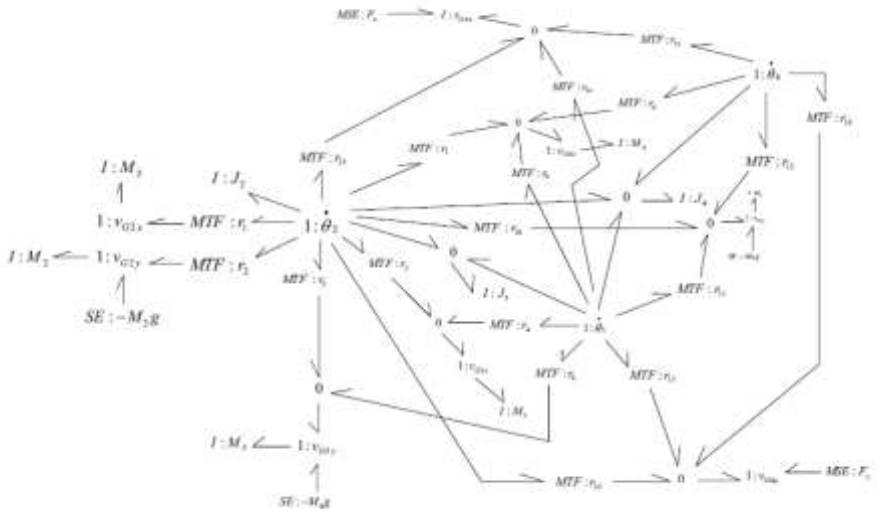

Figure 4.5: Bond Graph of Excavator Implements

4.4 Trajectory Planning

In a typical trajectory, all joints move simultaneously. For the typical trajectory selected here, the boom, arm, and bucket links move from their minimum to maximum positions and all joints start and finish moving at the same time, although different time limits can be programmed. Three common trajectories namely, trapezoidal trajectory, cubic polynomial trajectory, and quintic polynomial trajectory have been previously applied in trajectory planning for hydraulic manipulators. Among the three methods, the quintic polynomial trajectory has advantage in that;

- The velocity trajectory is smooth unlike in trapezoidal trajectory whose velocity profile has discontinuities where the link motion starts to settle at a constant velocity, and where the link starts to decelerate.

- The acceleration profile has values equal to zero at starting and finishing times of the trajectory, unlike in the other trajectories where the acceleration values at the start and final times have non zero values.

Therefore the trajectory to be adopted in this work is the quintic polynomial trajectory which is given by;

$$x(t) = a_0 + a_1 t + a_2 t^2 + a_3 t^3 + a_4 t^4 + a_5 t^5 \qquad (4.8)$$

The desired boundary conditions are; $x_{t=0} = x_{min}$, $x_{t=t_f} = x_{max}$, $\dot{x}_{t=0} = 0$, $\dot{x}_{t=t_f} = 0$, $\ddot{x}_{t=0} = 0$, $\ddot{x}_{t=t_f} = 0$

By taking the first and second derivatives of (4.8) and satisfying these boundary conditions, the coefficients of the polynomial can be obtained and substituted in the polynomial equation (4.8) to get the required displacement, velocity and acceleration trajectories as;

$$x(t) = x_{min} + \frac{10(x_{max}-x_{min})}{t_f^3} t^3 + \frac{15(x_{min}-x_{max})}{t_f^4} t^4 + \frac{6(x_{max}-x_{min})}{t_f^5} t^5 \qquad (4.9)$$

$$\dot{x}(t) = \frac{30(x_{max}-x_{min})}{t_f^3} t^2 + \frac{60(x_{min}-x_{max})}{t_f^4} t^3 + \frac{30(x_{max}-x_{min})}{t_f^5} t^4 \qquad (4.10)$$

$$\ddot{x}(t) = \frac{60(x_{max}-x_{min})}{t_f^3} t + \frac{180(x_{min}-x_{max})}{t_f^4} t^2 + \frac{120(x_{max}-x_{min})}{t_f^5} t^3 \qquad (4.11)$$

4.5 Model in the AMESim Modeling Environment

The figures below describe the modeling of the excavator implements Boom, Arm and Bucket in the AMESim modeling environment. The actuators are realized through the jack elements symbolized as A1, A2 and A3 in figure.

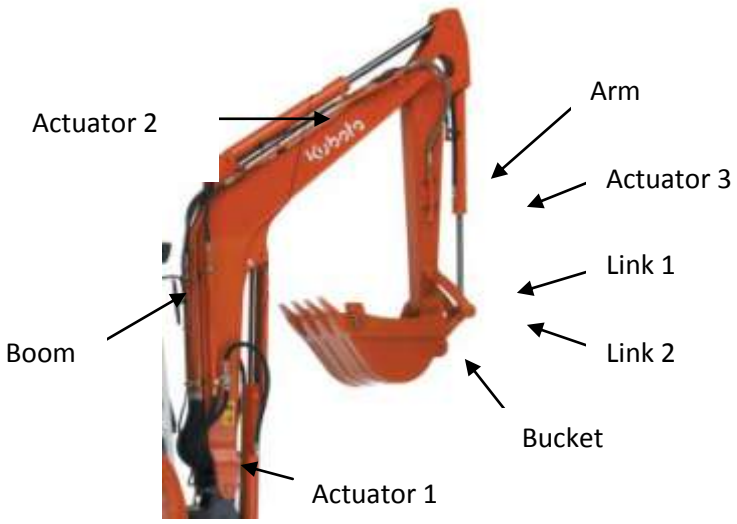

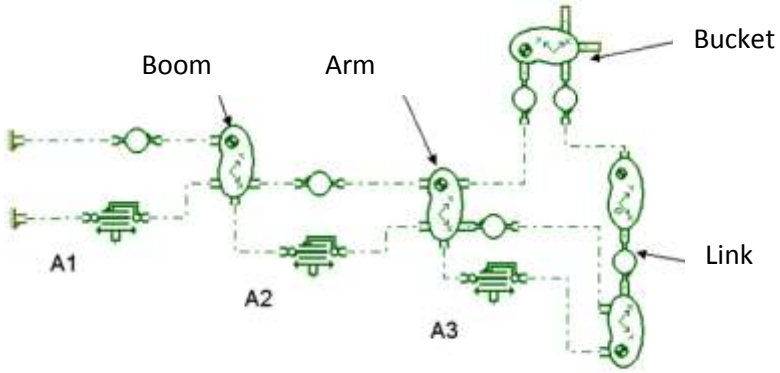

Model Capabilities

The developed models capabilities would describe the dynamics of the kinematics in terms of:

1. Implement instantaneous positions and velocities – the dynamic position of the main spool and it's characteristics of inlet orifice and meter out orifice.
2. Soil Interaction Model - The flow through the different chambers of the valve would account for the internal leakage through the main spool and pressure compensator. This would define the actual flow output from the valve.
3. Force on the actuators – The systems pressure dynamics is defined by the pressure rate rise equation and describes the pressure characteristics in the different chambers of the valve.

4. Pressure dynamics on the actuators – The pressure compensator dynamics provide information of the instantaneous spool position. The LS pressure and System pressures. Spool displacement and position. Flow through the damping orifice. Flow and pressure characteristics into and out of the intermediate chamber and the bridge.

4.6 References

[1] J. Denavit, and R. S. Hartenberg, "A kinematic notation for lower-pair mechanisms based on matrices," Journal of Applied Mechanics, pp. 215– 221. 1955.

[2] K.S. Fu, R. C. Gonzalez, and C. S. Lee, Robotics: Control, Sensing, Vision and Intelligence. McGraw Hill Book Publishing Company, 1987.

[3] J. J. Craig, Introduction to Robotics: Mechanics and Control. Addison-Wesley Publishers, USA, 1986.

[4] V. Anand, H. Kansal, and A. Singla, "Some aspects in bond graph modeling of robotic manipulators: Angular velocities from symbolic manipulation of rotation matrices," Technical Report, Department of Mechanical Engineering, Sant Longowal Institute of Engineering and Technology, 2003.

[5] H. M. Paynter, Analysis and Design of Engineering Systems. MIT Press Publishers, Cambridge, 1961.

[6] D. C. Karnopp, D. L. Margolis, and R. C. Rosenberg, System Dynamics;A Unified Approach. John Wiley and Sons Publishers, Newyork, 2nd ed., 1990.

[7] P. Breedveld, "Bond graphs," in Encyclopedia of Life Support Systems, Modeling and Simulation, 2003.

[8] O. M. Muvengei, "Design of an excavating mechanism to be used with juja diesel tractor jk01," Design Innovation, Department of Mechanical Engineering, J.K.U.A.T, 2006.

[9] A. Koivo, "Kinematics of excavator (back hoe) for transfering surface materials," Journal of Aerospace Engineering, vol. 7(1), pp. 7–31, 1994.

[10] J. Y. Luh, M. W. Walker, and R. P. Paul, "On-line computational scheme for

mechanical manipulators," Journal of Dynamic Systems, Measurement and Control, vol. 120, pp. 69–76, 1980.

[11] A REVIEW ON KINEMATICS OF HYDRAULIC EXCAVATOR'S BACKHOE ATTACHMENT, Bhaveshkumar P. Patel et al. / International Journal of Engineering Science and Technology (IJEST) Vol. 3 No. 3 March 2011

.

CHAPTER 5

Complete Model

A model has been developed for the simulation of vehicle behavior. Figure 5.1 depicts the complete model as it is in the present stage of model development. As it can be seen the model thus far represents and deals with the upper carriage system. The model is represented in three sections, the first section comprising of the pump model, the second section of the valve blocks and pressure feedback logic and the third section representing the rigid body linkage. As part of the present stage of model development, the pump and kinematics model have been linked together, using valve blocks and pressure compensated flow control valves with ideal characteristics. The pressures across all actuator ports have been compared to provide the maximum load at any instant of time to provide the LS pressure to the FC. The actuators in this model are linear actuators and have been modeled as components which include pressure dynamics in the volumes on either side of the piston, viscous friction, and leakage past the piston. In future work, detailed models of the valve block with compensators and actuators will be included to recreate the complete functioning of the system.

Model Capabilities

The developed models capabilities would describe the dynamics of the complete excavator in terms of:

1. Pump Swash Angle – the dynamic position of the swash plate that is identified by first order equations that balances the system pressure and the actuator pressure to define the swash plate position.
2. Flow characteristics of the pump - The flow out of the pump would account for the internal leakage through the fixed orifice which would define the leakage of the pump and in this way would describe the actual flow output from the pump.
3. Pump Pressure dynamics – The systems pressure dynamics is defined by the pressure rate rise equation.
4. Pump Flow compensator dynamics – The flow compensator dynamics provide information of the instantaneous spool position. The LS pressure and System pressures. Spring compressibility, displacement and position. Flow through the damping orifice. Flow and pressure characteristics into and out of the intermediate chamber.
5. Pump Pressure compensator dynamics - The pressure compensator dynamics provide information of the instantaneous spool position. System pressures. Spring compressibility, displacement and position. Flow through the damping orifice. Flow and pressure characteristics into and out of the intermediate chamber.
6. Valve Main Spool – the dynamic position of the main spool and it's characteristics of inlet orifice and meter out orifice.
7. Flow characteristics of the valve - The flow through the different chambers of the valve would account for the internal leakage through the main spool and pressure compensator. This would define the actual flow output from the valve.
8. Valve Pressure dynamics – The systems pressure dynamics is defined by the pressure rate rise equation and describes the pressure characteristics in the different chambers of the valve.
9. Valve Pressure compensator dynamics – The pressure compensator dynamics provide information of the instantaneous spool position. The LS pressure and System pressures. Spool displacement and position. Flow through the damping orifice. Flow and pressure characteristics into and out of the intermediate chamber and the bridge.
10. Valve Piston Check Assembly - The piston check assembly provides information of the instantaneous spool position, the bridge pressure used to displace the piston check assembly. System pressures. Spring compressibility, displacement and position. Flow and pressure characteristics from the bridge chamber.

11. Valve Intermediate chamber pressure – The dynamics of the intermediate chamber pressure between the main spool and pressure compensator can be determined.
12. Valve Spool Meter out - The dynamics of the meter out flow to tank can be determined as the work port drains the pressure and flow compensator and the control piston chamber can be determined.
13. Valve Load Sensing Signal – The dynamics of the LS signal can be determined and is fed back to the pump to stroke/destroke the pump.
14. Kinematics Implement instantaneous positions and velocities – the dynamic position of the main spool and it's characteristics of inlet orifice and meter out orifice.
15. Soil Interaction Model - The flow through the different chambers of the valve would account for the internal leakage through the main spool and pressure compensator. This would define the actual flow output from the valve.
16. Force on the actuators – The systems pressure dynamics is defined by the pressure rate rise equation and describes the pressure characteristics in the different chambers of the valve.
17. Pressure dynamics on the actuators – The pressure compensator dynamics provide information of the instantaneous spool position. The LS pressure and System pressures. Spool displacement and position. Flow through the damping orifice. Flow and pressure characteristics into and out of the intermediate chamber and the bridge.

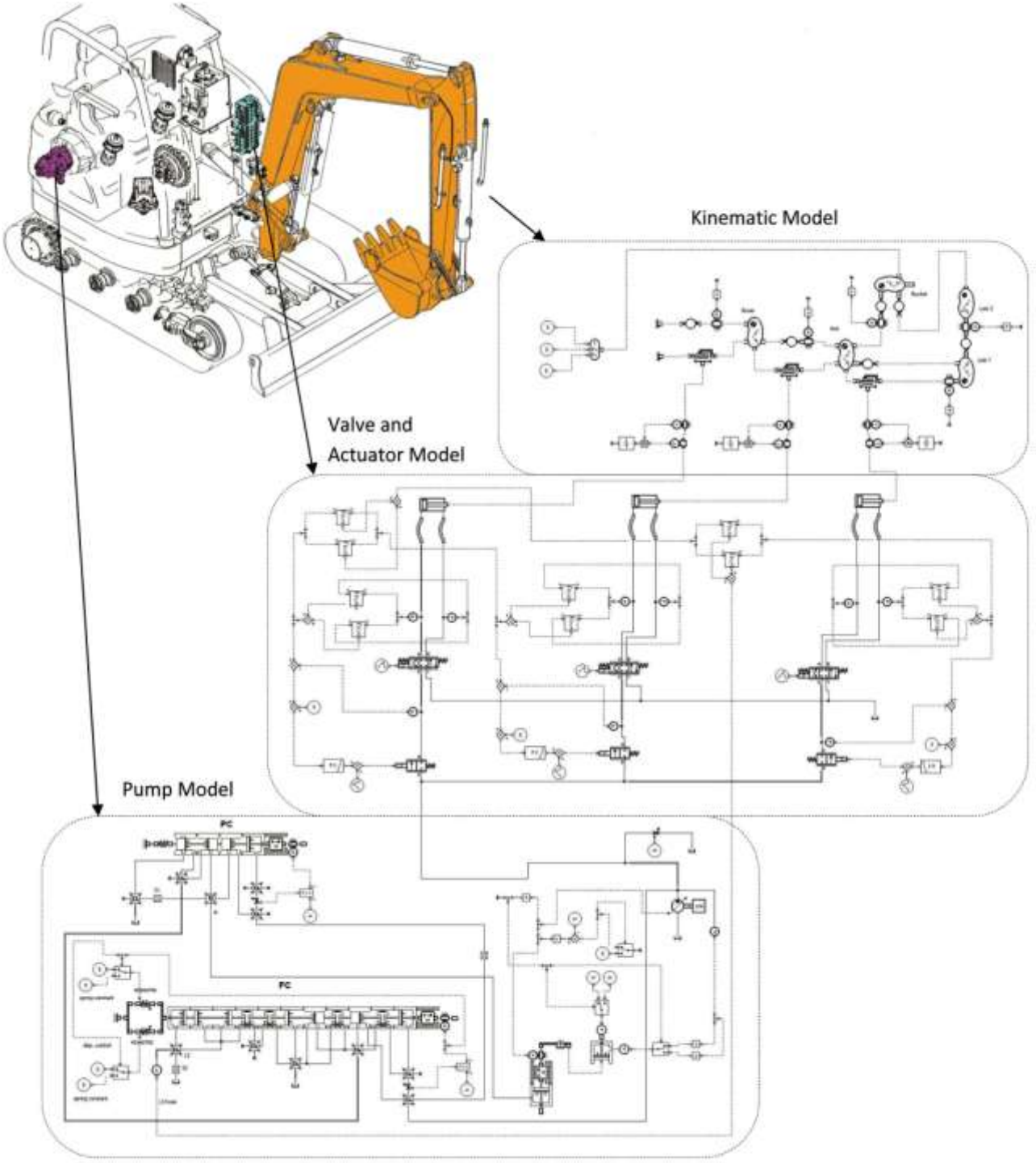

Figure 5.1. Overview of the Complete Model

CHAPTER 6

Experimental Setup

This chapter describes the experimental setup and the tests carried out to validate the different component models of the excavator that were devloped in the preceding chapters.

6.1 Scope of the Experiments

The objective of the experimental work carried out was to provide all data necessary for the completion of the simulation models. The different components that were validated were:

1. Flow Compensator
2. Pump MVP 60 – Flow Characteristics Identification
3. Pump with Pressure and Flow Compensator – MVP 60
4. Valve DPX 100 – Single Slice
5. Pump MVP 60 and Valve DPX 100
6. Valve DPX 100 – Two Slices

6.2 Laboratory Instrumentation

6.2.1. Test Bench

The test bench set up at the Laboratory of the Department of Industrial Engineering of Parma is an advanced test facility available for testing of hydraulic components and systems. The test facility has an integrated control and data acquisition device for complete physical parameter characterization related to hydraulic studies – such as pressure, flow, temperature, torque etc.

One of the major advantages of the test bench is a DC motor that is used to drive pumps for tests as well as motors. The DC electric machine can work on 4 quadrants and can provide high torques at low rotational velocities making it idea for pump/motor testing. The working interface of the test bench (Figure 6.1) has 3 suction lines and 4 free lines to tank. The test bench also has two ports connected to a flow meter and a pressure relief valve. For specifics the work port TC1 is a line of exhaust flow with a flow meter to measure flows of 150 l/min and a pressure relief valve to pressurize the line simulating loads of any kind; the work port TC2 has the same functionality but with a flow of 80 l/min. Inside the test bench there is a provision for a pressurised flow source. This is achieved through another electric motor 4-pole three-phase (Figure 6.2a) coupled to a an axial piston pump.

The functioning of the test bench is controlled by a control panel integrated with a personal computer with a specific software for data acquisition of the data for the sensors. The data acquisition modules are available for different sensor outputs. Apart from data acquisition it is possible to manage accurately the functioning of all the parameters of the functioning of the test bench such as the direction of rotation of the principle motor, the flow of the internal pump and opening and closing of the tank and pressure lines.

The oil used in the test bench is temperature regulated by a heat exchanger which monitors instataneously the temperature of the fluid and maintains it at a certain range. In this way

the fluid temperature can be maintained constant to limit the influence of the viscosity. There is a thermocouple inside the test bench that measures the tanks oil temperature and uses a series of resistance coils or a refrigeration cycle to maintain the fluid temperature (Figure 6.3).

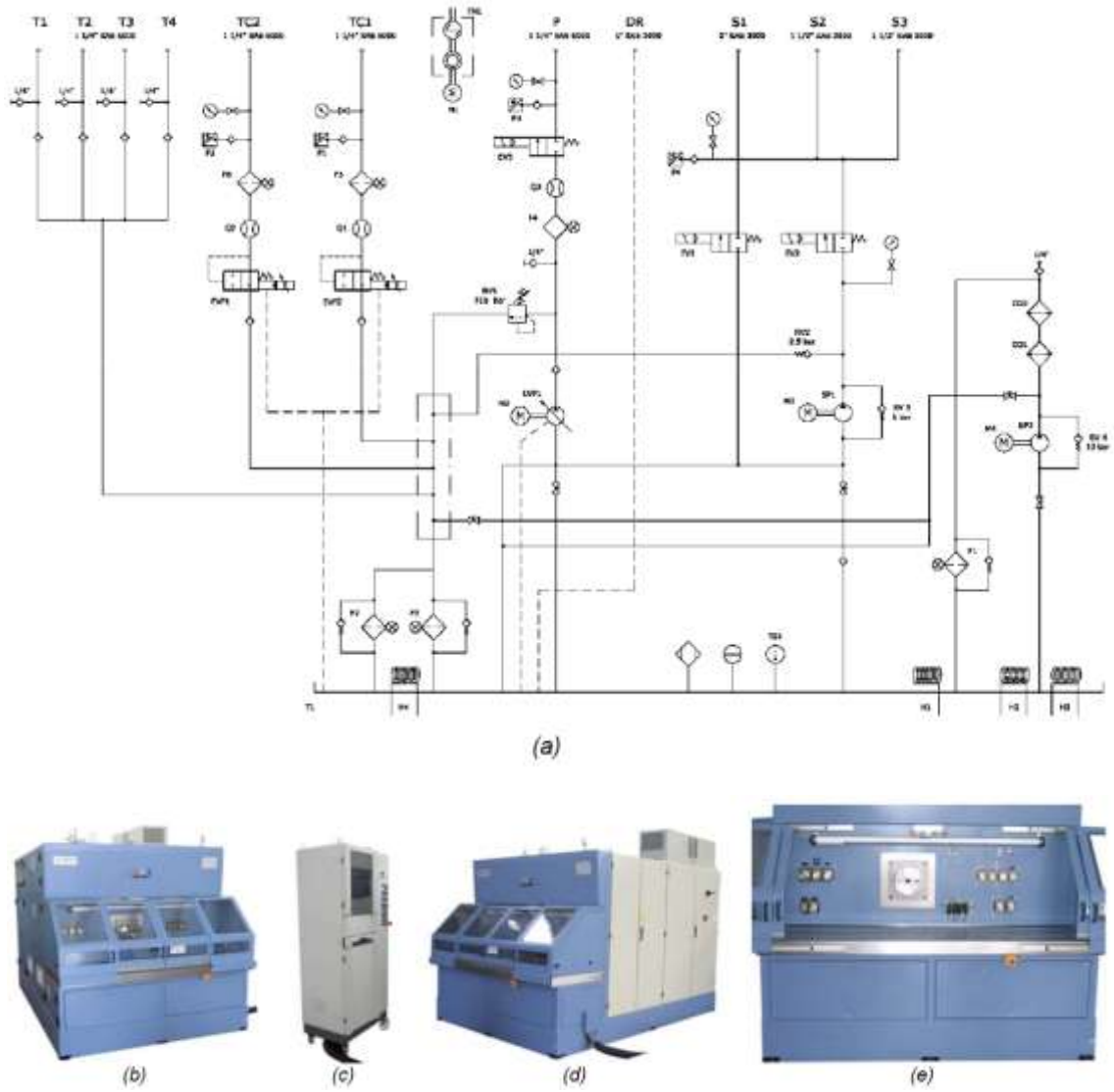

Figures 6.1 Test Bench for Hydraulic Components: a) ISO Circuit Schematic, b) front view of the test bench, c) Control Panel, d)Side view with electric control panel access, e) Details of the test bench .

(a) (b)

Figure 6.2 – (a) Sensor to measure oil temperature int eh tank; (b)Heat Exchanger.

To carry out tests to characterize components the internal pump inside the test bench can be used to provide a fluid power source (P) (please refer Figure 6.3a). This is achieved by an axial piston pump driven by an electric motor with a 75 KW capacity. Figure 6.3a depicts the pump inside the test bench.

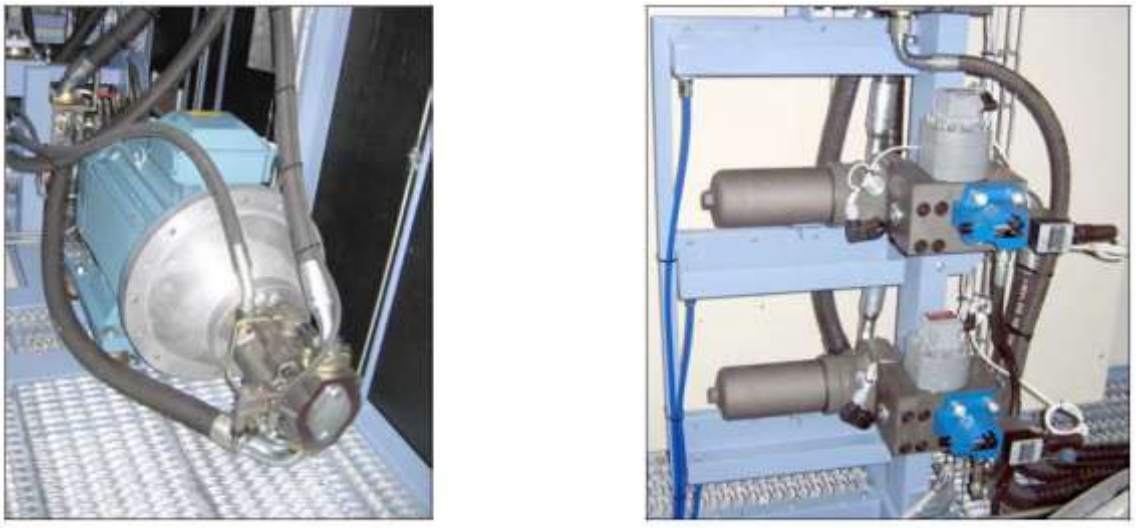

(a) (b)

6.3 a) Motor electric ABB, b)Pressure filters with connected flow meters

The presence of the filters in the test bench are for eliminating particles that could possibly damage the test components. Figure 6.4 illustrates the complete pump located inside the test bench with the ATOS PVPC controller.

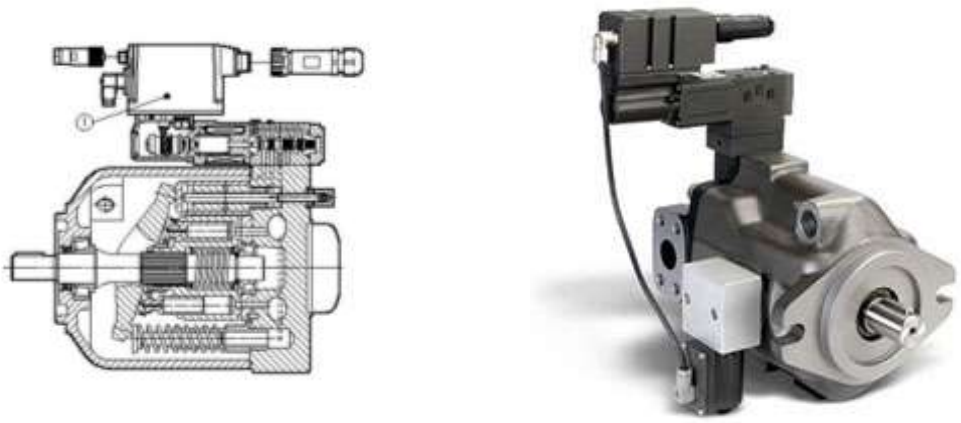

Figure 6.4 Describes the flow characteristics of the LVP 75. The curves are obtained ata d temperautre of 50 °*C* at an oil visccosity of 36 mm^2/s.

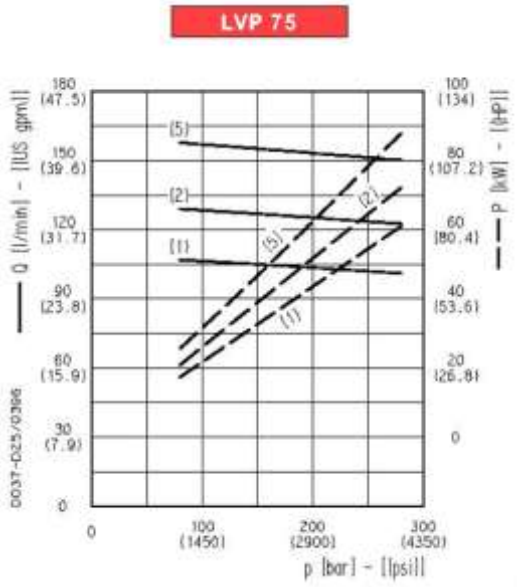

Figure 6.5 – Characteristic curves of the LVP 75 at 1500 r/min (1), a 1800 r/min (2), a 2200 r/min (5).

Tabel 6.1: Principle details of the test bench.

Caracterstics	*Specific*
Installed Power	*456 KVA – 160 kW*
Current Rating	*775 A*
Electric Motors	*M1, M2*

Motor M1	*ABB® DC, 75 kW, 4 quadranti*
Motor M2	*ABB® 4 Pole – 50 Hz*
Rating of Motor M2	*37 kW*
Rotatiotional Velcoity M2	*0 ÷1600 rpm*
Motor Control M2	*VFD*
Pump – P	*CASAPPA® Plata LVP 75 a cil. variable*
Pump Regulator	*Atos PVPC proporzionale elettroidraulica*
Maximum Flow	*140 l/min*
Displacement	*0 ÷ 83 cm^3*
Flow	*0 ÷ 140 l/min*
Pressure Relief Valve	*315 bar*
Maximum Pressure	*350 bar*
Maximum Flow	*150 l/min*
Inline Pressure Filter	*IKRON da 10 micron*
Inline Pressure Filter	*IKRON da 25 micron*
Pressure Sensor P1	*WIKA®, 0÷40 bar, accuratezza 0.25% FS*
Pressure Sensor P2,P3,P4	*WIKA®, 0÷400 bar, accuratezza 0.25% FS*
Flowmeter	*VSE® VS1, 0.05÷80 l/min, accurat. 0.3% v.m.*
Torque meter	*HBM® T, 0÷500 Nm, velocità limite 12000 r/min, classe accuratezza 0.05*
Encoder incremental	*HEIDENHAIN® ERN120, 3600 imp/r, limite 4000 r/min; accuratezza 1/20 del periodo*
Fluid Type	*Olio minerale ISO VG 46 – HVLP*
Temperature	*38 ÷ 42 °C*
Tank Capacity	*430 l*
Heat Exchanger	*Aria – Olio HPA 50/2 compact*
Portata di raffreddamento	*7450 m^3/h*
Massa totale a secco	*5000 kg*

6.2.2 Acquisition of Data and Transducers.

The test bench is controlled by a PC with a specific software to manage the programming and experimental testing on the test bench. The software permits a visualization and monitoring in real time of all the relevent data (Figure 6.6). It is possible to carry out certain acquisitions in the manual mode. In the automatic mode complete cycles can be programmed and the data acquired. At the end of the acquisition the measured data is

available as a text file for post processing. The data is acquired by the DAQ boards available on the controller with a maximum capability of acquisition of 32 channels.

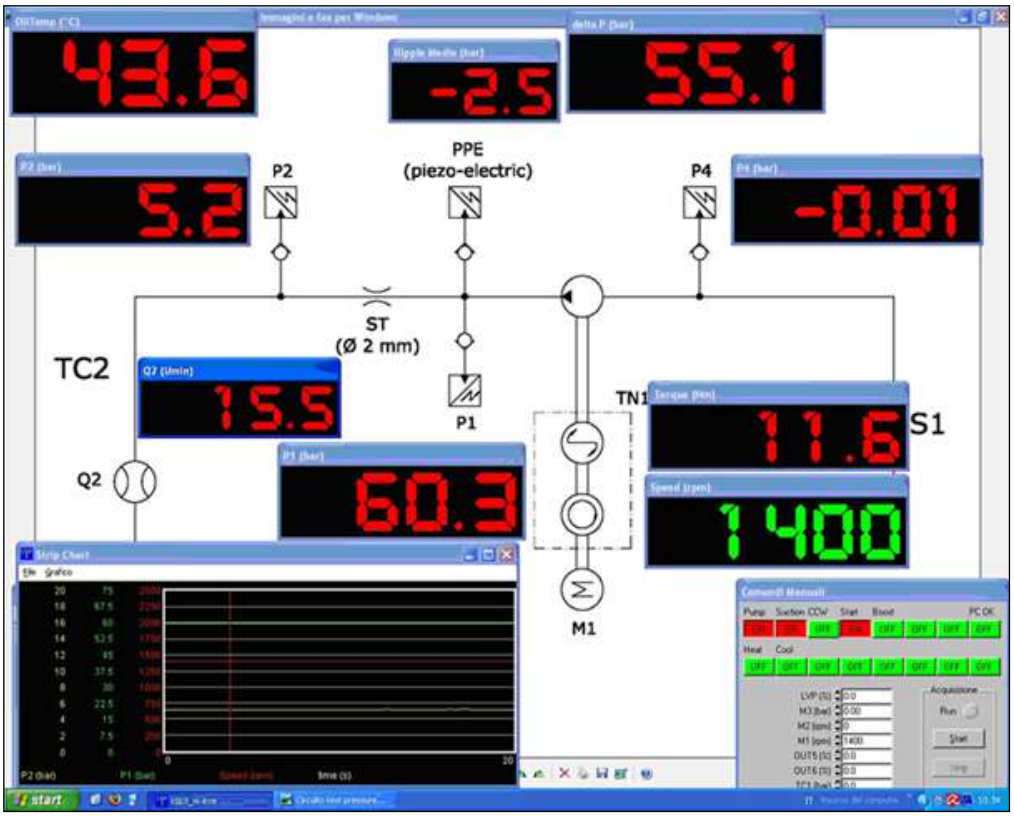

Figure 6.6 – Screenshot of the Acquisition software.

The acquisition interface (Figure 6.6) comprises of a system of signal conditioners and amplifiers. Manufactured by Electrostudio®, each electronic board provides an output of 24 V to power the transducers. The different boards available have the capacity to measure 0-10 V, 0-20 mA, 0-3 A, 0-50 V, Digital Signals and Thermocouple. There is a National Instruments® DAQ which is used to collect the data from the electronic DAQ boards. The PC with the installed software carries out the final processing of data and outputs all the data channels in the form of a text file (*.txt). Figure 6.7a represents the sensor connection with the PC of the test bench. In more detail we can observe Figure 6.7b, where the signal conditioning system and amplification of the transducer signals. Figura 6.7c illustrates in detail the acquisition scheme of the PCI installed in the computer.

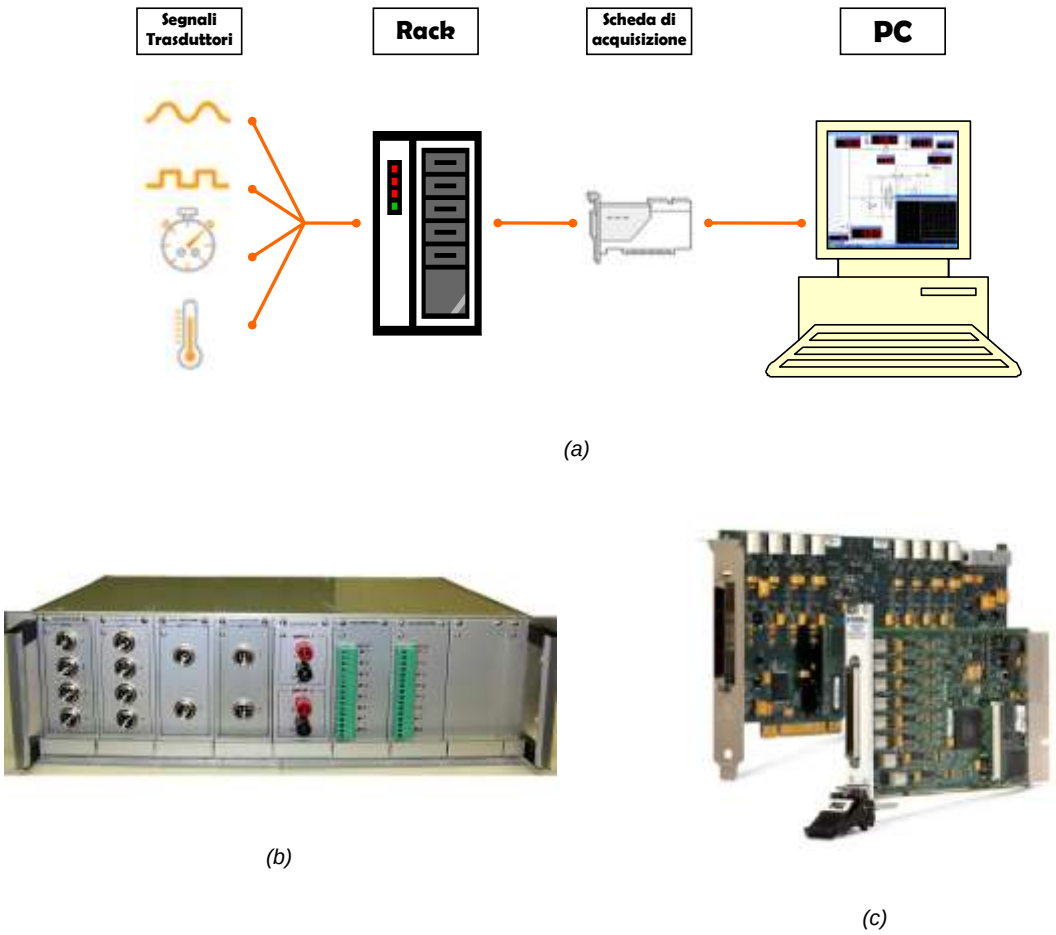

Figure 6.7 – (a) Schematic of the acquisition circuit; (b) Signal conditioning unit from Electrostudio®;(c) Acquisition board PCI National Instruments®.

The measurement of pressure is by an extensometric pressure transducer WIKA® S-10, with a range of 0 to 400 *bar* used on the lines TP1,TP2 and TP3 of the test bench. While the line T4 is fitted with a low pressure transducer 0 to 40 bar. These are powered by the Signal conditioning unit, and give out a signal of 4 to 20 mA depending on the pressure value. This value is converted to a voltage value of 0 to10 *V* which is then acquired by the National Instruments® board. The functioning of the pressure tansducer is based on the principle of the "strain-gage". A variable resistense effected by deformation and positioned on a membrane inside the sensor. The pressure, deforms the membrane and varies the

voltage due to the change in resistance which is measured through a Wheatstone bridge. Figure 6.8 reports an illustration of the pressure transducer.

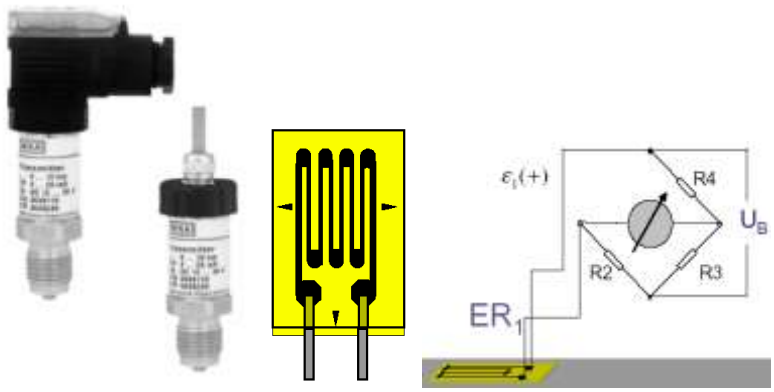

Figure. 6.8 – Pressure transducer WIKA®.

The measurement of flow is carried out by a volumetric flow measurement of a gear flow meter VSE® - VS 1 e VS 2, respectively from 150 *l/min* and from 80 *l/min* of maximum flow. Its functioning is analogous to an encoder. It measures with extreme precision the flow of the flowmeter. It is sufficient to measure the frequency of rotation per minute to determine the flow. A digital frequency signal is the output from which is then converted by the DAQ board to a 0-10V value and is then processed by the National Instruments®. Figure 6.9 illustrates an image of flow measurement; figure 6.10 is a graph that represents the leakage caused by load.

Figure 6.9– Flow Meter VSE®.

(a)

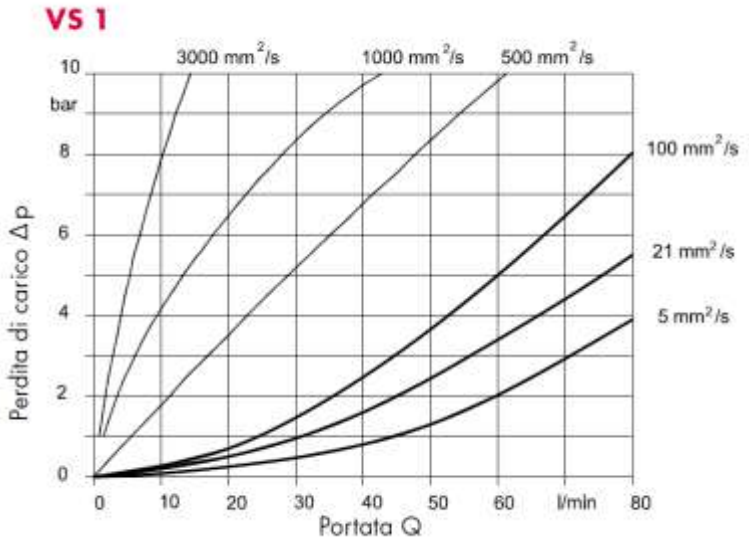

(b)

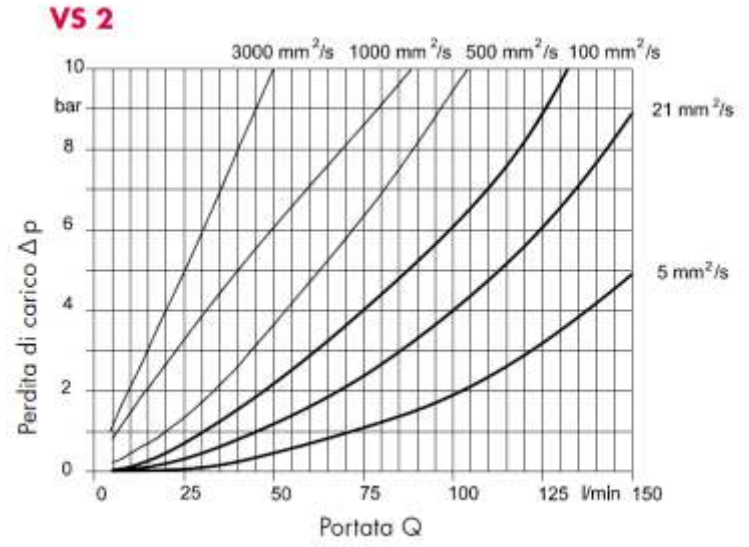

Figure 6.10 – Graph of flow-loss of load for the flow meterVSE®

The measurement of Torque and angular velocity is through a torsionmeter with encoder HBM® T10. The torque measurement is the range of 0 to 500 *Nm*, with a roational frequency of 12000 *r/min* Figure 6.11.

(a) *(b)*

Figure 6.11 – Torsiometro-encoder HBM® T10.

The measurement of temperature is very important in the test bench to gaurantee that the viscosity is maintained through out a test. This has been carried out in accordance to the norms UNI ISO 4409/90. The measurement of temperature is by a thermocouple Pt 100

To conclude the description of the instruments we describe the linear position transducer – LVDT. This is produced by Magnet Shulz and has a wet core so that it can be integral with the setup and allows for hydrostatic balancing of the moving core. The functioning of the LVDT is that a change in voltage is measured by the displacement of the moving core against the secondary windings. The output of the LVDT has the capability of providing an output of 0-10V or 4-20mA.

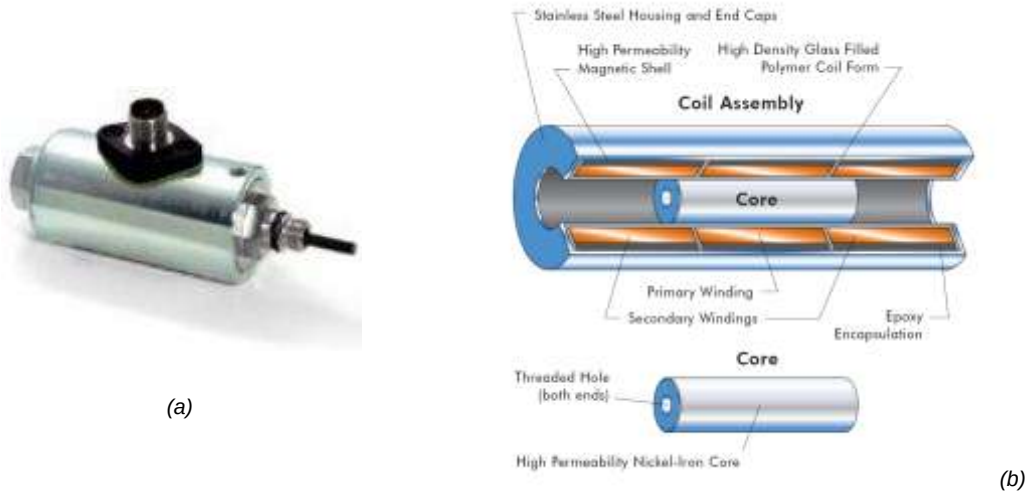

Figure 6.12 – (a) LVDT; (b) Functional descriprion.

6.3 Experimental tests on the Flow Compensator

6. 3.1 Circuit Configuration

Experimental tests were carried out on the Flow Compensator in order to obtain a complete steady state characterization. Tests have also been made to study the dynamic response using a step response. To carry out these tests two manifolds were machined such that the lower block allows the input pressure at the P ½ BSP threaded connection, which connects the pump line of the inlet of the manifold (Figure 6.13). The inlet line P replicates the pumps behaviour as though the flow compensator were mounted on it. The pressure reading on the pressure line is made accessible through a threaded hole which is ¼ BSP made on the left side of the upper manifold. The inlet pressure enters into the pressure inlet chamber of the flow compensator after which it causes the displacement of the spool against the flow compensator's spring setting and the LS pressure. The intermediate chamber of the flow compensator was connected to a connector that was left open to atmosphere so that the intermediate flow could be measured with a measuring jar. A flow control valve was used to create the load on the system.

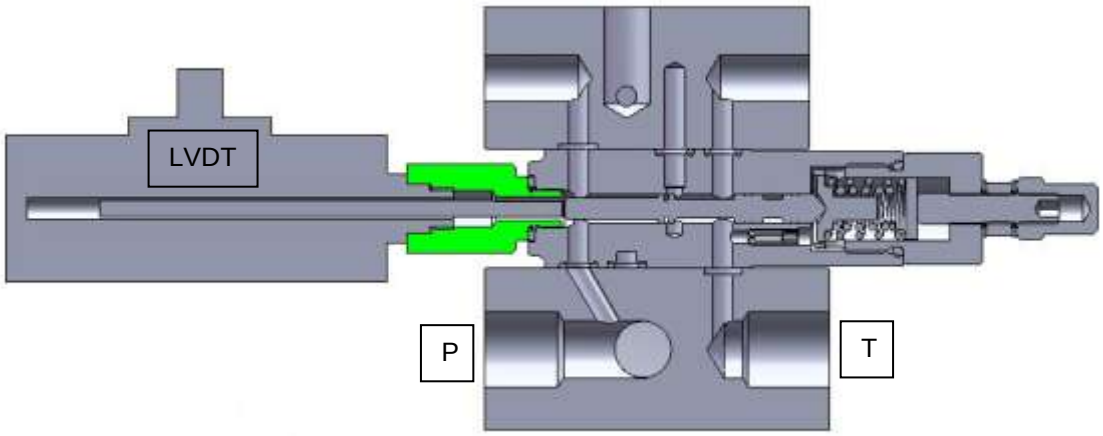

Figure 6.13 Flow compensator mounted on the manifolds

An LVDT was directly integrated with the flow compensator's spool to measure the spools displacement. Initially various types of adhesives were used to connect the LVDT's spool with that of the Flow Compensator. This method was found to be good for steady state tests but in the course of dynamic tests it was found that the LVDT got detatched from the flow compensator. To resolve this problem it was decided that the flow compensators spool be drilled and tapped such that the LVDT could be directly threaded to the flow compensator. The use of the LVDT in the testing cycle required the construction of a connector that would allow one end to be connected to the sensor and then other to the valve body. The figure describes the parts involved in connecting the LVDT with the flow compensators spool.

Figure 6.14 Parts of the assembly LVDT and flow compensator's spool

6.3.2 Component Calibration

An important step in the calibration of some components of the circuit. First it was necessary to set flow compensators pressure setting by adjusting R (Figure 6.12) of the valve. The R value was set to a value of 20 bar. The voltage signal output from the LVDT sensor which would be acquired by the PC of the test bench has been appropriately modified to express the instantaneous position of the valve spool. The following mathematical relationship has been adopted to set the value of the LVDT to exactly determine the flow compensators position:

$$\text{LVDT} = 3.75 \cdot (\text{Input Signal} - 8.018)\ [\text{mm}] \quad (6.1)$$

During the experimental tests two manual flow control valves were used to control the flow and set the working conditions of the valve. That of larger size (Figure 6.15a) was inserted in the circuit on the discharge line passing through the lower manifold, to play the role of the orifice in a load sensing circuit (highlighted in blue in Figure 6.18), after the flow control valve a line was tapped to connect to the LS line of the flow compensator and in this way the circuit was recreated. The smaller flow control valve (Figure 6.15b) was inserted on the line of the intermediate chamber so to recreate the situation of pressurization of the chamber of the actuator control of the swash plate. The flow characteristics of the flow control valve being fairly complex and nonlinear it was decided to map it's characteristics of flow versus number or rotations and insert these characteristics directly in the AMESim modeling environment, in this way the flow control valves could be recreated. (Figure 6.16 and 6.17).

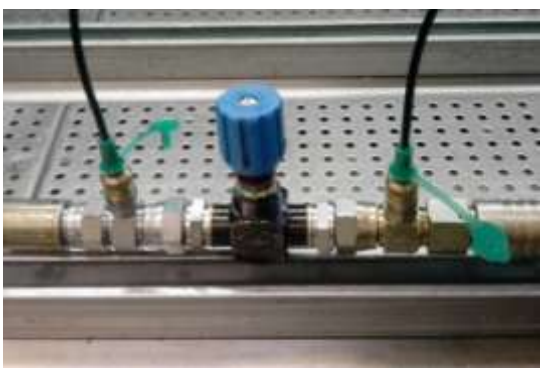

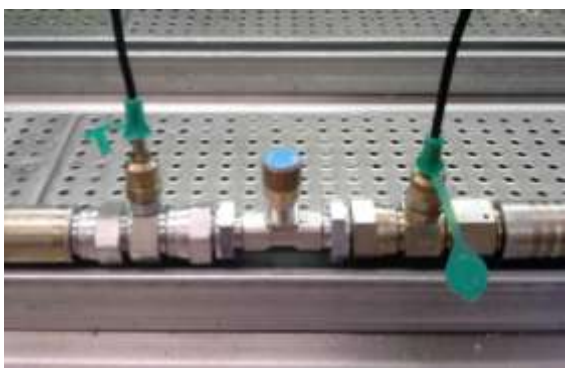

a) *b)*

Figure 6.15 Characterisation of the flow control valves on the test bench

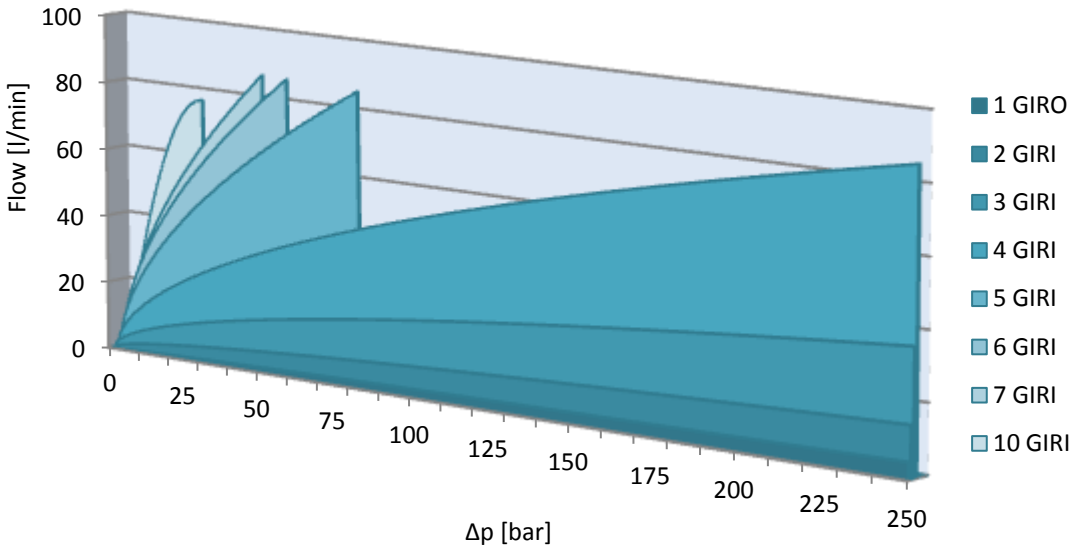

Figure 6.16 Characteristics of Flow vs Delta p for Figure 6.15 (a)

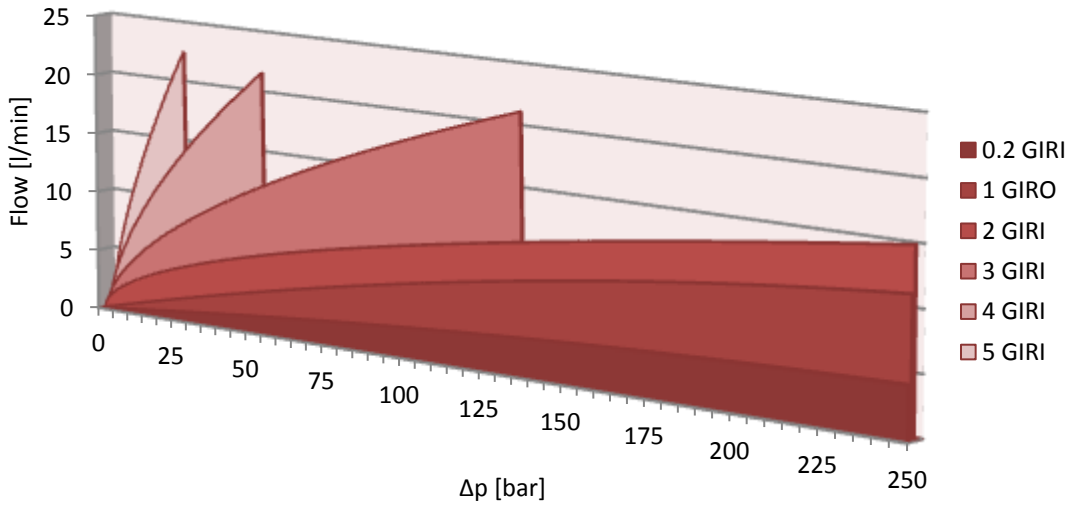

Figure 6.17 Characteristics of Flow vs Delta p for Figure 6.15 (b)

6.3.3 Steady State tests

The circuit implemented on the test bench as illustrated in Figure 6.18 has facilitated the test to be carried out in the following manner, that starting from the PC the flow line P can be controlled and set. The system could then be loaded by the manual flow control valve position to set the flow compensators spool position. For each position the following parameters were acquired - the values of Δp, the spool position, position of the manual flow control valve and the flow out of the intermediate line I.

In Figure 6.18 it can be seen that the intermediate line I is left open. This is due to the fact that the leakage flow rate through this chamber was too low to utilise the test benches flow meters. These tests were then carried out by using a a graduated container and a stopwatch. The tests were repeated for the entire stroke of the slider and have been repeated for different flow values, the results are reported in Chapter 8.

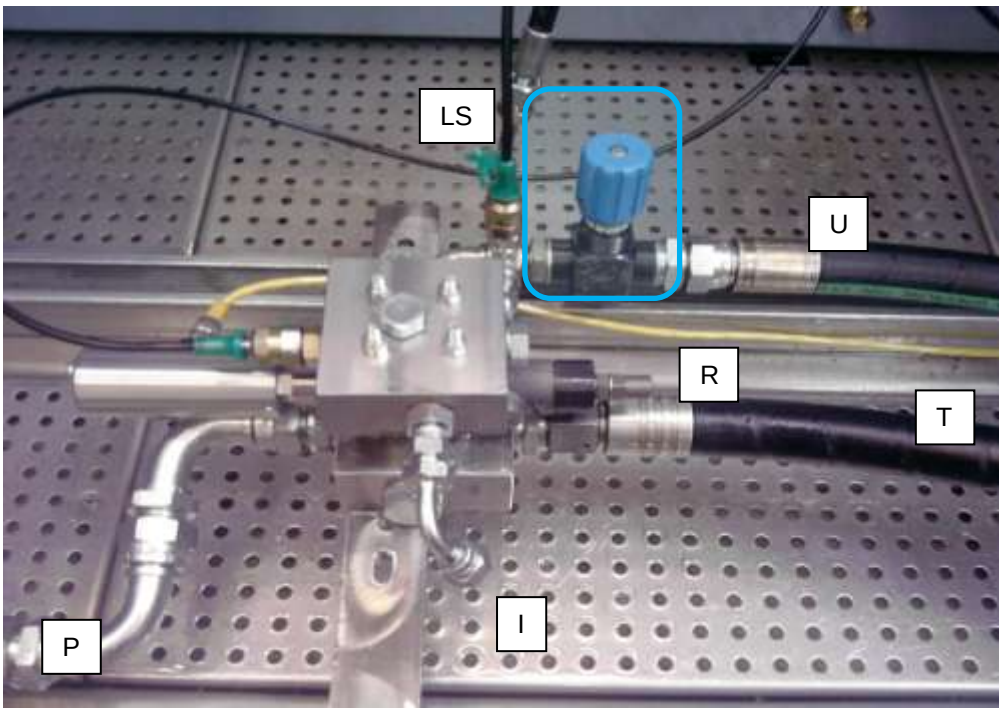

Figure 6.18 Circuit for the experimental tests of the flow compensator

6.3.4 Dynamic Test

The dynamic tests were done by acting on the line U (Figure 6.18) with the relief valve of the test bench, with a feedback-control the line. It has thus generated a load pulse, ie a sudden increase in pressure. In Figure 6.19 is shown for clarity the pressure curve on the line for a test in which the pressure generated on the line U has been a load of 120 bar from an initial condition of 30 bar.

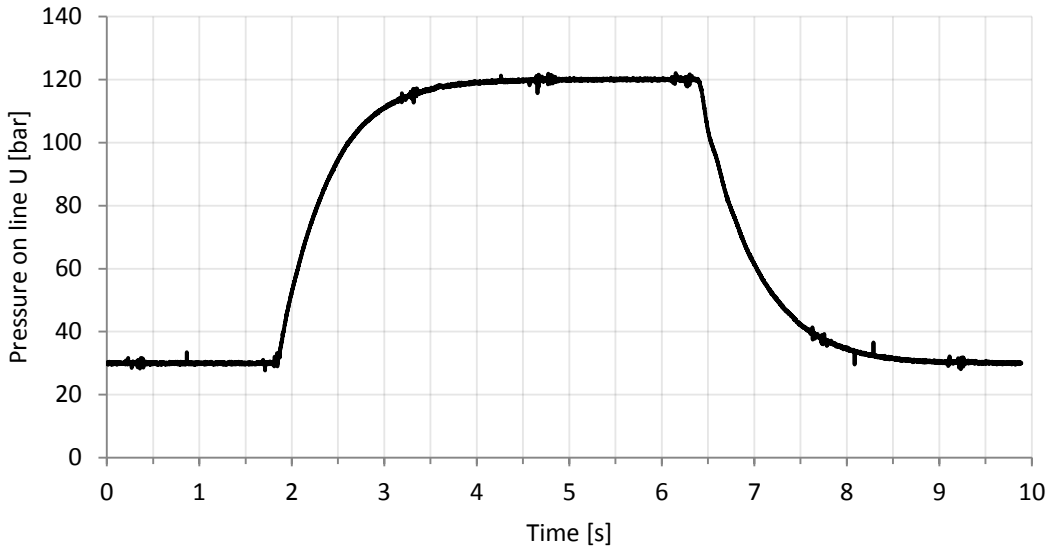

Figure 6.19:Generation of a load for input to the model

6.4. Experimental tests on the CASAPPA® MVP 60

The experimental work carried out on the axial piston pump tests were conducted in three different circuit configurations.

1. To collect a data set sufficient to complete the composition of the simulation model of the machine in AMESim ®.
2. To reproduce the actual operation of the pump so that the acquired data could validate the model.
3. Dynamic test of the pumps response in Frequency

6.4.1 Steady State Tests

The main components of this test stand are the variable displacement axial piston pump P, flow compensator FC, pressure compensator PC, ball valve and the prime mover which is a DC motor. The LS signal is tapped from the output of the ball valve and is measured using sensor P3. The actuator for controlling the swash plate is controlled by the FC/PC valve and the swash plate position is measured using an LVDT. The use of an LVDT to derive an angular value is justified by the fact that in this case, the curvature of the arc representing the swash plate rotation is extremely large and can be represented as a straight line. The system load is generated by a proportional relief valve, rated for 315 bar maximum pressure with a capacity to control the pressure for an inputted constant or mathematical function. The schematic diagram of the hydraulic circuit of the test facility is as depicted in Figure. 6.20 and the instrumentation used on the system is summarized in Table.1. Figure 6.21 is a photograph of the pump mounted on the test facility. The test rig is also equipped with an off line circuit (not represented in Fig.6.20) for oil temperature control, constituted by a system of heat exchangers, electronically regulated over a specified working temperature.

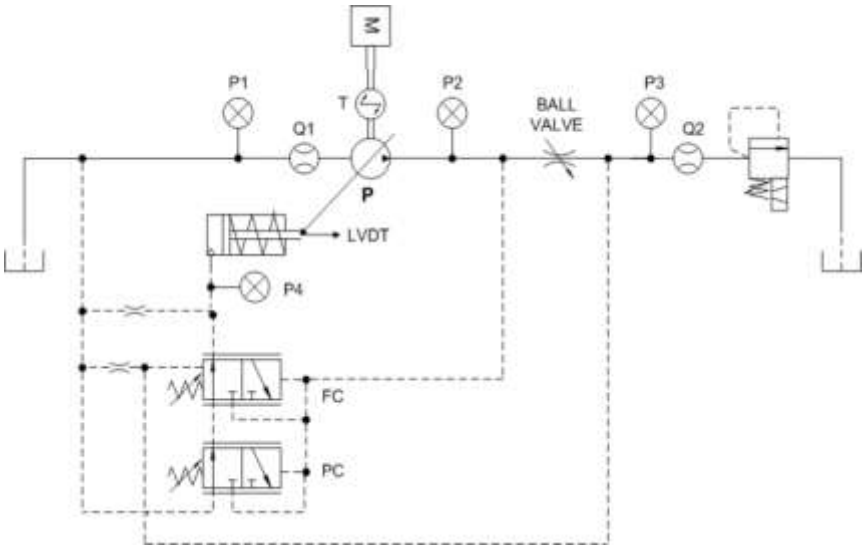

Figure 6.20: ISO Schematicof the first LS Pump test setup

Initially the pump was mounted on the test bench in a classical configuration with the load-sensing circuit connected (Figure 6.20). In some experiments the standard pressure compensator was replaced with the proportional solenoid MC10T pressure compensator produced by Walvoil. The MC10 has the same function of a standard pressure compensator except for the aspect of remote controllability. The pump is mounted on the main shaft and is driven by the motor M1, a manual ball valve has been inserted in the pump flow line and the signal at the outlet of the ball valve has been tapped to provide the LS signal. The flow in and downstream of the pump suction valve are also measured. Pressure transducers were mounted at the inlet and outlet of the ball valve in this manner the ball valves orifice area can be accurately characterised being a function of the differential pressure and flow.

It was necessary to study the and characterize the pump and to identify the pressure in the control actuator control of the swash plate. To achieve this a manifold was made such that it could be placed between the flow compensator and the pump housing interface.

A WIKA pressure sensor S 10 was connected to the line of interest. Of this manifold, shown in Figure 6.21 and shown in Figure 6.22 (item 2), Finally, the FC and the swash plate pump were also instrumented with two LVDT position sensors.

The preliminary phase involved the two valves PC and FC and the two position sensors. The maximum pressure relief valve was set to a value close to 300 bar while the setting of the FC was set to a value of 17 bar. The calibration of the LVDT sensor mounted on the valve FC had been made for the previous tests (Eq. 6.1), while for the LVDT sensor pump was necessary to insert a different equation that was to be derived by carrying out tests and determining the values of the swash plate at maximum and minimum inclination of the swash plate to define the range of the output signal, this is done using a simple linear relationship has allowed us to obtain the information directly in degrees

$$\theta = (Input\ signal - 2.28) * 3.732 \qquad (6.2)$$

Figure 6.21: of the pump mounted on the test rig

Table. 6.2. Features of sensors and main elements of the apparatus used in the present research

Sensor	*Type*	*Main features*
M	Prime mover	ABB®, 4-quadrant electric motor, 75 Kw
P	Pump	CASAPPA® MVP60, 84 cm^3/r
P1	Strain gage	WIKA®, Scale: 0..40 bar, 0.25% FS accuracy
P2 – P3 – P4	Strain gage	WIKA®, Scale 0..400 bar, 0.25% FS accuracy
Q1, Q2	Flow meter	VSE® VS1, Scale 0.05..80 l/min, 0.3% measured value accuracy
T	Torque/speed meter	HBM® T, Scale: 0..500 Nm, 12000 r/min Limit Velocity, 0.05 Accuracy Class
θ	Incremental encoder	HEIDENHAIN® ERN120, 3600 imp./r, 4000 r/min Limit velocity, 1/20 period accuracy

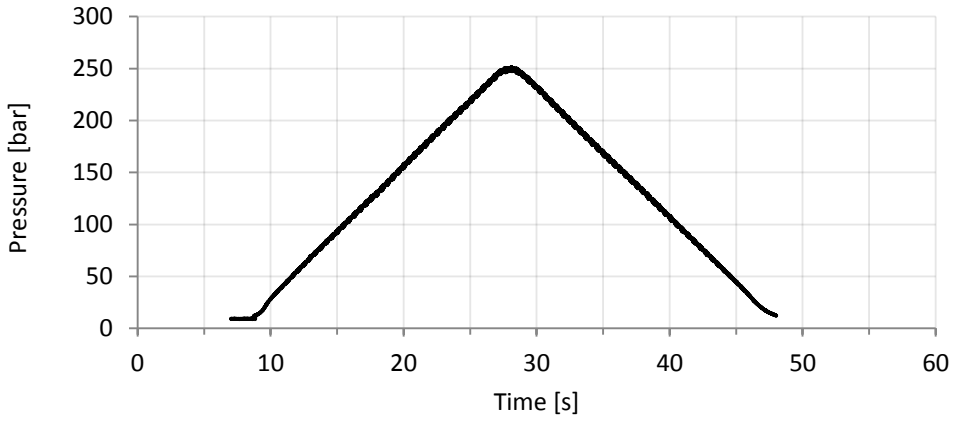

Figure 6.22: Pressure cycle maintained during the test

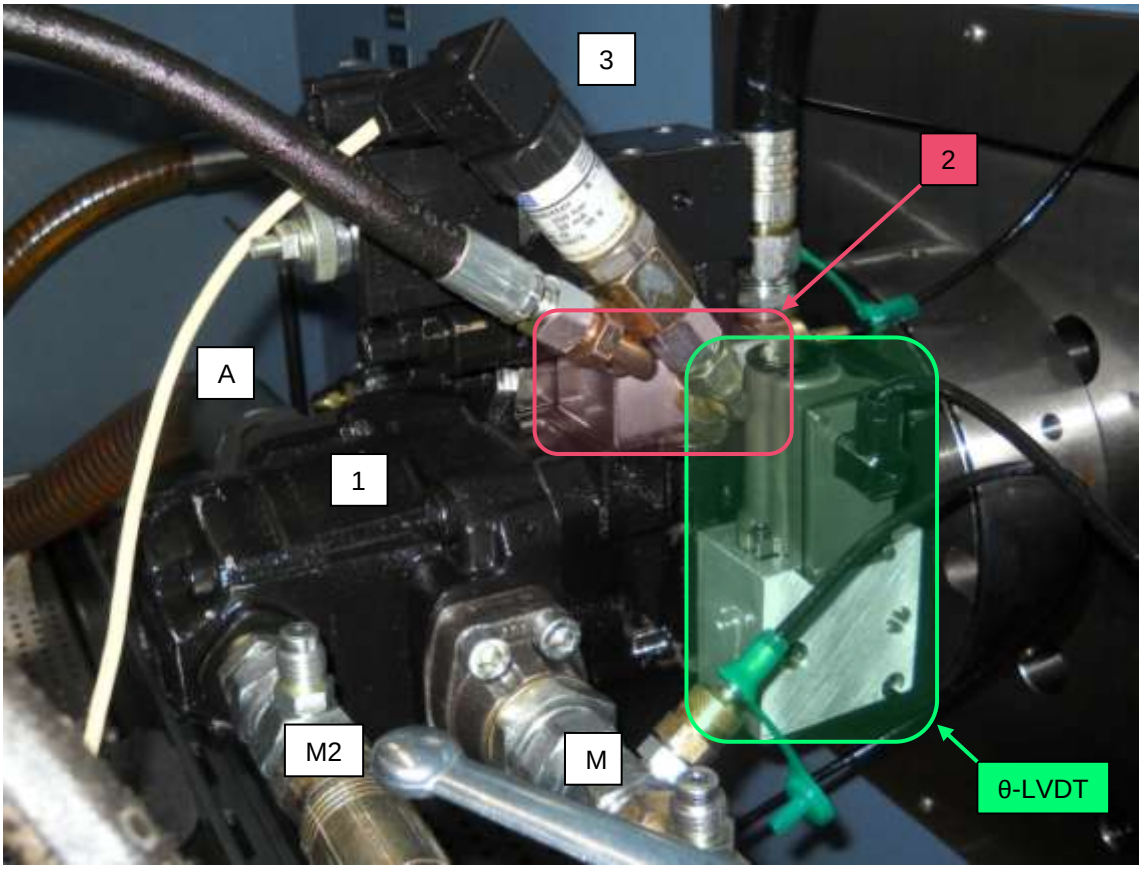

Figure 6.23: Details of instrumentation on the CASAPPA MVP60

The tests performed on the pump were carried out at variable load cycles (Figure 6.22) and in different working conditions in terms of speed. It was intended to capture the values which varied the pressure of the pump and pressure control actuator, as has already been

explained. The initial goal was to build a three-dimensional map to be included in the model built in AMESim ® such that, reading the values of the pump discharge pressure, pressure control actuator and speed of rotation the sub-model of the pump would be able to determine the swash angle, ie the swash plate (Figure 6.23). The tests were initially performed for a rotation speed of 1000 rpm starting from different angles of inclination of the swash plate (steps of 1° over the entire range of variation from 0 to 21°), obtained by placing the fine throttle valve at the outlet of the pump. These tests have allowed us to collect the initial data to construct a three-dimensional map, and have provided the background to understand the real functioning of the pump.

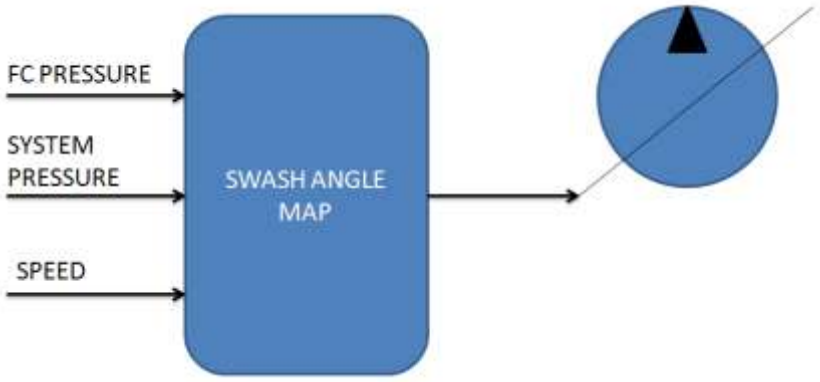

Figure 6.24 Initial modeling methadology

The second round of tests were carried out using a different circuit configuration, capable of performing cycles of zero displacement of the pump to vary the speed and delivery pressure. This was achieved by feeding the solenoid Walvoil MC10T placed above the compensator range.

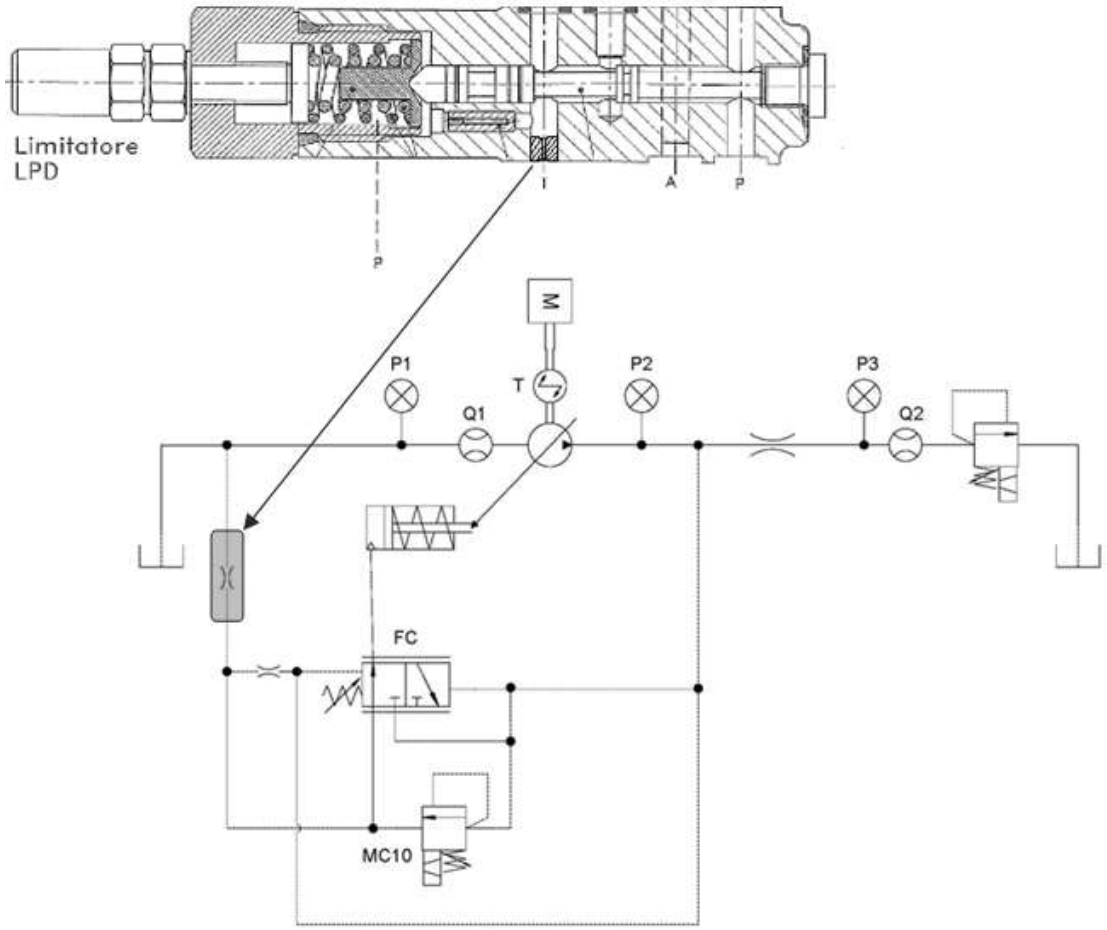

Figure 6.25 ISO Schematic of the MC 10 mounted on pump, with a restrictor in the T line

The circuit was modified by inserting a calibrated restrictor of a diameter of 1 mm on the exhaust line of the body of the flow compensator by this way allowing the pressurization of the internal environment that would lead to the actuator control of the swash plate. By exciting the solenoid MC10T it allows the oil passage from the entrance to the P line, then owing to the presence of the orifice shown in Figure 6.25 the flow to tank is limited and in this way pressurizes the chamber of the actuator. Another modification made in the circuit was that the LS line was connected directly to the Pump outlet, in this way the flow compensator would remain stationary and the actuator could be directly controlled by the MC 10 pressure compensator. The test was carried out by maintaing a fixed load and speed of rotation of the pump and by sending a linearly increasing excitation current to the valve MC10T with automatic cycles from the test bench set on the computer. It slowly increases the pressure in the actuator control until the pump is completely stroked and the

displacement is zero. The important parameter of these tests is to precisely determine the moment when the swash plate begins to move (Figure 6.26).

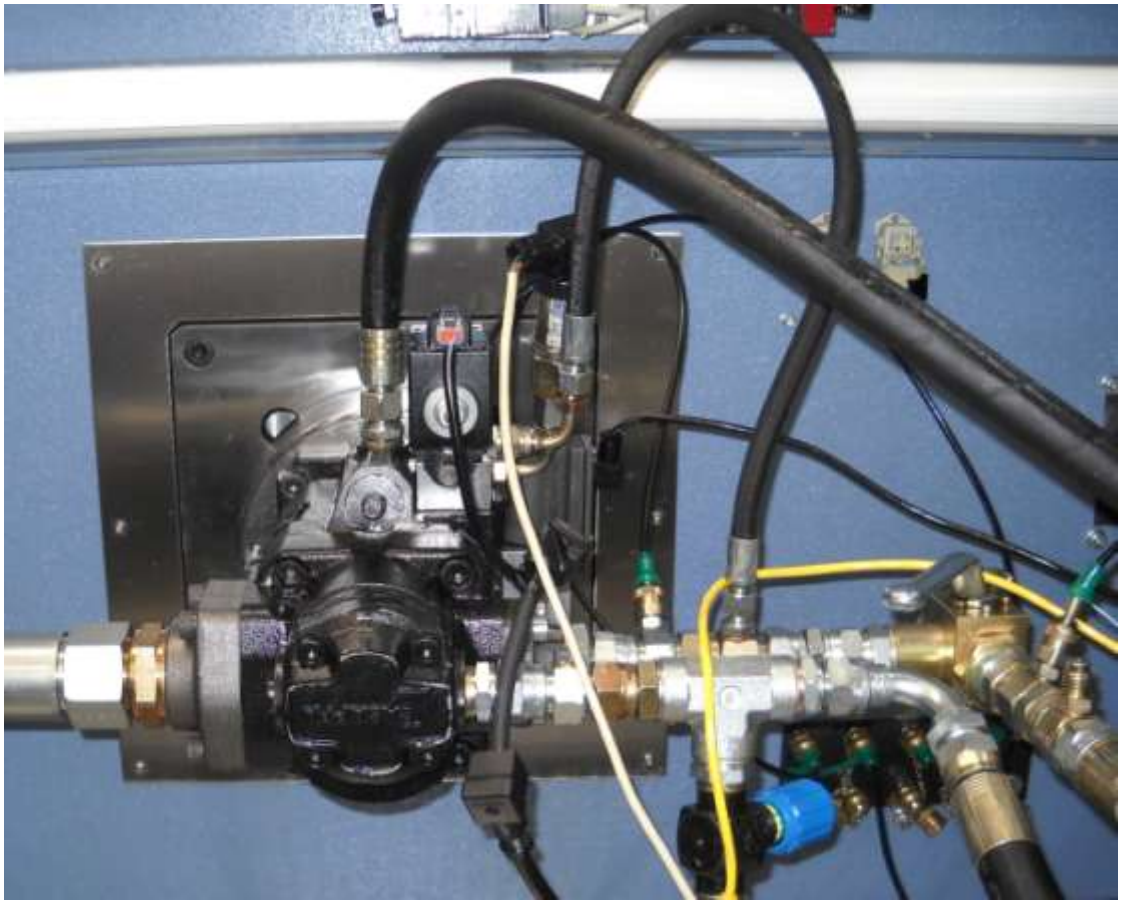

Figure 6.26: Pump mounted on the test rig in the second setupconfiguration

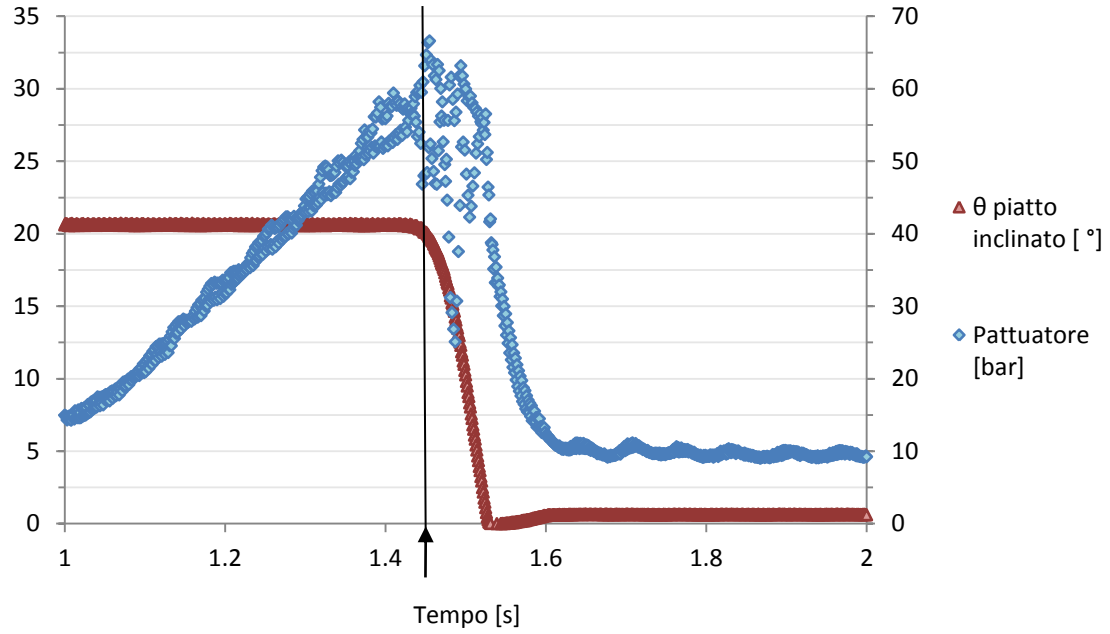

Figure 6.27 Cycle for stroking of the pump to reduce the displacement

To achieve the same kind of tests at low loads it was necessary to modify the circuit (third test configuration) as the solenoid MC10T only works with input pressures above 100 bar. The complete valve setup comprising of the pressure and flow compensators were replaced with a single manifold block that could be used to excite the contol actuator directly and in this way vary the swash angle. For simplicity the gear pump mounted on the rear of the axial piston pump was used to pressurize the chamber of the control actuator and in this way vary the displacement (Figure 6.27).

6.4.2 Dynamic Tests

After the preliminary tests on the pump that were required to complete the model, two types of pseudo-dynamic tests were carried out as part of the verification experiments to validate the pump model:

- Rapid transition back to zero and maximum displacement (Figure 6.28 a);
- Placement of intermediate random swash plate (Figure 6.28 b).

These tests have helped in recreating the complete working of the pump in different conditions. Where the compensators, swash plate and load sensing of the pump are all functional.

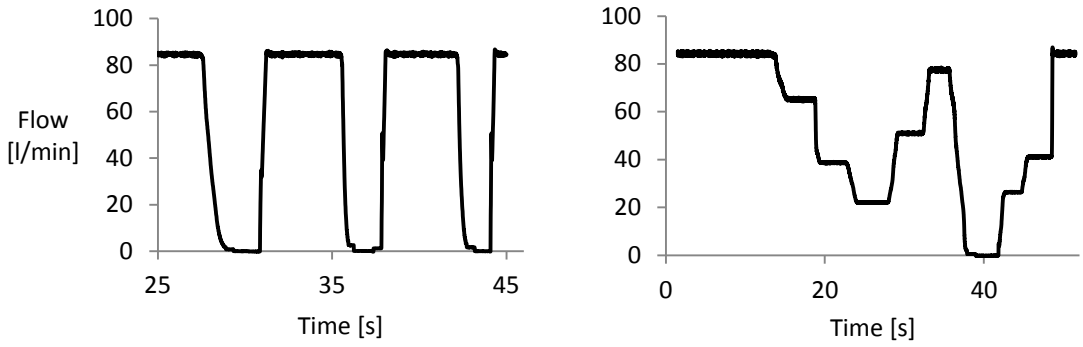

a) Stroking of the pump *b) Intermediate positions*

Figure 6.28: Dynamic tests of the pump

6.4.3 Tests to determine the frequency response of MVP 60

This section describes the frequency response tests that were carried out to ascertain the actual frequency response of the MVP 60. As can be seen in the Figure which illustrates the schematic of the test setup. The pump's load sensing line was connected directly to the pump's outlet port through a direction control valve. The direction control valve was a simple on-off solenoid with a very fast response. The response of the valve was in the order of 20ms. The solenoids were energised through a solid state relay switch that received its timing input from a function generator to control the frequency of switching and it was powered with a 24 Volts power supply. The load sensing line was connected to port P of the direction control valve and Port A was in turn connected to the LS on the Flow compensator. The port T was connected to tank and Port B was blocked. The sequence of operation was such that when the solenoid was excited in the 1st position the LS line would be connected to the flow compensator through the direction control valve as in P to A. When the other solenoid coil is energised the Flow compensators LS line would drain to tank A to T. This arrangement was adopted as the orifice inside the flow compensator provides a great restriction for free passage of oil to tank and thus delays the response of the pump to stroke and destroke. The test setup has LVDT's mounted on the Flow Compensator and the swash plate in this way the instantaneous position measurements can be made. Pressure transducers are mounted on the intermediate chamber, the LS line and system pressure line. Flow meter is connected at the outlet of the pump. The electric signals used to control the solenoids of the direction control valve are acquired using a current and voltage transducer.

Table. 6.3. Features of sensors and main elements of the apparatus used in the present research

Sensor	*Type*	*Main features*
M	Prime mover	ABB®, 4-quadrant electric motor, 75 Kw
P	Pump	CASAPPA® MVP60, 84 cm^3/r
P1	Strain gage	WIKA®, Scale: 0..40 bar, 0.25% FS accuracy
P2 – P3 – P4	Strain gage	WIKA®, Scale 0..400 bar, 0.25% FS accuracy
Q2	Flow meter	VSE® VS1, Scale 0.05..80 l/min, 0.3% measured value accuracy
T	Torque/speed meter	HBM® T, Scale: 0..500 Nm, 12000 r/min Limit Velocity, 0.05 Accuracy Class
θ	Incremental encoder	HEIDENHAIN® ERN120, 3600 imp./r, 4000 r/min Limit velocity, 1/20 period accuracy
DCV	Direction Control Valve	Bosch Rexroth

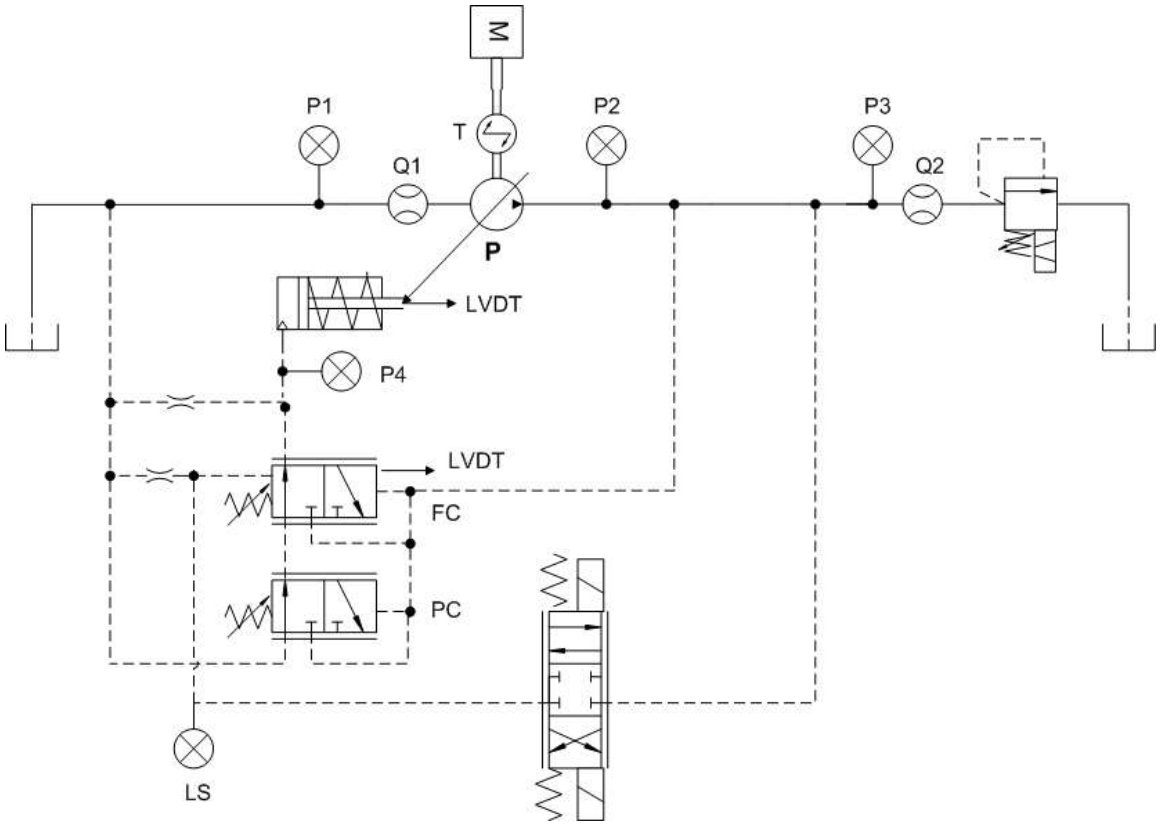

Figure 6.29: Frequency response test on MVP 60

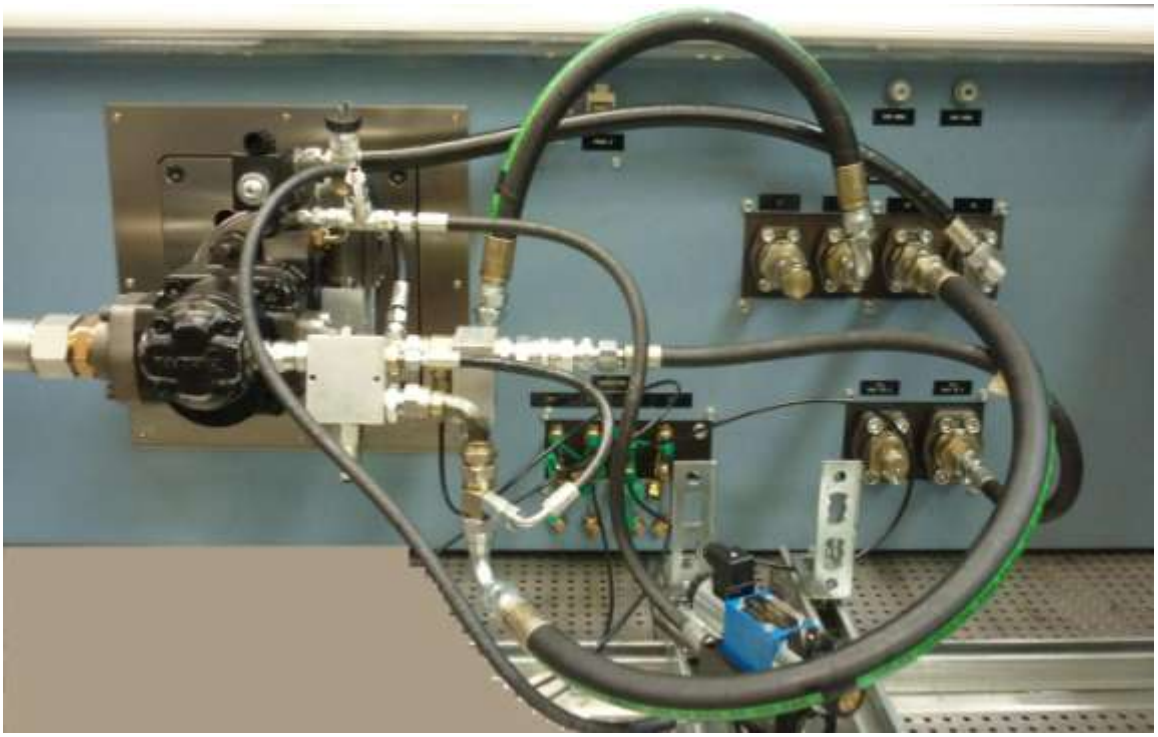

Figure 6.30: Frequency response test mounted on the test bench

The figure depicts the frequency response test setup with the pump, direction control valve and associated connections that were made to perform the test.

6.5 Experimental tests on the WALVOIL® DPX 100

This section describes the tests that were carried out on the Walvoil DPX 100 valve block. As desccribed earlier the DPX 100 is a fairly complex valve block. The experimental tests that would have to be carried out to validate its functioning would have to be very detailed to firstly gather a deeper understanding of the valve secondly to study the variation of all the physical parameters in the course of operation.

The study of all the essential parameters of the DPX 100 is very elaborate requiring a large number of instruments. The table lists the instruments that were used to study the functioning of the DPX 100 along with the corresponding measuring points.

Table. 6.4 Features of sensors and main elements of the apparatus used in the present research

Parameter to be measured	Sensor Used
Inlet pressure to valve	Pressure transducer (0 – 400 bar range)
Bridge pressure	Pressure transducer (0 – 400 bar range)
Load Sensing Pressure	Pressure transducer (0 – 400 bar range)
Work port A	Pressure transducer (0 – 400 bar range)
Work port B	Pressure transducer (0 – 400 bar range)
Pilot Pressure	Pressure transducer (0 – 400 bar range)
Main Spool Displacment	Linear Variable Differential Transformer (-15 to +15)
Pressure Compensator Dispalcement	Linear Variable Differential Transformer (-15 to +15)
Inlet flow measurement to valve	Flow meter
Outlet flow measurement port A	Flow meter
Outlet flow measurement port B	Flow meter

The figure describes the details of the manifold, pressure tapping points and LVDT attachment

Table 6.5: Description of the parts in the figure

Part No.	Description
1	Rear Manifold plate
2	Solenoid
3	Linear Variable Differential Transformer
4	LVDT attachment for connection to main spool
5	Front Manifold plate
6	Bridge pressure tapping point
7	LVDT connected to pressure compensator

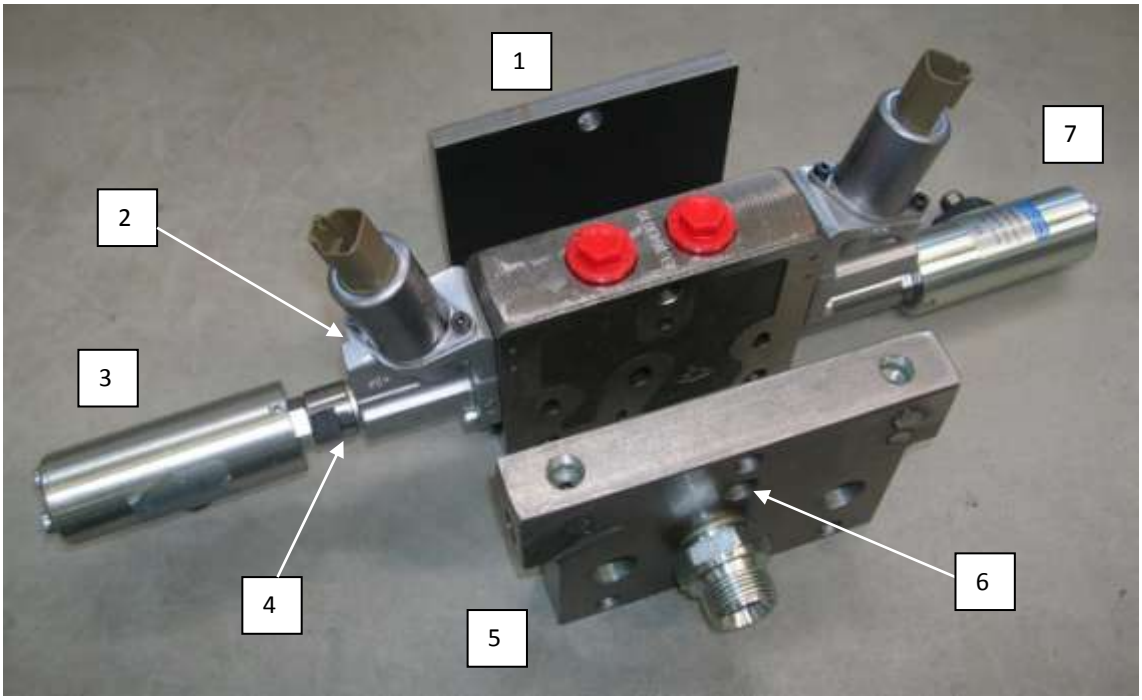

Figure 6.31 Manifold for DPX 100 with instruments and pressure tapping points

The figure 6.32 shows a detailed view of the attachment of the LVDT to the main spool. As it can be seen in the illustration part 4 is an attachment to connect the LVDT body with the housing of the pilot chamber. Part 8 is another attachment made to connect the LVDT spool with the main spool of the DPX 100. In this manner the LVDT has been rigidly connected to the main spool.

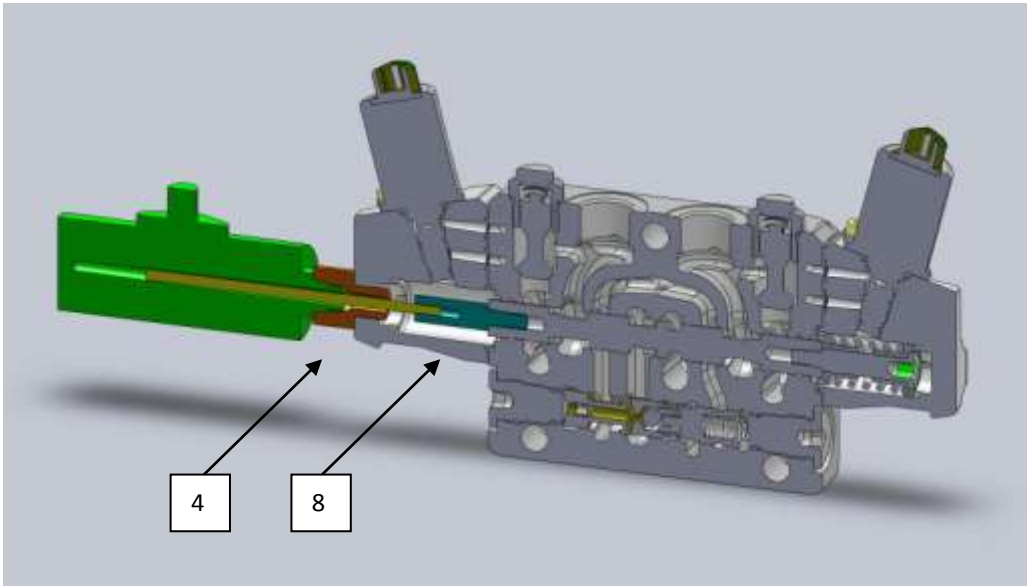

Figure 6.32 CAD model of the LVDT and main spool connection

The connection of the pressure compensator was done in a similar manner as can be seen in figure. The complexity in rigidly connecting the LVDT to the pressure compensator is that the PC has a fine orifice which has to be recreated in any attachment that is developed. This has been realised by using part A which has a small orifice of 0.5mm drilled and then a 1mm hole drilled at right angles to allow the sensed pressure to pass through. The complete attachment comprises of LVDT part 7 connected to the valve housing through part 9. Part 10 is the special LVDT and Pressure Compensator spool attachment.

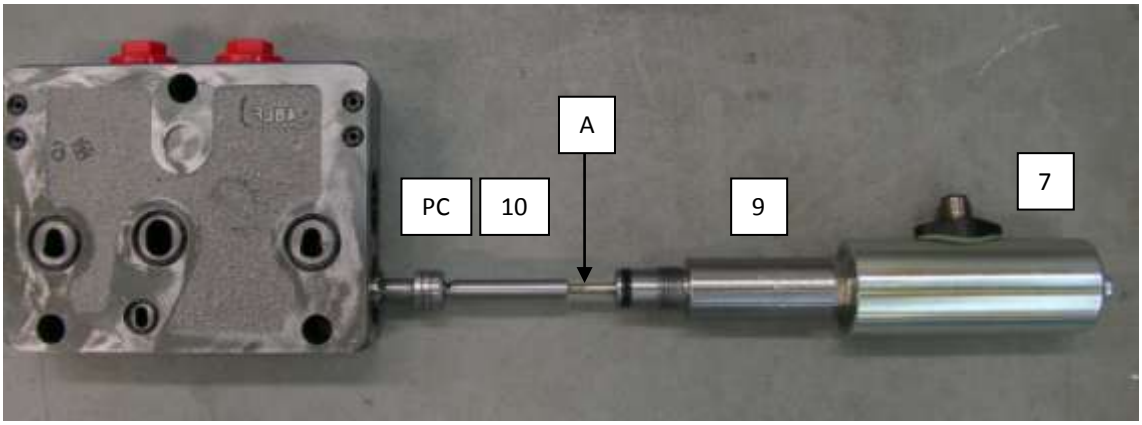

Figure 6.33 Instrumentation of the pressure compensator

The figure depicts the view of the valve block DPX 100 with the LVDT's and LVDT attachments to connect to the main spool and to the pressure compensator.

Figure 6.34: Exploded view of the complete position measurement setup on the valve

Two types of the tests were carried out using the instruments that were mounted on the valve block and are described in this section:

1. The functioning of the DPX 100 as a single slice.
2. The functioning of two DPX 100 slices

6.5.1 Functioning of the DPX 100 as a Single Slice

Table.6.6. Features of sensors and main elements of the apparatus used in the present research

Sensor	*Type*	*Main features*
M	Prime mover	ABB®, 4-quadrant electric motor, 75 Kw
P	Pump	CASAPPA® MVP60, 84 cm^3/r
P1	Strain gage	WIKA®, Scale: 0..40 bar, 0.25% FS accuracy
P2 – P3 – P4 – P5 – P6 – P7– P8	Strain gage	WIKA®, Scale 0..400 bar, 0.25% FS accuracy
Q2	Flow meter	VSE® VS1, Scale 0.05..80 l/min, 0.3% measured value accuracy
T	Torque/speed meter	HBM® T, Scale: 0..500 Nm, 12000 r/min Limit Velocity, 0.05 Accuracy Class
Θ	Incremental encoder	HEIDENHAIN® ERN120, 3600 imp./r, 4000 r/min Limit velocity, 1/20 period accuracy
LVDT	Linear variable differential transformer	Magnet Schuz AVAX 015

The figure represents the schematic of the test setup that was developed to test the functioning of the DPX 100 functioning as a single slice. To carry out the test it was decided that it would be best to study the valve with a fixed displacement pump, in this way the effects of LS compensation and feedback could be eliminated. To achieve this the pump's load sensing line was connected to the pump outlet and in this way the flow compensator was kept in a fixed position and the pump always maintained maximum displacement. A flow meter was set at the inlet of the valve and a pressure transducer to determine the inlet system pressure. The main spool was actuated by setting a pilot pressure of 35 bar with the gear pump following which the current to the proportional flow control solenoids were altered to displace the main spool.

The following tests were carried out on a single slice and the following parameters studied:

1. Spool Displacement:

    - The current to the solenoids were linearly increased to a maximum current of 1.2 A to actuate port A and then the current brought back to zero.
    - During the course of the rise in current the spool displacement was monitored using the LVDT mounted on the main spool.
    - The displacement of the pressure compensator was studied as the main spool was shifted to maximum displacement and then closed.
    - The flow and pressure out of port A was measured during the course of the test.
    - The same test was repeated for Port B

2. Pressure Compensator and Piston Check Displacement:

    - The current to the solenoids were linearly increased to a maximum current of 1.2 A to actuate port A and then the current brought back to zero.
    - During the course of the rise in current the spool displacement was monitored using the LVDT mounted on the main spool.
    - The displacement of the pressure compensator was studied as the main spool was shifted to maximum displacement and then closed.
    - At the maximum displacement of the spool a pressure peak of 250 bar was created so as to excite the bridge pressure to force the piston check assembly to mechanically close the pressure compensator.
    - The flow and pressure out of port A was measured during the course of the test.
    - The same test was repeated for Port B

3. Effect of Load Sensing Pressure Test:

- The current to the solenoids were linearly increased to a maximum current of 1.2 A to actuate port A and then the current brought back to zero.
- During the course of the rise in current the spool displacement was monitored using the LVDT mounted on the main spool.
- The displacement of the pressure compensator was studied as the main spool was shifted to maximum displacement and then closed.
- At the maximum displacement of the spool the ball valve was quickly closed and opened to create an instantaneous pressure rise in the LS chamber. This pressure rise would cause the Pressure Compensator to close to adjust its pressure according to the pump pressure and the piston check would return to its home position..
- The flow and pressure out of port A was measured during the course of the test.
- The same test was repeated for Port B

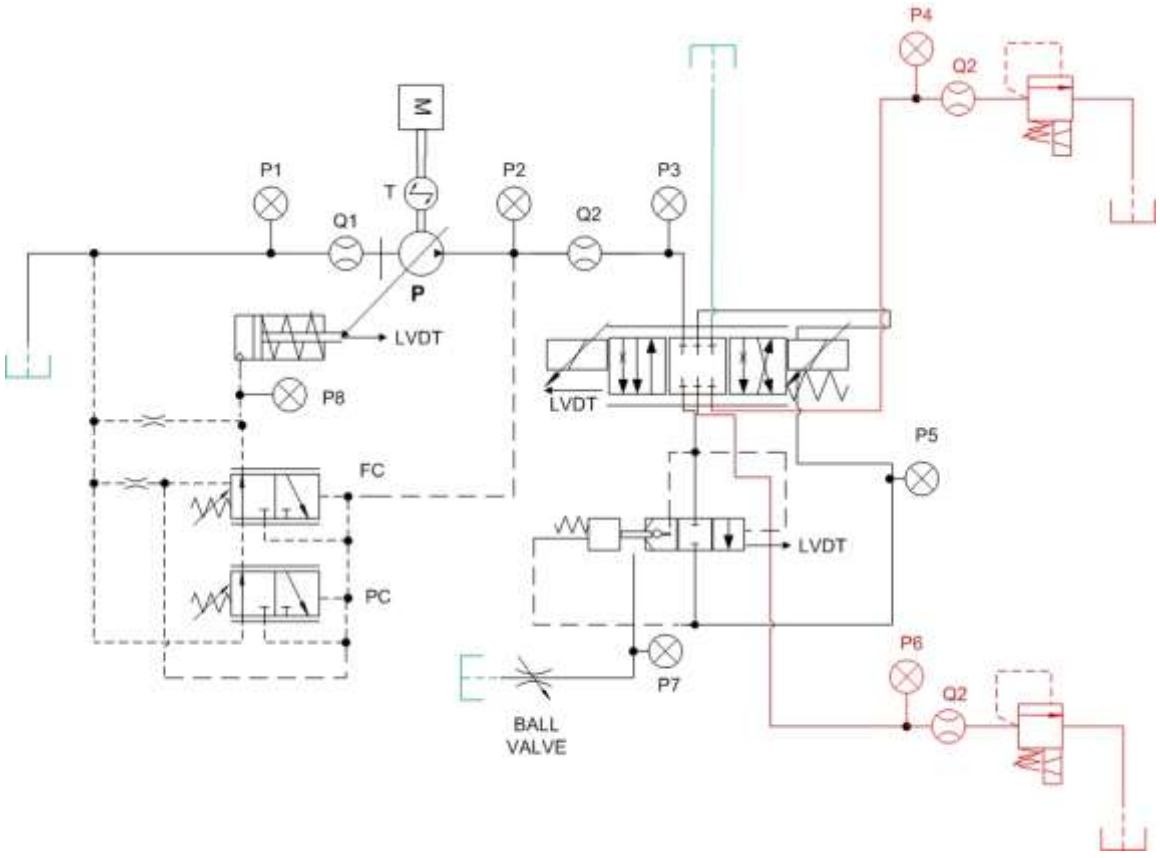

Figure 6.35: DPX 100 – I slice and ball valve to close LS line

Figure 6.36: Physical layout of Figure 6.35

6.5.2 Functioning of the MVP 60 and DPX 100 Single Slice with LS feedback

Table. 6.7 Features of sensors and main elements of the apparatus used in the present research

Sensor	*Type*	*Main features*
M	Prime mover	ABB®, 4-quadrant electric motor, 75 Kw
P	Pump	CASAPPA® MVP60, 84 cm^3/r
P1	Strain gage	WIKA®, Scale: 0..40 bar, 0.25% FS accuracy
P2 – P3 – P4 – P5 – P6 – P7– P8	Strain gage	WIKA®, Scale 0..400 bar, 0.25% FS accuracy
Q2	Flow meter	VSE® VS1, Scale 0.05..80 l/min, 0.3% measured value accuracy
T	Torque/speed meter	HBM® T, Scale: 0..500 Nm, 12000 r/min Limit Velocity, 0.05 Accuracy Class
Θ	Incremental encoder	HEIDENHAIN® ERN120, 3600 imp./r, 4000 r/min Limit velocity, 1/20 period accuracy
LVDT	Linear variable differential transformer	Magnet Schuz AVAX 015

The figure represents the schematic of the test setup that was developed to test the functioning of the MVP60 and DPX 100 single slice working together. The test was carried out by connecting the LS line from the valve block to the pumps flow compensator. To prevent the LS line from saturating a 0.75mm bleed off orifice was integrated into the line. This helped the system dynamics by preventing saturation of the LS line and ensuring that there was no delayed response in the reaction of the pump owing to the time taken to drain out of the orifice within the flow compensator. A flow meter was set at the inlet of the valve and a pressure transducer to determine the inlet system pressure. The main spool was actuated by setting a pilot pressure of 35 bar with the gear pump following which the current to the proportional flow control solenoids were altered to displace the main spool.

The following tests were carried out on the pump and valve single slice combination:

1. Spool Displacement:
    - The current to the solenoids were linearly increased to a maximum current of 1.2 A to actuate port A and then the current brought back to zero.
    - During the course of the rise in current the spool displacement was monitored using the LVDT mounted on the main spool and the variation of the swash angle on the pump.
    - The displacement of the valves pressure compensator and the pumps flow compensator was studied as the main spool was shifted to maximum displacement and then closed.
    - The flow and pressure out of port A was measured during the course of the test.
    - The same test was repeated for Port B

2. Pressure Compensator and Piston Check Displacement:
    - The current to the solenoids were linearly increased to a maximum current of 1.2 A to actuate port A and then the current brought back to zero.
    - During the course of the rise in current the spool displacement was monitored using the LVDT mounted on the main spool and the pumps swash angle was monitored.

- The displacement of the pressure compensator was studied as the main spool was shifted to maximum displacement and then closed as well as that of the pump's flow compensator.
- At the maximum displacement of the spool a pressure peak of 250 bar was created so as to excite the bridge pressure to force the piston check assembly to mechanically close the pressure compensator.
- The flow and pressure out of port A was measured during the course of the test.
- The same test was repeated for Port B

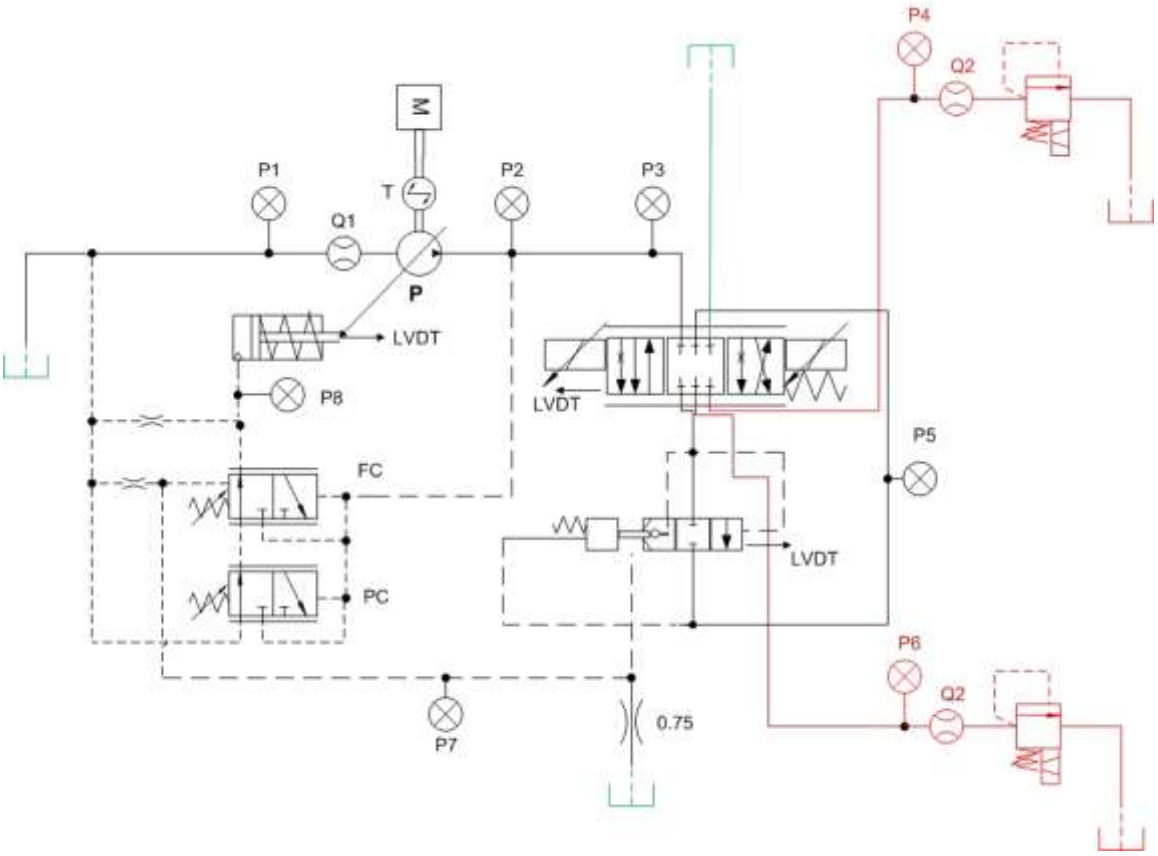

Figure 6.37: Pump and DPX 100 1 slice working together

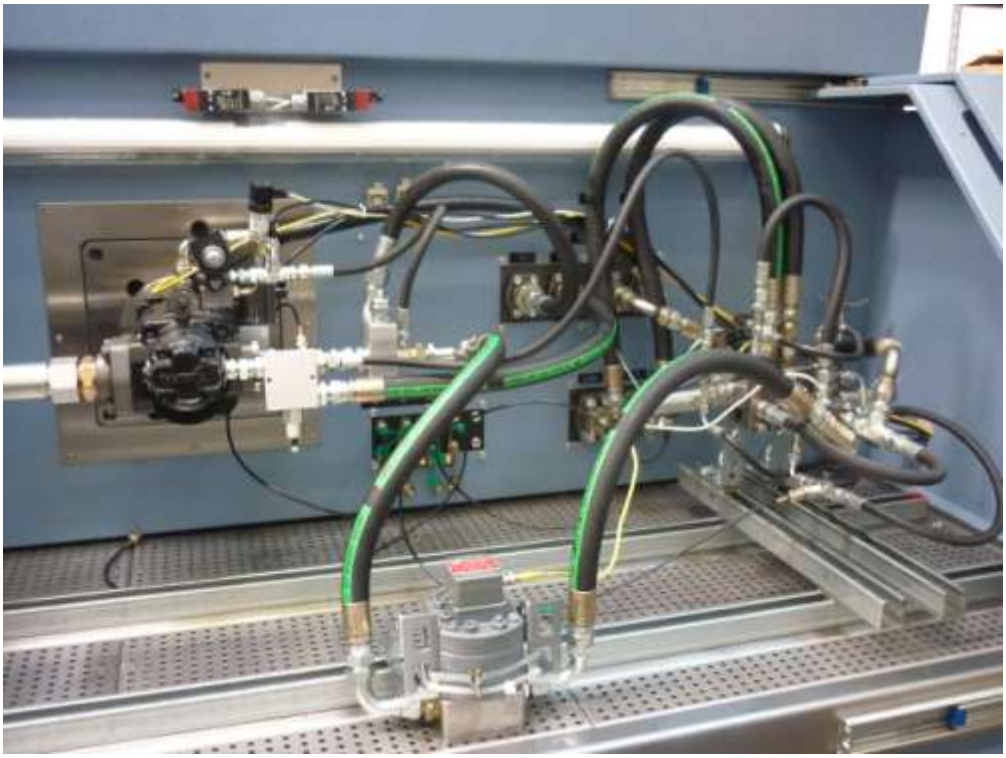

Figure 6.38: Pump and valve block mounted on the test bench for combined operation

6.5.3. Functioning of the MVP 60 and DPX 100 Dual Slice with LS feedback

Table. 6.8. Features of sensors and main elements of the apparatus used in the present research

Sensor	*Type*	*Main features*
M	Prime mover	ABB®, 4-quadrant electric motor, 75 Kw
P	Pump	CASAPPA® MVP60, 84 cm^3/r
P1	Strain gage	WIKA®, Scale: 0..40 bar, 0.25% FS accuracy
P2 – P3 – P4 – P5 – P6 – P7– P8	Strain gage	WIKA®, Scale 0..400 bar, 0.25% FS accuracy
Q2	Flow meter	VSE® VS1, Scale 0.05..80 l/min, 0.3% measured value accuracy
T	Torque/speed meter	HBM® T, Scale: 0..500 Nm, 12000 r/min Limit Velocity, 0.05 Accuracy Class
Θ	Incremental encoder	HEIDENHAIN® ERN120, 3600 imp./r, 4000 r/min Limit velocity, 1/20 period accuracy
LVDT	Linear variable differential transformer	Magnet Schuz AVAX 015

The figure represents the schematic of the test setup that was developed to test the functioning of the MVP60 and DPX 100 dual slice working together. The test was carried out by connecting the LS line from the valve blocks to the pumps flow compensator. To prevent the LS line from saturating a 0.75mm bleed off orifice was integrated into the line. This helped the system dynamics by preventing saturation of the LS line and ensuring that there was no delayed response in the reaction of the pump owing to the time taken to drain out of the orifice within the flow compensator. A flow meter was set at the inlet of the valve and a pressure transducer to determine the inlet system pressure. The main spool was actuated by setting a pilot pressure of 35 bar with the gear pump following which the current to the proportional flow control solenoids were altered to displace the main spool.

The following tests were carried out on the pump and valve single slice combination:

1. Spool Displacement:
    - The current to the solenoids were linearly increased to a maximum current of 1.2 A to actuate port A of the first slice and simultaneously port B of the second slice, both slices were then brought back to zero.
    - During the course of the rise in current the spool displacement was monitored using the LVDT mounted on the main spools and the variation of the swash angle on the pump.
    - The displacement of the valves pressure compensator and the pumps flow compensator was studied as the main spool was shifted to maximum displacement and then closed.
    - The flow and pressure out of port A was measured during the course of the test.
    - The same test was repeated for Port B

2. Pressure Compensator and Piston Check Displacement:
    - The current to the solenoids were linearly increased to a maximum current of 1.2 A to actuate port A of the first slice and simultaneously port B of the second slice, both slices were then brought back to zero.

- During the course of the rise in current the spool displacement was monitored using the LVDT mounted on the main spool and the pumps swash angle was monitored.
- The displacement of the pressure compensator was studied as the main spool was shifted to maximum displacement and then closed as well as that of the pump's flow compensator.
- At the maximum displacement of the spool a pressure peak of 250 bar was created so as to excite the bridge pressure to force the piston check assembly to mechanically close the pressure compensator.
- The flow and pressure out of port A was measured during the course of the test.
- The same test was repeated for Port B

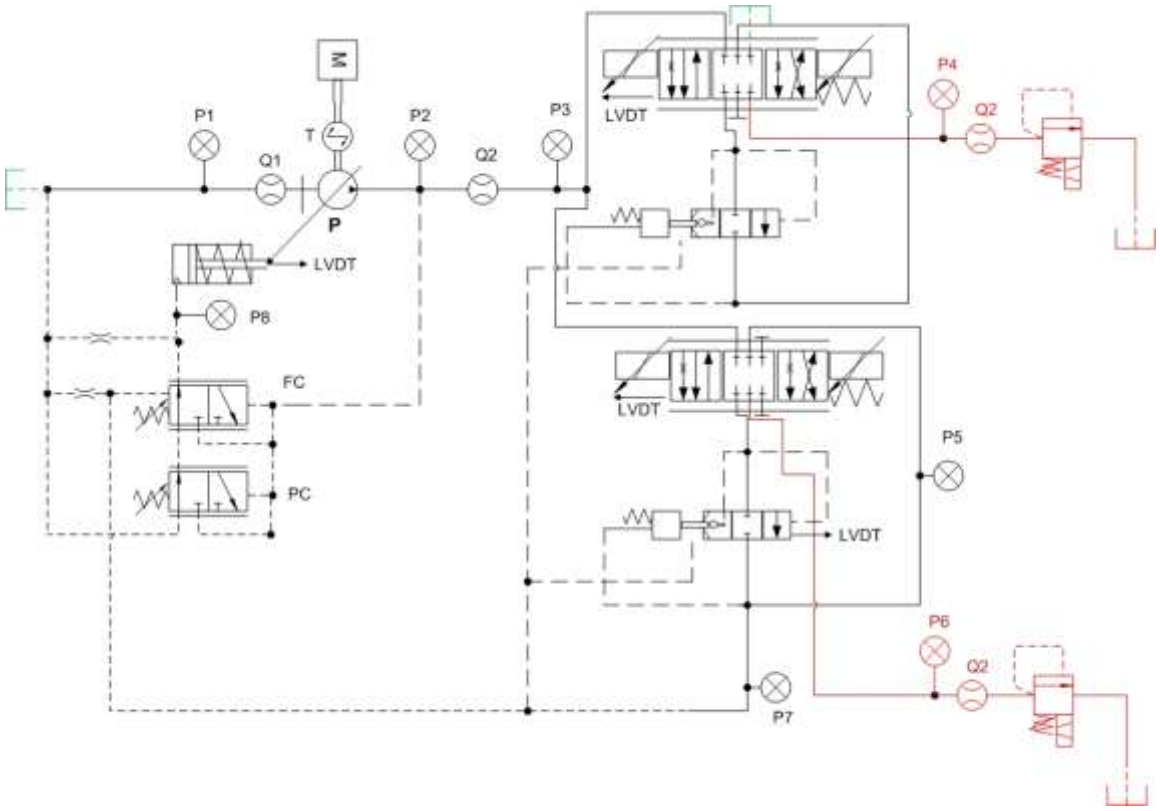

Figure 6.39: DPX 100 – 2 slices

6.6 Experimental test on the Excavator SAMPIERANA – EUROCOMACH® ES 850 ZT

This section describes the experimental activity that was carried out on the mini excavator that was being modeled. The digging cycle tests on the excavator were carried out to measure the pumps response to different excavation cycles. The data from the excavation cycles were used to verify and validate the functioning of the simulation model of the excavator. Digging cycles were carried out at different engine speeds to verify the functionality of the pump response at different operating conditions and load cycles. Figure 20 depicts the excavator that was used to carry out the experimental field tests and Table 2 describes the instrumentation used to measure the represented data as well as verifying the mathematical model. Tests were carried out at three different engine speeds: 1000r/min, 1500r/min and 1750r/min as. For the DPX 100 only the pilot pressure was measured to serve as an input to control the functioning of the valve. Due to space limititations it was not possible to install more instrumentation.

The sensors used to carry out the test are as listed in the table. Pressure transducers were mounted on the boom actuator and on the bucket actuator. The data from these transducers were used to define the loads on the excavator. The pump was instrumented with a swash angle sensor, load sensing signal pressure transducer and pump outlet pressure transducer. The valve block DPX 100 was instrumented with a pressure transducer on the pilot signal, so that the data could be used to control the valve spool movement.

Table. 6.9. Features of sensors and main elements of the apparatus used on the excavator

Sensor	*Type*
Pump Output Pressure	Strain gauge
Swash Angle Sensor	Inclination Sensor
Load Sensing Pressure	Strain Gauge
Valve Pilot Pressure	Strain gage
Actuator Extension Pressure	Strain Gauge
Actuator Retraction Pressure	Torque/speed meter
Output Flow	Flow Meter
Engine Speed	RPM Sensor

Figure 6.40 Excavator Sampierana® ES 850 ZT used for the test

Table 6.10 Excavator test scheme

Test N.	Implement	Action	Angular Velocity
1	Bucket	Extension + Retraction + Extension	1000
2	Bucket	Extension + Retraction + Extension	1500
3	Bucket	Extension + Retraction + Extension	1750
4	Bucket	Extension + Retraction + Extension	2000
5	Bucket	Extension + Retraction + Extension	2350
6	Arm	Extension + Retraction + Extension	1000
7	Arm	Extension + Retraction + Extension	1750
8	Arm	Extension + Retraction + Extension	2000
9	Arm	Extension + Retraction + Extension	2350
10	Arm + Bucket	Scavo: Extension (BR) con Retraction(BE) + Retraction (BR) with Extension (BE) + Extension (BR) con Retraction (BE)	1500
11	Arm + Bucket	Scavo: Extension (BR) con Retraction(BE) + Retraction (BR) with Extension (BE)	1750

		+ Extension (BR) con Retraction (BE)	
12	Arm + Bucket	Scavo: Extension (BR) con Retraction(BE) + Retraction (BR) with Extension (BE) + Extension (BR) con Retraction (BE)	2000
13	Arm + Bucket	Scavo: Extension (BR) con Retraction(BE) + Retraction (BR) with Extension (BE) + Extension (BR) con Retraction (BE)	2350

CHAPTER 7

RESULTS

7.1 Verification of Pump MVP 60 – Flow Compensator

The stationary tests performed on the flow compensator of the pump were compared with simulation results obtained with the flow compensator model in Figure 7.1. The data to be verified was that of the Δp maintained by the valve and the flow exiting from the intermediate chamber (Q_{OUT} in Figure 7.1) at various positions of the spool. The test is carried out in the following manner the inlet flow to the system is set and the sytem pressure would be maintained by an ideal relief valve identified in Figure 7.1 as VL2. An FCV is connected in series to create the functioning of the load orifice and the output of the FCV was connected to the LS line. The tests were performed for flow rates of 5, 10, 20 and 30 l/min and data were acquired with steps of 0.1 mm displacement of the flow compensator spool, starting from the critical condition of the immediate orifice opening to maximum displacement of approximately 3.9 mm (this occurs in the case where the valve is closed externally by the cap screwed on the body, but instrumented with LVDT position sensor that increases the total travel of the inner cursor from 3.7 to 4.8 mm).

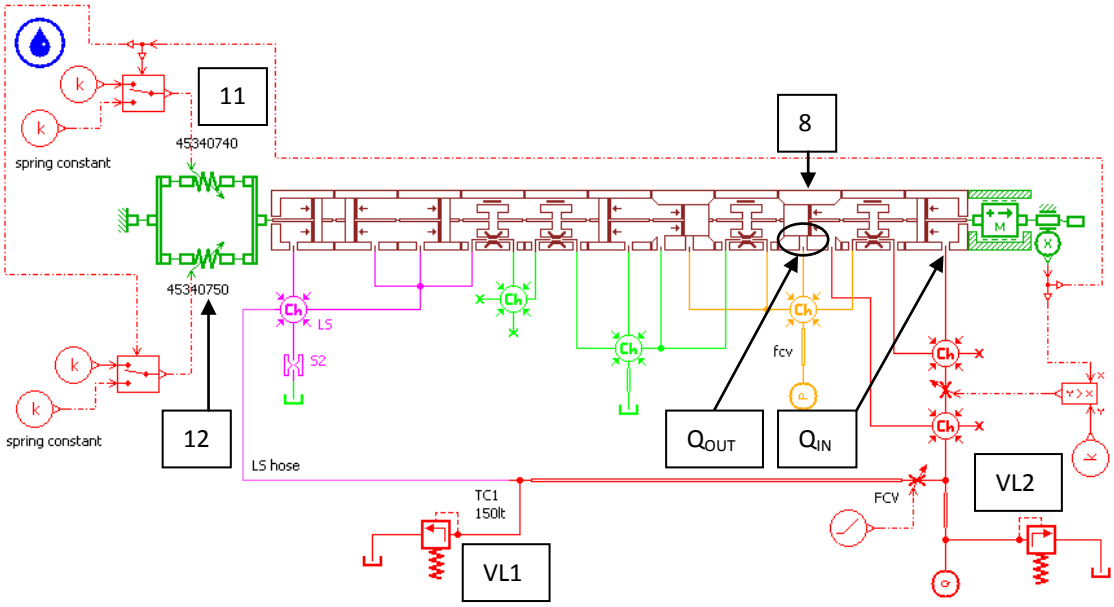

Figure 7.1 AMESim® model of the FC utilsed for reproducing the steady state tests of the FCV

From an initial comparison between the experimental and simulated curves it was noted that only in the vicinity of the position of the immediate orifice opening, with a proper setting of the compensator concentric springs, the model could replicate with good approximation the values of pressure drop measured on the test bench. For positions of the spool at its stroke limit the differences between the data were rather high. The model was then adjusted for better replication of the real behavior of the valve going to increase the spring constant of the internal spring, which was initially taken from the Casappa data sheet. This has also increased the value of the initial oriifce opening that allows oil to flow in the intermediate chamber and then the actuator to control the pump swashplate. The modified values in the model are listed in Table below:

Table 7.1: Modified table parameters of the Flow Compensator

Element	Parameter	Value	Unit
8	*Diameter*	*5*	*mm*
	Underlap	*-3.87*	*mm*
11	*Precompression (17bar)*	*$-0.5*10^{-3}$*	*mm*
	Elastic Constant	*9'950*	*N/mm*
	Switch threshold	*-0.5*	*adim*
12	*Precompression (17bar)*	*$-3.3*10^{-3}$*	*mm*
	Elastic Constant	*72'450*	*N/mm*
	Switch threshold	*-3.3*	*adim*
VL1	*Relief setting*	*5*	*bar*
VL2	*Relief setting*	*300*	*bar*

By comparing the results obtained, it shows a good approximation for all test conditions the pressure drop required to place a precise point in the internal piston is faithfully reproduced by the model. If the features are almost perfectly linear simulation, this is not always the case for the real characteristics. This is due to several phenomena including the non-linearity of the elastic elements, the leakage of oil etc.. Regarding the characteristics of the flow control valve model, they are modeled perfectly to a shift of about 4.3 mm of the drawer, or in the first phase of opening. From this point on, the flow is larger than experimental simulation with an error that reaches a peak of about 20% in terms of the spool being fully extended and very high flow rate (Figure 7.2b). All this, however, has little value considering the conditions under which the component usually works: the displacement of the internal piston is less than 3.9 mm for all conditions in which the pump is supplying lines with high flow at low load, if instead the pressure drop across the valve distributor tends to increase over the registry value, this shift will exceed the critical value of 3.9 mm, while making the actuator control of the swash plate to maintain the condition of controllability in the speed of all users. In this phase of operation of the internal piston valve will continue to oscillate near the critical condition of the orifice opening to "compensate" the oil drain valve with a discontinuous pressurization actuator control, and to adapt as quickly as possible varying load conditions. Only in a very short transient, it will be in the fully open position, and then the residual error of the outgoing flow characteristic in these conditions will be less crucial to replicate the operation.

Tabel 7.2 of results with $\mathbf{Q_{IN}}$ **= 5 l/min**

Test N.	Spool Position [mm]	Δp Experimental [bar]	Δp Simulation [bar]	Flow Experimenta [l/min]	Flow Simulation [l/min]
1	**3.9**	19.8	20.08	12*10^(-3)	0.04
2	**4.0**	22.2	22.22	0.3	0.47
3	**4.1**	23.7	24.37	1.1	1.15
4	**4.2**	25.6	26.51	2.0	2.03
5	**4.3**	28.6	28.65	3.5	3.12
6	**4.4**	30.8	30.80		.39

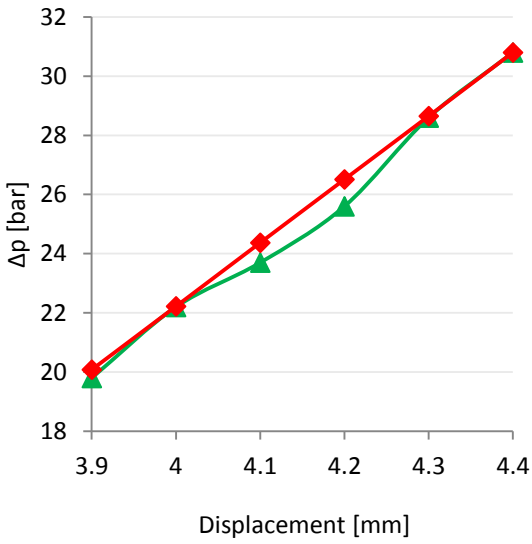

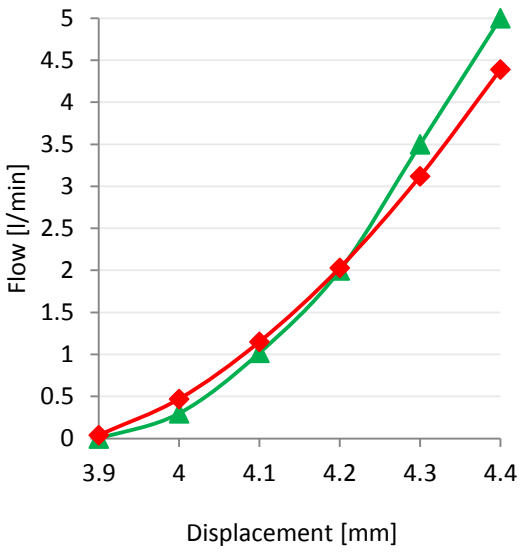

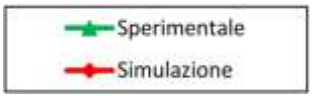

7.2 a) Pressure drop in function of spool displacement for Q_{IN} = 5 l/min

7.2 b) Flow in function of spool displacement for Q_{IN} = 5 l/min

Table 7.3 of results with Q_{IN} = **10 l/min**

Test N.	Spool Position [mm]	Δp Experimental [bar]	Δp Simulation [bar]	Flow Experimenta [l/min]	Flow Simulation [l/min]
1	**3.9**	19.9	20.08	19*10^(-3)	0.04
2	**4.0**	22.0	22.21	0.3	0.47
3	**4.1**	24.0	24.35	1.0	1.15
4	**4.2**	25.9	26.50	2.3	2.03
5	**4.3**	28.7	28.64	3.5	3.12
6	**4.4**	31.1	30.79	5.2	4.39
7	**4.5**	33.4	32.92	7.0	5.84
8	**4.6**	35.6	35.07	8.9	7.46
9	**4.7**	38.5	37.22	10.0	9.26

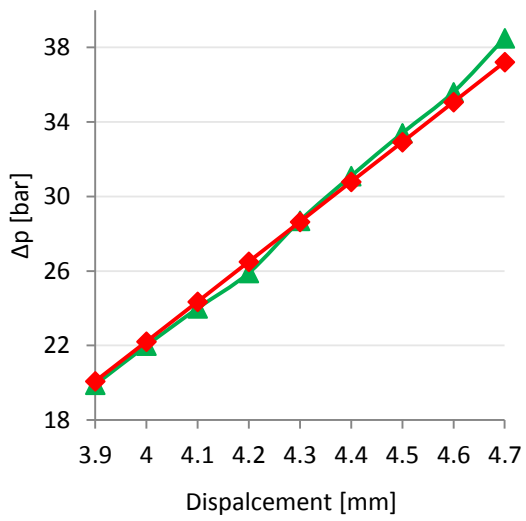

7.3 a) Pressure drop vs spool displacement for Q_{IN} = 10 l/min

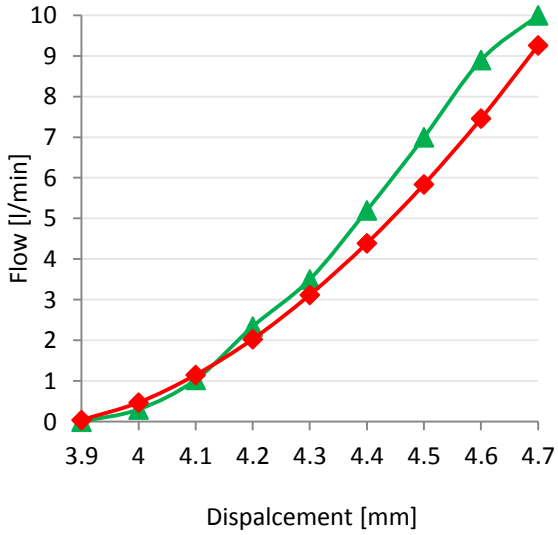

7.3 b) Flow vs spool displacement for Q_{IN} = 10 l/min

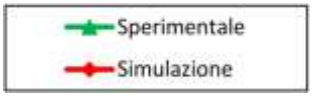

Table 7.4 of results with Q_{IN} ***= 20 l/min***

Test N.	Spool Position [mm]	Δp Experimental [bar]	Δp Simulation [bar]	Flow Experimenta [l/min]	Flow Simulation [l/min]
1	**3.9**	19.9	20.04	15*10^(-3)	0.04
2	**4.0**	21.8	22.20	0.3	0.47
3	**4.1**	24.0	24.33	1.1	1.15
4	**4.2**	26.0	26.48	2.0	2.04
5	**4.3**	28.5	28.62	3.5	3. 2
6	**4.4**	30.9	30.78	5.2	4.40
7	**4.5**	33.2	32.91	7.1	5.85
8	**4.6**	36.8	35.05	9.2	7.47
9	**4.7**	44.9	37.20	12.0	9.26

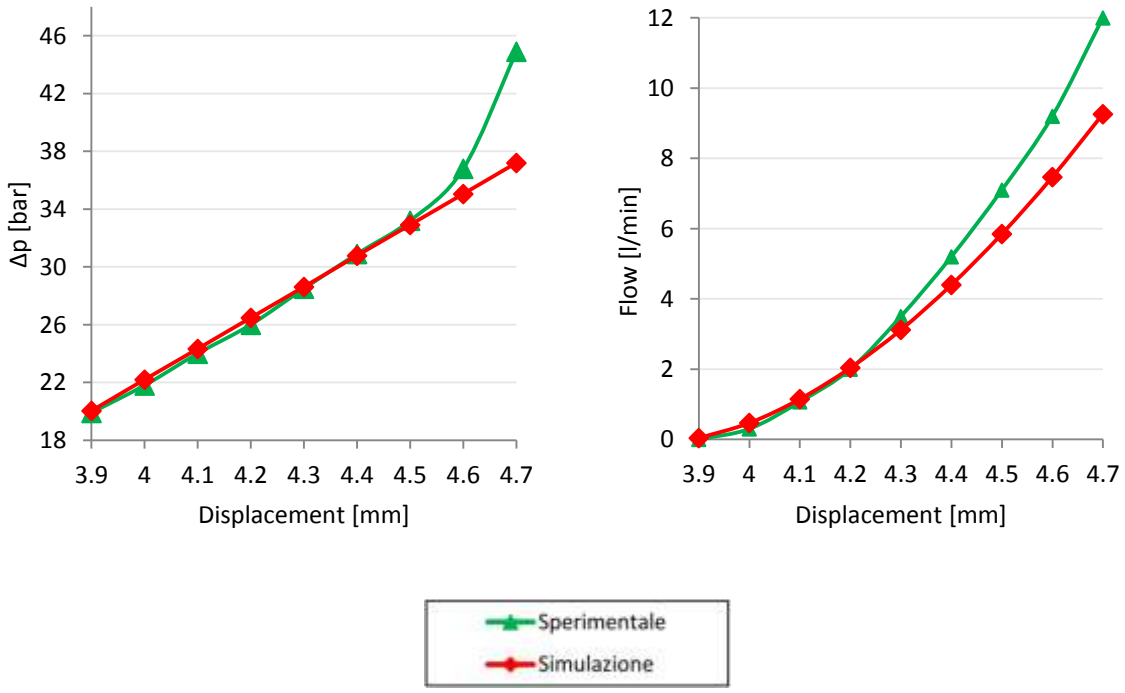

7.4 a) Delta P vs Spool Displacement for Q_{IN} *= 20 l/min*

7.4 b) Flow vs Spool Displacement for Q_{IN} *= 20 l/min*

Tabel 7.5 of results with Q_{IN} ***= 30 l/min***

Test N.	Spool Position [mm]	Δp Experimental [bar]	Δp Simulation [bar]	Flow Experimenta [l/min]	Flow Simulation [l/min]
1	**3.9**	19.7	20.02	16*10^(-3)	0.04
2	**4.0**	21.8	22.16	0.3	0.47
3	**4.1**	23.8	24.30	0.9	1.15
4	**4.2**	25.9	26.45	2.0	2.04
5	**4.3**	28.3	28.60	3.5	3.12
6	**4.4**	31.7	30.74	5.	4.39
7	**4.5**	33.1	32.88	7.2	5.84
8	**4.6**	36.5	35.02	9.4	7.47
9	**4.7**	42.8	37.17	11.9	9.27

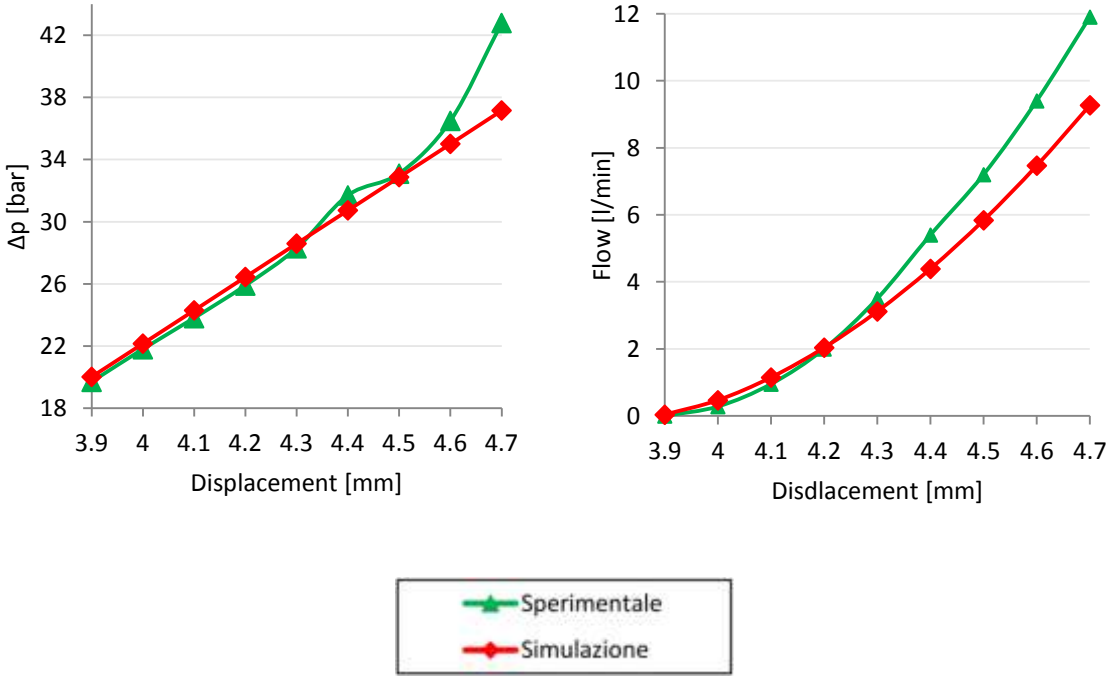

Figure 7.5 a) Delta P vs spool displacement Q_{IN} *= 30 l/min*

Figure 7.5 b) Flow vs Spool Displacement Q_{IN} *= 30 l/min*

Dynamic tests performed on the flow compensator of the pump were then compared with simulation results obtained on the model of flow compensator. In these experimental tests the flow compensator has been subjected to a load step imposed by the test bench, with the aim of instantaneously pressurizing the line and determine the dynamic response of the

component. Tests were run in three configurations, namely with a load steps at 110, 120 and 150 bar. The values of the pressure upstream and downstream of the valve were then used in a file format data in the model as boundary conditions to compare the simulation if the response was similar to that of the actual valve. Compared to the circuit of Figure 7.1, the ideal source of capacity has been replaced with a pressure source that reads the values of upstream pressure measured during the tests. While the valve VL in Figure 7.1 has been commanded to reproduce a load identical to the one generated at the test bench.

In Figure 7.7 a) and b) we see that for the first 2 seconds of the test the compensator is working to maintain a delta pressure which is equal to about 20 bar. To achieve this the piston oscillates at the critical opening position and allows the flow of oil through the intermediate chamber I. When the load suddenly starts to increase the first effect that it has is the pressurization of the LS chamber and the balance of power shift to the right of the cursor inside that closes the intermediate opening (condition highlighted in red in Figure 7.6) and reaches a displacement of approximately 3.6mm (more than the initial state in which it is in contact with the cap right, that is the right limit). The system pressure P rises to catch the load and as soon as the delta pressure rebalances then you reopen the intermediate chamber and the flow path back to compensate. For the transient effect of load dropping what occurs is the inverse of the previous point: the pressure downstream of the line suddenly starts to diminish. The pressure drop increases and the spool is pushed to the left in order to allow a greater amount of flow of oil on the middle line, with the intent to restore the previous fall on the distributor subjecting it to a lower flow rate (in green condition).

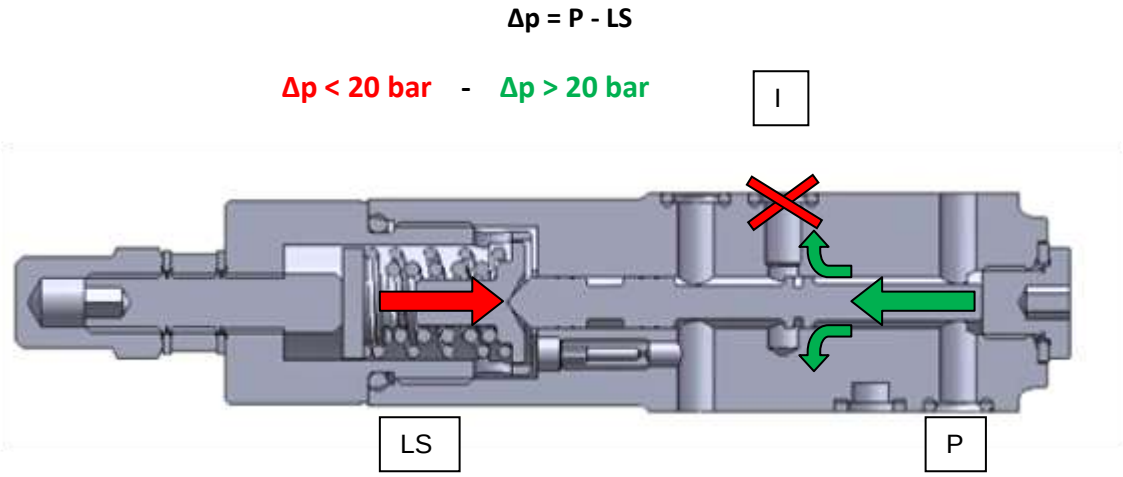

Figure 7.6 Functioing Logic of the Flow Compensator

*Dynamic tests at **a pressure of 110 bar***

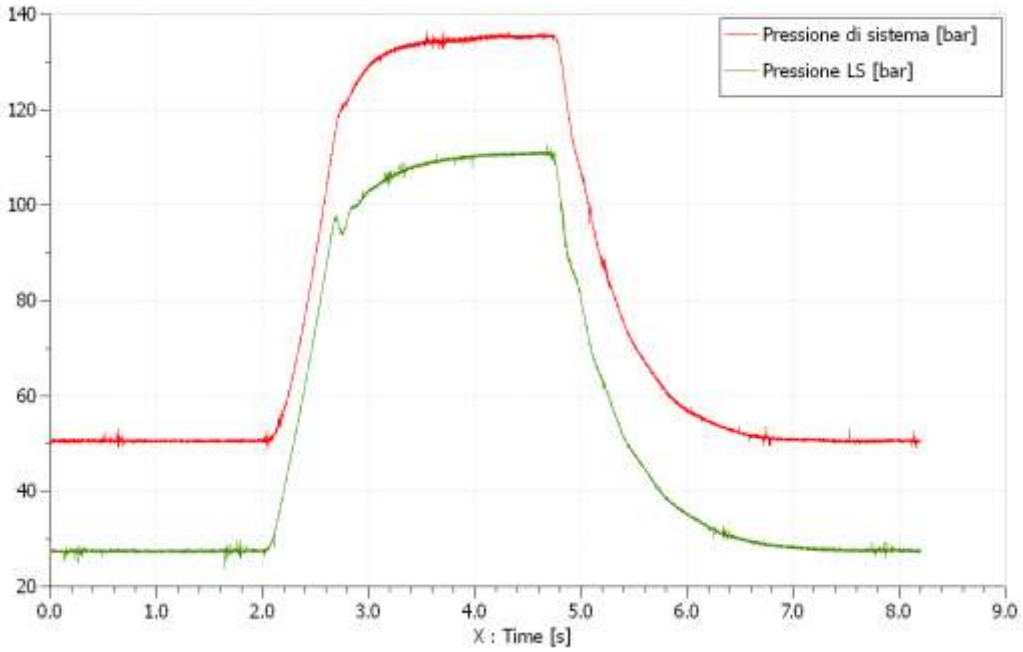

Figure 7.7 a) Experimental pressure characteristics used as an input for the model (test at 110bar)

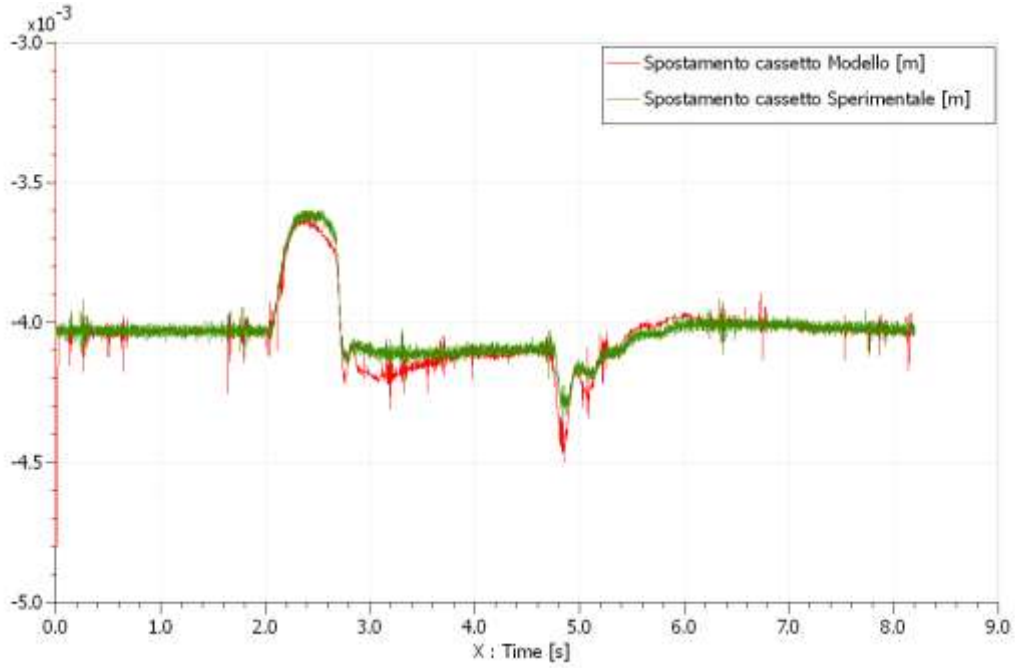

Figure 7.7 b) Comparison of experimental tests with simulation of spool position (test a 110bar)

Dynamic Tests for a load of **120 bar**

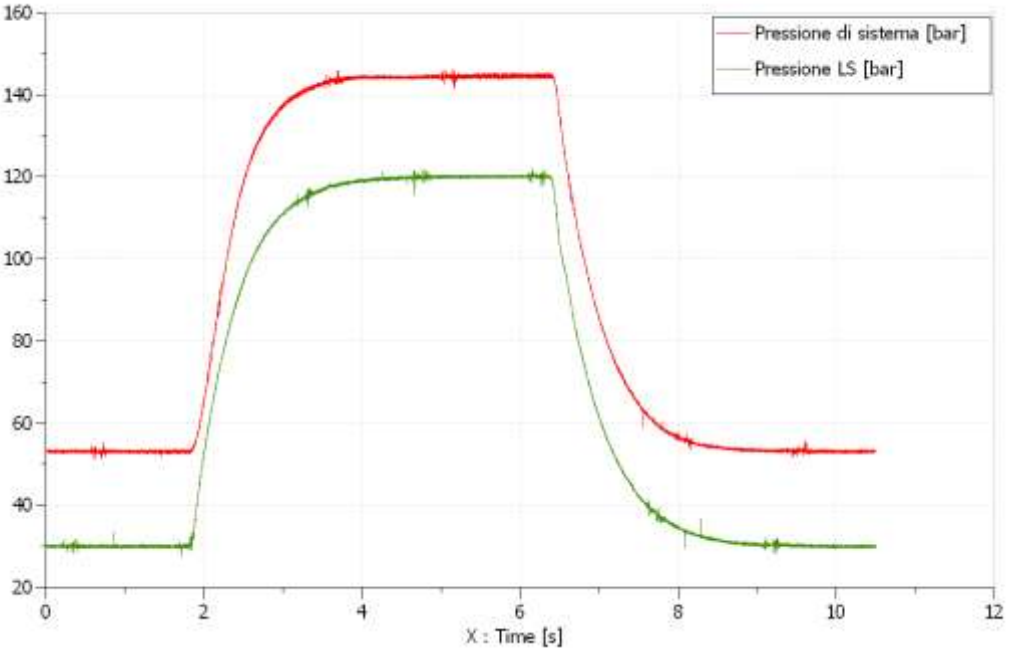

Figure 7.8 a) Pressure characteristics curve used as input for the model (test a 120bar)

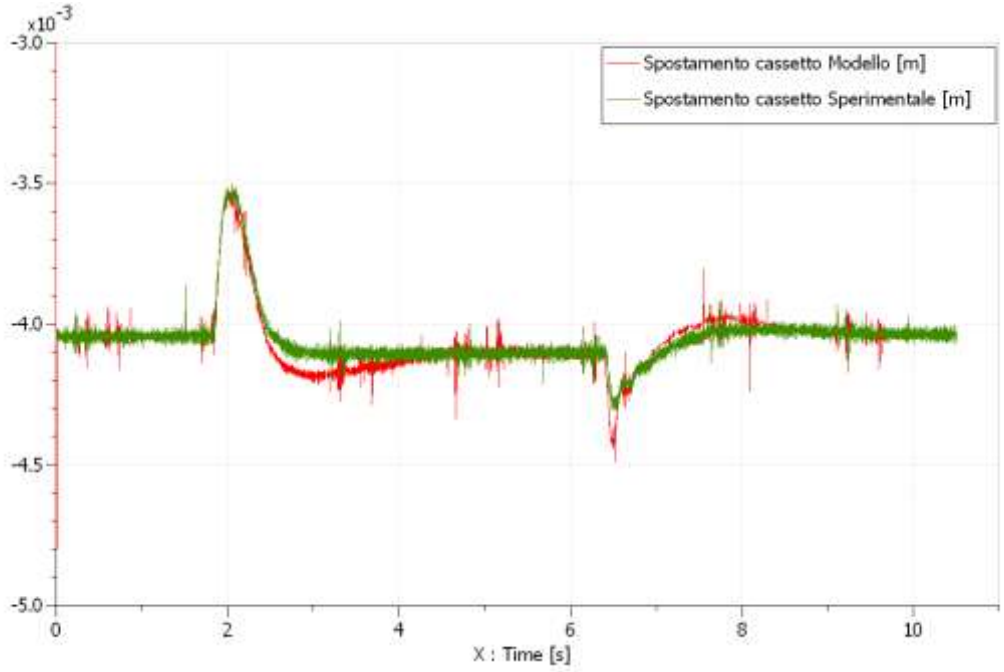

Figure 7.8 b) Comparison of Experimetanl and Simulation results of the spool (test a 120bar)

Dynamic Test for a Load of **150 bar**

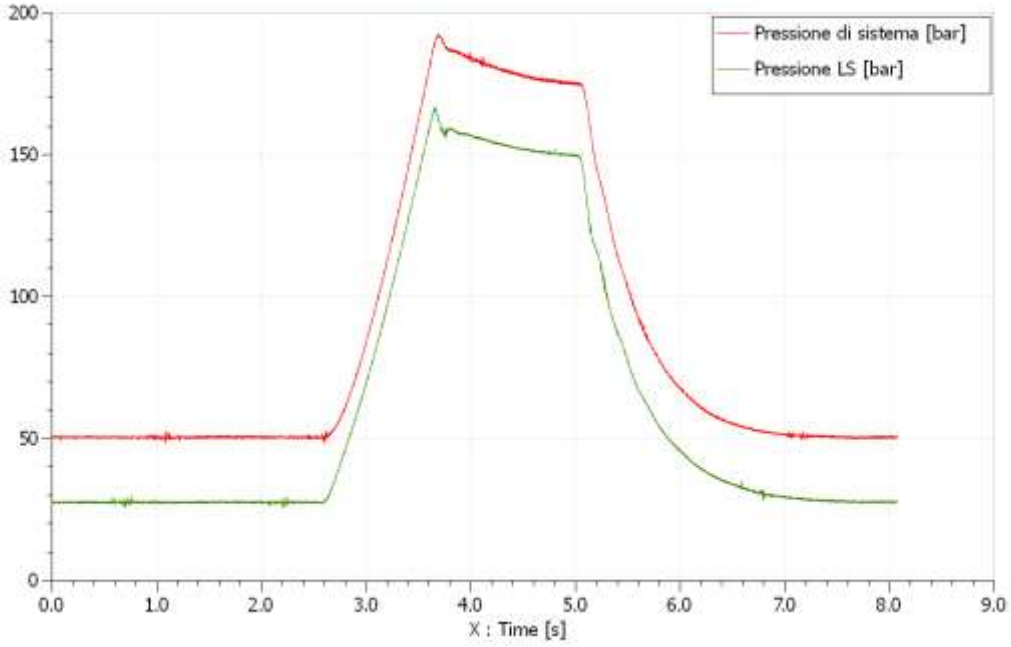

Figure 7.9 a) Pressure characteristics used to drive the simulation model (test at 150bar)

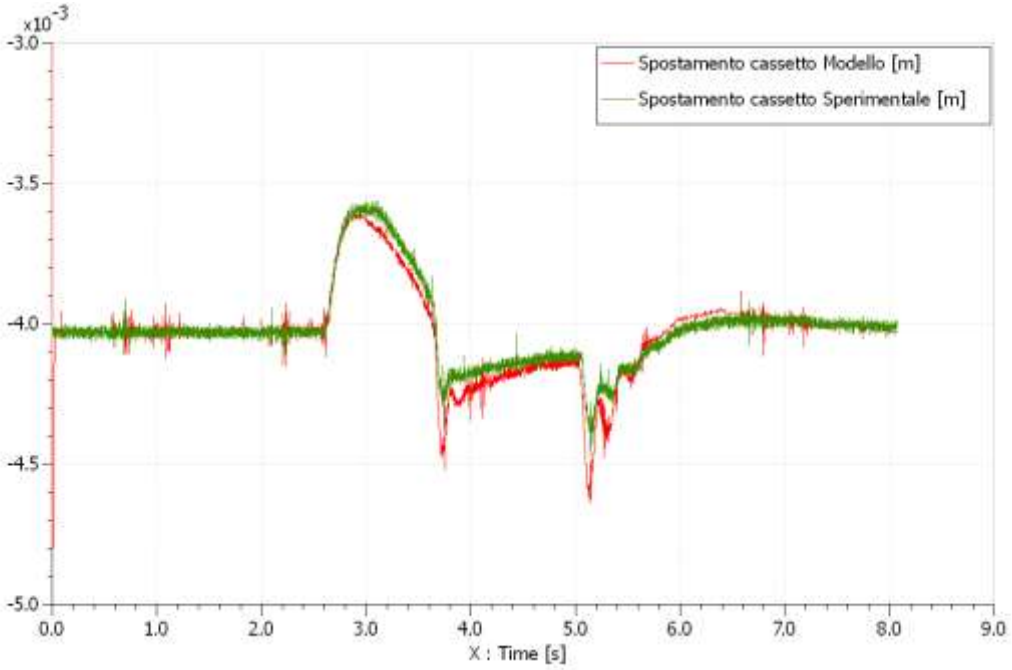

Figure 7.9 b) Comparison between simulation and experimental results (test a 150bar)

7.2 Results Relating to the Pump Simulation

The first experimental tests have been performed on the pump, as mentioned in Chapter 6, according to the classical circuit configuration with LS with increasing load cycles - at a speed of 1000 rpm, repeating the test for different positions of the manual valve to determine different positions of the swash plate (step one degree through out the operating range of 0 to 21°). As an example, take the test at $\theta = 3$ °, for which we have obtained the curves of pressure load and discharge PLS PS shown in Figure 7.10a), the angle of inclination of the swash plate is changed by about 0.9° as shown in Figure 7.10b) and the pressure in the actuator control has increased with the load as

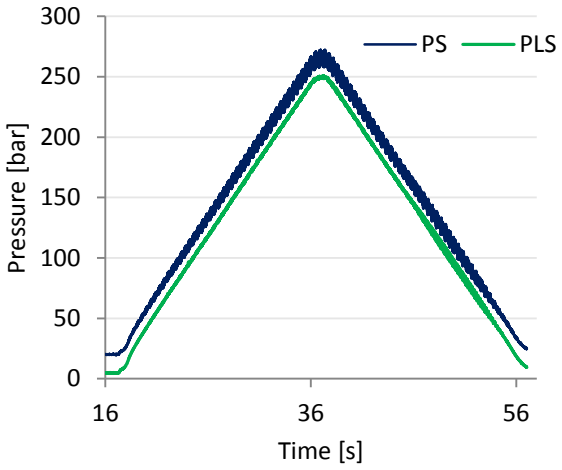

Figure 7.10 a) Pressure curve of system and LS for θ_{IN} = 3°

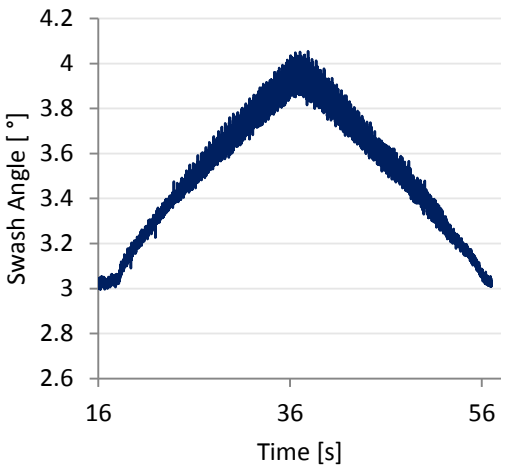

Figure 7.10 b) Variation of the swash angle θ_{IN} = 3°

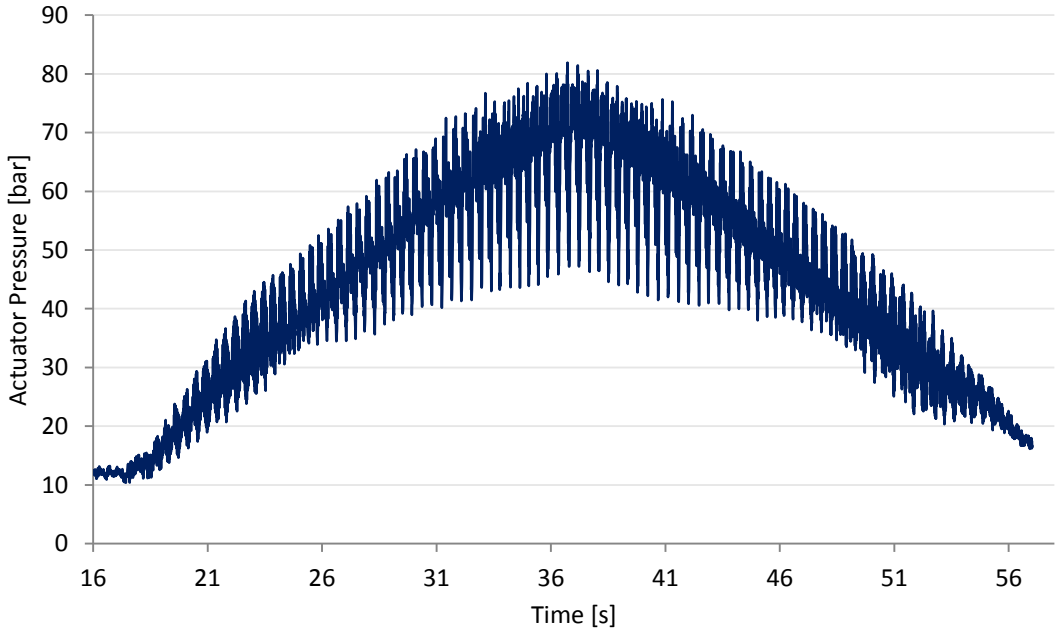

Figure 7.11 Variation of the actuator pressure for θ_{IN} = 3°

seen from Figure 7.11. The data from all trials were filtered using linear or quadratic fit to then define three-dimensional curves in which the angle θ of the swash plate was expressed as a function of system pressure PS and the actuator PACT (Figure 7.12). It was hoped that a three-dimensional surface plot could be obtaine that could be defined uniquely as the output angle θ, once defined PS and PACT and n, and then build a table useful for the completion of the model. From the processed data we see that there are not unique plots for each swash angle instead all curves are almost overlapping. This would

makes it impossible to achieve the objective of creating a table to define the position of the swash angle. Fortunately this data allowed us to use the collected data in another way to define the model the pump.

On further study of the curves it has been found that the intermediate positions of the swash plate is obtained by a relation between P_S and P_{ACT} that keeps in balance the swash plate and overlapping features found, (Figure 7.15), shows that this report does not change with change in θ (the straight line interpolation of the curves is described by Eq. shown in green in the Figure), which means that for all intermediate positions of the swash plate P_{ACT} needed to keep it in balance, ie to balance the force due to the P_S, is almost constant. In other words, the "Barrel Force", for an operating condition, is almost constant with change in θ (= SA).

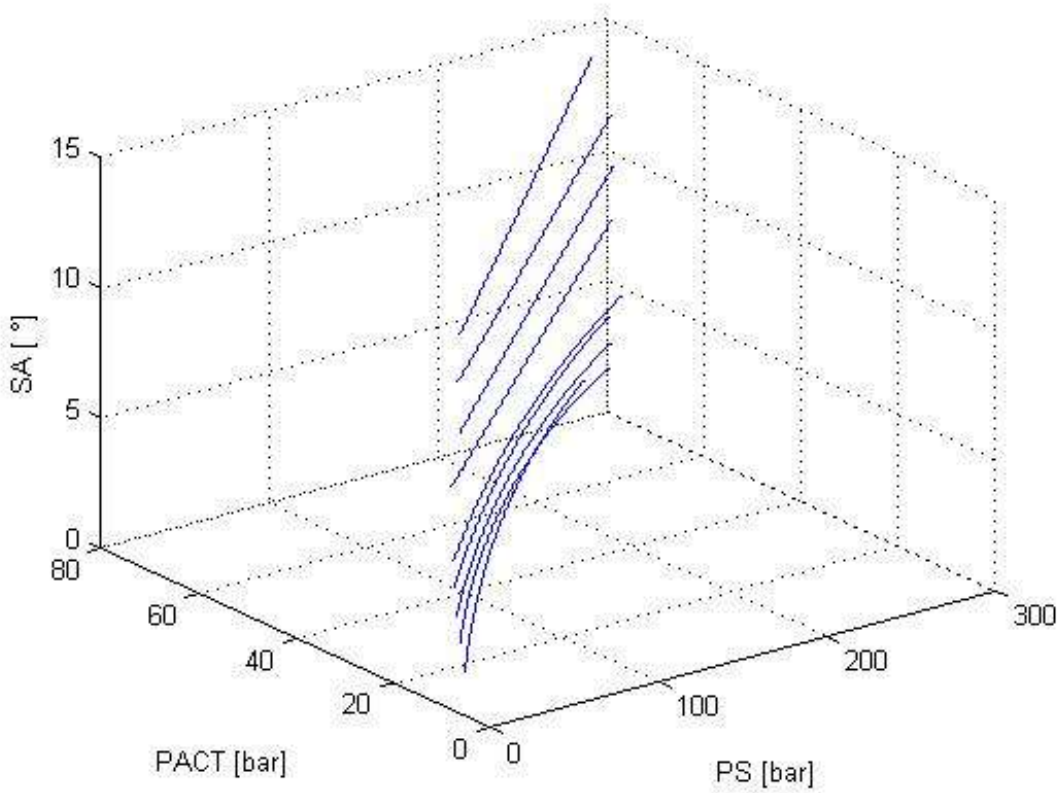

Figure 7.12 3D Graph with regressed curve obtained from the first experimental test

In the second and third round of testing the experimental pump was carried out by excitation of the proportional pressure relief MC10T Walvoil, with ramps of pressurising the chamber of the actuator to de-stroke the pump to minimum displacement in various working conditions. Initially it was set to the rotation speed of 1000 rpm and 5 iterations were performed for each test, loads between 20 and 250 bar in steps of 15 ÷ 20 bar between one and another. As can be seen in Figure 7.13 the angle of inclination of the plate (Swash Angle) changes from values close to 21 ° when you are in conditions of maximum displacement to zero values (minimum displacement) from the moment the

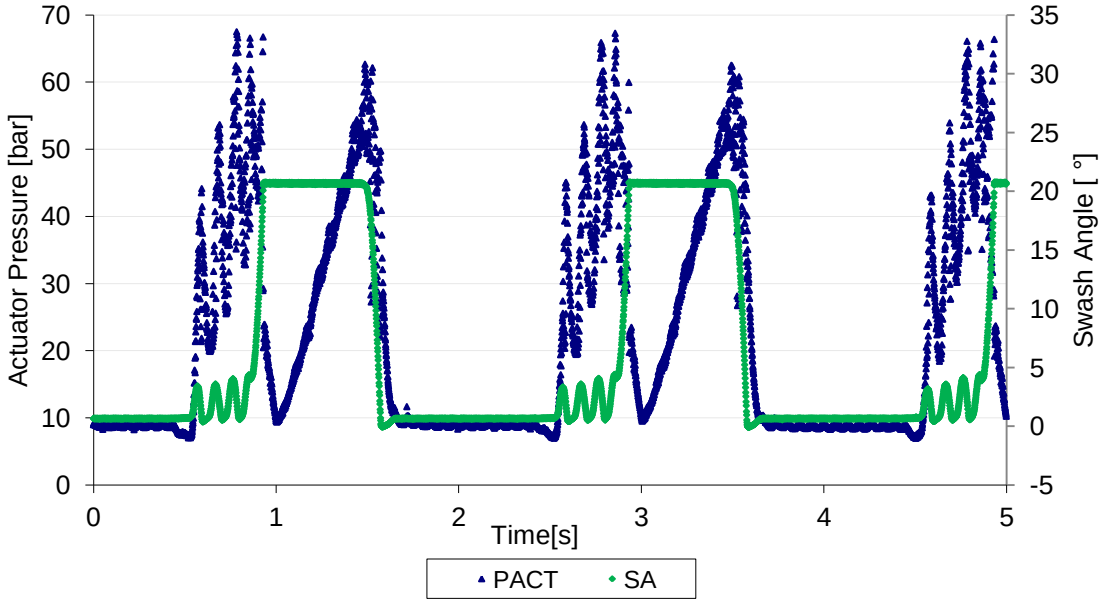

Figure 7.13 Iterative tes carried out to determine the pumps displacement at 1000 rpm with a load of 135 bar

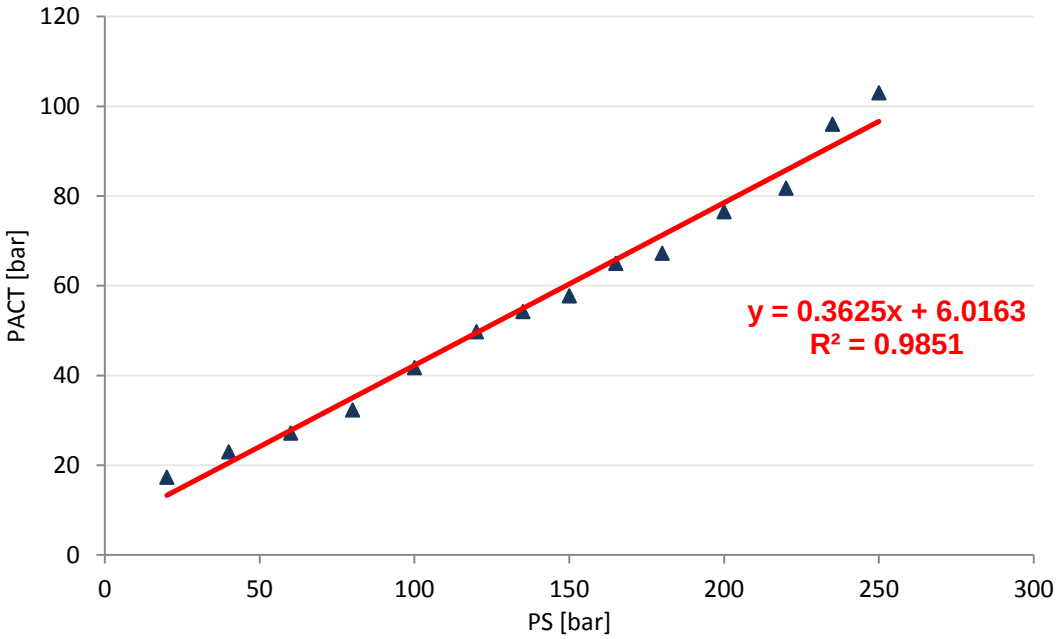

Figure 7.14 Results for the test carried out at 1000 rpm

force generated by the increasing pressure in the actuator control overcomes a force of the pistons: it is at that moment that you have collected the values of P_S and P_{ACT}. In Figure 7.14 shows the values were obtained from these tests: you can see how they are distributed roughly along a straight line, namely as the actuator pressure required to destabilize the system increases linearly with the pressure of the pump. In other words you can describe the relationship between the force of the cylinder block and the actuator force on the oscillating plate with the simple equation of the straight line interpolation of the results shown in Figure 7.14: the confidence in these value is further confirmed by the regression coefficient near to 1.

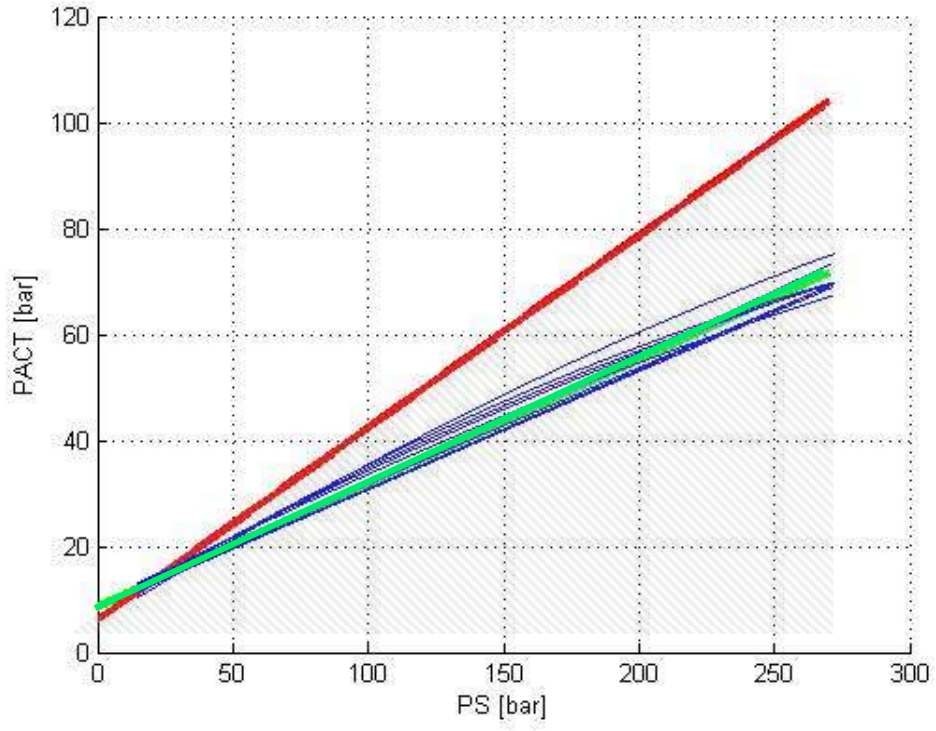

PACT = 0.3625* PS + 6.0163 **PACT = 0.2333* PS + 8.5**

Figure 7.15 Superimposing the curve of figure 7.14, with the regression curve (in green), and the characteristics of the figure in 7.14 (in red)

This report describes what happens in the initial condition of the pump's maximum displacement, whichever is superimposed on the characteristics and is obtained in the first round of tests (Figure 7.15) shows a significant divergence is between the two. Figure 4.12 describes the curves that are integral in the balance of forces between the control piston actuator and barrel forces. The figure illustrates that once the swash plate is displaced from its max position of 21° which is described by the equation of the red line it falls into the zone where all the intermediate angles can be defined by the equation of the green line, which is obtained by interpolating 20 curves.

The determination of the characteristic PS-PACT was also performed at speeds of 500 rpm and 1500: the data are shown in Table below. What is known is that the characteristic changes little with change in n: ultimately the final model pump will also take account of this effect and will be enough to create a table of coefficients depending on the value of n

which works the pump generate a different balance of forces on the lever that acts as a swash plate.

Table 7.6 Parameters to Define the equations which is represented in figure 7.16

Angular Velocity	500 [rpm]	1000 [rpm]	1500 [rpm]
PS [bar]	PACT [bar]	PACT [bar]	PACT [bar]
20	16.7	17.3	18.3
40	24.8	23.0	22.8
60	35.7	27.2	27.2
80	44.2	32.3	34.0
100	49.4	41.8	40.6
120	56.3	49.8	45.3
135	64.1	54.3	49.3
150	71.6	57.8	51.6
165	79.3	65.0	56.8
180	87.1	67.3	63.3
200	97.0	76.5	71.9
220	107.0	81.8	77.8
235	117.3	96.0	83.0
250	124.8	103.0	87.5
Linear interpolated relation	**PACT = 0.4632* PS + 4.9647**	**PACT = 0.3625* PS + 6.0163**	**PACT = 0.3048* PS + 9.5305**

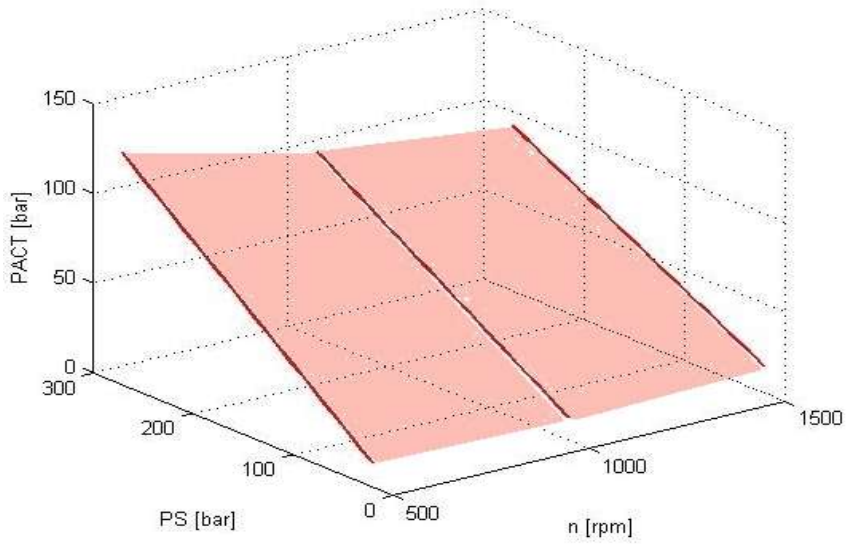

7.16 Characteristics of PS-PACT destoking of the pump at different angular velocities

Subsequent tests were performed on the simulation pump to determine the ability of the model to replicate the operation of the real pump. As mentioned previously with the classical configuration of the pump circuit, the LS Signal is fedback to the flow compensator after passing through a ball valve. The ball valve has been instrumented with pressure transducers and a flow meter so that the orifice area can be determined analytically. These tests were carried out at 1000 rpm. The load characteristics were acquired from the test bench and were used to drive the simulation model.

The simulation models input parameters were obtained from the actual experimental test data to compare the results. The control inputs of the model, highlighted in yellow in Figure 7.17, are the experimental data load (relief valve) on the pump outlet line and a signal to represent the dimensionless orifice that acts as a distributor.

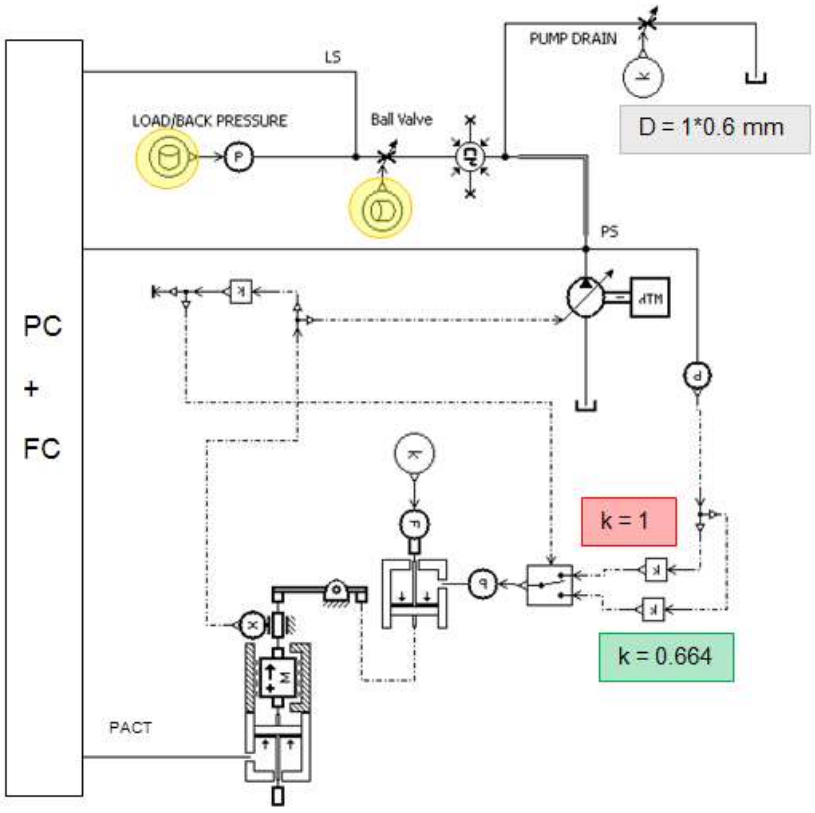

Figure 7.17 AMESim model of the flow characteristics model

Test Results: **Destroking of the pump without load**

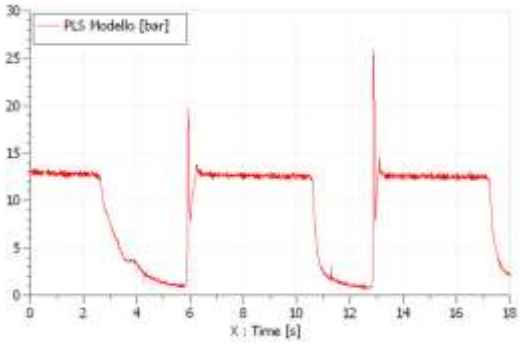

Figure 7.18 a) Backpressure of the test bench

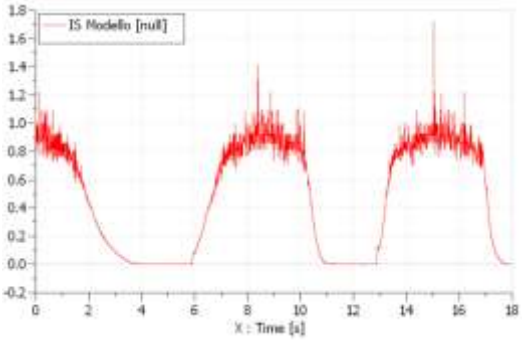

Figure 7.18 b) Dimensionless signal to represent the orifice (D = 14mm)

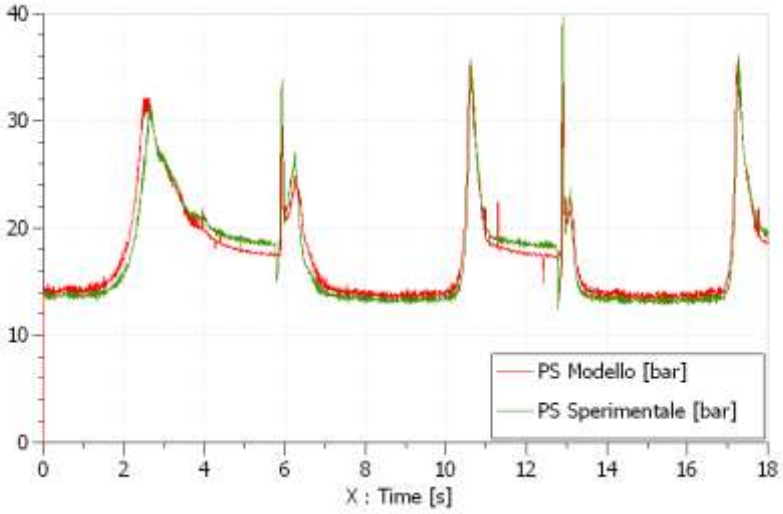

FIgure 7.18 c) Comparison of simulation and experimental simulation pressure

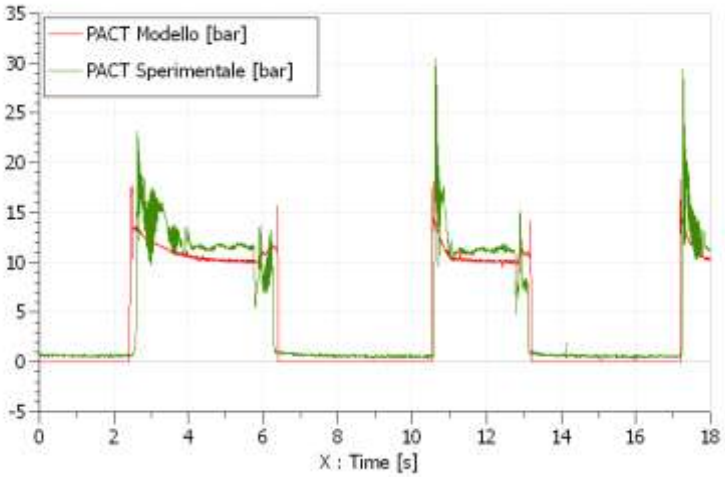

Figure 7.18 d) Comparison of the experimental and simulation actuator pressure

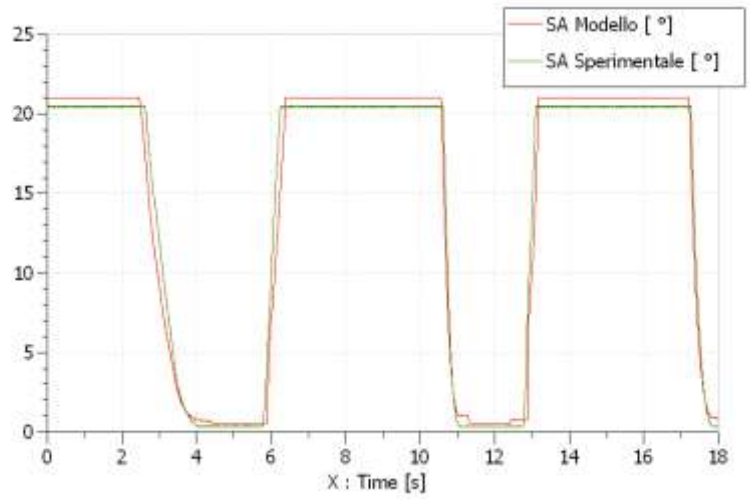

FIgure 7.18 e) Comparison of the swash angle

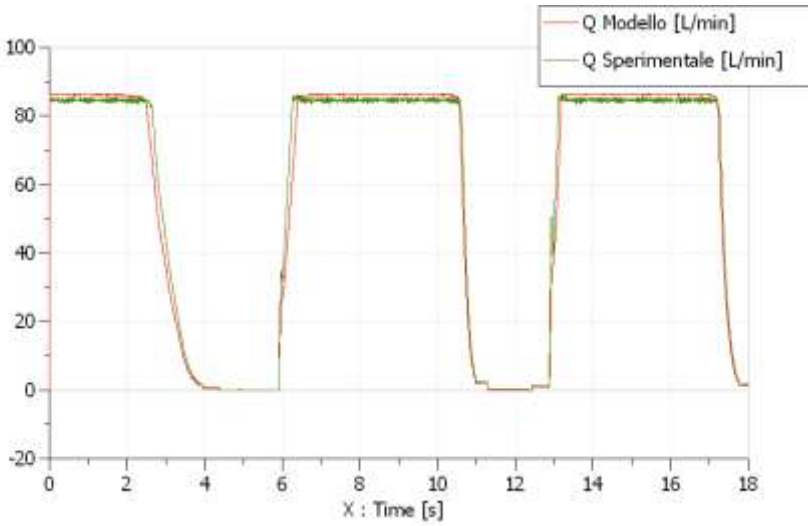

FIgure 7.18 f) Comparison of the flow

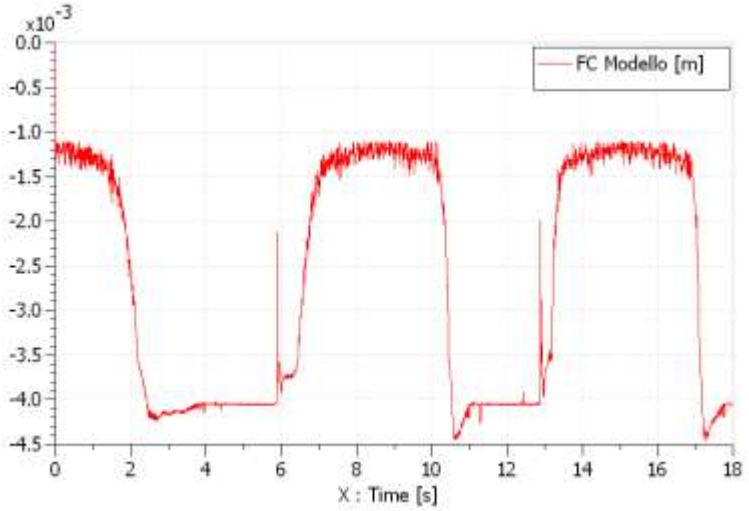

FIgure 7.18 g) Displacement of the flow compensator

Test Results: **Destroking at 150 bar**

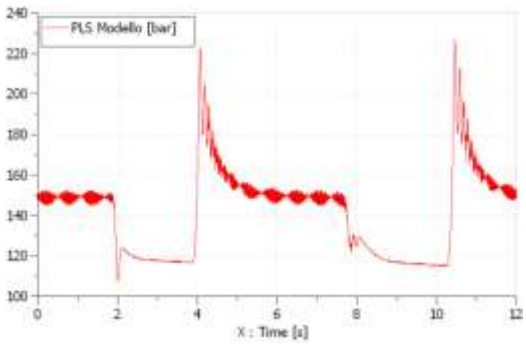

FIgure 7.19 a) Load on the supply line

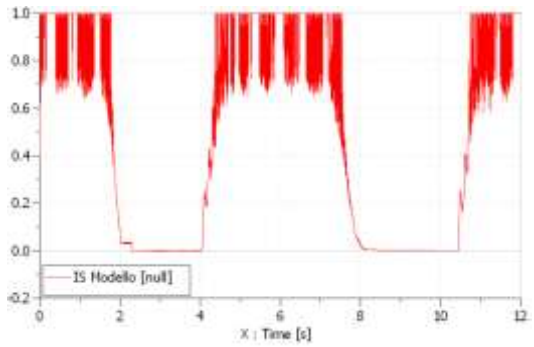

Figure 7.19 b) Dimensionless signal to control the orifice (D = 14mm)

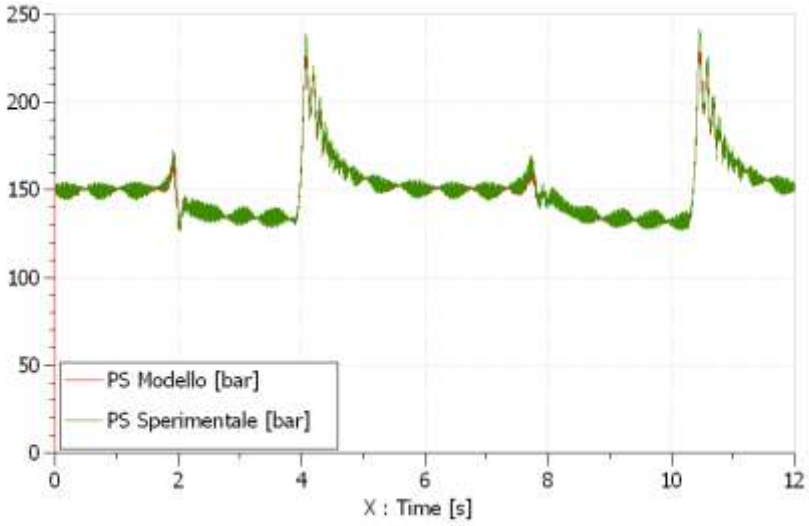

FIgure 7.19 c) Comparison of system pressure – experimental and simulation

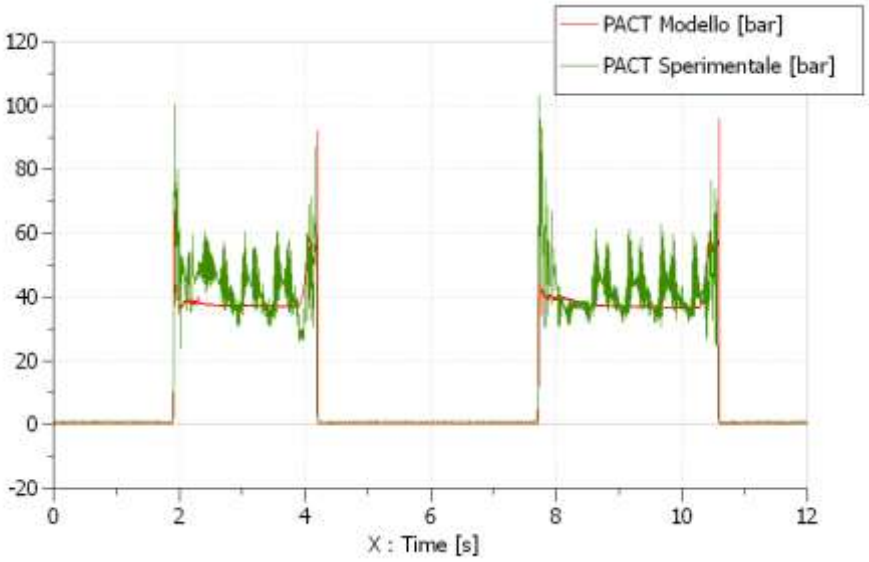

FIgure 7.19 d) Comparison of the simulation of the actuator pressure

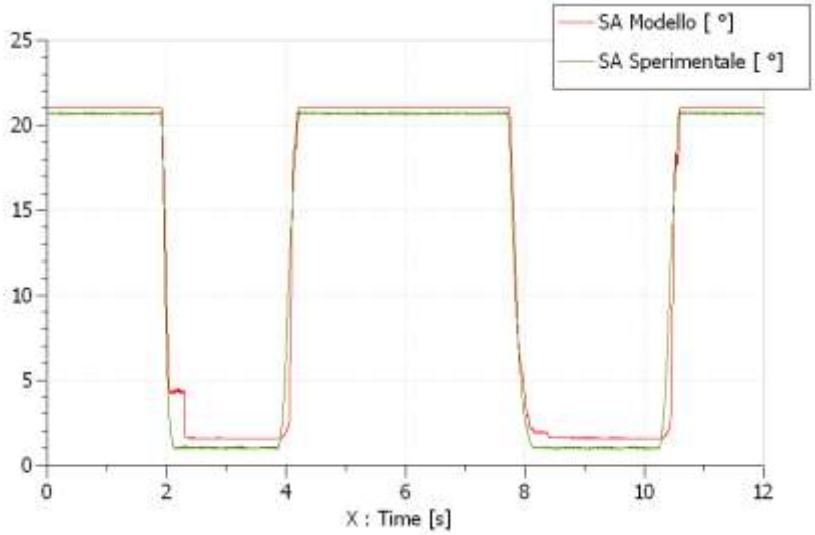

FIgure 7.19 e) Comparisonof the swash angle

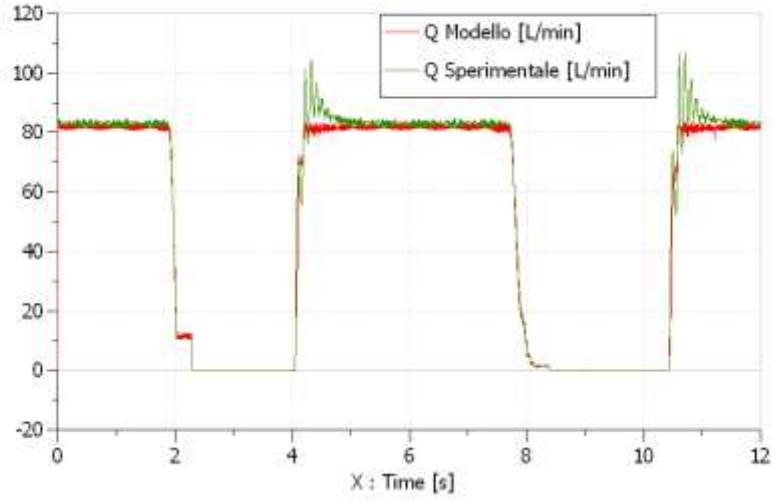

FIgure 7.19 f) Comparison of the flow

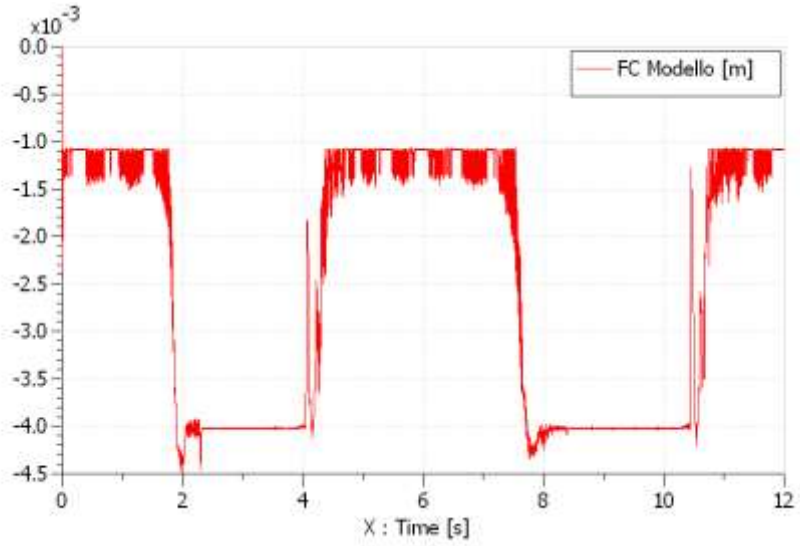

FIgure 7.19 g) Displacement of the flow compensator

Test Results: **Random load test**

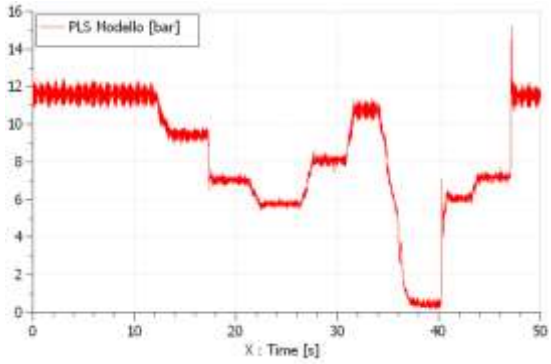

FIgure 7.20 a) Line pressure of the supply line

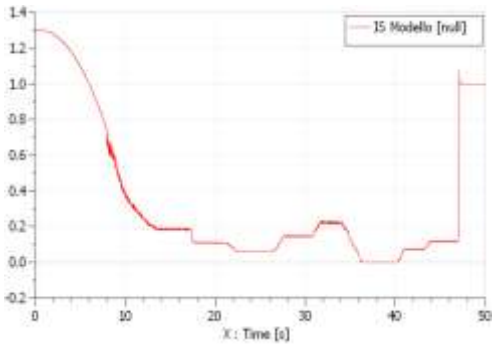

FIgure 7.20 b) Dimensionless orifice signal (D = 14mm)

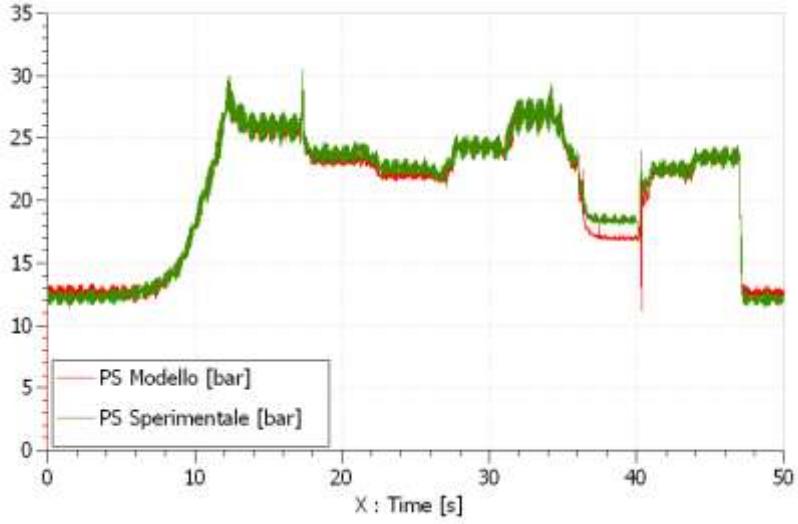

FIgure 7.20 c) Comparison of the system pressure – Simulation and Experimental

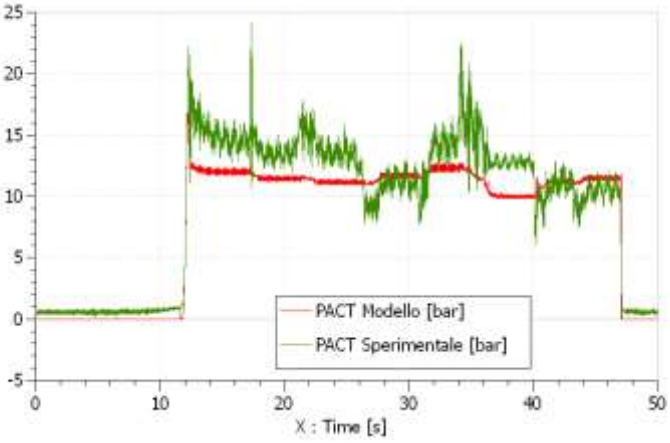

FIgure 7.20 d) Comparison of the actuator pressure – Simulation and

Experimental

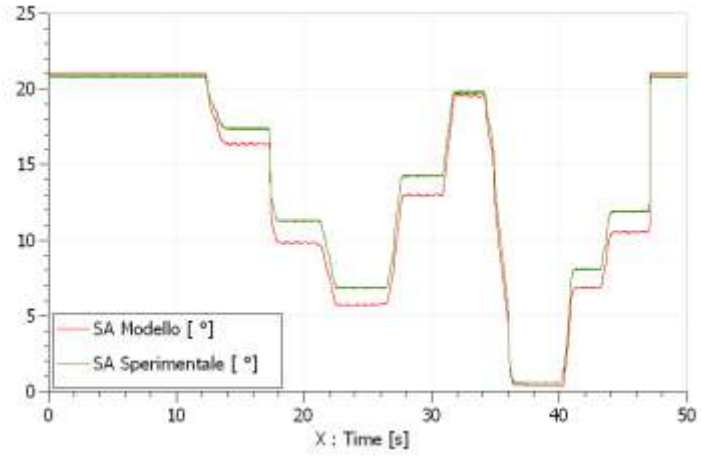

FIgure 7.20 e) Comparison of the swash angle

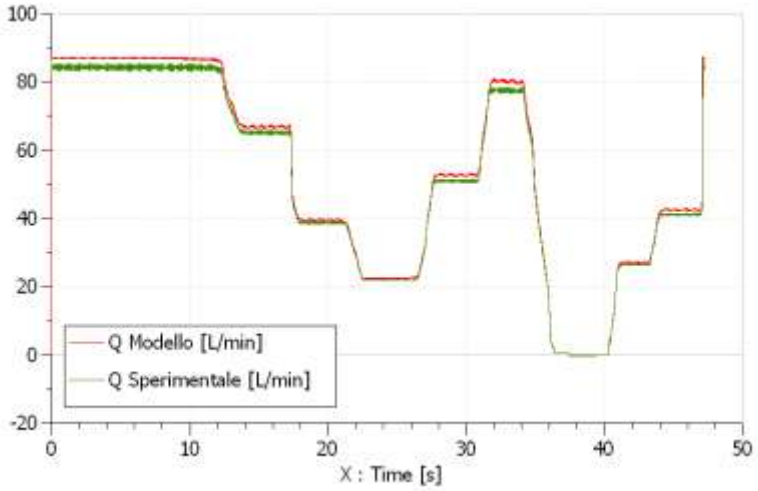

FIgure 7.20 f) Comparison of flow

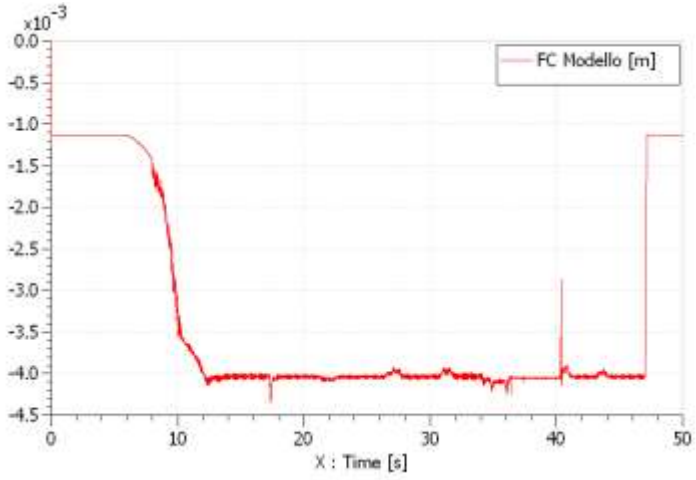

FIgure 7.20 g) Displacement of the compensator

Test Results: **Random positions at 230 bar**

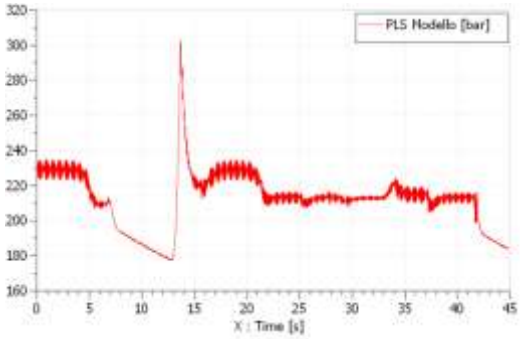

FIgure 7.21 a) Load on the pump output flow line

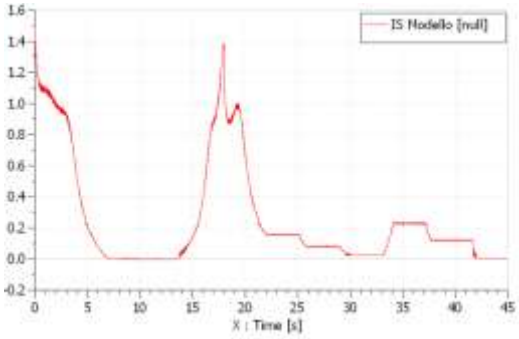

FIgure 7.21 b) Dimensionless signal for orifice area (D = 14mm)

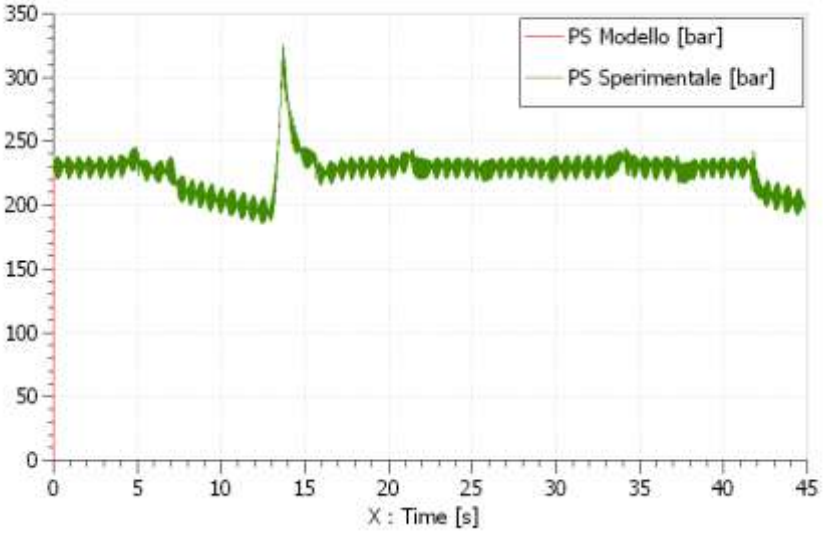

FIgure 7.21 c) Comparison of the system pressure

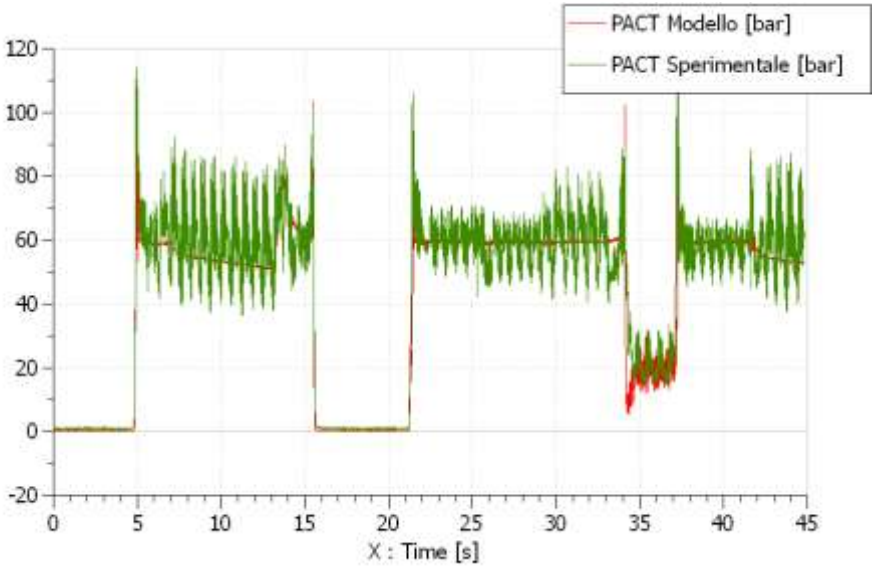

FIgure 7.21 d) Comparison of the actuator pressure

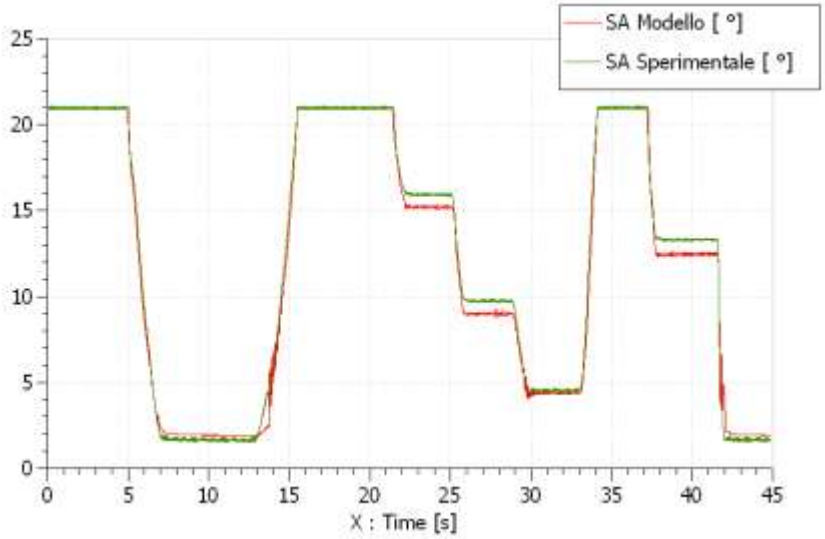

FIgure 7.21 e) Comparison of the swash angle

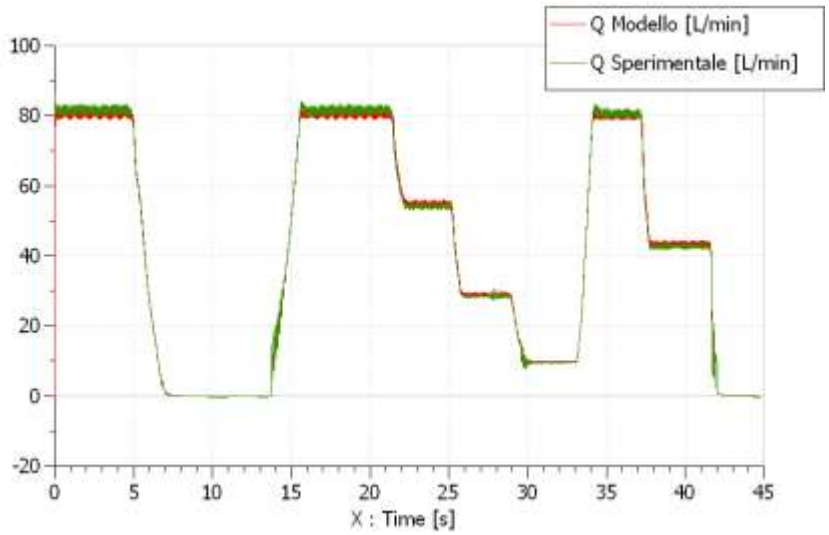

FIgure 7.21 f) Comparison of the flow

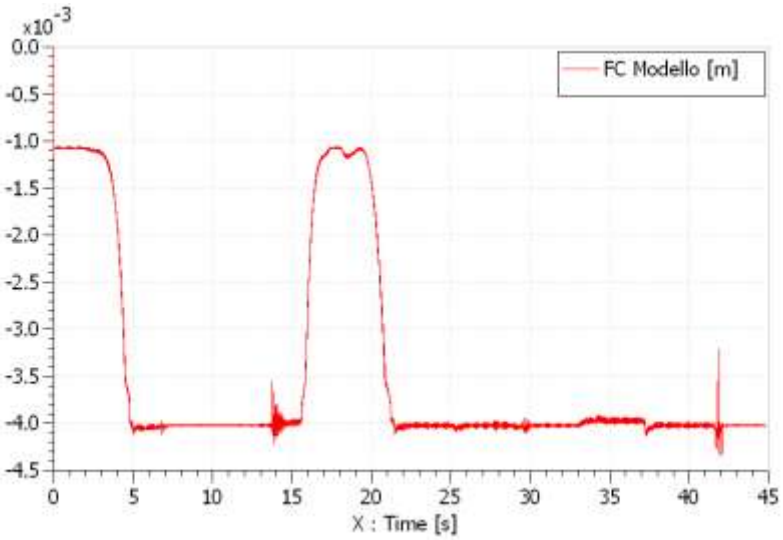

FIgure 7.21 g) Displacement of the flow compensator

With regard to the test of destroking the pump (Figure 7.18 and 7.19) can be observed that the discharge pressure of the pump model is in fact identical to the real one, and this means that the flow compensator is working properly. It is also seen that if the oscillations and the noise of the measurement are filtered the pressure to the actuator in the model provides a good approximation of the force in the pump. This validates the method by which the model was built and set the balance relations of forces. To complete the analysis of the output of the pump flow rates are compared and elaborated. In this case the values are almost identical in both the maximum displacement is transient.

The dynamic tests performed while keeping the pump swash plate in intermediate positions (Figure 7.20 and 7.21) are also satisfactory, although the deviations of the data model are greater than the experimental ones. The scope and therefore the inclination of the plate model faithfully replicate the behavior of the machine during the simulation the plate of the pump, subject by the same boundary conditions, reproduces well the transient and takes positions that have maximum errors of about one degree (5% FS). Without the volumetric efficiency of the pump (to simplify the drainage with a fixed orifice) and the approximate area of passage defined by the valve (following the method by which this signal has been inserted) are certainly among the causes of this unacceptable error. It can also be seen that the drain inserted in the model underestimates the volumetric loss of the machine as in all conditions intermediate values of the model remains at θ slightly smaller than the actual pump.

The delivery pressure of the pump is replicated accurately, while the pressure of the actuator model is slightly different from the experimental one: this can be justified by the considerable dispersion observed in the experimental data of the tests described above (the curves of Figure 7.12 are not perfectly superimposed).

The simulation data for the flow compensator shows that near the critical condition of opening of the orifice (3.9 ÷ 4.0 mm) in all periods in which the pump should remain in intermediate positions.

7.2.1 Frequency response test of the MVP 60-80

This chapter deals with the experiments that were carried out to quantify the response time of the pump. The pumps dynamic response offers the key inputs required to design controllers for characteristic a frequency response analysis is the response of the system to a sinusoidal input. It is important for understanding the propagation of variability through a process, but it is not normally used for tuning or designing industrial controllers. The speed of a process is important to take into consideration before choosing the frequency of the set-point variation. It is important to understand the feedback control behavior of a process in order to effectively control it and keep it stable. To study the effect of sinusoidal

inputs over a range of frequencies, a Frequency Response Analysis must be used. The analysis involves generating data about how the open loop process reacts to input changes of varying frequencies.

The figure below depicts a process with a sinusoidal input.

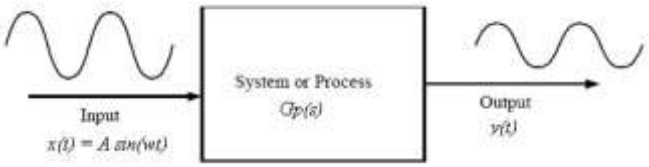

Figure 7.22: Process being tested with a sinusoidal input

When using experimental results, frequency response data is taken on an open loop, proportional-only control. To gather data for the Bode plot, the following steps are to be taken:

1. Open the control loop between the sensor and controller.
2. Turn off integral and derivative control by setting τ_I to infinity and τ_D to zero.
3. Set $K_c = 1$.
4. Input a sinusoidal variation at a range of frequencies and measure the phase angles (φ) of the outputs.
5. Record the amplitude value of the variation and system response versus time.

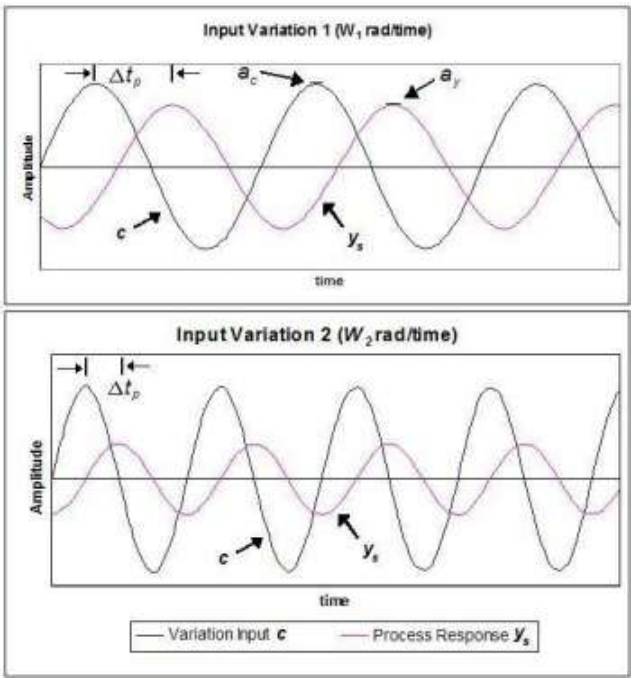

The graphs above can be read as follows:

1. The curve labeled *c* shows the sinusoidal variations to the set-point (input)
2. The sine wave labeled y_s models the process response (output)
3. A_r is the amplitude ratio. The amplitude ratio is the amplitude of of y_s divided by the amplitude of *c*. In the graph above a_y and a_c are labeled to show where the values for computing A_R can be found.

$$A_r = a_y/a_c$$

The phase angle of a system is also important for understanding and interpreting a Bode plot in the frequency response analysis. The phase angle (φ) indicates how much the controller output lags behind the controlled variable. To calculate the phase angle, the time difference between peaks, Δt_p, is converted into an angle.

$$\varphi = (\omega\ \Delta t_p / 2\pi)* 360°$$

The frequency of the input variables, ω, is measured in radians per second. Also, the Δt_p is assumed to be positive when *c* lags y_s.

The Bode plot of the process can then be constructed by plotting the logarithm of amplitude ratio (log A_r) and phase angle (φ) versus the logarithm of frequency (ω).

The Bode stability criterion:

> If the open-loop amplitude ratio is greater than unity (one) at a phase angle of -180°, the system is unstable under close-loop conditions.

Critical frequency, ω_c

> The frequency at which the phase angle is equal to -180°

Crossover frequency, ω_{co}

> The frequency at which the amplitude ratio is equal to 1

The Phase and Gain Margins of Stability occur at the point when the closed-loop system will sustain an oscillatory response to a step or impulse disturbance. At this point the system is on the brink of instability. The PM and GM values are a measure of how close the system is to instability. The large these values are for a system, the more conservative

the controller tuning. However, a larger value of the Gain Margin also causes a slower response of the controller, so it is desirable for it to be as close to one as possible. More nonlinear processes and disturbances of larger magnitude require larger values of PM or GM. GM values usually range from 1.4 to 1.8 and PM values range from 30° to 40°.

Phase Margin of Stability (PM): the difference between a phase angle corresponding to an amplitude ratio of 1 and a phase andgle of -180°. To find the PM:

1. Find ω_{co} when $A_r = 1$ by locating the point (ω_{co}, 1) on the amplitude ratio portion of the Bode plot. On a log scale, this point is found at (ω_{co}, log 1 = 0).
2. Find $\varphi_{Ar=1}$ on the phase angle portion of the Bode plot using the ω_{co} found in step 1 by locating the point (ω_{co}, $\varphi_{AR=1}$).
3. PM = $\varphi_{Ar=1}$ + 180°.

When PM > 0°, the system is stable.

Gain Margin of Stability (GM): The inverse of the amplitude ratio at the critical frequency. To find the GM:

1. Find ω_c (critical frequency) by locating the point (-180°, ω_c) on the phase angle portion of the Bode plot.
2. Find A_r using the value of ω_c found in step 1 by locating the point (A_r, ω_c) on the amplitude ratio portion of the Bode plot. On a log scale plot, $A_r = 10^{(\text{y-value at the point where } x = \omega_c)}$.
3. GM = $1/A_{r \text{ at } \omega c}$.

When GM > 1, the system is stable. If GM = 1 the system will have sustained oscillations.

Experimental results of frequency test

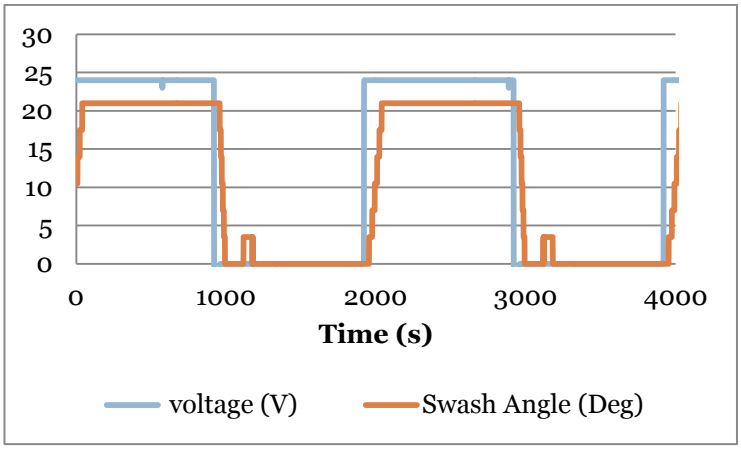

Figure 7.23: Pump response at 0.5 Hz step response

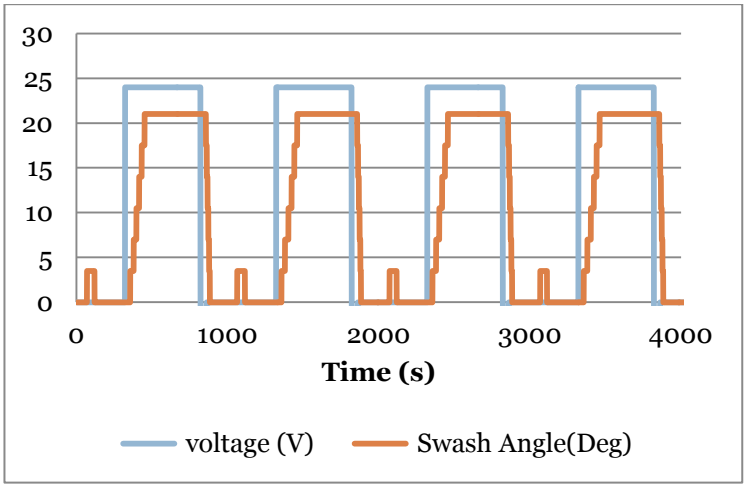

Figure 7.24: Pump response at 1 Hz step response

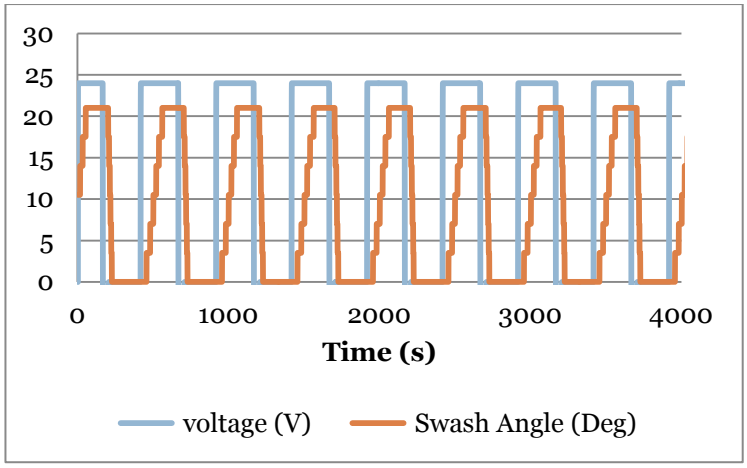

Figure 7.25: Pump response at 2 Hz

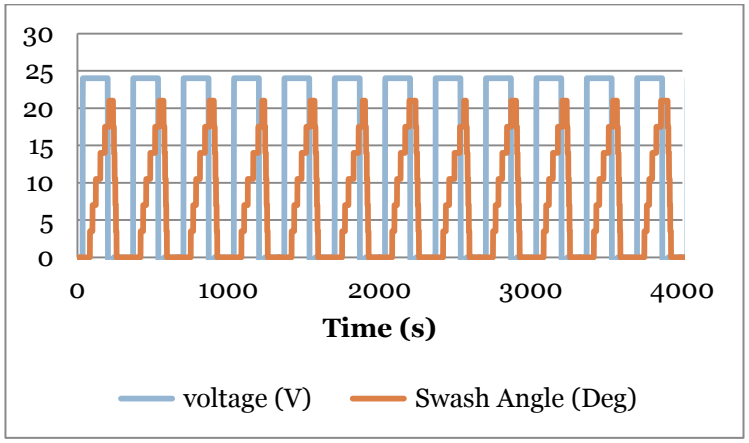

Figure 7.26: Pump response at 3 Hz

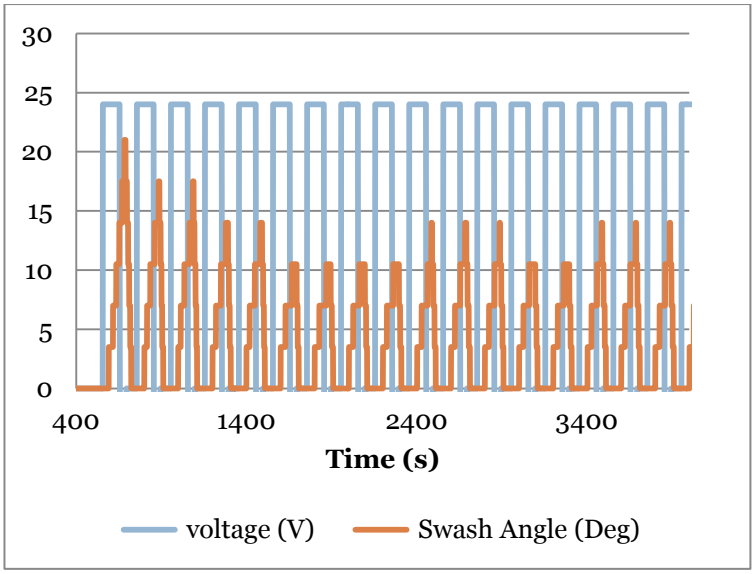

Figure 7.27: Pump response at 5 Hz

Table 7.7: Frequency response for destroking the pump

Frequency	Ac	Ay	Time (21-0)	Amplitude Ratio	Deg down
0.5	24	8	62	0.333	-11.16
1	24	8	73	0.333	-26.28
2	24	8	60	0.333	-43.2
3	24	8	58	0.333	-62.64
5	24	5	56	0.208	-100.8

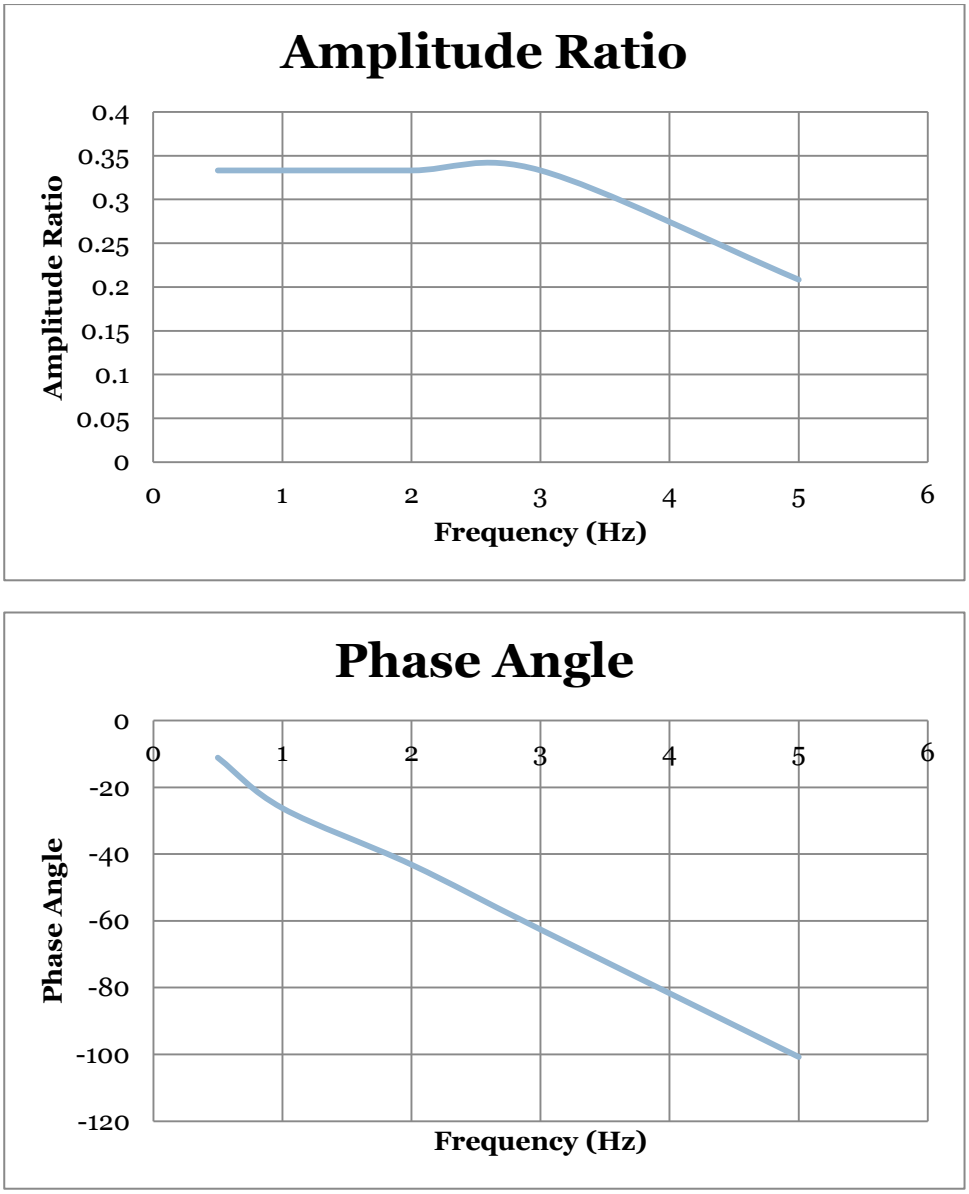

Figure 7.28 Bode Plot for destroking the pump

Table 7.8: Frequency response for stroking the pump

Frequency	Ac	Ay	Time (0-21)	Amplitude Ratio	Deg up
0.5	24	8	136	0.333	-24.48
1	24	8	118	0.333	-42.48
2	24	8	144	0.333	-103.68
3	24	8	176	0.333	-190.08
5	24	5	107	0.208	-192.6

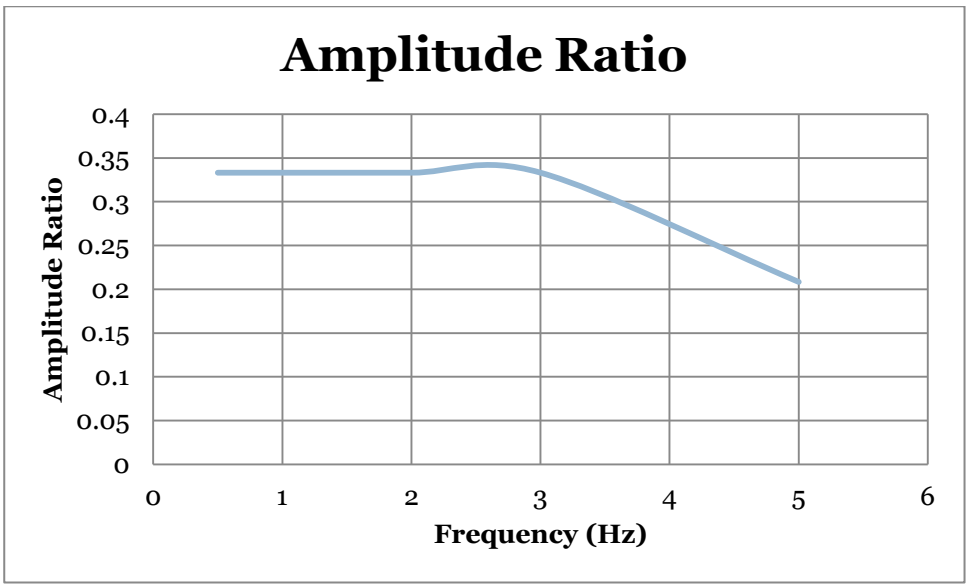

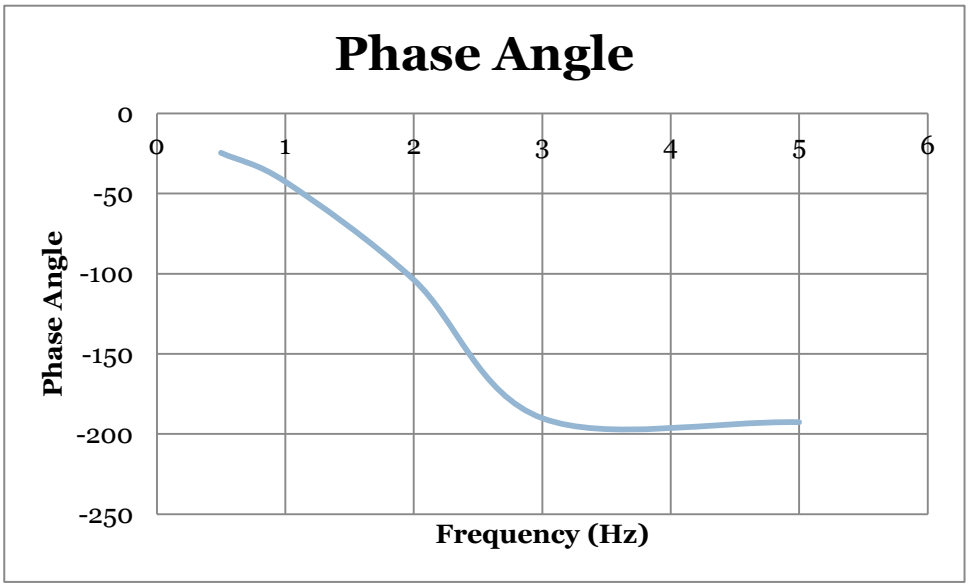

Figure 7.29: Bode Plot of Stroking the Pump

From Figure relating to the bode plot of the destroking of the pump we can clearly see that the pump has a maximum response frequency of 3.5 Hz for destroking the pump, after which the pump goes out of phase. At 3 Hz we see that the pump is - 60 Degrees out of phase. After this value this frequency there is a change in the amplitude so the pump cannot be used for operations requiring frequencies higher than 3 Hz.

From Figure relating to the bode plot of the stroking of the pump we can clearly see that the pump has a maximum response frequency of 1.8 Hz for stroking the pump, after which the pump goes out of phase. At 2 Hz we see that the pump is - 106 Degrees out of phase. After this value this frequency there is a change in the amplitude so the pump cannot be used for operations requiring frequencies higher than 3 Hz.

The data presented in this chapter is purely experimental to gain a better idea of the maximum frequency capacities of the pump. Future work could include modifying the linear equation of the pump model to replicate these high frequency tests. Though it might not be necessary as excavator response is generally less than 0.5 Hz.

7.3 Results of Walvoil DPX 100

This section describes the testing of the Walvoil DPX 100 as described in Chapter 6. The different experimental settings that were explained in the previous chapter are individually explained here, some results are a comparison of the experimental and simulation results and the others are purely experimental results that can be used by future researchers to take the model development forward.

Model Test Environment in AMESim

The figure describes the Walvoil DPX 100 single slice model in the virtual test environment, wehre it is linked with the real world inputs. The systems inputs are the flow

into the valve block defined as the system pressure which is modeled as an ideal flow element reading data from the actual experimental flow of the test bench. A relief valve has been used to set the inlet system pressure. The relief valve model used in Figure is that of an ideal relief valve to replicate the relief valve that was used to set the maximum system pressure of the test setup. The pressures of work port A and B were derived from the test bench and were directly fed to the simulation model using data table controllable relief valves. The main spools displacement was directly driven by a displacement transducer that read the data table from the experimnet on the main spools position and used the data to move the spool accordingly.

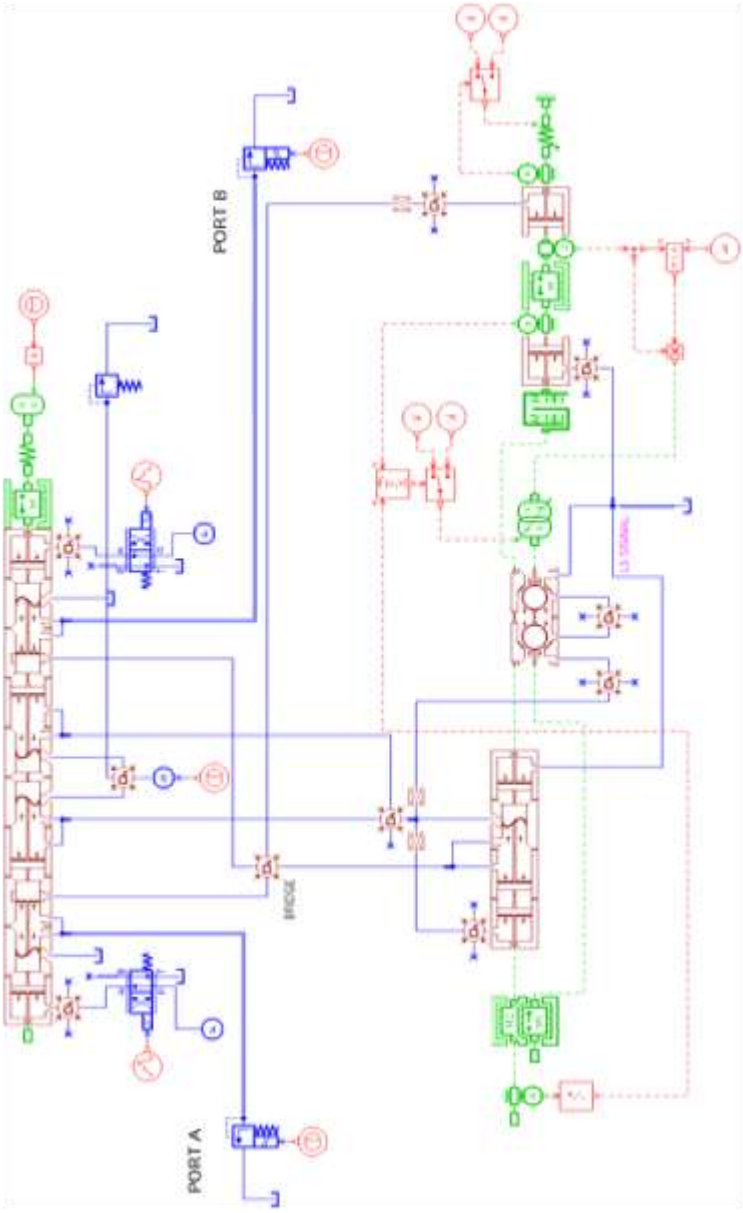

Figure 7.30: Model validation setup with test bench inputs in the AMESim environment

7.3.1.Test of a DPX 100 Single slice

1. Test 1 Analysis of Results:
    - The spools displacement as it can be seen the motion of the spool in the direction of Port A is more controlled as against the control in direction Port B. This is due to the different PWM settings on the controllers used to control the proportional solenoid
    - The system pressure defines the variation of the system pressure during the course of the experiment as the main spool opens and closes.
    - The bridge pressure provides insight into the pressures available to the work ports and conditions where the piston check valve is closing due to the increase in bridge pressure in respect to system pressure.
    - Port A pressure describes the pressure characteristics of the utility port as the load is controlled by the test benches relief valve.
    - Port A flow compares the experimental and simulation flow characteristics of the flow out of the valve as it can be seen there is a good correlation between the comparisons of results.
    - Port B pressure describes the pressure characteristics of the utility port as the load is controlled by the test benches relief valve.
    - Port B flow compares the experimental and simulation flow characteristics of the flow out of the valve as it can be seen there is a good correlation between the comparisons of results.

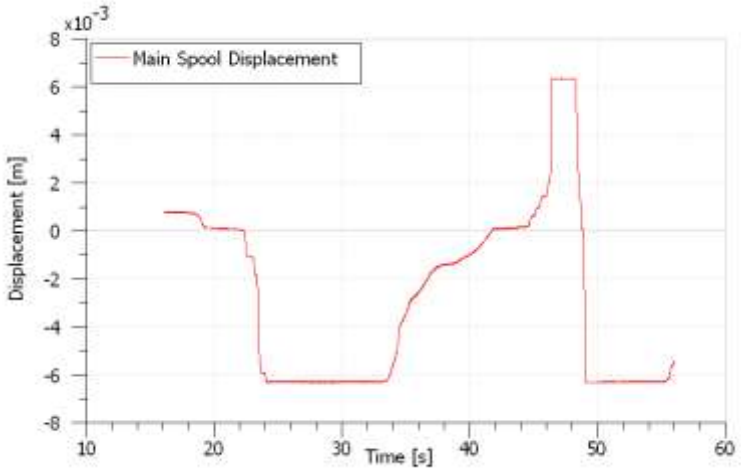

Figure 7.31 a: Main Spool Displacement

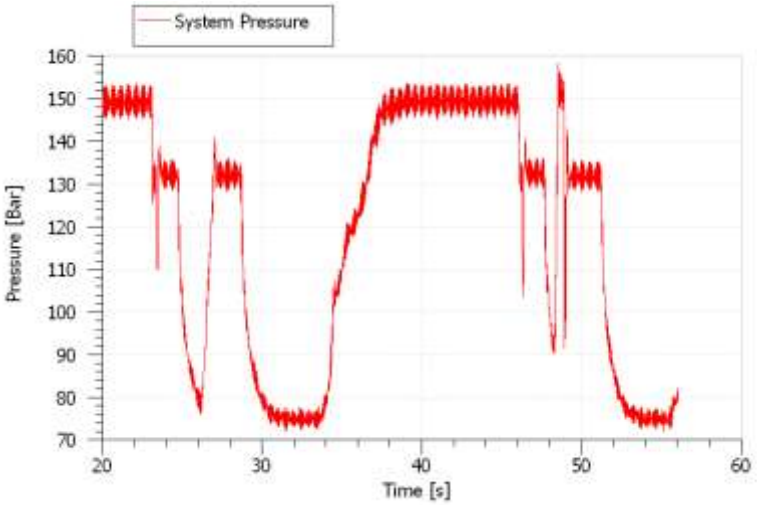

Figure 7.31 b: System Pressure

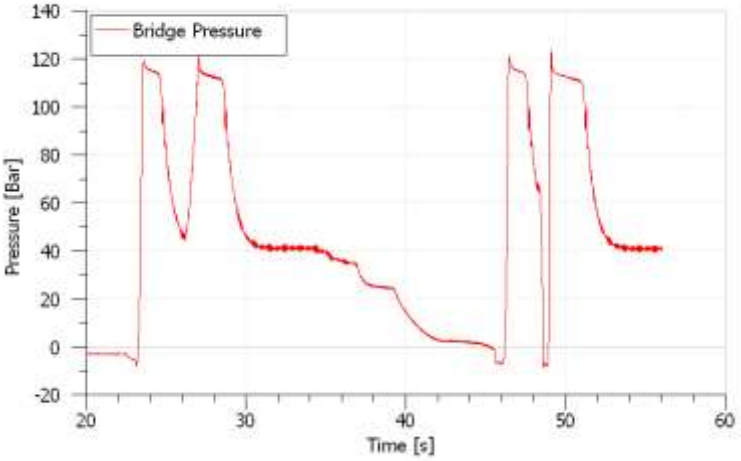

Figure 7.31 c: Bridge Pressure

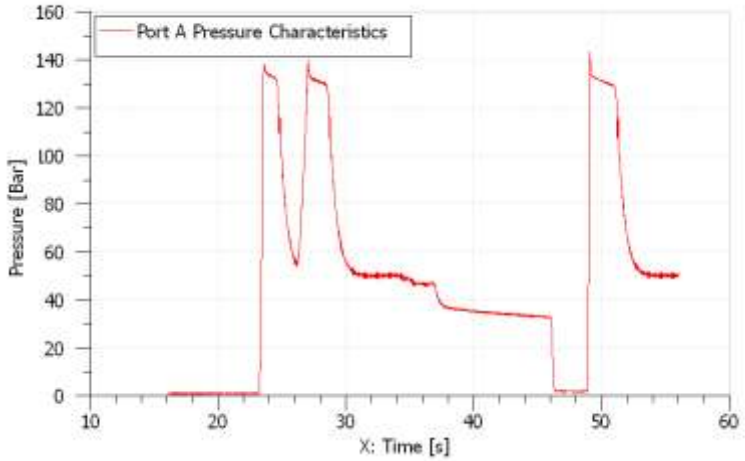

Figure 7.31 d: Port A Pressure Characteristics

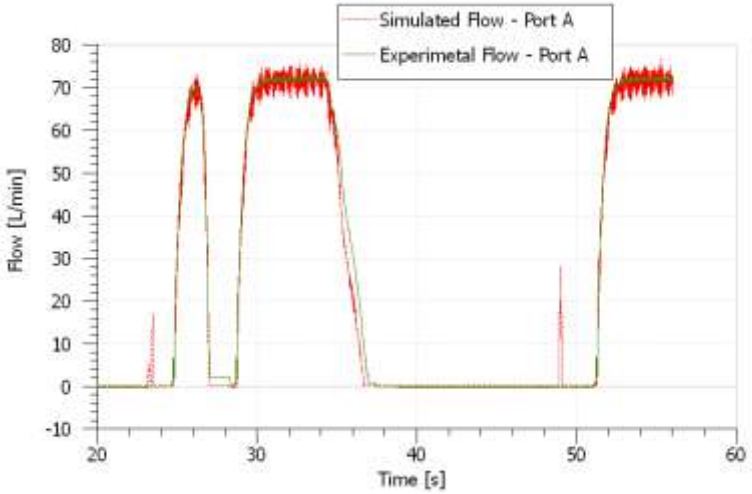

Figure 7.31 e: Port A Flow characteristics

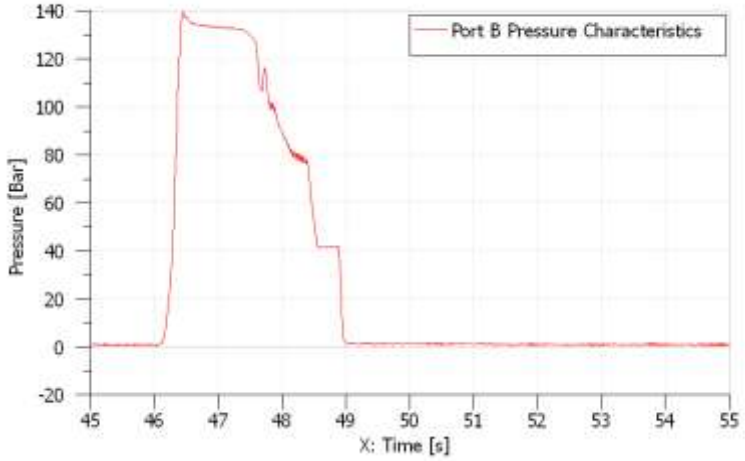

Figure 7.31 f: Port B Pressure Characteristics

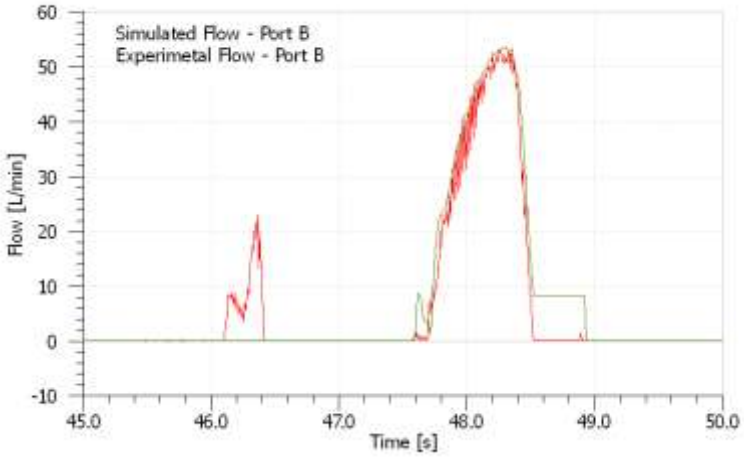

Figure 7.31g: Port B Flow characteristics

7.3.2 Test 2 DPX 100

2. Test 2 Analysis of Results:
    - The spools displacement as it can be seen the motion of the spool in the direction of Port A is more controlled as against the control in direction Port B. This is due to the different PWM settings on the controllers used to control the proportional solenoid
    - The system pressure defines the variation of the system pressure during the course of the experiment as the main spool opens and closes.
    - The bridge pressure provides insight into the pressures available to the work ports and conditions where the piston check valve is closing due to the increase in bridge pressure in respect to system pressure.
    - Port A pressure describes the pressure characteristics of the utility port as the load is controlled by the test benches relief valve.
    - Port A flow compares the experimental and simulation flow characteristics of the flow out of the valve as it can be seen there is a good correlation between the comparisons of results.
    - Port B pressure describes the pressure characteristics of the utility port as the load is controlled by the test benches relief valve.

- Port B flow compares the experimental and simulation flow characteristics of the flow out of the valve as it can be seen there is a good correlation between the comparisons of results.

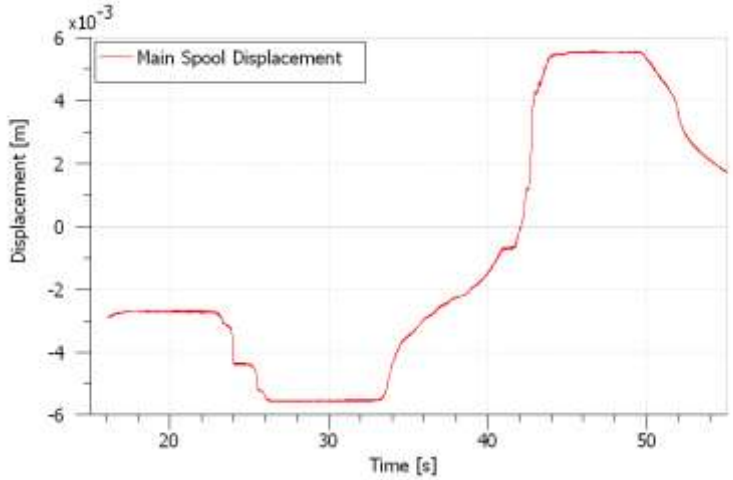

Figure 7.32 a: Main Spool Displacement

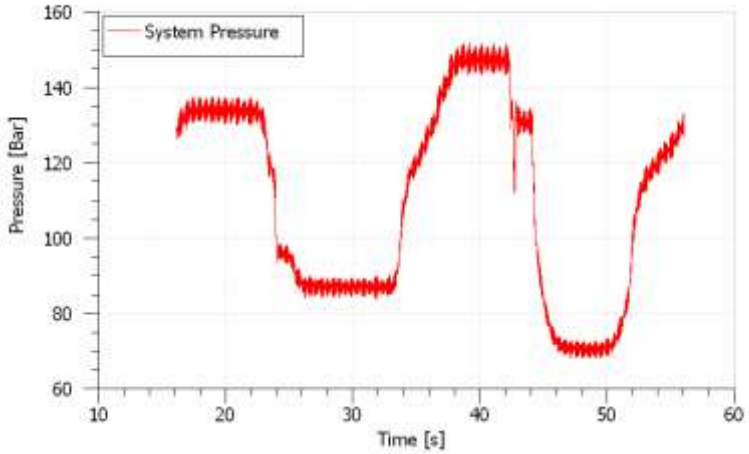

Figure 7.32 b: System Pressure

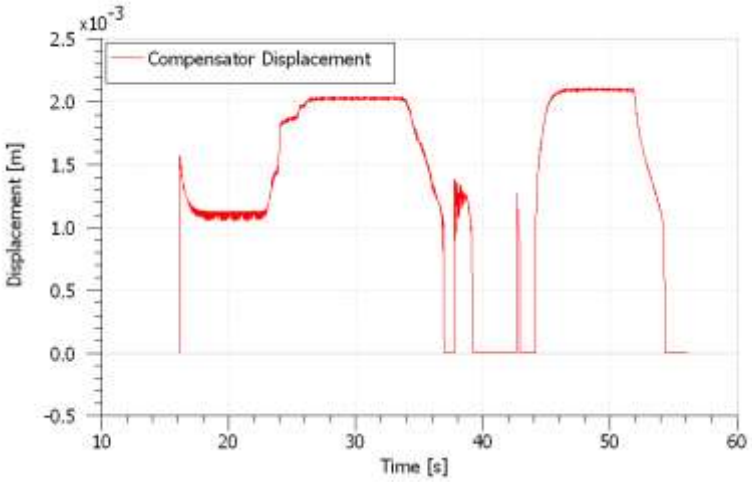

Figure 7.32 c: Compensator Displacement

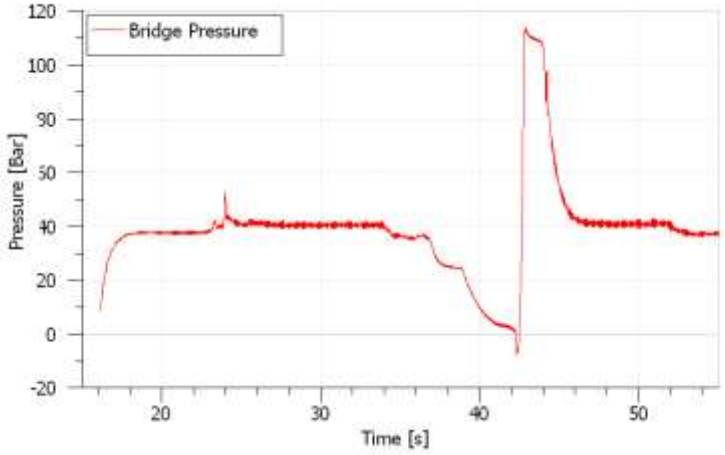

Figure 7.32 d: Bridge Pressure

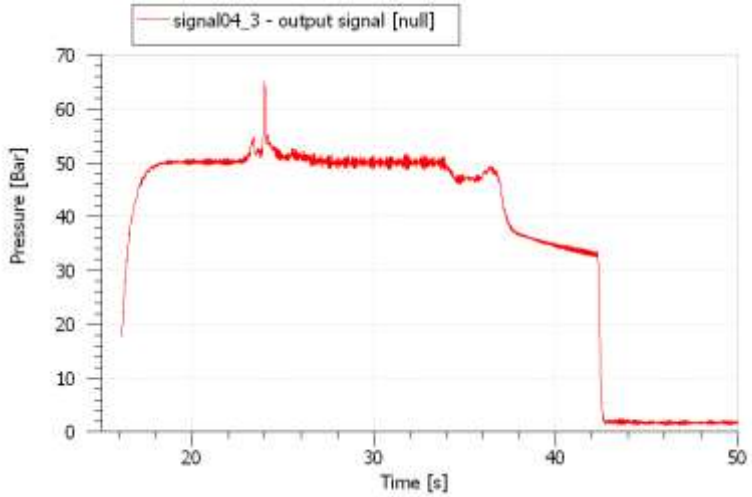

Figure 7.32 e: Port A Pressure

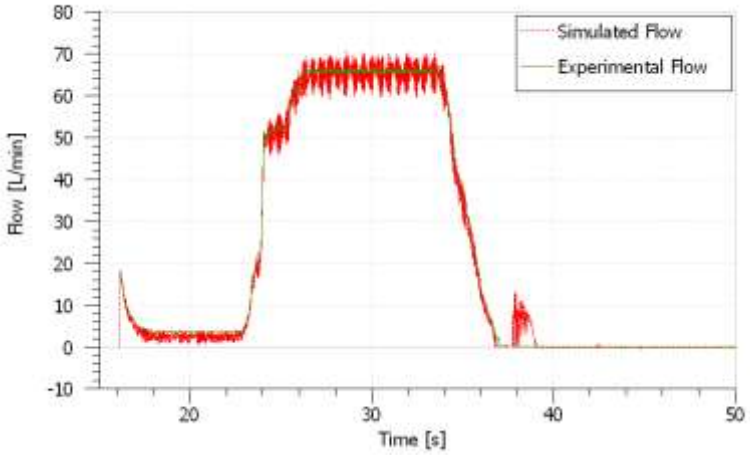

Figure 7.32 f: Port A Flow

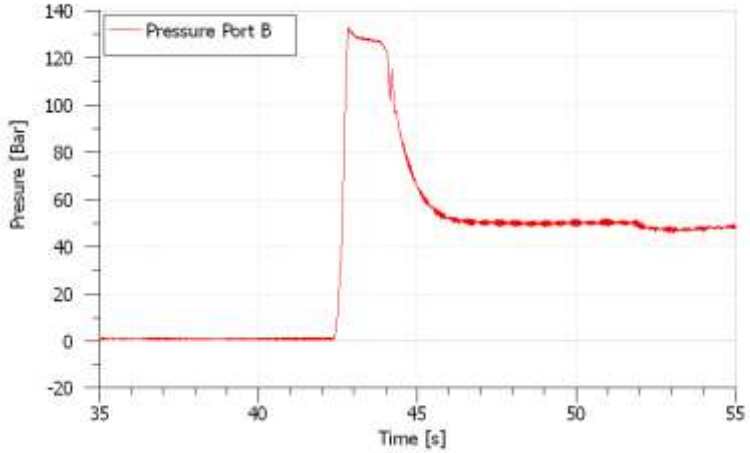

Figure 7.32 g: Port B Pressure

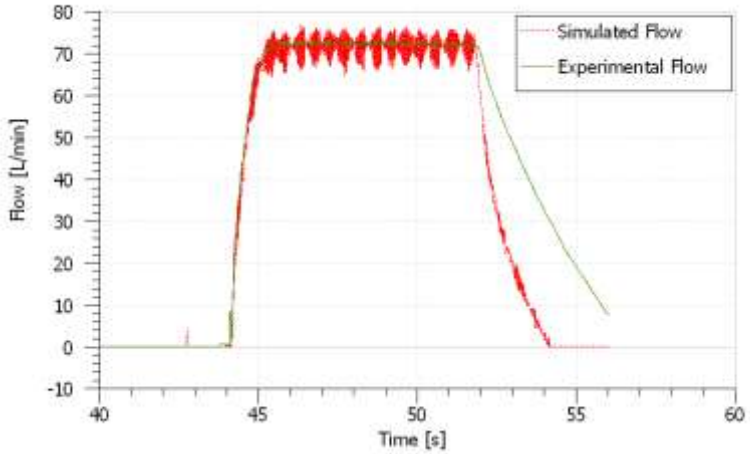

Figure 7.32 h: Port B Flow

7.4 Results relating to the excavator tests

7.4.1 Comparison of results – Field tests on an Excavator for Pump Characteristics

The digging cycle tests on the excavator were carried out to measure the pumps response to different excavation cycles. The data from the excavation cycles were used to verify and validate the functioning of the simulation model of the excavator. Digging cycles were carried out at different engine speeds to verify the functionality of the pump response at different operating conditions and load cycles. Figure 7.33 depicts the excavator that was used to carry out the experimental field tests and Table 2 describes the instrumentation used to measure the represented data as well as verifying the mathematical model. The simulation plots were verified at three different engine speeds: 1000r/min, 1500r/min and 1750r/min as can be seen in figures 7.33 respectively. Figure 7.33 describes the valve input signal that was used to actuate the valve on the excavator; this data was measured and used to drive the simulation model as an input signal.

Table. 7.9. Features of sensors and main elements of the apparatus used on the excavator

Sensor	*Type*
Pump Output Pressure	Strain gauge
Swash Angle Sensor	Inclination Sensor
Load Sensing Pressure	Strain Gauge
Valve Pilot Pressure	Strain gage
Actuator Extension Pressure	Strain Gauge
Actuator Retraction Pressure	Torque/speed meter
Output Flow	Flow Meter
Engine Speed	RPM Sensor

The verification of the actual pumps response can be seen in the following graphs as compared to the simulation model of the pump. The comparison of the experimental and simulation data shows that the simulation model has the capability of replicating the actual characteristics of the real pump. The difference in the plot results arrive from the actual excavator valve having non-linear orifice opening characteristics, whilst the model of the valve on the excavator has ideal orifice opening characteristics. This issue will be dealt with in future work, where the generic valve model will be replaced with a detailed mathematical model of the valve capable of recreating the non-linear orifice characteristics, thereby replicating the actual behavior of the pump.

Figure 7.33 a. Photograph of the Excavator used for the verification of the simulation model

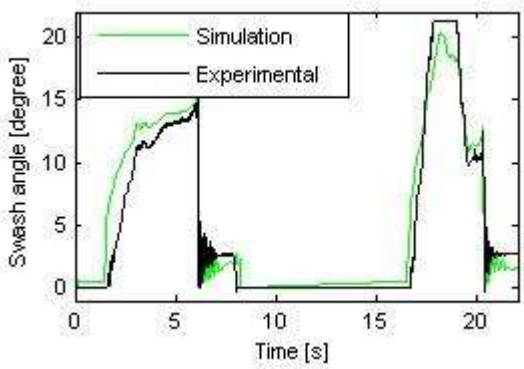

Figure 7.33 b. Swash angle at 1000 r/min

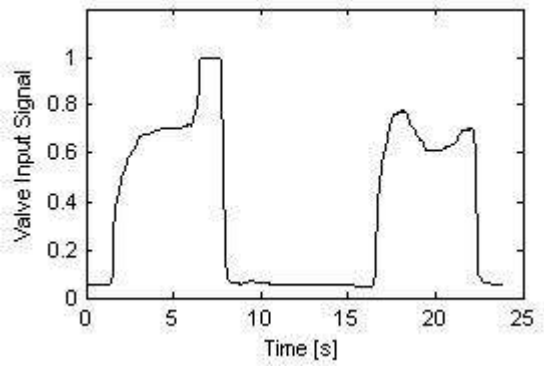

Figure 7.33 c**.** Valve Input Signal for 1000 r/min

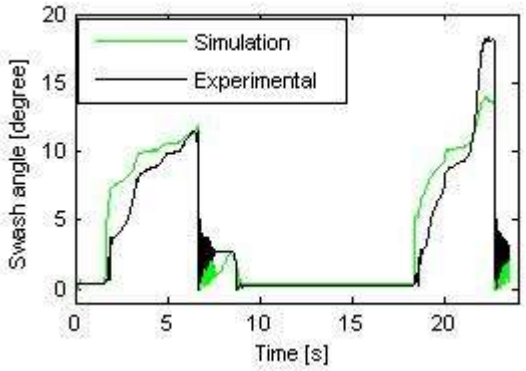

Figure 7.33 d**.** Swash Angle at 1500 r/min

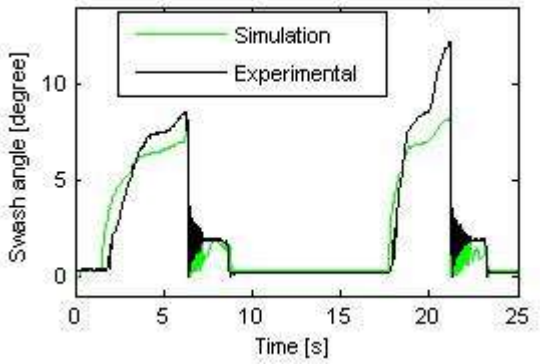

Figure 7.33 e**.** Swash Angle at 1750 r/min

7.5 Results relating to the complete excavator simulation

7.5.1 Excavator Model executing a digging cycle with boom, arm and bucket

On analysis of results presented in the previous section, it is evident that the pump model is capable of reproducing actual conditions. Thus the model was extended to include the valve blocks and the kinematics as depicted in Figure 11 and described in section 2.3. The complete system was subjected to a duty cycle as described in Table.3. The values from Table.3 were used to control the valve opening for respective implements. The pump's maximum displacement used for this simulation was 84 cm^3/rev and the engine speed was set at 1000 r/min. Figure 7.34 describes the initial condition of the excavator in the simulation model. Figure 7.34 describes the forces on the implements and the effects of these forces can be seen in Figures 7.34 in pressure terms on the boom, arm and bucket actuators. Figure 7.34 describes the pressures across the FC, as it can be seen the LS pressure is the instantaneous maximum pressure

of the system derived from the actuators and the pump pressure is the instantaneous system pressure. Figure 7.34 describes the differential pressure across the FC, which is equal to the pump margin set to about 17 bar. Figures 7.34 describe the spool displacements of the PC and FC respectively: the FC provides a flow path through the spool when the displacement is greater than 3.90 mm and the PC when the displacement is greater than 2.10mm. Figure 7.34 describes the pump swash angle controlled by the flow across the FC and PC spools.

Table. 7.10. Duty cycle – Control Signals to Valve Block for Boom, Arm, Bucket Motion

Implement Name	*Time [s]*	*Valve Opening [%]*	*Actuator Action*
Boom	0 - 2	0 – 30 (ramp)	Retraction
	2 - 7	0	-
	7 - 10	0 – 30 (ramp)	Extension
	10 - 13	0	-
Arm	0 - 2.5	0	-
	2.5 - 7.5	100 – 50 (ramp)	Extension
	7.5 - 10	0 – 50 (ramp)	Retraction
	10 - 13	0	-
Bucket	0 - 2.5	0	-
	2.5 - 7.5	100	Extension
	7.5 - 10	0	-
	10 - 13	0 – 50	Retraction

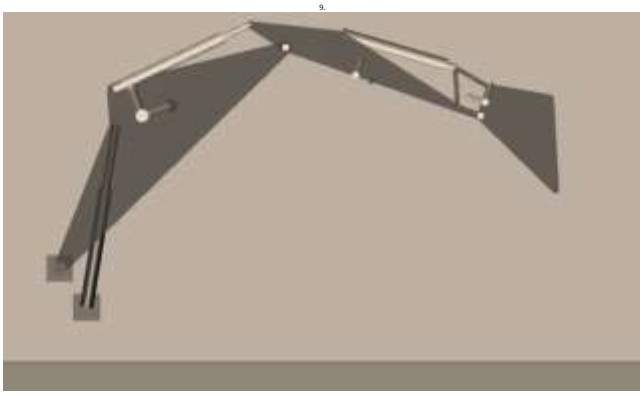

Figure 7.34 a**.** Initial position of the Excavator

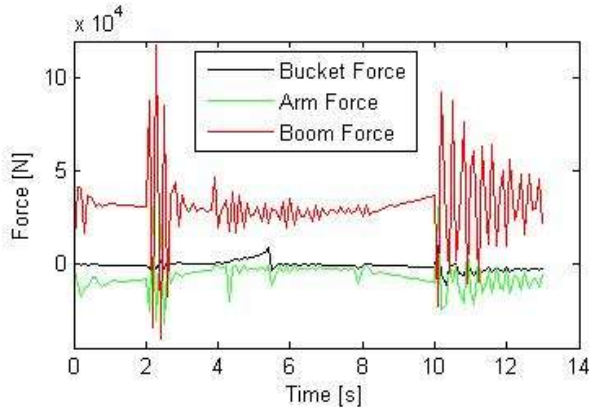

Figure 7.34 b**.** Actuator Forces

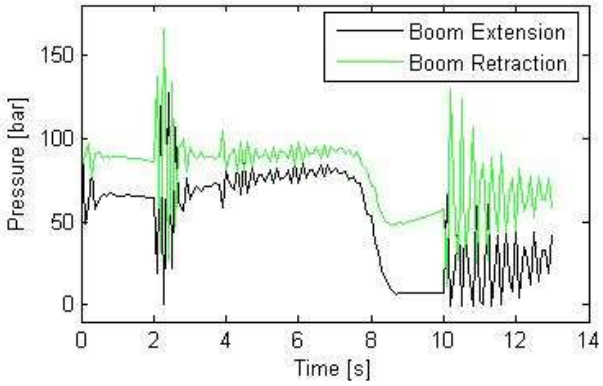

Figure 7.34 c**.** Pressure in Boom Actuator

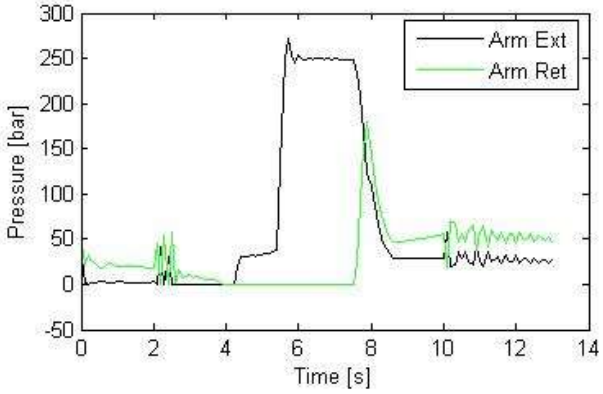

Figure 7.34 d**.** Pressure in Arm Actuator

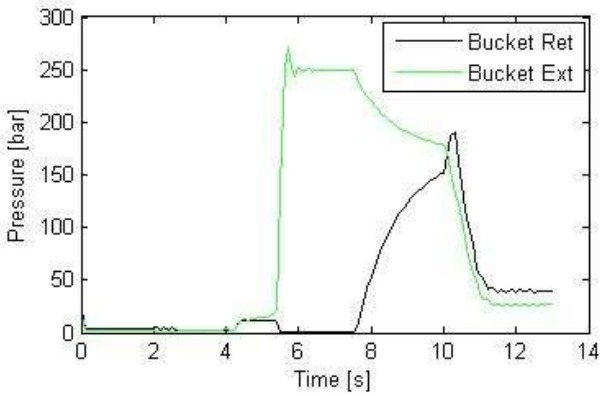

Figure 7.34 e**.** Pressure in Bucket Actuator

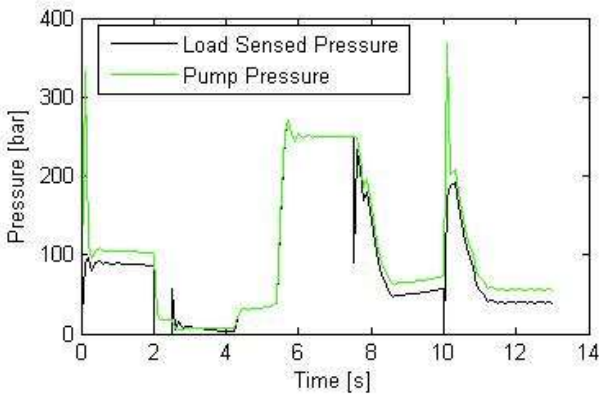

Figure 7.34 f**.** Pressure Across the FC

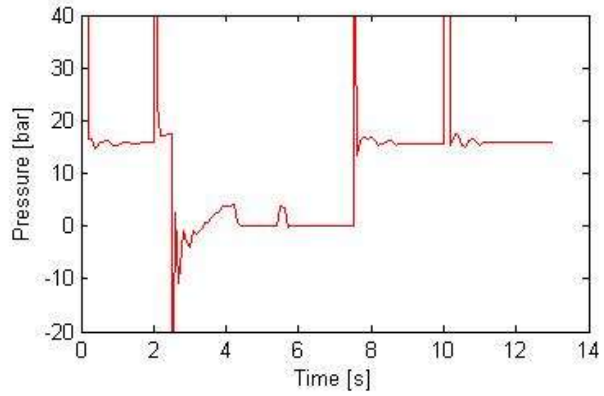

Figure 7.34 g**.** Differential pressure across the FC

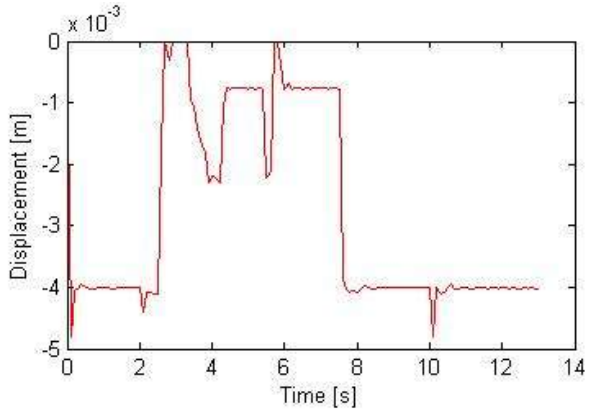

Figure 7.34 h**.** Displacement of the FC

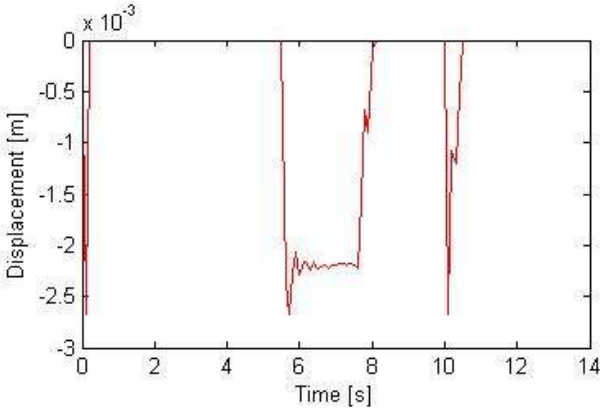

Figure 7.34 i**.** Displacement of the PC

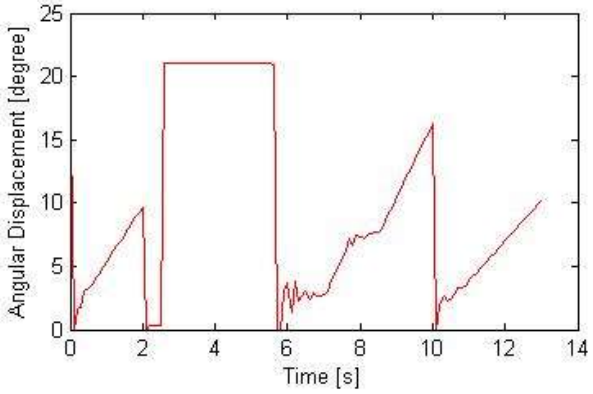

Figure 7.34 j**.** Swash Angle

Conclusion

The document has presented the analysis of an excavator control system. The model has been developed with the objective of creating a fast simulation model. The model is described by the models of a: hydraulic grey box model of the LS variable displacement axial pump, detailed model of the LS flow sharing valve block and a 2D kinematic model to simulate the excavator's body elements.

The detailed hydraulic model described is that of the main hydraulic pump, which has been conceived as a grey box model; where the flow and pressure compensators have been modeled as white box models and the actual flow characteristics of the pump as a black box model. The black box model to obtain the swash plate positions has been developed using a relation between the control piston pressure and the net torque acting on the swash plate through the system pressure. A linear relation between these pressure characteristics were derived from experimental results and was used to simulate the functioning of the pump. This methodology has the advantage of being easily applicable to pumps of different types and sizes, by changing the gain values and the constants of the linear equation. The model of the variable displacement pump has been validated on the basis of a preliminary set of experimental data collected at particular operating conditions. It has permitted the necessary verification of the interaction between the hydraulic and structural linkage/mechanical model.

A detailed model of the LS flow sharing valve block has been developed. This model owing to its complexity and non linearity has been developed as a white box model. This approach has been adopted owing to the complexity of the orifices integrated into the central section of the main orifice and the meter out orifices of the main spool. The pressure compensator of the valve block has a very complex function of being integrated

with a piston check valve, to force close the pressure compensator when the bridge pressure rises. There is another fuction where the sensed LS pressure if greater than a section, will cause the pressure compensator to close and the piston check to return to its home position. This offers a great modelling complexity as there occurs a situation of mechanical contact or fluid contact. Creating this discontinuity in the model has been a fair challenge. This has finally been integrated with the use of a special air gap damper spring arrangement, where the spring properties have been changed to rigid links and the air gap to recreate the fluid contact situation. The valve model requires complex verification of displacements, pressures and flow characaterisitcs. This has lead to an extensive validation campaing to carry out the complete verification of the valve.

A 2D kinematic/mechanical model has been developed to simulate the body elements of the excavator. This would reproduce the motion of the boom, arm and bucket. The kinematic model also includes a developed soil interaction model, which has been used to study and effect the soil interaction properties on the excavator implements in the course of an excavation cycle. This has assisted the model development in the creation of a unique simulation environmen where the hydraulic models can be loaded with realistic load characteristics on the systems from the implements.

The model has been validated completely in terms of the pump characteristics and the pumps response and behaviour in a complete excavator. These tests of the pumps behaviour have been carried out and verified using field tests on an excavator. Tests and verification of the characteristics of the LS flow sharing valve have been carried out. There is a good amount of confidence in the models capabilities of recreating the flow characteristics of the flow sharing valve.

This study has been a very interesting and challenging one, where the capabilities and potential of the completely developed autonomous model are paramount. It offers a futuristic approach to studying the complete excavator. The fact that there is a mix of modelling approaches used in the recreation of the system model offers the capability of the development of a complete fast model. Where the model can be used to study complete excavation cycles and the systems performance during the process.

Dott. Ing. Alvin Anthony

Future work

The model offers a host of capabilites for system developement:

- The model can be used to study the sytem behavior of the complete system.
- The model can be used to study the development of new control strategies for optimal and robust control of the pump and valve.
- The model can be used to carry out Hardware in the Loop studies where the simulation environment can be used by an expert operator and the simulation models pump and valve be studied by the manufacturers to understand the systems behavior.
- The model can be used to carry out a complete energy study of the excavator system.
- The pump model could be improved by studying a higher order curve fitting to improve the transient response of the pump.
- Detailed models of the actuators can be included to the complete system.

Modeling and Analysis of Tractor Rear Hitch Controls

PART - II

This part of the thesis describes the work carried out towards mathematical modeling and analysis of a tractor rear hitch control valve (HCV). The HCV operates in two modes namely lifting and lowering. The lifting circuit incorporates a pressure compensated flow control valve, while the lowering circuit is gravity assisted. The HCV is a load-sensing system; load-sensing systems and pressure compensated valves are classified as feedback systems. Systems with feedback offer scope for tuning and towards this objective the pressure compensator has been linearised and its characteristics analyzed. The objective of this study is to develop a complete mathematical model of the HCV. This would help to better understand its functionality and to quantify the energy losses across its components.

Index

CHAPTER 1

Introduction

Hydraulic circuits with fast dynamic response are often characterized by low power efficiency; on the other hand, energy-efficient circuits under certain circumstances, can demonstrate slow transient responses. Continuously rising energy costs combined with the demand on high performance has necessitated that hydraulic circuits become more efficient yet still demonstrate superior dynamic response. Towards this purpose this part of the thesis will deal with the study and analysis of energy efficiency of a Hitch control valve and will further analyze in depth the pressure compensator.

Hydraulic systems are used to transfer energy by converting mechanical energy to fluid energy, and then back to mechanical energy. The principle reason for converting to fluid energy is the convenience of transferring energy to a new location. Hydraulic drives have many advantages over other technologies. The ratio of weight, volume and inertia to available power is significantly lower than in electromechanical drives, especially for linear motion. The dynamic performance is superior when compared to electrical or electrical-mechanical drive systems in large power drive systems [1]. For those systems that require an output power larger than 10 kW and a fast response speed, hydraulic drive systems are often the appropriate choice. Hydraulic systems are especially suitable for those operations characterized by abrupt loading, frequent stops and starts, reversing and speed variations that cause sharp peak, cyclic and fluctuating power demands. These

advantages make them very popular in applications such as aircraft, mobile equipment, lifting machines and forest machines.

Compared with other systems (e.g., mechanical electrical system), hydraulic systems can be energy inefficient. The typical efficiency for a single mechanical gearbox is about 98%~99% and for a triple reduction gearbox is above 95%. However, the typical efficiency for a hydraulic pump or motor is only 85%. The overall efficiency for a very simple pump-controlled hydraulic system under ideal operating conditions is about 70% [2]. The total efficiency of a pump/motor combination is much less when the system operates in a low rotational speed range. If hydraulic control valves are included to control the actuators in hydraulic drive systems, the overall efficiency can be substantially reduced under certain loading conditions. Poor efficiency can translate into other problems in hydraulic systems. Not only is power consumption increased, but also exhaust emissions (in the case of internal combustion engines) and operating costs increase which lead to the necessity of installing larger pumps and more elaborate cooling equipment to dissipate the heat.

In the past, power efficiency has not been a high priority for hydraulic circuit and component design. Much attention has been oriented towards the pursuit of high system performance and to the fulfillment of the demanded functions. In recent decades, high performance still remains a priority, but systems which are energy efficient have been the focus of much study; this is primarily due to fuel economy and environmental considerations. The demand for highly efficient hydraulic drives (especially when compared with their electrical and mechanical counterparts) has also increased. If the efficiency of hydraulic drive systems cannot be improved, many traditional applications in which they are found will be converted to other power drive systems.

In summary, continuously rising fuel costs and increasing environmental pollution concerns combined with the challenge from other competing technologies has meant hydraulic drives must become more efficient yet still demonstrate competitive cost and superior dynamic responses

1.2 Achievements in Improving Power Efficiency

The power efficiency of hydraulic systems is affected by both the component and system design. Because of the interest in improving hydraulic system efficiency, individual components (pump, motor, actuator, valve etc) have been studied extensively by component manufactures and researchers; much progress over the past decade has been made on the improvement of the component efficiency. However, what is more important for system efficiency is how these components are combined to meet the load demands. There are many combinations of components which can be used to accomplish a single task. For example, a variable displacement pump/fixed displacement motor, a fixed displacement pump and motor with a variable speed motor drive or a fixed displacement pump and motor with a flow modulation valve can all be used to vary the rotational speed of a load. However, the efficiency of each system can be vastly different depending on the loading conditions even though the efficiency of pumps and motors can be very similar. Thus circuit design is the most important factor for power efficiency consideration.

Any kind of power transmission technology must be controllable yet efficient. The control of a hydraulic system is achieved by modulating the flow rate of the fluid. Four main methods are used to control flow: (1) controlling the power supply unit (engine or electric motor), (2) controlling the displacement of the hydraulic pump, (3) modulating flow through hydraulic valves, and (4) controlling the displacement of the hydraulic actuator (rotary). Each method will now be considered in relationship to their operation and relative efficiency.

1.2.1 Valve Control and Load Sensing System

Valve control is widely used in hydraulic systems because of its high controllability and good performance. A "conventional" valve-controlled system consists of a fixed displacement pump (non-pressure compensated), a relief valve, a flow modulating valve and an actuator (cylinder or motor). The output flow from the pump is constant. If loading conditions are such that the load flow demand is less than the output flow from the pump, then the excess flow must be diverted to tank through a relief valve (R.V). The pump pressure is now at a value dictated by the relief valve setting. This results in flow passing through the R.V to tank at a substantial pressure drop (all wasted power) and a pressure

drop across the flow modulating valve (also wasted power). These losses are demonstrated schematically in Figure 1.1(a). In this case, PS is the pump pressure, PL is the load pressure, QS is the flow from the pump and QL is the demanded flow to the load (QS-QL is the flow which passes through the R.V). The shaded areas indicate the power that is lost across the R.V. and control valve (C.V). As the load pressure and load flow demands decrease, the efficiency of the circuit drops. These losses are compounded if a symmetric valve is used to control an asymmetric cylinder due to the discontinuity of the pressure in the two sides of cylinder when the direction of cylinder movement is changed [3]. In general, the pump/valve/actuator system is simple, reliable and inexpensive, and has good controllability. However, it can be very inefficient as illustrated in this figure.

The pressure losses of conventional systems are often unacceptable, hydraulic systems, which use variable pressure and/or variable flow, are often employed. One such system is shown schematically in Figure 1.1(b). Variable pressure control uses a "load sensing unloading valve" to sense the load pressure. The directional valve includes a load sensing port which is connected to the unloading valve. Flow from the pump not required by the load is diverted to tank at a pressure, 70-140 kPa higher than the load pressure via the load sensing unloading valve. This system is the same as the conventional system except that the "effective" relief valve setting (via the unloading valve) is always 70-140 kPa above the load pressure. The losses are shown by the shaded regions in Figure 1.1(b).

A third system shown in Figure 1.1(c) uses a "pressure compensated" pump. This system is called a demand flow system because the pump supplies only the flow which is required. However because the pressure of the pump is fixed by the compensator, metering losses across the control valve still exist (see shaded area). For pressure compensated systems, a variable displacement pump is always required.

Although variable pressure or pressure compensated systems can be used to improve efficiency, loss across the flow valve or control valve still exists. This has led to the development of a different "load sensing system", which is commonly found in mobile hydraulics as a "driving concept" with high running efficiency [5]. Load sensing systems

use a load-sensing valve (Figure 1.1(d)) to sense the load pressure which is then fed back to a pump compensator. By means of a compensator control valve, the displacement of the pump is adjusted to deliver the required flow and maintain a pressure 70-140 kPa higher than the load pressure. This desired constant pressure difference across the flow metering valve is set by the compensator. Thus the pump pressure follows changes in the load pressure, while the pump provides only the flow demanded by the metering valve. As illustrated in Figure 1.1(d), the power losses of a load sensing system are substantially smaller than other systems.

Load sensing systems are very efficient in single load applications. However, they are often used in multiple load applications (single pump/multiple load). The pressure at each load is sensed: only the pressure which has the highest value is fed back to the compensator. This means the pump pressure will follow the load with the highest pressure demand. This results in an efficient circuit for that particular load. If load pressures of all other loads are less than the one with the highest load, then the pressure drop across each valve can be substantial and some power losses are introduced into the other circuit.

One problem with load sensing systems for multi load applications is stability which can arise from load interactions through the feedback line. To minimize these interactions, pressure compensated (PC) control valves are often used. Although they are not more efficient than the traditional load sensing systems, they can be used to minimize interactions [11].

Another problem with load sensing systems is the risk of instability which can occur through the pressure feedback line (or load sensing line). To make the load sensing system more stable, different kinds of hydraulic “signal filters” (such as the combinations of orifices, check valves and accumulators) may be used in the load sensing line. However, in many cases, this kind of filtering slows down the system dynamic response. Many studies have attempted to improve the dynamics of load sensing systems, such as using electric hydraulic load sensing systems [6] and [10]. In their studies, the load pressure was measured using a pressure transducer on the load sensing valve; in addition the pump was

equipped with an electro-hydraulic directional valve to control the displacement of the pump. The load sensing line was replaced by an electric signal line including a pressure transducer, electrical controller/filter and an electrically controlled load sensing pump. With this electric load sensing line, different control strategies would be implemented. With the help of an electronic filter and controller, any oscillation in the load sensing signal would be attenuated; thus, it was possible to design a load sensing system that was stable but still demonstrated fast response.

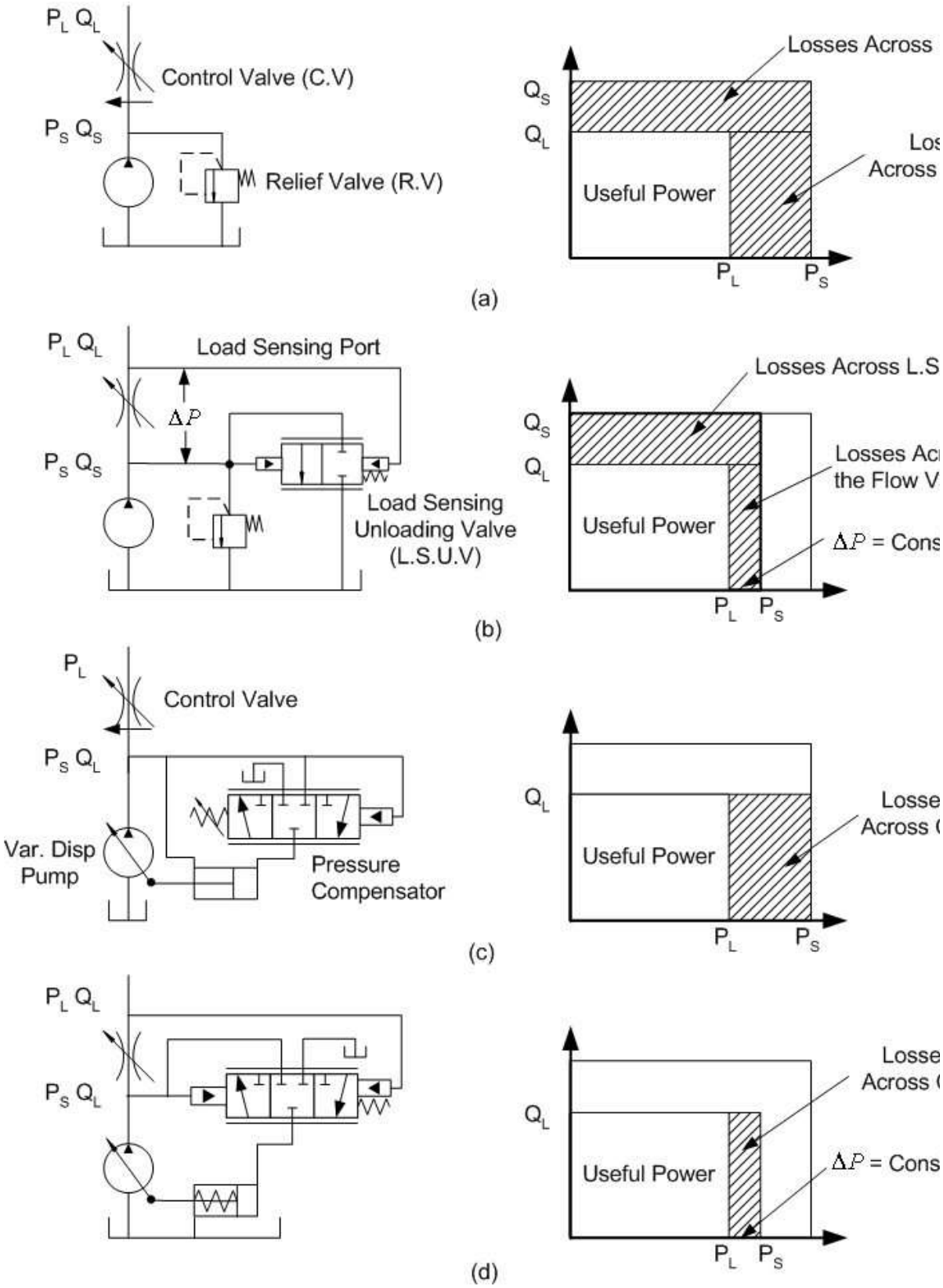

Figure 1.1 Power losses of valve-controlled systems

The Hitch Control System is a system for controlling the lifting and lowering of the implement. The HCV described in this work pertains to the type used on Case New Hollands, T7000 Agriculture tractor series. The layout of the tractor is as described in the figure

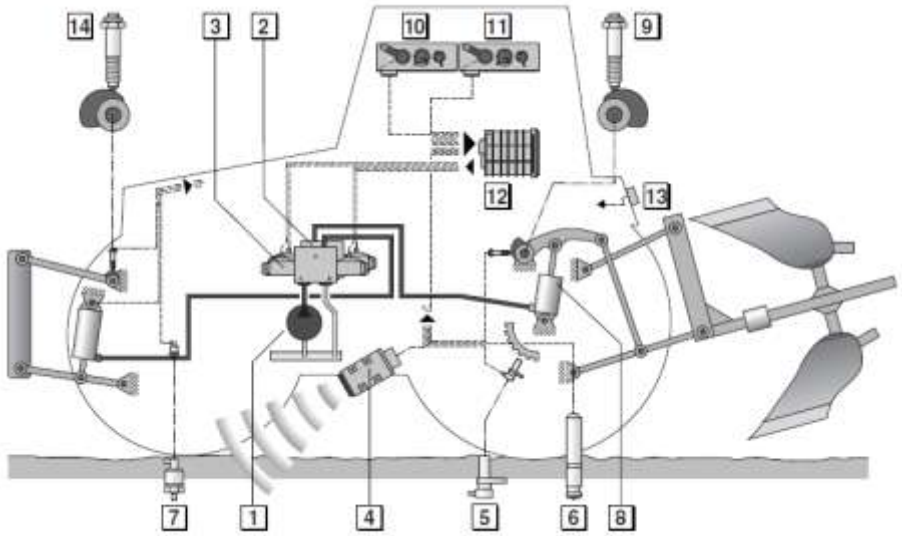

Figure 1.1: Hitch Control Physical Layout on a Tractor

Table 1.1: Tractor Layout Description

Ref No.	DESCRIPTION	Ref No.	DESCRIPTION
1	Main Pump	8	Hydraulic Cylinder
2	Valve Block	9	Position Sensor
3	Valve Block	10	Operator Controls
4	Velocity Sensor	11	Operator Controls
5	Hitch Position Sensor	12	Electronic Control Unit
6	Draft Sensor	13	Manual Command
7	Pressure Sensor	14	Position Sensor

Heavy equipment such as agricultural tractors employ fluid power systems to control their loads by way of valve adjustment in a pump-valve control configuration. Most of these systems have low energy efficiency as a result of pressure drops across control elements. A solution to save energy in a pump-valve system would be to use a Load-Sensing (LS) feature. This feature would permit the reduction of the number of pumps in a system, but introduces the disadvantage of power losses incurred by throttling.

Fluid temperature increases because of these losses causing additional problems in terms of heat removal. The function of a pressure compensator (PC) valve in hydraulic circuits is to control flow rate through the valve, while minimizing the effect of pressure drop across the valve under both steady-state and dynamic operating conditions [11]. In order to understand the design and operation of a PC valve, a good first step is to develop a mathematical model.

The kind of HCV model presented is that of a phenomenological model, therefore it uses physical equations which describe the behavior of the internal elements and their connections. The hydraulic circuit for the HCV comprises two proportional flow control valves (FCV) that control lifting and lowering of the hitch. The lifting portion of the circuit incorporates a pressure compensated valve (PC) which is a flow control device. The compensator's orifice area is modulated to maintain a fixed pressure drop across the control orifice. This feature of PC valves in hydraulic circuits is used to control the flow rate through the valve by minimizing the effect of pressure drop under both steady state and transient operating conditions. The analysis of the hydraulic circuit incorporated in the HCV has been carried out following both a numerical and an experimental approach. The numerical analysis has been developed by means of mathematical models and has been realized in the AMESim® simulation environment. The results of the mathematical model have been validated against experimental data and the first results are presented herein. Thereby an energy analysis pertaining to the power losses across the HCV components and the useful power available to the load is presented.

As introduced, the pressure compensated valve (PC system) is a flow control device which consists of a fixed or adjustable orifice and a compensator valve. The compensator valve modulates its opening in order to maintain a fixed pressure drop (Ps - Pm) across the fixed or adjustable orifice. There usually are two configurations for PC systems1: (a) hydrostat upstream and (b) hydrostat downstream as shown in Figure 1.3. Their purpose for flow control is same, that is, to maintain a constant pressure drop across the fixed orifice independent of changes in load pressure, thus flow is maintained constant and is independent of changes in the load pressure. The hydrostat upstream, configuration (a), has been studied by many researchers [7] and [11]. From a practical viewpoint, in this study, it was very difficult to install transducers to measure the spool displacement, *xpc*, and the

intermediate pressure, *Pm*, for the hydrostat upstream due to the compact structure of these valves. However, PC systems with the hydrostat downstream can be fitted with appropriate transducers to measure *xpc* and *Pm*. Therefore, only the hydrostat downstream configuration is studied in this thesis. There is no loss in generality here because if the model can be verified with the hydrostat downstream then the approach can be applied to the case of the upstream hydrostat with some confidence. For the duration of this thesis, a hydrostat downstream will be assumed.

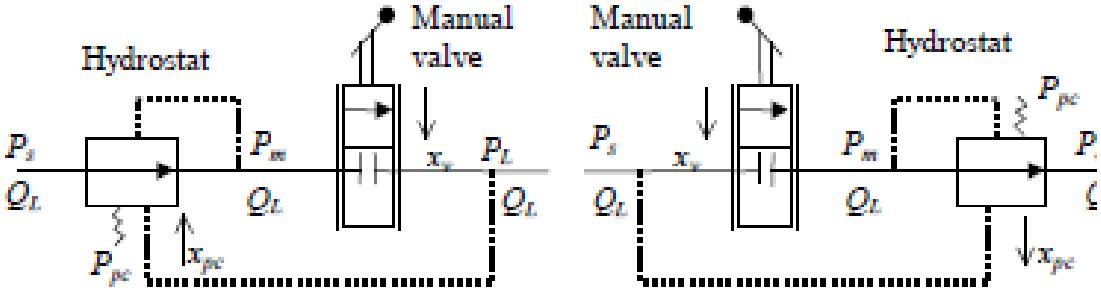

(a) Hydrostat upstream configuration (b) Hydrostat downstream configuration

Figure 1.3 Comparison of Two Types of PC Systems

There usually are two configurations for PC systems:

- hydrostat upstream
- hydrostat downstream

as shown in Figure 1.3. Their purpose for flow control are same, that is, to maintain a constant pressure drop across the fixed orifice independent of changes in load pressure, thus flow is maintained constant and is independent of changes in the load pressure. The hydrostat upstream, configuration (a), has been studied by many researchers [7] and [11]. From a practical viewpoint, in this study, it was very difficult to install transducers to measure the spool displacement, *xpc*, and the intermediate pressure, *Pm*, for the hydrostat upstream due to the compact structure of these valves. However, PC systems with the hydrostat downstream can be fitted with appropriate transducers to measure *xpc* and *Pm*. Therefore, only the hydrostat downstream configuration is studied in this thesis. There is no loss in generality here because if the model can be verified with the hydrostat downstream then the approach can be applied to the case of the upstream hydrostat with some confidence. For the duration of this thesis, a hydrostat downstream will be assumed.

CHAPTER 2

Modeling of the Tractor Rear Hitch Control Valve

As described in the introduction, the HCV is a manifold block which includes a lifting and a lowering circuit, figures. 2.1 and 2.2. The lowering circuit is gravity assisted and does not involve pump flow. It consists solely of a proportional FCV, which is used to control the flow of oil out of the actuator. The lifting circuit comprises a pressure compensator in conjunction with another proportional FCV and a load-sensing check valve. A bleed off flow control is also included in the lifting circuit. The lifting and lowering circuits are separated by a check valve. The HCV's system pressure is defined by a relief valve which also incorporates an anti-cavitation feature.

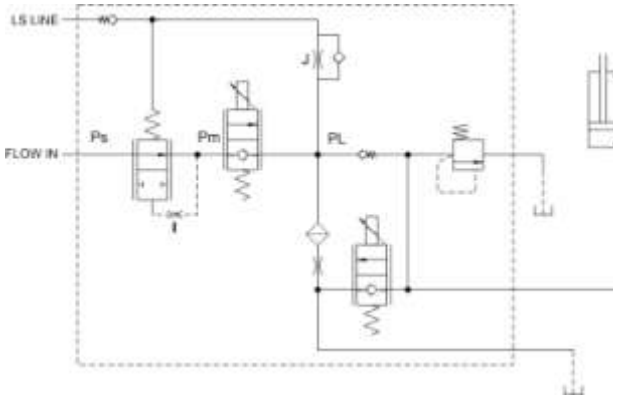

Figure 2.1: Hydraulic Schematic of the Tractor Rear Hitch Control

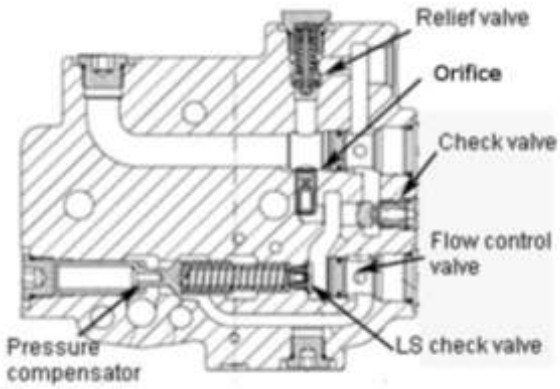

Figure 2.2: Sectional view of the rear hitch controller valve

The following subsections describe the mathematical model of the components in Figure 2.2. The HCV control structure consists of a pump, compensator valve (more commonly known as a hydrostat), and a fixed orifice (Figure 2.3). The system consists of (or valve combination) in which the pressure(s) is piloted to a pressure compensator valve (A) in Figure 2.3, (located downstream from a fixed or adjustable orifice (E)). This compensator valve modulates its opening in order to maintain a fixed pressure drop (*Ps* - *Pm*) across the fixed or variable orifice (E). Consider the situation in which the load (D) experiences a change during operation; subsequently, the pressure, *PL*, would also change. This causes an instantaneous decrease in the pressure drop, *Pm – PL*, which results in a decrease in the flow rate, *QL*, to the load. The "unperturbed" flow through the fixed orifice (E) encounters a resistance at (B). Because of the very small chamber volume between the fixed and compensator orifice, the intermediate pressure, *Pm*, would suddenly increase. The pressure increase is sensed in the feedback sensing line (C) and is exerted on the spool of the compensator valve (A). The orifice created by the compensator spool is modulated by the force unbalance across the spool (created by *Ps*, *Pm* and a bias spring, *Ppc*). An increase in *Pm* increases the compensator spool orifice opening, *xpc*, which results in an increase in the flow, *QL*, through the compensator. The increase in the flow rate via the compensator (A), in turn, results in a decrease in *Pm*. The aforementioned processes continue until a new force balance is re-established across the compensator spool (A). The original pressure drop across the fixed orifice is restored and flow control is accomplished. Thus for a specific orifice setting, the flow is independent of the variation in *PL* (and similarly, *Pm*).

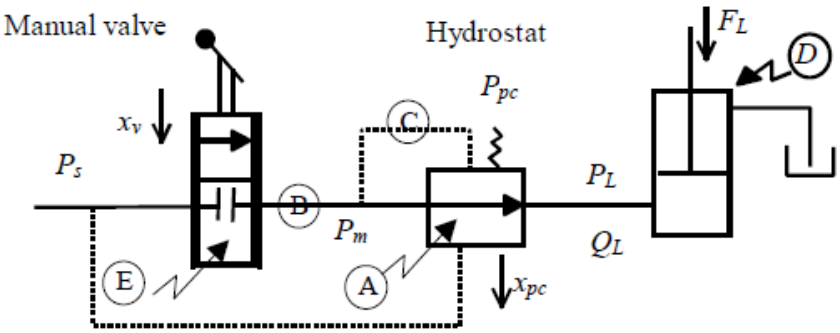

Figure 2.3: Schematic of Pressure Compensated (PC) System

For the LS system previously discussed, a problem associated with changes in the load was identified. This same situation exists for this kind of PC system. However, because the mass of the spools of the compensator is small compared to the mass of the pump swash plate, the response of the valve is very fast compared to the pump and rapid flow recovery is possible. When used in circuits with multiple loads, the second problem discussed previously does not exist because each load is isolated by a separate PC valve and hence *Ps* is approximately constant. For all PC systems, the supply from the pump is established by the pressure compensator on the pump or from the relief valve setting. This means that a substantial pressure drop exists across all (PC) flow control valves. This can result in substantial energy losses in the system. This loss is highly dependent upon the load pressure and the supply pressure set at the pump.

2.1 Modeling of the Pressure Compensator

This section presents the nonlinear governing equations used as a guideline for the modeling of the pressure compensated flow control valve in the AMESim® modeling environment, as well as to facilitate the comprehension of section 4 of this paper. The advantages of implementing the model in AMESim® are the ability to account for a detailed geometry of the valve and to evaluate viscous forces related to leakages.

The operation of the pressure compensated FCV is such that it modulates its opening in order to maintain a fixed pressure drop across the FCV independent of changes in the load pressure: figure 2.5 shows a simplified drawing of the PC spool.

In order to understand the functioning of the lifting circuit of the HCV it is a good approach to describe the defining or control equations pertaining to the valve. The pressure compensator incorporated in this HCV is of the upstream type, the generic model of a downstream PC by [10] has been adapted and modified to represent the upstream PC of the HCV which is the objective of this paper.

The control equations that describe the flow into the HCV comprise of:

The flow rate through the pressure compensator orifice Q_{LPC}, this is defined by equation (2.1). In the case mentioned here the orifice of the pressure compensator has a crescent type shape and the orifice area A_{pc} is a function of the spool displacement x_{pc}

$$Q_{LPC} = C_{dc} \cdot A_{pc}(x_{pc}) \cdot \sqrt{\frac{2}{\rho} \cdot (P_s - P_m)} \tag{2.1}$$

The flow rate out of the HCV through the proportional FCV Q_{LV} is defined by equation (2.2). The FCV is a two stage fine regulating flow control valve and the pilot stage is controlled by a proportional solenoid. The orifice geometry of the FCV is that of a crescent type. The orifice area A_v is a function of the spool displacement x_v

$$Q_{LV} = C_{dv} \cdot A_v(x_v) \cdot \sqrt{\frac{2}{\rho} \cdot (P_m - P_L)} \tag{2.2}$$

The dynamic force balance across the pressure compensator's spool is defined by equation (2.3)

$$\begin{aligned} M_{pc}\ddot{x}_{pc} + B_{pc}\dot{x}_{pc} + K_{pc}x_{pc} \\ = A_{pcs}\{P_{pc} - (P_I - P_J)\} - K_{ff} \cdot A_{pc}(x_{pc}) \cdot (P_s - P_m) - \rho L\dot{Q}_{LPC} \end{aligned} \tag{2.3}$$

This dynamic equation is used to determine the balance of forces across the pressure compensator spool. The terms on the left hand side of the equation relate to acceleration of the spool mass, damping coefficient of the spool and the coefficient of the pre-compressed spring. The first term on the right hand side of the equation is the force that relates to the pressure on either side of the spool. The value P_{pc} is an equivalent pressure value caused by the compression force of the spring on the spool area. The second term on the right hand side reflects the steady state flow forces, where K_{ff} is the steady state flow coefficient and is obtained by substituting:

$K_{ff} = 2C_{dc}C_v\cos(69°) = 0.7C_{dc}$. The steady state flow force is proportional to the flow area of the orifice and pressure drop across the pressure compensator. The last term on the right hand side refers to transient flow forces. The damping length *L* is defined as the axial length between the incoming and outgoing ports of the compensator spool.

Now, considering the flow continuity equations of chamber V2 and chamber V3, as the HCV is a compact valve the chamber sizes are small in comparison to the bulk modulus of the medium, thereby the equations for P_I relating to the pressure in chamber V2 and P_J relating to the pressure in chamber V3 would equate to an infinitesimally small value and can be neglected. This would result in equations (2.4) and (2.5):

$$P_I = P_m + A_{pcs} \cdot R_I \dot{x}_{pc} \tag{2.4}$$

$$P_J = P_L + A_{pcs} \cdot R_J \dot{x}_{pc} \tag{2.5}$$

The term R_I and R_J represent the hydraulic resistance offered by the orifices *I* and *J*.

Finally, the flow continuity equation for the intermediate chamber between the pressure compensator orifice and the flow control valve orifice is defined by equation (2.6), here again as the volumes are infinitesimally small in comparison to the bulk modulus the equation is reduced:

$$Q_{LPC} - Q_{LV} - A_{pcs} \cdot \dot{x}_{pc} = 0 \tag{2.6}$$

These are the nonlinear control equations that define the functioning of the pressure compensated flow control valve and have been used as the basis to develop a more detailed model in the AMESim® modeling environment. In the AMESim® detailed model the valve behavior is described by the interaction between a fluid-dynamic model (FDM) and a mechanical-geometrical model (MGM). The FDM calculates pressures inside volumes and the flow rates between adjacent volumes; the MGM calculates the dynamic forces acting on the spool and determines the orifice flow areas. The FDM is based on a lumped parameter framework. The pressure inside each control volume is assumed uniform and is time dependent, while the continuity equation determines the pressure values using equation (2.7):

$$\frac{dp_{\mathrm{i}}}{dt} = \frac{\beta}{\rho_{\mathrm{i}}} \cdot \frac{1}{V_i(x)} \left(\sum \dot{m} - \rho_{\mathrm{i}} \cdot \frac{dV_{\mathrm{i}}(x)}{dt} \right) \tag{2.7}$$

Fluid temperature is assumed constant and fluid density is evaluated as a function of pressure as described in [4]. As described by Equations 2.1 and 2.2, the net volumetric flow rate and chamber volumes are derived from the instantaneous position of the spool. Mass exchange through orifices are calculated under quasi-steady conditions and the flow area is constant for fixed orifices. An appropriate value of the coefficient of discharge is set at each connection, using either experimental data or values reported in literature. Thereafter the instantaneous coefficient of discharge value is evaluated as a function of the Reynolds number to account for partially developed or fully turbulent conditions [5]. Annular leakages past spool bodies have been evaluated using the annular leakage equation [6]. The advancement in the implementation of the model in the AMESim® environment is the ability to evaluate viscous forces related to the leakages in the dynamic force balance Equation (2.3).

For a more detailed description of the modeling of the HCV please refer [8]. Figure 2.6 describes the AMESim model pertaining to the Pressure Compensator, Load Sensing

Check Valve and FCV. The objective of figure 2.6 is to provide a visual idea of the complexity that has been incorporated into the AMESim® model.

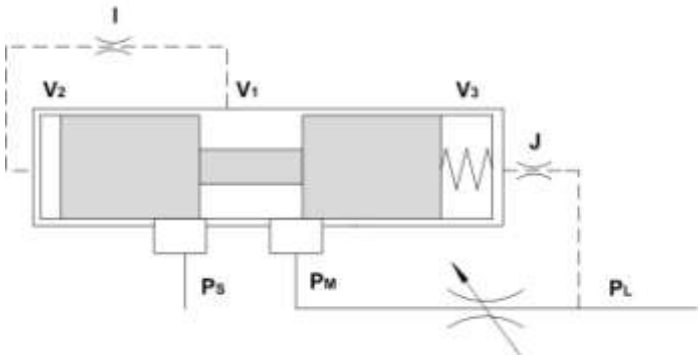

Figure 2.4: Simplified sketch of the Pressure Compensated Flow Control Valve

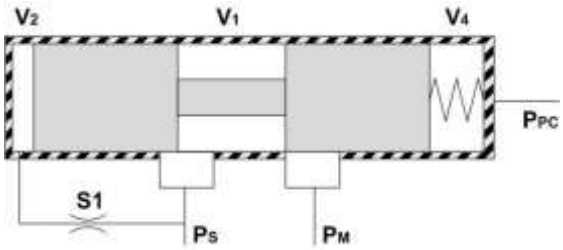

Figure 2.5: Sectional drawing of PC spool

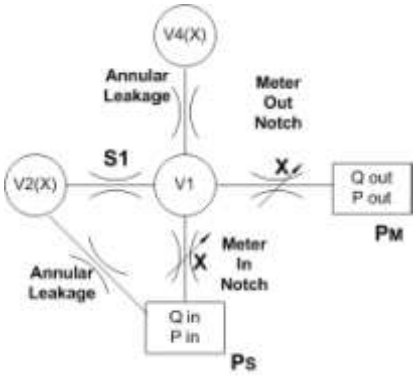

Figure 2.6: Schematic of the fluid dynamic model

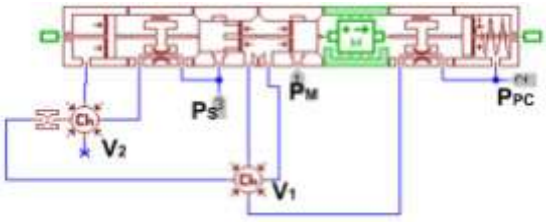

Figure 2.7: AMESim® model of the PC spool

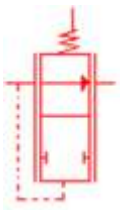

Figure 2.8: AMESim® super component

2.2 Modeling of the Two Stage Flow Control Valve (FCV)

The FCV is a fine regulating flow control valve. It consists of a pilot and main stage; figure 2.9 shows a simplified sketch of this valve. The pilot stage is controlled by a proportional solenoid. The mathematical model has been formulated utilizing the same modeling method as described in section 2.1. The FDM of the FCV (Figure 2.10) includes control volumes (V_6, V_7, V_8, V_9) whose pressure dynamics is defined by eq. (2.1), the mass exchange by equations. (2.2 and 2.3). The AMESim® sketch of the FCV is reported in figure 2.11. The main stage is actuated by means of an external force generated by the proportional solenoid. The implementation of the model is fairly complicated as it involves interaction between the pilot stage and main stage.

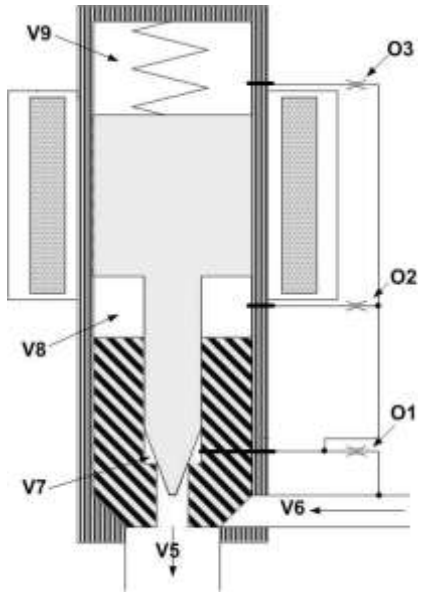

Figure 2.9: Simplified Sketch of FCV

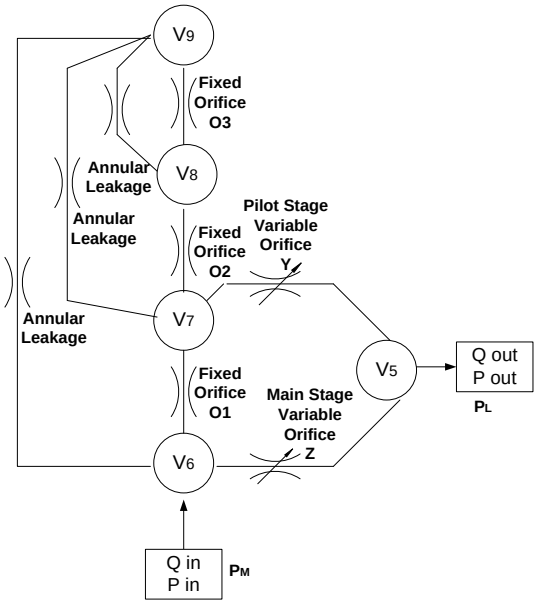

Figure 2.10: Schematic of the Fluid Dynamic Model of FCV

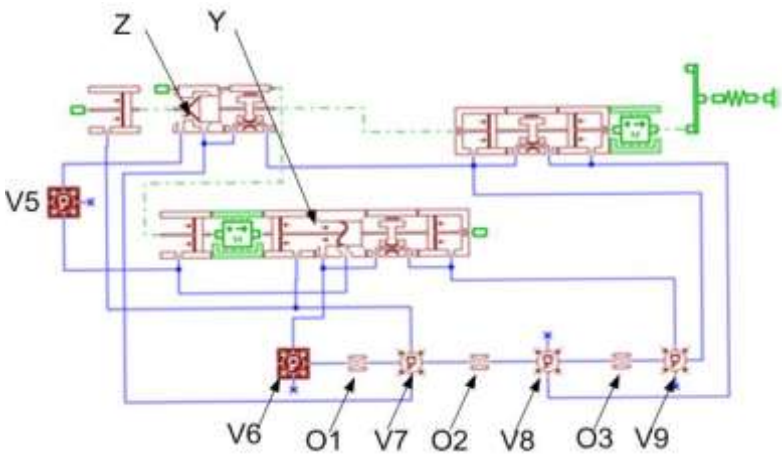

Figure 2.11: AMESim® Sketch of the FCV

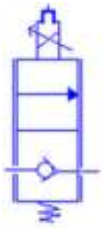

Figure 2.12: AMESim® Super component

2.3 Modeling of the Proportional Solenoid (PS)

At this point of research the electrical specifications of the solenoid were unavailable. This model was required to study the functioning of the HCV in the automatic control modes available on the tractor. In this case, in place of a phenomenological model an empirical one was developed to control the solenoid. In order to create the control of the PS which is determined by a function of current input with spool position as the output, a common parameter had to be identified to link the experimental and simulation data. This was achieved by using flow rate as the reference parameter. The fact used to support the selection of this parameter was that a PS generates a constant force for a given air gap /Nor00/ which is achieved in our case by the displacement of the FCV pilot stage spool. Consequently, flow rate was considered to be the independent variable for comparing the experimental values of flow rate achieved to current control of the PS, with the simulation values obtained through position control of the FCV's spool, figure 2.13.

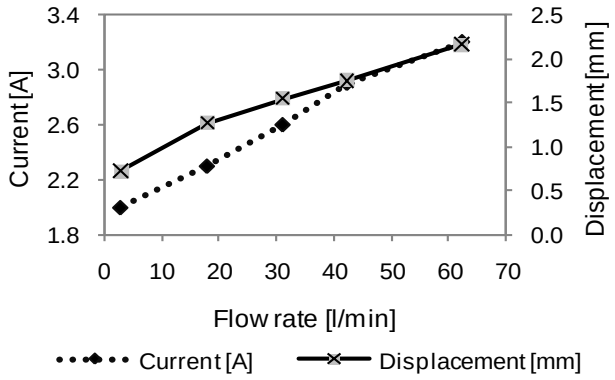

Figure 2.13: Graph of Displacement and Current vs. Flow rate

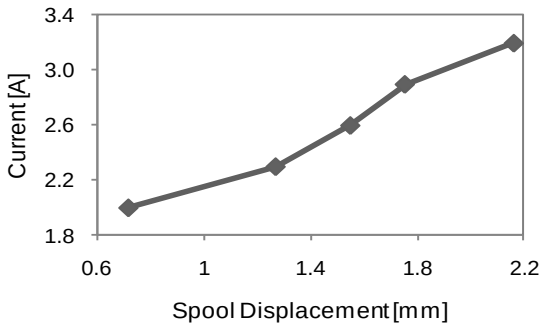

Figure 2.14: Graph of Current vs. Displacement

Figure 2.14 shows the spool position for a corresponding current value at constant force. For a given spool displacement the force required to maintain the spool position can be obtained from the simulation model, thereby creating figure 2.15 which describes the force value for a given current value. For a given current it was observed that the force varied very slightly at different pressure values. This effect was due to a shift in the spool position which was in the order of a few microns and was caused by the pressures acting on the spool; to account for this non linearity a reference look up table, figure 2.16, comprising force values for a discrete set of current and pressure value was created. Figure 4.1 describes the validation tests carried out to compare the manufacturers specifications of the PS with that of the simulation model using the reference table Figure 2.16. The results using the reference table 3.1 can be seen in figure 4.2.

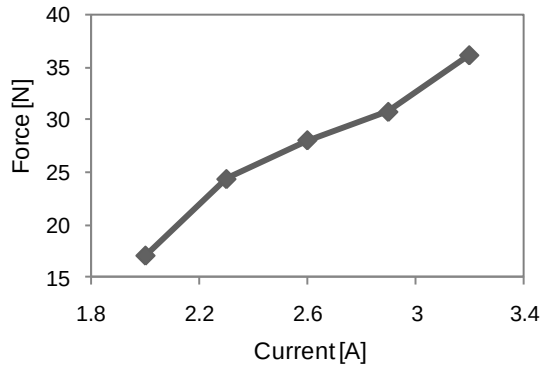

Figure 2.15: Graph of Force vs. Current

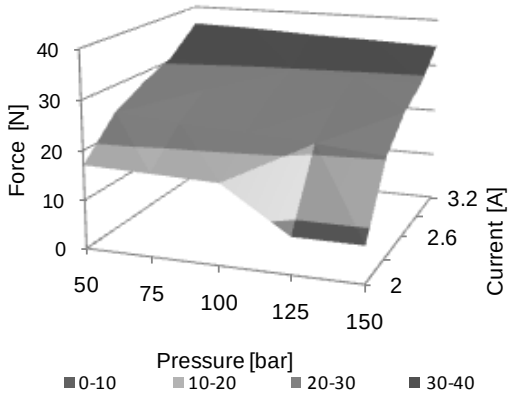

Figure 2.16: Surface plot describing the force values for a given current and pressure

2.4 Load-Sensing (LS) Check Valve

The function of the LS Check valve is to facilitate a pressure feedback to the pressure compensator spool, figure 2.2. When the load pressure increases the check valve is unseated and a flow path is established to the LS line of the system. The schematic of the fluid dynamic model, figure 2.17, describes the operation of the LS Check Valve. The valve has been modeled as two control volumes. In figure 2.17 the fixed orifice 1 provides the pressure feedback to the compensator. When the load pressure increases it unseats the check valve and a flow path is established through the fixed orifice 2 and also through the annular leakage. The LS Check valve has been modeled in the AMESim® environment (figure 2.18).

2.5 Modeling of the Relief Valve and Bleed Off Flow Control

The relief valve in the circuit is of the direct acting type and includes a spring loaded check valve, the latter working as an anti-cavitation feature. This component has been modeled following the same approach as described earlier and has an in-depth evaluation of flow forces. Further details can be found in [9].

The rear hitch lifting circuit incorporates a bleed off circuit. The fluid dynamic model of the bleed off flow control circuit includes a sharp edged short orifice. The flows through the fixed orifices are defined by equation (2.2).

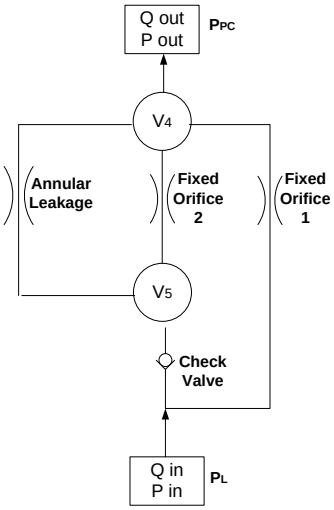

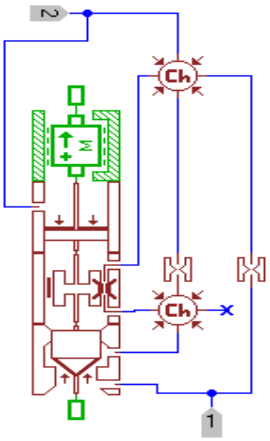

Figure 2.17: LS Check valve - Schematic of the fluid dynamic model

Figure 2.18: AMESim® sketch of the LS Check valve

2.6 Modeling of the Rear Hitch Kinematics

The rear hitch consists of a four bar linkage and can be described as a double lever mechanism. The kinematic model has been incorporated as a lumped parameter model that accounts for angular position, relative coordinates, distances between links, relative velocity, relative acceleration and the output forces. Joint forces of contact and stiffness are also considered in the model. The kinematic model was used to create a realistic load on the actuator. Considering the benefits of having the kinematic model integral with the hydraulic simulation model, the linkage parameters were coupled to the hydraulic simulation model using the Planar Mechanics library of AMESim®. This makes understanding of the dynamic loads on the hydraulic cylinder easier. The cylinder (A in figure 2.19) is modeled as a jack in the kinematic library. The jack receives its input from the displacement of the cylinder in the hydraulic model and returns the load of the kinematic linkage to the cylinder. The links C, E and G are modeled as 3, 2 and 2 port bodies respectively /LMS09/. These bodies contain the mathematical model based on the Lagrange equations using the Lagrange multipliers method. The revolute pairs B, D, F and H have been modeled as Lagrange multipliers and are calculated from the Baumgarte stabilization method applied to the constraint equations [8].

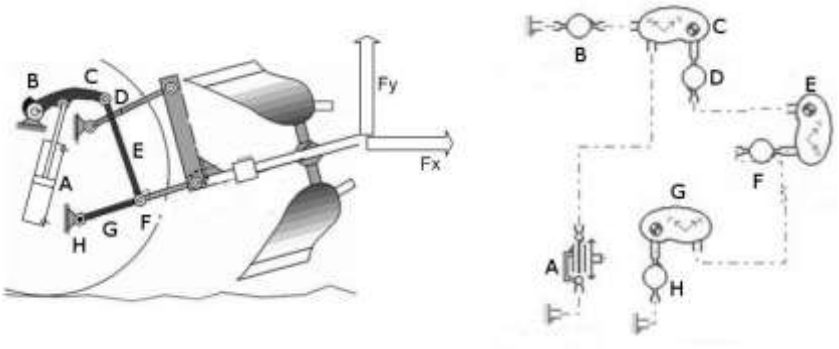

Figure 2.19: Kinematic and AMESim® Planar Mechanics Model

2.7 An overview of the complete model

Figure 2.20 describes the complete mathematical model as implemented in AMESim®.

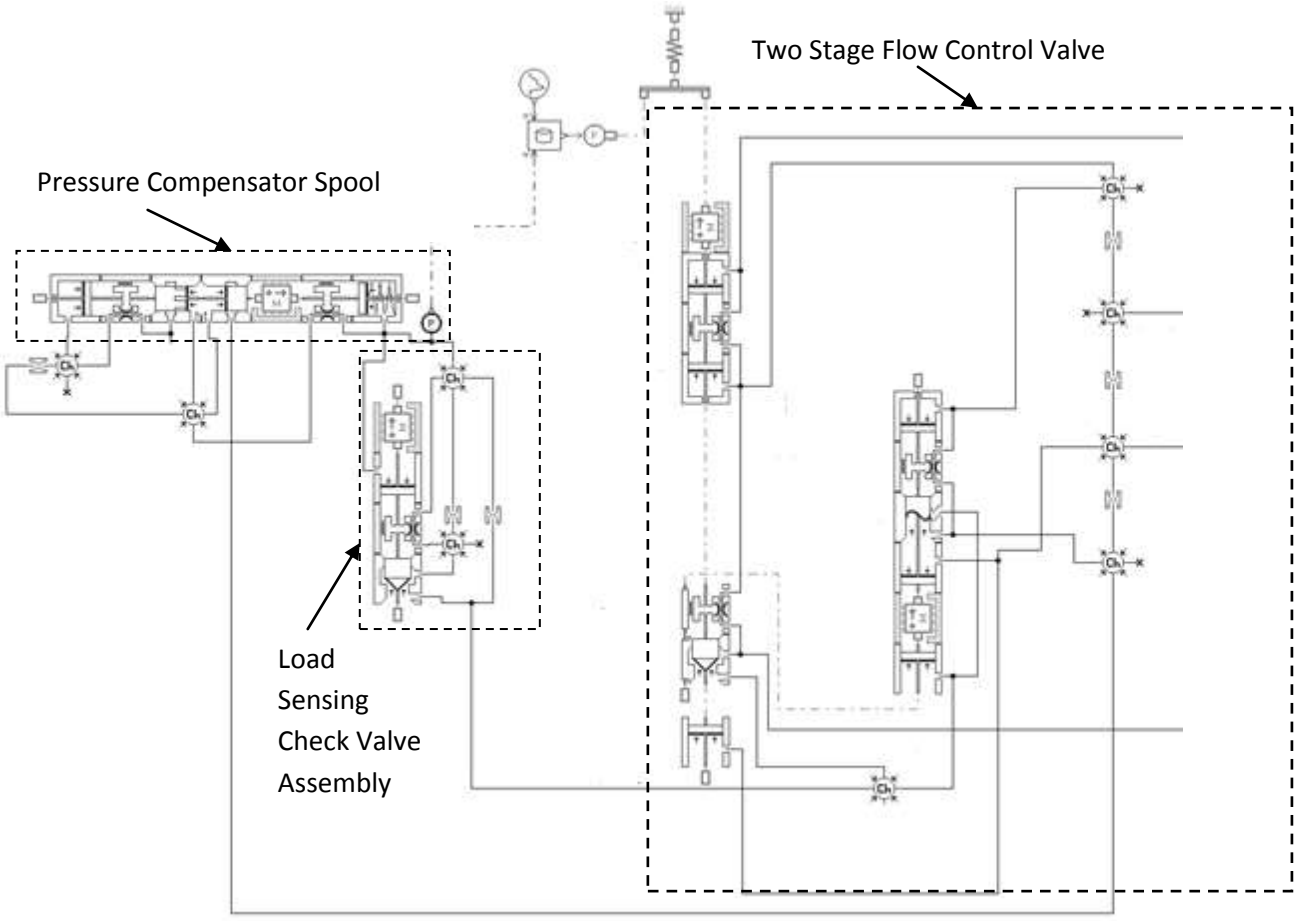

Figure 2.20: AMESim® representation of the Pressure Compensator and Flow Control Valve

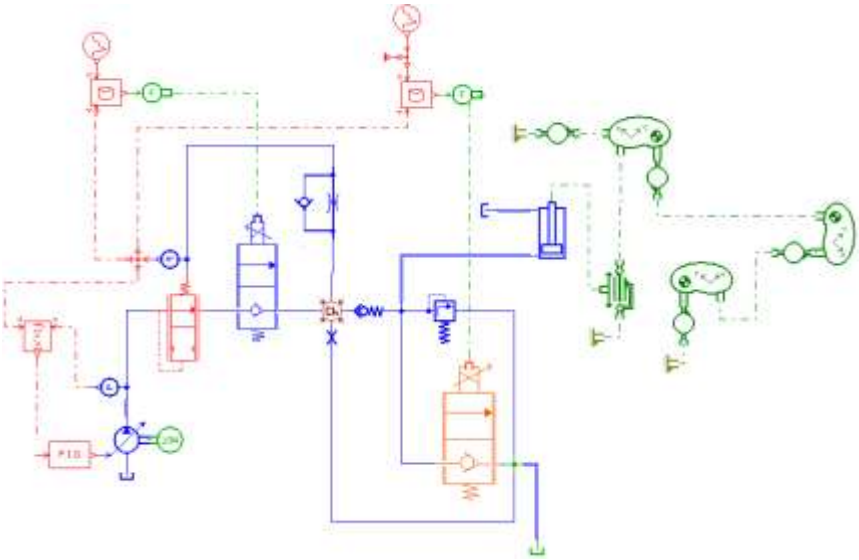

Figure 2.21: Schematic of the complete mathematical model described as AMESim® super components

CHAPTER 3

Experimental Test Setup

The manifold block inclusive of the rear hitch control valve was mounted on a test rig of the IED laboratory. The schematic of the test setup is depicted in figure 3.1. The test setup comprising a variable pump, associated instrumentation in terms of pressure, flow rate and temperature transducers were connected to the inlet and outlet ports. A loading valve was used to create the system load. Data were acquired using a dedicated data logger at an acquisition rate of 1 kHz. The details of the test rig are explained in Part 1 – Chapter 6 of this document.

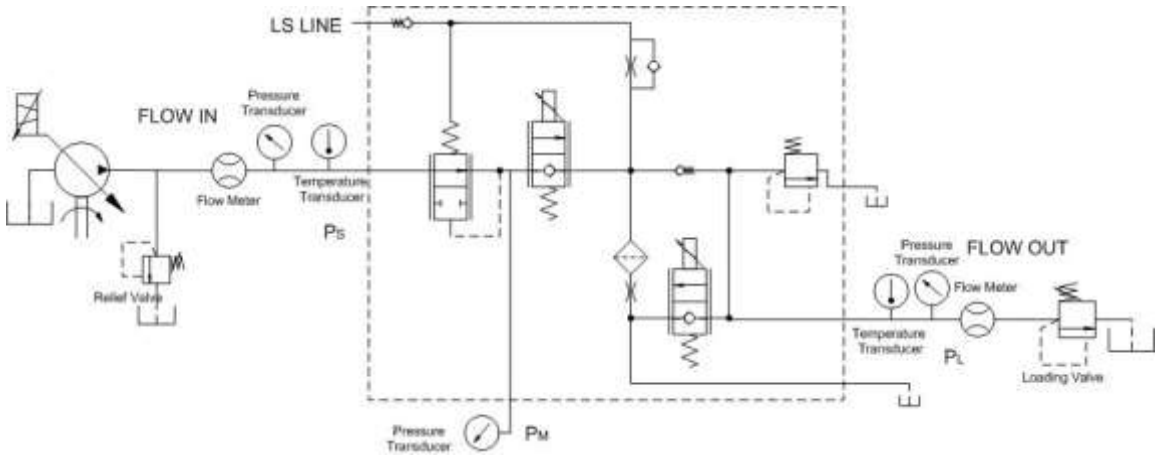

Figure 3.1: Schematic of the experimental test setup

Table 3.1: Instrumentation used in the Test Circuit

Sensor (Figure 3.1)	Type	Features
T1, T2	*resistive*	Scale: -50°;+200°C; 1%FS accuracy
P1, P2, PM	*strain gage*	WIKA®, Scale 0;400bar, 0.25 FS accuracy
Q1, Q2	*flow meter*	VSE® VS1, Scale 0.05; 80l/min, 0.3% measured value accuracy
S	*speed meter*	HBM® 12000 r/min^{-1} Limit Velocity

The following tests were carried out on the hitch control valve and the following parameters studied:

1. Flow rate vs. current of the FCV:

    - The current to the solenoids were linearly increased to a maximum current of 3.2 A to actuate the Flow Control Valve.
    - During the course of the rise in current the flow rate across the FCV was monitored.
    - The data was used to plot the current versus flow characteristics of the FCV.

2. Flow rate vs. pressure characteristics of the rear hitch control valve:

    - The current to the solenoids was set at different fixed values upto a maximum current setting of 3.2 A.
    - During the course of the rise in current the flow rate across the HCV manifold block was monitored.
    - The pressure and flow characteristics for each current setting were measured and plotted.

CHAPTER 4

Comparison between experimental and simulated results

Figure 4.1 as described in section 2.3 compares numerical results with data from the manufacturer's specifications with respect to flow rate vs. current of the FCV. It can be seen that there is a fairly good agreement.

Figure 4.2 describes the flow rate vs. pressure characteristics of the rear hitch control valve. The results represented are a comparison of the experimental and simulation results, for different current settings. As experimental and simulation results match satisfactorily, it is evident that the model is fairly accurate.

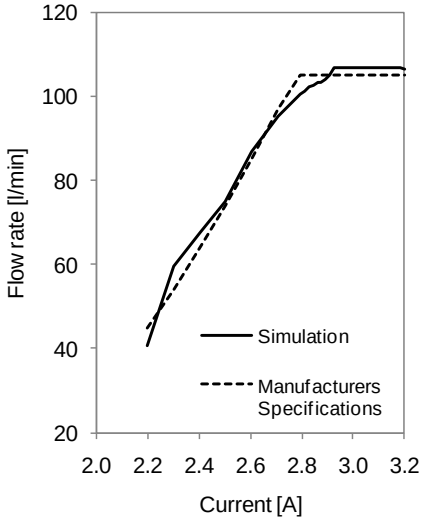

Figure 4.1: Comparison between manufacturers specifications and simulation results for the FCV

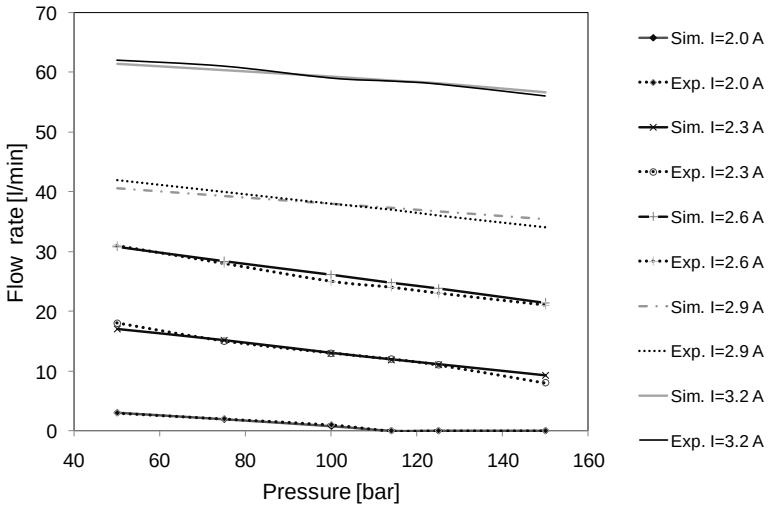

Figure 4.2: Rear Hitch Control Valve - experimental and numerical characteristic

CHAPTER 5

Energy Analysis of the HCV

This section describes the capability of using the mathematical model to perform an energy analysis of the HCV. Figure 5.1 describes the instantaneous pressure and flow characteristics of the system. Three load conditions have been considered: 10 kN, 20 kN and 10 kN on the HCV in conjunction with a secondary user, the system load being defined by the secondary user. The figure describes the pressures at the inlet of the HCV described as the System Pressure P_S, the intermediate chamber pressure P_M and the load pressure P_L. The flow rate across the valve is also plotted. In this way by calculating these paramters the power consumed and thereby the energy consumed by the system can be determined.

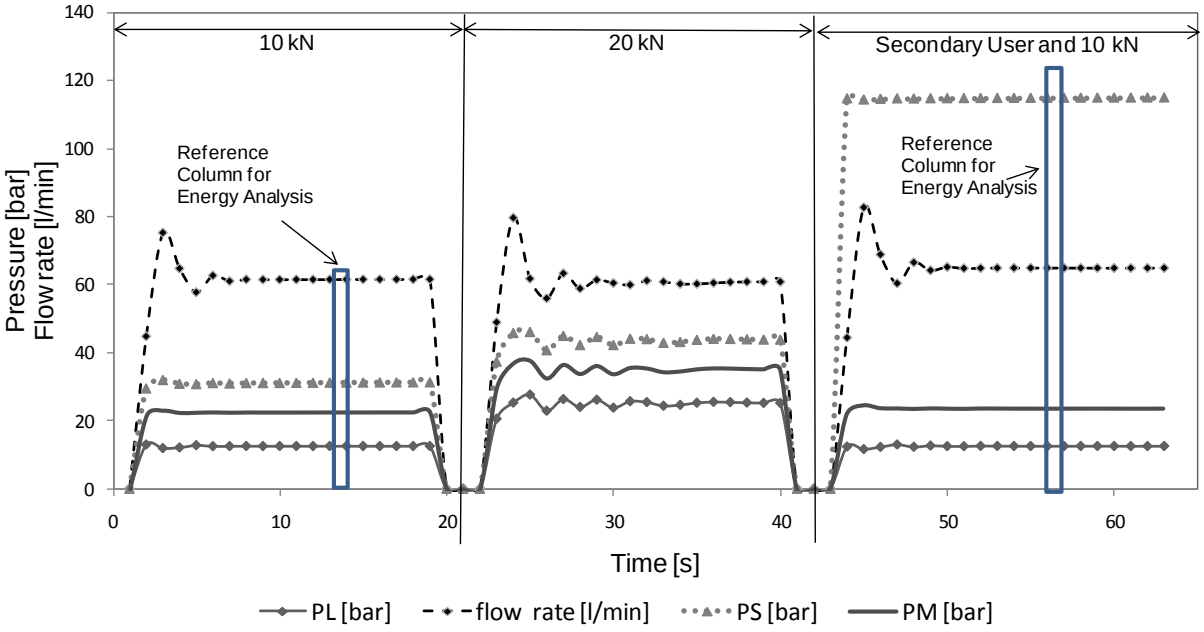

Figure 5.1: Simulated instantaneous pressures and flow rate through the HCV

.

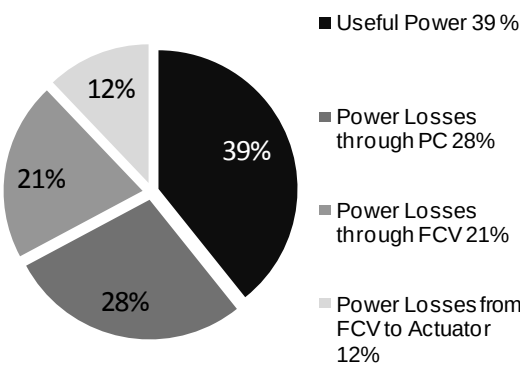

Figure 5.2: Energy chart for a single user LS System

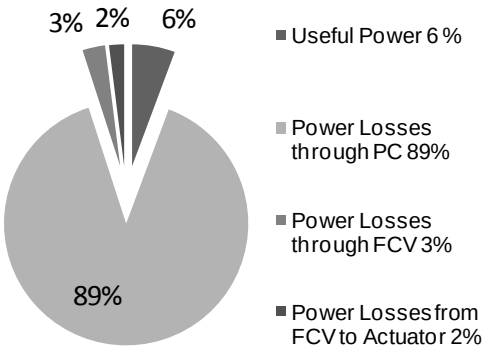

Figure 5.3: Energy chart for a secondary user system

Figure 5.2 describes the energy losses and the power available for lifting 10 kN in a system where the HCV is the only user. This pie chart is obtained by interepreting the time domain data presented in Figure 5.1. The figure 5.2 describes that the actual lifting power avaialble to the actuator is 39% of of the systems inlet power. The figure reveals that a major loss of power transmission, almost 28% occurs at the pressure compensator and that the flow control valve has a power loss of 21% across the valve. These are useful values to help determine how the systems design and effieicncy can be determined. The data represents that if the FCV is appropriately sized the systems efficiency can be improved by 11%. Thereby improving the systems overall efficiency to 50%. The data represents that if

the FCV and the pressure compensator are both improved the systems efficiency can be improved to almost 67%. This graph shows us how appropriate design changes can improve the overall efficieincy of the system and gives us a complete view of the efficiency of the individual components.

The Figure 5.3 describes the power breakdown in the case where the HCV is a secondary user: this time the lifting power share is 6%. This is because the experiment has been carried out considering that the secondary user is the heavily loaded user thereby the energy map represents that the majority of power is consumed by the secondary user in the system and the components of the primary user show very insignificant values.

CHAPTER 6

Dynamic Analysis of the Pressure Compensator

Chapters 2 to 5 have investigated the steady state and dynamic performance of the HCV system. A main problem in the LS system is the poor relative stability. In this chapter, a comprehensive model and analysis of the PC valve is presented. A general non linear dynamic model of a typical PC valve and its linearized equations is developed. As introduced earlier, the pressure compensated valve (PC system) is a flow control device which consists of a fixed or adjustable orifice and a compensator valve. The compensator valve modulates its opening in order to maintain a fixed pressure drop (Ps - Pm) across the fixed or adjustable orifice.

The PC system investigated in this study was a PC flow control valve manufactured for use with CNH Tractors Hitch control circuits. The PC system consists of the valve case, a hydrostat spool (automatically controlled) and an adjustable spool (manually or electrically). Its operation principle has been explained and is not repeated here. The state variables used to describe the dynamic behavior are the displacement, *xpc*, of the hydrostat spool, the pressure, *Psh*, in chamber (2) and the intermediate pressure, *Pm* (see Figure 2.3). The input variables include the upstream pressure, *Ps*, the downstream pressure, *PL*,

and the opening, *xv*, of the adjustable orifice. This chapter presents the process used to linearize the nonlinear relationships.

6.1 Linearized model

To carry out an analysis of the HCV lifting system in the frequency domain a linearized model of the defining control equations has to be formed. Linearization refers to finding the linear approximation to a function at a given point. In the study of dynamic systems, linearization is a method for assessing the local stability of an equilibrium point of a system of nonlinear differential equations. By linearizing the control equations it would be possible to take advantage of a number of well defined frequency response techniques to understand the characteristics of the system under study. The state variable for the system are, the intermediate pressure P_m and pressure compensator spool positionx_{pc}.

Linearizing the flow through the pressure compensator orifice, equation (2.1) and the flow out of the HCV through the proportional FCV, equation (2.2), the following equations (6.1) and (6.2) are obtained:

$$\Delta Q_{LPC} = K_{qpc}\Delta x_{pc} + K_{cpc}(\Delta P_s - \Delta P_m) \tag{6.1}$$

$$\Delta Q_{LV} = K_{qv}\Delta x_v + K_{cv}(\Delta P_m - \Delta P_L) \tag{6.2}$$

Where $K_{qpc}$and K_{qv} are the flow gains of the PC's orifice and the FCV's orifice. K_{cpc} and K_{cv} are the flow pressure coefficients of the PC and FCV orifice respectively. This model follows the linearized model of flow across an orifice.

The flow gain of the PC orifice K_{qpc}

$$K_{qpc} = C_{dc}\sqrt{\frac{2}{\rho}(P_s - P_{m0})} \cdot \frac{dA_{pc}}{dx_{pc}}(x_{pc0}) \tag{6.3}$$

The flow gain of the FCV orifice K_{qv}

$$K_{qv} = C_{dv}\sqrt{\frac{2}{\rho}(P_{m0} - P_L)} \cdot \frac{dA_v}{dx_v}(x_v) \tag{6.4}$$

The flow pressure coefficient of the PC orifice K_{cpc}

$$K_{cpc} = \frac{C_{dc} \cdot A_{pc}(x_{pc0})}{\sqrt{2\rho(P_s - P_{m0})}} \tag{6.5}$$

The flow pressure coefficient of the FCV orifice K_{cv}

$$K_{cv} = \frac{C_{dv} \cdot A_v(x_v)}{\sqrt{2\rho(P_{m0} - P_L)}} \tag{6.6}$$

Linearizing equation (2.3) the dynamic force balance across the pressure compensators spool and substituting the values for P_I equation (2.4) and P_J equation (2.5), results in equation (6.7). In the linearized model the value P_{pc} is left out as it is neither an input variable nor a state variable. P_{pc} affects the dynamic behavior of the system only through the steady state operating point.

$$\begin{aligned} M_{pc}\Delta\ddot{x}_{pc} + \{B_{pc} + \rho L K_{qpc} + A_{pcs}^2(R_J - R_J)\}\Delta\dot{x}_{pc} \\ - \left\{K_{pc} + K_{ff} \cdot \frac{dA_{pc}}{dx_{pc}}(x_{pc0}) \cdot (P_s - P_{m0})\right\}\Delta x_{pc} - \{K_{ff} \cdot A_{pc}(x_{pc0}) - A_{pcs}\}\Delta P_m \\ = A_{pcs}\Delta P_L - K_{ff} \cdot A_{pc}(x_{pc0}) \cdot \Delta P_s \end{aligned} \tag{6.7}$$

Linearizing equation (2.6) the flow through the intermediate chamber

$$\Delta Q_{LPC} - \Delta Q_{LV} - A_{pcs}\Delta\dot{x}_{pc} = 0 \tag{6.8}$$

Substituting the linearized values of ΔQ_{LPC} and ΔQ_{LV} equations (6.1) and (6.2) in the equation (6.8) yields

$$K_{qpc}\Delta x_{pc} - \left(K_{cpc} + K_{cv}\right)\Delta P_m = A_{pcs}\Delta \dot{x}_{pc} - K_{cpc}\Delta P_s - K_{cv}\Delta P_L + K_{qv}\Delta x_v \tag{6.9}$$

6.2 Dynamic model of the lifting circuit

Based on the linearized dynamic model the frequency response model of the lifting circuit, which comprises of a pressure compensated flow control valve, can be developed. Taking the Laplace transform for the linearized force balance across the pressure compensator Equation (6.7), equation (6.9), equation (6.1) and solving the Laplace transforms for the flow rate across the pressure compensator as a function of the variables pertaining to the opening of the variable orifice $X_v(s)$, pressure into the system $P_s(s)$ and the pressure at the load $P_L(s)$ the following transfer function is obtained:

$$Q_{lpc} = G_{xv}(s)X_v(s) + G_{psl}(s)(P_s(s) - P_L(s)) \tag{6.10}$$

Where, $G_{xv}(s)$ is the flow gain transfer function, equation (6.11) and $G_{psl}(s)$ is defined as the flow pressure coefficient transfer function equation (6.12)

$$G_{xv}(s) = K_{xv}\frac{s^2 + b_{xv1}s + b_{xv0}}{s^2 + a_1 s + a_0} \tag{6.11}$$

$$G_{psl}(s) = K_{psl}\frac{s^2 + b_{psl1}s + b_{psl0}}{s^2 + a_1 s + a_0} \tag{6.12}$$

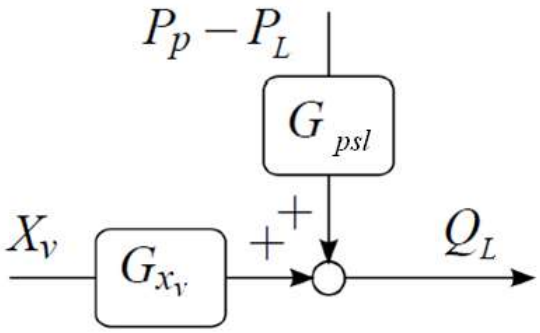

Figure 6.1: Block Diagram derived from Transfer Functions

The gains and coefficient values for $G_{xv}(s)$ and $G_{psl}(s)$ are:

$$K_{xv} = \frac{K_{cpc}K_{qv}}{K_{cpc} + K_{cv}} \tag{6.13}$$

$$K_{psl} = \frac{K_{cpc}K_{cv}}{K_{cpc} + K_{cv}} \tag{6.14}$$

$$a_1 = \frac{B_{pc} + \rho L K_{qpc} + A_{pcs}^2(R_I - R_J)}{M_{pc}} + \frac{A_{pcs}\{K_{ff} \cdot A_{pc}(x_{pc0}) - 1\}}{M_{pc}(K_{cv} + K_{cpc})} \tag{6.15}$$

$$a_0 = \frac{K_{pc} + K_{ff} \cdot \frac{dA_{pc}}{dx_{pc}}(x_{pc0}) \cdot (P_s - P_{m0})}{M_{pc}} + \frac{K_{qpc}\{K_{ff} \cdot A_{pc}(x_{pc0}) - A_{pcs}\}}{M_{pc}(K_{cv} + K_{cpc})} \tag{6.16}$$

$$b_{xv1} = \frac{B_{pc} + \rho L K_{qpc} + A_{pcs}^2(R_I - R_J)}{M_{pc}} \tag{6.17}$$

$$b_{xv0} = \frac{K_{pc} + K_{ff} \cdot \frac{dA_{pc}}{dx_{pc}}(x_{pc0}) \cdot (P_s - P_{m0})}{M_{pc}} - \frac{K_{qpc}\{K_{ff} \cdot A_{pc}(x_{pc0}) - A_{pcs}\}}{M_{pc}K_{cpc}} \tag{6.18}$$

$$b_{psl1} = \frac{B_{pc} + \rho L K_{qpc} + A_{pcs}^2(R_I - R_J)}{M_{pc}} + \frac{A_{pcs}^2}{M_{pc}K_{cv}} \tag{6.19}$$

$$b_{psl0} = \frac{K_{pc} + K_{ff} \cdot \frac{dA_{pc}}{dx_{pc}}(x_{pc0}) \cdot (P_s - P_{m0})}{M_{pc}} - \frac{K_{qpc}K_{ff} \cdot A_{pc}(x_{pc0})}{M_{pc}K_{cpc}} \tag{6.20}$$

6.3 Analysis of the lifting circuit of the hcv

For a particular operating condition when the flow control valve was at its maximum opening, particular flow instability was observed in the AMESim® nonlinear numerical simulation, figure 6.2. A fixed input flow rate was assumed as an input to the system, this does not reflect the actual case as is found on the tractor. The reason for choosing this mode of simulation was to quantify the functionality of the Pressure Compensated Flow Control Valve at various flows and pressures.

For the model developed, the data pertaining to the operating point was obtained from the AMESim® non-linear model and these parameters (refer Table 6.1) were used to obtain the frequency plots in Matlab® figures. 6.3, 6.4. The displacement of the pressure compensator (x_{pc}) for this particular condition was $0.5 \cdot 10^{-3}$ m and of the FCV orifice (x_v) $2.05 \cdot 10^{-3}$ m.

Table 6.1: Parameters of the Pressure compensator spool and FCV

Parameters	Value
Fluid Density, ρ	850 kgm^{-3}
Fluid Temperature, T	40° C
Discharge Coefficient of the pressure compensator orifice, C_{dc}	0.7
Discharge Coefficient of the control orifice, C_{dv}	0.7
Spring Stiffness, K_{pc}	$38 \cdot 10^{-3}$ Nm^{-1}
Spool Diameter, D_{pcs}	$19.03 \cdot 10^{-3}$ m
Spool Damping Coefficient, B_{pc}	10 Nsm^{-1}
Damping Length, L	$28.39 \cdot 10^{-3}$ m
Flow area of pressure compensator, $A_{pc}(x_{pc})$	$8.37 \cdot 10^{-6}$ m^2
Equivalent Width of Pressure compensator orifice, $\frac{dA_{pc}}{dx_{pc}}(x_{pc})$	$15.625 \cdot 10^{-3}$ m
Supply Pressure, P_s	20 MPa
Intermediate Pressure, P_m	6 MPa
Load Pressure, P_L	5.4 MPa
Spool Mass, M_{pc}	0.133 kg
Flow area of Control Orifice, $A_v(x_v)$	$37.83 \cdot 10^{-6}$ m^2
Equivalent Width of Control orifice, $\frac{dA_v}{dx_v}(x_v)$	$18.42 \cdot 10^{-3}$ m

Using the data provided in the table the following frequency response parameters were obtained:

$$G_{xv}(s) = 0.02 \cdot \frac{s^2 + 223.4s + 1.11 \cdot 10^8}{s^2 - 466.8s + 5.91 \cdot 10^6} \tag{6.21}$$

$$G_{psl}(s) = 3.6 \cdot 10^{-11} \cdot \frac{s^2 - 508.9s - 5.14 \cdot 10^5}{s^2 - 466.8s + 5.91 \cdot 10^6} \tag{6.22}$$

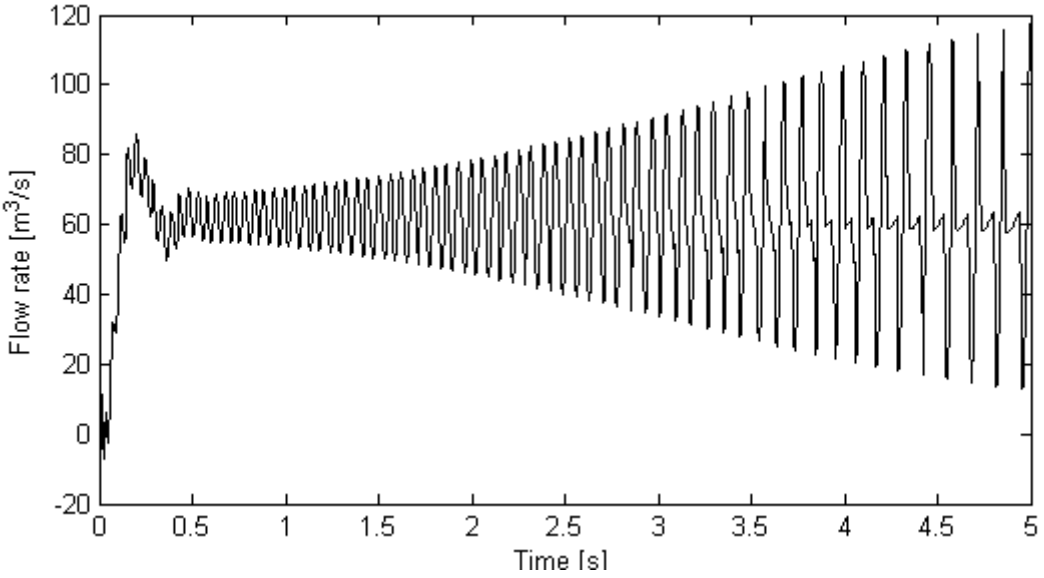

Figure 6.2: Flow Characteristic at the Load – Original System

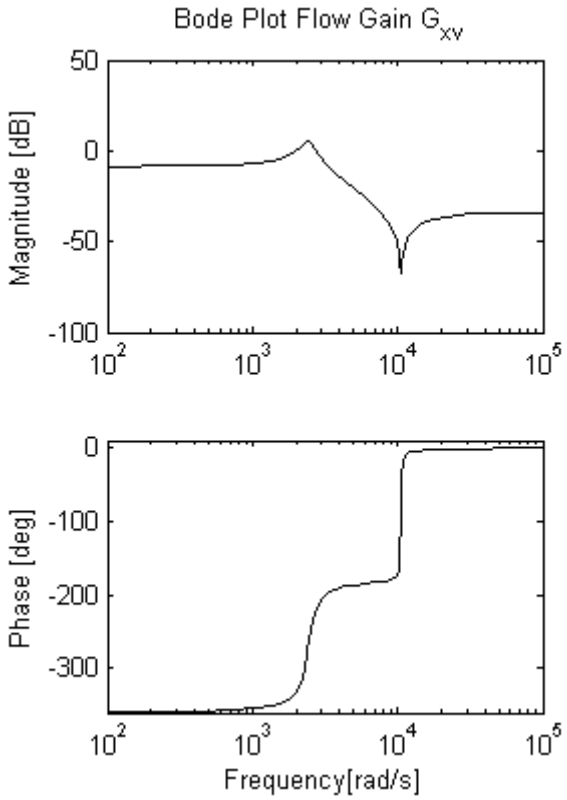

Figure 6.3: Frequency response of flow gain, G_{xv}

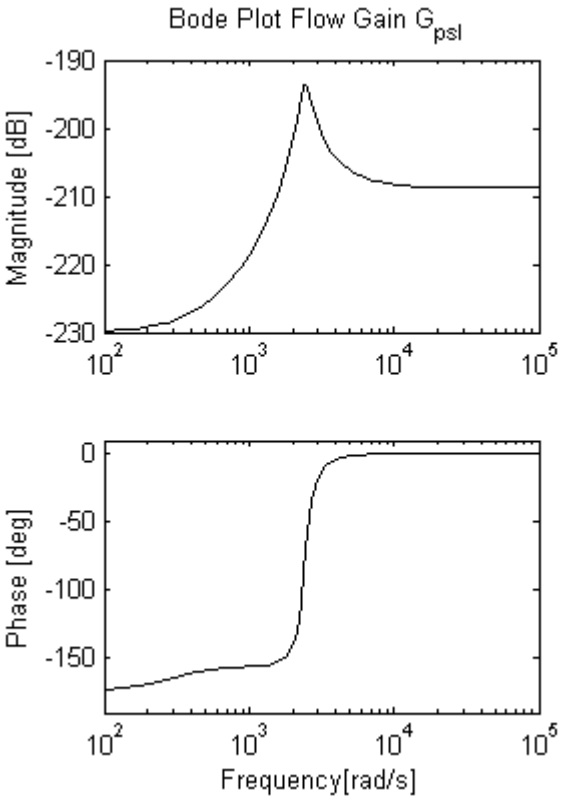

Figure 6.4: Frequency response of flow-pressure coefficient, G_{psl}

Figure 6.2 shows that the flow characteristic at this particular operating position of the valve is unstable, resulting in a divergent flow characteristic. From the analysis of figure 6.3 the frequency response of the flow gain, it is evident that the frequency bandwidth of flow control is very wide. This is understood from the magnitude plot of G_{xv}, which describes the bandwidth of flow gain to the corner frequency. The damping ratio of the system is 0.1. From figure 6.4 relating to the flow pressure coefficient it can be seen that at very low frequencies, near steady state conditions, the phase of the flow pressure coefficient transfer function is -180° and can be defined as an undercompensated condition.

6.4 Interpreting the frequency plots

The flow gain transfer function $G_{xv}(s)$ is a low pass filter because the value of a_0 is smaller thanb_{xv0}. That is, it allows low frequency signals but attenuates signals higher than the

cut-off frequency. Thereby it removes the short-term oscillations. The damping in the system is affected by the hydraulic resistance offered by the two orifices *I* and *J*. To calculate the effect of the damping orifice, we consider the flow rate through the orifice which would be laminar as it is a very small value. The flow being laminar can be commonly specified as the pressure – flow ratio; the hydraulic resistance. On this basis the hydraulic resistance can be defined by the Hagen Poiseulle's equation and can be expressed as:

$$R = \frac{128 \cdot \mu}{\pi \cdot d^3} \tag{6.23}$$

Where, the values for the hydraulic resistance *R* can be calculated by inserting the appropriate diameter (*d*) for the orifice *I* or *J*. To obtain an appropriate damping ratio the sizes of these two orifices must be carefully calculated. The damping ratio is a parameter, usually denoted by ζ, which characterizes the frequency response of a second order ordinary differential equation. An ideal situation would be to have ζ critically damped, this is achieved when the PC system has a pair of conjugate poles (a real part in the attenuation parameter), with a damping ratio of 0.7.

The flow-pressure coefficient is used to minimize the effect of pressure drop across the valve on flow rate. The flow pressure coefficient transfer function is a high pass filter. A high-pass filter is a linear time invariant filter that passes high frequencies well but attenuates frequencies lower than the cut-off frequency. In order to have a minimum effect of pressure on flow, the magnitude of the flow pressure coefficient should be as small as possible in all frequency regions. This is particularly important in the low frequency regions near the steady state operating condition. It is possible to reduce the flow pressure coefficient by designing a proper set of dynamic parameters such as the M_{pc}, B_{pc}, K_{pc}, and *R*. Another approach to decrease the magnitude would be to decrease the zero value of *Gpsl(s).*[10].

6.5 Results

From the analysis of figures. 10, 11 and 12 in comparison with those of figures. 7, 8 and 9, the parameters that have been used to improve the pressure compensated flow control valve can be identified. To comply with the objective of effecting an improvement in the flow response characteristic while keeping the casting dimensions unchanged, it was decided that the damping parameter of the valve would be improved. This objective can be achieved by maintaining the phase of the flow pressure coefficient critically damped, that is a phase of 0° as seen in Figure 11; this in comparison to figure 9 where the phase is -180 ° which relates to an under damped condition. By increasing the damping a diverging flow characteristic (obtained from the nonlinear AMESim® model) Figure 7 was changed to fig 12 a converging characteristic. The changes incorporated were to modify the orifice dimensions *I* and *J* to 0.67mm and 1mm respectively. By incorporating these changes a better flow characteristic can be achieved while not afflicting expensive manufacturing changes in terms of modification of the casting; thus providing a feasible and viable solution.

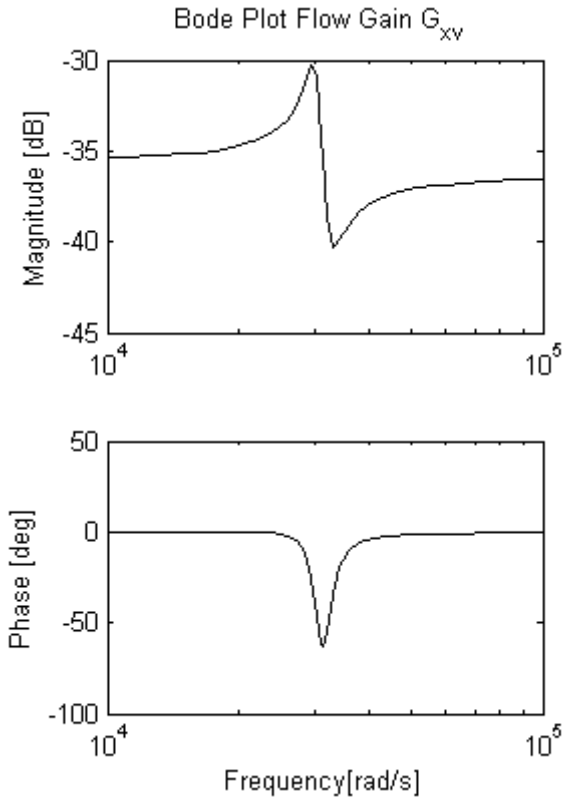

Figure 6.5: Modified System Frequency

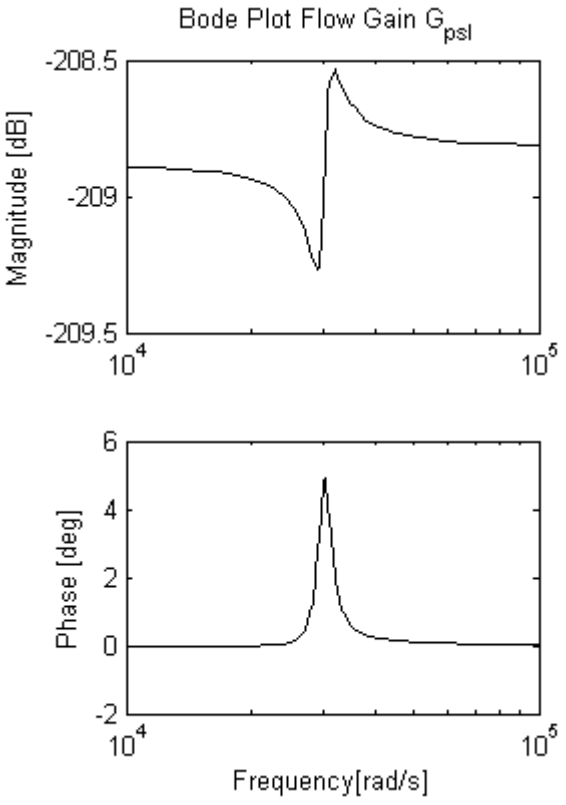

Figure 6.6: Modified System Frequency

response of flow gain, G_{xv} response of flow-pressure coefficient, G_{psl}

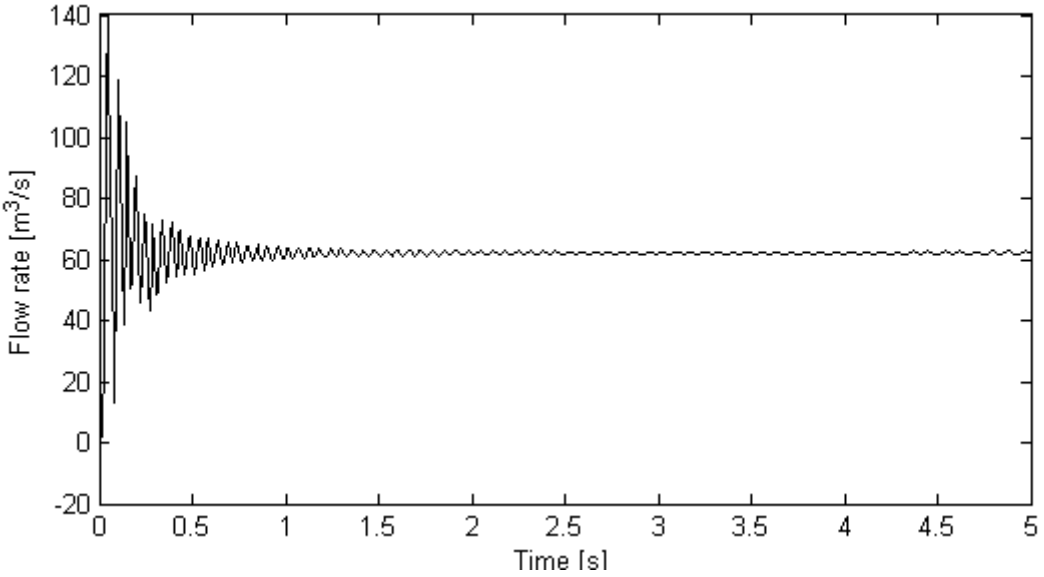

Figure 6.7: Flow Characteristic at the Load – Modified System

It is know that to specify a manufacturing dimension of 0.67mm is unrealistic for large scale manufacturing. The value 0.67 presented here represents an ideal damping characteristic related to this work. The value 0.67 was chosen after it was found that good damping characteristics were achievable with an orifice hole in the range of 0.65 to 0.8mm. On verifying machining data for tolerance limits on drills, which describes that for a 0.65mm drill, the upper tolerance limit would result in a size of 0.75mm. Based on this data it was decided that an exact value for the calculated orifice be represented, as it would fall within the tolerance range for a standard drill of the 0.65 size. All the hole diameters in the range of 0.65 to 0.75mm provide good damping characteristics, while the size of 0.67mm provides the ideal characteristic.

Conclusion

The document describes a nonlinear and linearized model of an agricultural tractors rear hitch control valve lifting control system. It comprises of a pressure compensated flow control valve. A pressure compensated valve employs a pressure control valve to maintain a constant pressure drop across an orifice. With a constant pressure drop the flow through the orifice is directly proportional to the orifice area and load independent. The validity of the nonlinear numerical model is demonstrated by comparing it with experimental results. The numerical model demonstrates the capability of reproducing experimental results, thus providing confidence in the models capabilities. An energy analysis has been carried out using the numerical model after validation. It describes the functioning of the hitch control valve under three different load conditions. The first condition with a 10kN load, the second condition with a 20kN load and the third condition with a secondary user being the highest load. This type of a load analysis provides the feasibility of studying the power losses across the various components of the hitch control valve and gives us information on the power consumed by different components.

The study has been extended to study a linearized model of the pressure compensator. This is used to perform a frequency analysis of the valve and to ascertain the parameters affecting its performance for a particular operating condition. The flow characteristic in the time domain was found to be divergent. The frequency analysis plots have been interpreted and used to modify and improve the valve's performance. The improvement in performance is evident from the flow bounded condition.

Dott. Ing. Alvin Anthony

List of Notations

A_{PC}	Orifice area of PC	m^2
A_{PCS}	Area of PC spool	m^2
A_v	Orifice area of FCV	m^2
B_{PC}	Damping coefficient of PC spool	Nm/s
C_{dc}	Coefficient of discharge PC orifice	
C_{dv}	Coefficient of discharge FCV orifice	
C_v	Flow velocity coefficient (approx. 0.98)	
G_{xv}	Flow gain TF	m^2/s
G_{psl}	Flow pressure coefficient TF	m^5/sN
K_{qpc}	Flow gain of PC valve	m^2/s
K_{cpc}	Flow pressure coefficient of PC valve	m^5/sN
K_{qv}	Flow gain of FCV	m^2/s
K_{cv}	Flow pressure coefficient of FCV	m^5/sN
K_{PC}	Spring stiffness of PC	N/m
K_{ff}	Flow force coefficient	
K_{xv}	Gain of the flow gain TF	
K_{psl}	Gain of the flow pressure coefficient TF	
L	Damping length of compensator spool	m
M_{PC}	Mass of PC spool	kg
P_S	Supply Pressure	Pa
P_M	Intermediate pressure	Pa
P_L	Load Pressure	Pa
Q_{LPC}	Flow rate through the PC	m^3/s
Q_{LV}	Flow rate through the FCV	m^3/s
R_I	Hydraulic resistance of damping hole I	sN/m^5
R_J	Hydraulic resistance of damping hole J	sN/m^5
x_{pc}	Displacement of PC spool	m
x_v	Displacement of FCV spool	m
ρ	Fluid Density	kg/m^3
Acronyms		
FCV	Flow Control Valve	
FDM	Fluid Dynamic Model	
HCV	Hitch Control Valve	

LS	Load Sensing
MGM	Mechanical Geometric Model
PC	Pressure Compensator
TF	Transfer Function

References

[1] **Blakburn J. F., Reethof G. & Shearer J. L..** *Fluid Power Control*. USA: MIT Press, 1966. ISBN 0262520044.

[2] **Handroos, H. M, Vilenius, M. J**, *Flexible Semi-Emprical Model for Hydraulic Flow Control Valves,* Transactions of the ASME, Sep 1991

[3] **Karnopp. D,** *Computer simulation of stick slip friction in mechanical dynamic systems,* ASME Journal of Dynamic Systems, Measurement and Control, March 1985

[4] **LMS Imagine - AMESim** Reference manual 2009

[5] **McCloy, D., Martin, H. M,** *The control of Fluid Power*, Longman, London, 1973

[6] **Merrit, H. E.**, *Hydraulic Control Systems*, Wiley, New York, 1967

[7] **Norvelle. F. D,** *Electro hydraulic Control Systems*. Prentice Hall, 2000. ISBN 0137163592.

[8] **Shih-Tin Lin,** *Stabilization of Baumgarte's Method Using the Runge-Kutta Approach,* ASME Journal of Mechanical Design, December 2002

[9] **Vacca. A, Greco. M, Fornaciari. A,** *A Methodology for the development of a Relief, Antishock and Anticavitation Cartridge Valve*, 6 IFK, Dresden, Germany 2008

[10] **Wu, D., Burton, R., Schoenau, G., Bitner, D.,** *Analysis of a Pressure - Compensated Flow Control Valve*, ASME Journal of Dynamic Systems, Measurement and Control, March 2007

[11] **Casoli, P.; Vacca, A.; Anthony, A.; Berta, G.L.** (2010). Numerical and Experimental Analysis of the Hydraulic Circuit for the Rear Hitch Control in Agricultural Tractors. *Proceedings of the 7th International Fluid Power Conference, Aachen.*

[12] **Manring, N. D.** (2005) *Hydraulic Control Systems*, John Wiley & Sons Inc

Acknowledgement

I would like to thank God for having blessed me to carry out my Doctoral research in Italy, a wonderful and blessed country with the nicest people in the world. It has truly been an enlightening experience.

I would like to thank Prof. Paolo Casoli for being a friend, a guide and a good support through the development of my research. Working with whom truly has been a pleasure.

I would also like to thank Prof. Gian Luigi Berta, Prof. Agostino Gambarotta and Giorgio Toderi for providing a nice and friendly environment at the Industrial Engineering Deparrtment.

My thanks to the teams at Casappa (R. Casappa, Guidetti, Lettini, Dardini, Pietropaolo). Walvoil (Fornaciari, Dolcin, Gannasi, Havermann) and CNH (Riccordo Morselli) for all their help in terms of lively discussions and for test components.

I would like to thank my friends from UNIPR - Gabriele, Michele, Manuel, Iacopo, Luca, Gianluca, Cora, Alex, Davide, Marco, Alessandro, Giovanni and Andrea Vacca. You have all been great people to work with and I had an interesting time interacting with all of you.

My special thanks to our friends from Parma – Anila, Armando, Atim, Elisa, Fred, Greg and Leo for always being there for us.

I would like to thank my parents and in-laws for all their support and help.

Special thanks are due to Mr. Vasudevan Ramamurthy for introducing me and mentoring me in the wonderful world of fluid power.

I would like to thank my daughters Michelle and Arielle for being such wonderful and accomodating children during the course of the Doctoral program inspite of the fact that I never could spend too much time with them. Both of them always were a continuous source of joy, encouragement and are the biggest source of happiness in my life.

My deepest and most heartfelt thanks to my wife Mythili, who held fort and took care of everything on the family front. Thank you from the bottom of my heart, you are my biggest blessing from God.

Alvin Anthony